



University of Bradford eThesis

This thesis is hosted in [Bradford Scholars](#) – The University of Bradford Open Access repository. Visit the repository for full metadata or to contact the repository team



© University of Bradford. This work is licenced for reuse under a [Creative Commons Licence](#).

New C-C Chemokine Receptor Type 7 Antagonists

Mohaned Saad Abdalla AHMED

Submitted for the Degree of Doctor of Philosophy

Institute of Cancer Therapeutics

University of Bradford

2016

Abstract

Mohaned Saad Abdalla AHMED

New C-C Chemokine Receptor Type 7 Antagonists

Key words: Cancer, Metastasis, Chemokines, Receptor, CCR7, CXCR4, antagonist, GPCR, medicinal chemistry, agarose spot assay.

Chemokines are chemotactic cytokines which play an important role in the migration of immune cells to distant tissues or compartments within tissues. These proteins have also been demonstrated to play a major role in cancer metastasis. The C-C chemokine receptor type 7 (CCR7) is a member of the chemokine receptor family. CCR7 along with its ligands CCL19 and CCL21 plays an important role in innate immune response by trafficking of lymphocytes. In cancer, tumour cells expressing CCR7 migrate to lymphoid organs and thus disseminate to other organs. Neutralizing the interactions between CCL21/CCR7 would therefore be expected to inhibit the progression and metastasis of many different types of cancer to regional lymph nodes or distant organs. Our objective was to identify a potent small molecule antagonist of CCR7 as a prelude to the investigation of the role of this axis in cancer metastasis. In this study, we provided a brief description of chemokines and their role in health and disease with an emphasis on the CCR7/CCL19/CCL21 axis, as well as identification of a CCR7 antagonist "hit". The potency of the CCR7 antagonist "hit" was optimised by

synthesizing different CCR7 antagonist analogues. The “hit” optimization process has led to discover the most active compound amongst a series of different analogues which have the ability to bind and block CCR7 receptor. The efficacy of the most active compound and other analogues were evaluated *in vitro* using a calcium flux assay which is based on detecting fluorescent light emitted upon release of calcium ions. To identify a suitable cell line, which expresses CCR7 and capably respond to it, amongst a panel of cell lines for *in vitro* assessment of potency of synthesised compounds, we used Western blot assay and later by flow cytometry assay. The activity and selectivity of the most effective compound against CCR7 receptor was evaluated *in vitro* by other functional assays such as “configured agarose spot assay” and scratch assay. We first configured the existing under agarose assay to fulfil our requirements and then used it to assess activity and selectivity of compounds. The configured agarose spot assay also describes the application of the agarose spot for evaluation of cells chemotactic response to multiple chemokines under identical experiment conditions.

Acknowledgement

My sincerest gratitude is toward my supervisor Dr. Kamyar Afarinkia for giving me the opportunity to work on this interesting project and for his continuous guidance and support.

I would specially like to express my thanks to my family, my mother, my father, my wife and my two daughters, Fatima and Jannat for the support and my government of Libya for providing me with funding.

I am very grateful towards Dr. Victoria Vinader and Dr. Steve Shnyder for their encouragement and continuous guidance.

It is a pleasure to thank all staff and students, at the Institute of Cancer Therapeutics, University of Bradford, who helped and supported me during my lab work over the last three years of my PhD.

Table of Contents

Abstract.....	i
Acknowledgement.....	iii
Table of Contents.....	iv
Abbreviations	vi
1. Chapter 1 Chemokines and their role in disease.....	1
1.1. Introduction	2
1.2. Chemokines and chemokine receptors.....	4
1.3. Function of Chemokines in Health and Disease	9
1.4. Chemokines signalling Pathways	11
1.5. The CXC Chemokine Receptor Type 4.....	15
1.6. The C-C Chemokine Receptor Type 7.....	19
1.7. Aims and Objectives	37
2. Chapter 2: Synthesis of CCR7 receptor antagonists.....	38
2.1. Introduction	39
2.2. Synthesis of compound 1, ICT5189.....	39
2.3. Structure activity relationship: summary of findings	88
3. Chapter 3: Pharmacological characterization of CCR7 receptor antagonists	92
3.1. Introduction	93
3.2. Characterization of CCR7 receptor antagonists potency using calcium flux assay.....	95

3.3.	Characterization of CCR7 Receptor expression using Western blot.	
		97
3.4.	Determining the efficacy of the agonist.....	99
3.5.	Determining the efficacy of the antagonists	106
3.6.	Agarose spot method for <i>in situ</i> analysis of chemotactic responses to multiple chemoattractants.....	109
3.7.	Concluding remarks and future works	144
4.	Chapter 4: Experimental.....	149
4.1.	Experimental Section.....	150
5.	References.....	235
Appendix I	Evaluating activity of Different compounds using calcium flux assay.	256
Appendix II	CCR7 and CXCR4 membranous receptor expression using flow cytometry assay.....	266
Appendix III	Evaluating the cytotoxicity of some compounds using MTT assay.	268
Appendix IV	Evaluating efficacy of compound 75 using scratch assay. ...	269

Abbreviations

Ac	acetyl
aq	Aqueous
ATCC	American Type Culture Collection
BSA	Albumin, from bovine serum
Bu	butyl
CAFs	cancer associated fibroblasts
cAMP	Cyclic adenosine monophosphate
cat	catalyst
CCL19	Chemokine C-C motif ligand 19
CCL21	Chemokine C-C motif ligand 21
CCR7	C-C chemokine receptor type 7
CD4	cluster of differentiation 4
COSY	Correlation Spectroscopy (NMR)
CXCL12	Chemokine CXC motif ligand 12 aka Stromal-derived factor 1 (see SDF1)
CXCR4	CXC chemokine receptor type 4
DCC	N,N'-Dicyclohexylcarbodiimide
DCM	Dichloromethane

DEPT	Distortionless Enhancement by Polarisation Transfer
DMAP	4-(N,N-Dimethylamino)pyridine
DMF	N,N-Dimethylformamide
DMSO	Dimethyl sulfoxide
ECM	Extracellular matrix
ELR	glutamic acid–leucine–arginine
ERK	extracellular-signal-regulated kinases
ESI	Electrospray Ionization
Et	ethyl
FCS	Foetal Calf Serum
GAGs	glycosaminoglycan
GDP	guanosine diphosphate
GEFs	guanine nucleotide-exchange factors
GPCR	G-protein coupled receptor
GPI	glycosylphosphatidylinositol
GTP	Guanosine triphosphate
G _α	G protein alpha subunit
G _{βγ}	G beta-gamma complex

HBSS	Hanks Balanced Salt Solution
HEVs	high endothelial venules
HIF	Hypoxia inducible factor
HIV	Human immunodeficiency virus
IC ₅₀	half maximal inhibitory concentration
IFN- γ	Interferon-gamma
IgG	Immunoglobulin G
IL-1 β	Interleukin-1 beta
IL-6	Interleukin 6
IP-10	interferon- γ -inducible protein-10
IR	Infrared (spectroscopy)
<i>J</i>	Coupling Constant (NMR)
JAK	Janus kinase
kDa	kilodalton
LDA	Lithium diisopropylamide
LN _s	lymph nodes
m.p.	melting point
MCP-1	monocyte chemoattractant protein-1 aka CCL2

Me	methyl
mg	Milligram
ml	Millilitre
mM	Millimolar
μ M	micromolar
MMPs	Matrix metalloproteinases
MS	Mass Spectrometry
NCI	National Cancer Institute
NF- κ B	nuclear factor kappa-light-chain-enhancer of activated B cells
NMR	Nuclear Magnetic Resonance spectra
p38 MAPK	p38 mitogen-activated protein kinase
PAK	p21-activated kinase
PE	petroleum ether (bp fraction 60-80 °C)
PF4	platelet factor 4
Ph	phenyl
PBS	phosphate buffered saline
PI3K	phosphatidylinositol 3-kinase
PIP3	phosphatidylinositol 3, 4, 5-triphosphate

ppm	parts per million
rpm	Revolutions per minute
RT	Room temperature
SAR	Structure-activity relationship
SCCHN	Squamous cell carcinoma of the head and neck
SCID	severe combined immunodeficient
SDF-1	stromal cell derived factors
SDS	sodium dodecyl sulfate
siRNA	Small interfering RNA
STAT	signal transduction and activators of transcription
TAMs	tumour-associated macrophages
TBAF	Tetra-n-butylammonium fluoride
THF	Tetrahydrofuran
TLC	Thin layer chromatography
TMS	trimethylsilyl
TNF α	tumour necrosis factor alpha
Tyr	Tyrosine
VCAM-1	vascular cell adhesion molecule-1

VEGF	vascular endothelial growth factor
vHTS	virtual high-throughput screening
WB	Western blot

1. Chapter 1 Chemokines and their role in disease

1.1. Introduction

Uncontrolled cell growth is an important characteristic of cancer. In most body tissues and organs, a balance is kept between cell proliferation and cell death. Sometimes, cells lose their ability to respond to the normal growth control mechanism and thus never stop their replication. This results in large clusters of cells that can be considered as a tumour or neoplasm. Tumours can be classified as benign or malignant depending on their behaviour, such as how fast they grow and how likely they tend to spread to certain parts of the body. Benign tumours are typically slow-growing and rarely spread to other parts of the body ¹. However, malignant tumours tend to grow faster and have the potential to invade surrounding tissue and metastasise to distant organs. Malignant tumours (cancer) are defined as group of uncontrolled diseases characterized by self-sufficient in growth signals, by pass apoptosis, insensitivity to tumour suppressor gene, induce angiogenesis, ability to invade and metastasise to certain organs, immortality, avoiding immune destruction, promote inflammation, genome instability and cellular energetics deregulation ². Metastatic cancer cells are uniquely characterised by their spreading throughout the body. They migrate from a primary site to other locations in the body. This process is called metastasis and it's the major difference between benign and malignant cell growth. The process of tumour progression to metastasis is very complicated and only a few cells survive the whole processes to reach the invasion step ³. Following initial growth of preliminary tumours, malignant cells invade surrounding tissues and enter blood circulation. Circulating tumour cells migrate out of the blood vessels into distant tissues ⁴. Tumour cells can

spread and migrate along tissue surfaces and into many different tissue spaces and cavities, however the main two routes of metastatic spread are through lymphatic and blood vessels ⁵. Tumour metastasis is the main cause of mortality in patients with malignant tumours. Different tumours metastasise to certain organs of the body based on the origin of the primary tumour. For instance, breast and prostate cancer cells tend to metastasise to bone while melanoma mainly metastasises to the brain, lung and liver. Secondary tumour site formation is based on many factors like blood flow, and the expression of specific receptors can accelerate metastasis ⁶. Cancer is the most widespread disease affecting people throughout the world. Although improved treatment regimens have reduced the death-rate resulting from cancer, it is still the major cause of death. The mortality rates of cancer have risen quickly in the world, especially in the last two decades, which has brought more attention to cancer research ⁷. Most physicians prescribe adjuvant therapy for patients with solid tumour as additional therapy after primary surgery to eliminate micro-metastatic disease. The adjuvant treatment is dependent on prognostic signs such as tumour size, grade, and most substantially, the existence of tumour cells in distant organs. Indeed, lymphatic metastasis is a marker for distant metastatic disease ⁸. Although many molecules are involved in cancer metastasis, there is no single precise mechanism of tumour cell migration to specific organs. The “seed and soil” theory describes directional metastasis, taking into account that certain organs have the suitable environment for cancer cells from the first organ ⁹. A wide range of the tumour host factors including growth factors, cytokines and chemoattractants support tumour cell growth, proliferation and migration.

Cytokine family members known as chemokines are involved in many steps of malignant transformation and tumour invasion and metastasis. Many different functions and mechanisms of action have been proposed for chemokines and their receptors in the growth and progression of tumours ¹⁰.

1.2. Chemokines and chemokine receptors.

The inflammatory cells, such as phagocytic leukocytes of the immune system, undergo accelerated controlled movement in response to a chemical stimulus toward the inflammation site which have the highest concentration of chemokine (chemoattractant gradient) to serve as a first line of defence against infection ¹¹. Phagocytic leukocytes are part of the innate immune system which are involved in protecting the body from inflammation and foreign invaders. During injury, infected cells release chemotactic factors which recruit phagocytic leukocytes to the inflammation site through endothelial receptors. The interaction between chemotactic factors and phagocytic leukocyte initiate changing in ion fluxes, increasing integrin avidity and transmembrane potential, changes in cell shape, production of superoxide anions, as well as improved locomotion ¹². The chemotactic gradient released from cells attract leukocytes toward the site of injury or infection. Eventually they transmigrate and exit the bloodstream toward infected tissue and engulf infected cells or recruit the adaptive immune system to eradicate or stop pathogen growth.

There are two well-known types of chemoattractants that have been identified. These chemoattractants are bacterial-derived *N*-formyl peptides and lipid molecules such as leukotriene B₄ and platelet-activating factor

which all are activators of leukocytes ¹³. There are a number of chemotactic cytokines that have been shown to be selective for leukocyte subpopulations and these are called chemokines ¹⁴. Chemokines are a large family of structurally related cytokines which are involved in activation and migration of many different types of leukocytes ¹⁵. Unlike cytokines which were first discovered by observation of soluble bioactivities, chemokines were verified by molecular cloning efforts. The first ever chemokine discovered was in 1961 and called platelet factor 4 (PF4). It took about three decades after identifying the first chemokine before several new members were discovered that described the common structural feature of the chemokine family ¹⁶.

To date, more than 50 chemokines and 20 chemokine functional receptors have been identified ⁴. Chemokines play a key role in development, angiogenesis and haematopoiesis ¹⁷. They are 8–14 kDa, mostly basic, heparin-binding cytokines and small peptide ligands that play a major role by interacting with cell surface proteins, including integrins, to direct different types of cells toward specific anatomical sites ¹⁸. In general, chemokine receptors have about 340 to 370 amino acids length with a relatively small extracellular acidic N-terminus, plus large numbers of serine and threonine in the short intracellular C-terminal tail ¹⁹. They are classified into four groups (CXC, CX3C, CC and C). This classification is structural rather than functional and is based on the spacing of conserved cysteine residues near the N-terminus which dictate chemokines tertiary structure. C chemokines have only two conserved cysteines, whereas CXC, CC, and CX3C chemokines all have four conserved cysteines ²⁰. The first and second cysteine residues in CXC and CX3C chemokines are separated by one or

three amino acids, whereas the first two cysteines of CC chemokines are adjacent ²¹ (**Figure 1**).

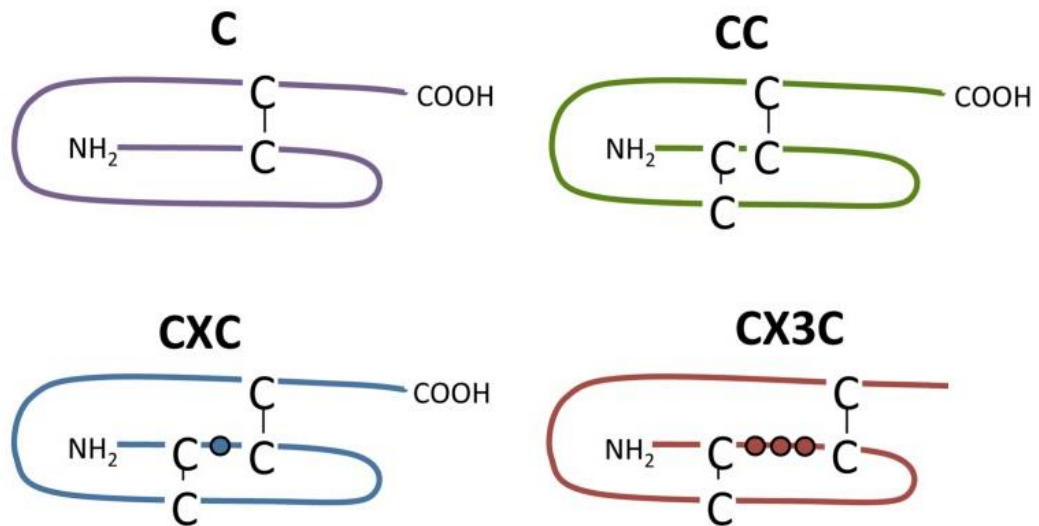


Figure 1 Schematic illustrations of chemokines (C, CC, CXC, CX3C) and chemokine receptors (CR, CCR, CXCR, CX3CR) classification based on the spacing of conserved cysteine residues near the N-terminus ²².

CXC subfamily are further classified into two groups based on the presence or absence of a tripeptide motif glutamic acid–leucine–arginine (ELR) in the N-terminal domain ²⁰. The following chemokines, CXCL1, CXCL2, CXCL3, CXCL5, CXCL6, CXCL7 and CXCL8 are all ELR-positive chemokines.

Figure 2 shows different chemokine receptors and their known chemokine ligands. The NH₂ terminal group plays an important role in attraction between chemokines and neutrophils and also participating in angiogenic characteristic of these chemokines ²³. Chemokines and their receptors are highly interconnected and have complex relationships: a single chemokine recognises and binds to many different receptors, while one chemokine receptor identifies several chemokines ²⁴.

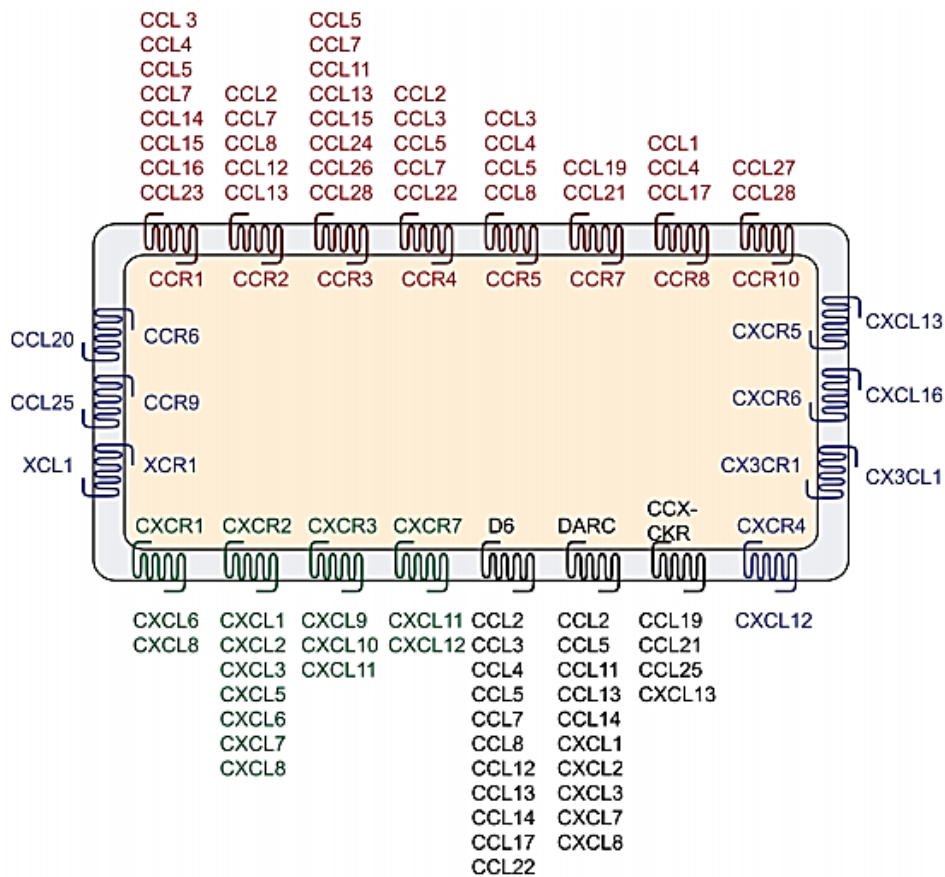


Figure 2 Schematic diagram shows known chemokines and chemokine receptors. There are 10 CCR family subunits and 7 CXCR family subunits as well as XCR1 and CX3CR1 which are known as decoy receptors that only bind to ligand and do not elicit signal transduction ²⁵.

Based on their biological function, chemokines are also classified into homeostatic and inflammatory chemokines. The homeostatic chemokines are normally produced and secreted in many different organs or tissues in the absence of inflammatory stimuli and they have many different functions ²⁶. For example, they orientate the migration of lymphocytes to lymphoid tissues, are involved in immune surveillance, they function to localize T or B cells with antigens in the lymphatic system and they work to create a balance of lymphocytes throughout the lymphatic system ²⁷. Inflammatory chemokines are only produced by cells in the presence of infection or pro-

inflammatory stimuli. The function of inflammatory chemokines is to enhance the trafficking of the white blood cells toward the injured or infected tissues²⁸. Even though these chemokines are classified into two classes, inflammatory and homeostatic, it shouldn't be viewed as absolute. For example, one of the inflammatory chemokines is MCP-1 (CCL2) which, together with its receptor CCR2, is involved in controlling the migration of monocytes and macrophages in an inflammatory setting. However, this chemokine MCP-1 along with its receptor CCR2 have also been shown to have great effect on the development of polarized T helper cell responses, which shows that chemokines in some cases can work as both inflammatory and homeostatic²⁹.

Most known chemokine receptors have the same monomeric structure and share very similar tertiary structures. They consist of chemokine domain at the flexible N terminal region which comes before the first cysteine residue and is responsible for receptor stimulation and activation. The N-terminus is followed by 10- to 20-amino acids that form an N-terminal loop, which is believed to be involved in receptor specificity, followed by a helix that contains 310 residue, a β -sheet with three antiparallel β -strands and a C-terminal, cytoplasmic tail, and an α -helix that set against the β -sheet³⁰. The loops which connect the first β -strand with the second and the second with the third β -strand are similar in structure. They differ only in the chirality of the disulphide bonds. The first connecting loop is called 30s and the second connecting loop is called 40s. The disulphide bond of the CXCR chemokines and the CCR chemokines are identical. The only difference is that the CXCR chemokines contain disulphide bonds in the first cysteine residue with right-

handed chirality. However, the CCR-binding chemokines contain disulphide bonds with left-handed chirality. However, the second disulphide bond is left-handed in the two families¹⁸. Some exceptions are found in the CXCR4 receptor in which both bonds are left-handed. The monomeric structure of the CCR-binding chemokines is identical to the monomeric structure of the CXCR-binding chemokines. The only considerable differences were found in the dimeric and tetrameric structure. The chemokine receptor CCR4 was the first receptor to be identified as dimeric. The amino terminal of CCR-binding chemokine is rigid, not flexible as in case of CXCR-binding chemokines. The rigidity of the N-terminus is a result of forming the dimeric interface which makes the protein elongated with each helix. Other chemokines like CCR2 was discovered to have a tetrameric structure³¹.

1.3. Function of Chemokines in Health and Disease

Recently, chemokines and their receptors have received much attention due to their important role in tumour invasion and metastasis. Initially, they are described because of their correlation with inflammatory response, and by activation of leukocytes in the time of inflammation³². The main function of chemokines is to facilitate the trafficking and migration of leukocytes between circulation and tissues. Chemokines and their receptors are involved in attracting leukocytes from blood circulation to the inflammation site. Chemokine receptors are expressed on the leukocyte cell surface and their ligands are released by the infected or inflamed cells. Chemokines bind to their receptors leading to increasing avidity of integrins, located on the leukocyte cell surface, to their ligands which provide firm attachment of the leukocyte to the endothelium. The interaction between chemokines and their

receptors initiate and activate downstream signalling which is responsible for enhancing leukocytes locomotion and transmigration. Once the leukocytes reach the site of inflammation, they come into contact with the inflamed tissue and eradicate the inflammation. Chemokines play a significant role in both innate and adaptive immunity. They are crucial in attracting different sets of inflammatory cells to the inflammation site depending on whether inflammation is innate or adaptive ³⁶. The innate immune response is enhanced by the recruitment of neutrophil and monocyte cells to the site of inflammation. Other different cells like naive and memory CD4 cells are involved in the adaptive immune response which is induced by different type of chemokines and their receptors ³⁷.

Beside their role as regulators of immune cell circulation, chemokines are involved in many different other physiological and pathological processes such as maintenance of tissue homeostasis, controlling cell multiplication, tissue morphogenesis, angiogenesis, tumorigenesis, and metastasis ³³. They promote angiogenesis during new formation of blood vessels in case of wound healing, tissue repair and embryonic development ³⁴. For example, different chemokine receptors are expressed by platelets, leukocytes and endothelial cells during wound healing. These chemokines have an angiogenic effect on the endothelium to activate neovascularization of the granulation tissue. They also promote angiogenesis in different pathogenic conditions as observed in tumour growth and formation ³⁵. Chemokines and chemokine receptors control angiogenesis in the tumour microenvironment. They promote tumour growth by regulating the formation of vascular networks from surrounding tissue ⁵⁶. Different members of CXC chemokine

receptors family are identified to have regulatory effect on angiogenesis. It has been well studied that CXC chemokines promote blood vessel formation⁵⁴. Chemokines that have positive ELR motif support tumour to form new blood vessels and are called angiogenic factors these include, CXCL1, CXCL2, CXCL3, CXCL5, CXCL6, CXCL7 and CXCL8, which exert an angiogenic effect in prostate cancer. Conversely, chemokines that are ELR negative (ELR⁻), except CXCL12, show inhibitory effects on angiogenesis and block tumour vascularisation in a way that is still not defined³⁹.

Chemokine receptors are highly expressed in certain types of cancer and are involved in cancer growth and progression. Normal tissue such as breast tissue expresses many types of chemokine like, CXCL1, CXCL2, CXCL3, CXCL5, CXCL6, CXCL7 and CXCL8, as well as tumour necrosis factor alpha (TNF α) and Interleukin 6 (IL-6), but at very low concentrations. However, these chemokines are found to be highly expressed during malignancy such as breast cancer, among these are CXCL8, CCL2, CCL4 and CCL5 which are the most studied chemokines³⁸. Following the binding between chemokines and their receptors, a series of multiple intracellular downstream signals are activated and this lead to activation of transcription factors which are responsible for tumour growth and progression. Chemokines also have the ability to guide metastasising tumour cells toward secondary organs by similar process which guide leukocyte toward inflammation site³⁹.

1.4. Chemokines signalling Pathways

In order for circulating white blood cells to reach intercellular sites, they must go through protective barriers such as the endothelium and the epithelium⁴⁰. Transmigration of leucocytes occurs in several steps including a sequential

cascade of pro-inflammatory cytokines, adhesion molecules and chemokines. Pro-inflammatory cytokines, such as TNF- α , IFN- γ and IL-1 β activate endothelium and as a result, chemokines are secreted ⁴¹. Chemokines are molecules that control metastatic spreading of tumour cells to particular sites. They are expressed in the places where the tumour cells reside, whilst their ligands are expressed in distant tissues. For example CCL21 ligand is highly expressed in lymph nodes whilst its receptor CCR7 is highly expressed in breast cancer tissue ⁴².

Chemokines exert their effects through G protein coupled receptors which contain seven transmembranous domains ⁴³. The chemokine first bind to a specific and highly sulphated protein called glycosaminoglycan (GAG). They are linear heterogeneous polysaccharides which are often covalently bound to core proteins that are available on the membrane of cells or within the extracellular matrix ⁴⁴. GAGs family are classified into many members including heparan sulfate which is known to function in association with many different biological processes such as cell adhesion, blood coagulation, angiogenesis, morphogenesis, and regulation of growth factors and cytokine effects ⁴⁵. Heparan sulfate are further classified into many other families based upon their core protein structure. The two major families of the heparan sulfate are called glypicans and syndecans, which are linked to the plasma membrane by a glycosylphosphatidylinositol (GPI) linkage or a transmembrane domain respectively ⁴⁶. These two families interact with several chemokines and enhance their local concentration and help in the formation of a chemokine gradient to guide the migration of cells from the circulation to the site of chemokine production ⁴⁷. Chemokine receptors are

coupled to heterotrimeric $G_{\alpha\beta\gamma}$ proteins. $G_{\alpha\beta\gamma}$ subunits are dissociated following chemokines binding and induce release of G_{α} subunits and $G_{\beta\gamma}$ subunits. A wide variety of enzymes, including phospholipid kinases, lipases and GEFs (guanine nucleotide-exchange factors), are activated following the release of the $G_{\beta\gamma}$ subunits. These enzymes, in turn will activate and regulate other downstream signalling pathways that are important in growth and transcription ⁴⁸. These pathways include: calcium mobilization and the activation of extracellular signal-regulated kinases 1 and 2 (ERK1 and ERK2), p38 mitogen-activated protein kinase (p38 MAPK), phospholipase- $C\beta$, phosphatidylinositol 3-kinase (PI3K), RAS, the RHO family of GTPases, p21-activated kinase (PAK), and NF- κ B which are all involved in enhancing tumour cells growth and metastasis ⁴⁹.

Additionally, the released G_{α} subunits activate cyclic adenosine monophosphate (cAMP) via adenylate cyclase, and tyrosine kinases. Tyrosine kinases are important enzymes that work as mediators in the signal transduction pathway which lead to cell growth, proliferation and migration. They phosphorylate and activate the JAK (Janus kinase) and STAT (signal transduction and activators of transcription) signalling pathway which regulate transcription processes ⁵⁰ (**Figure 3**).

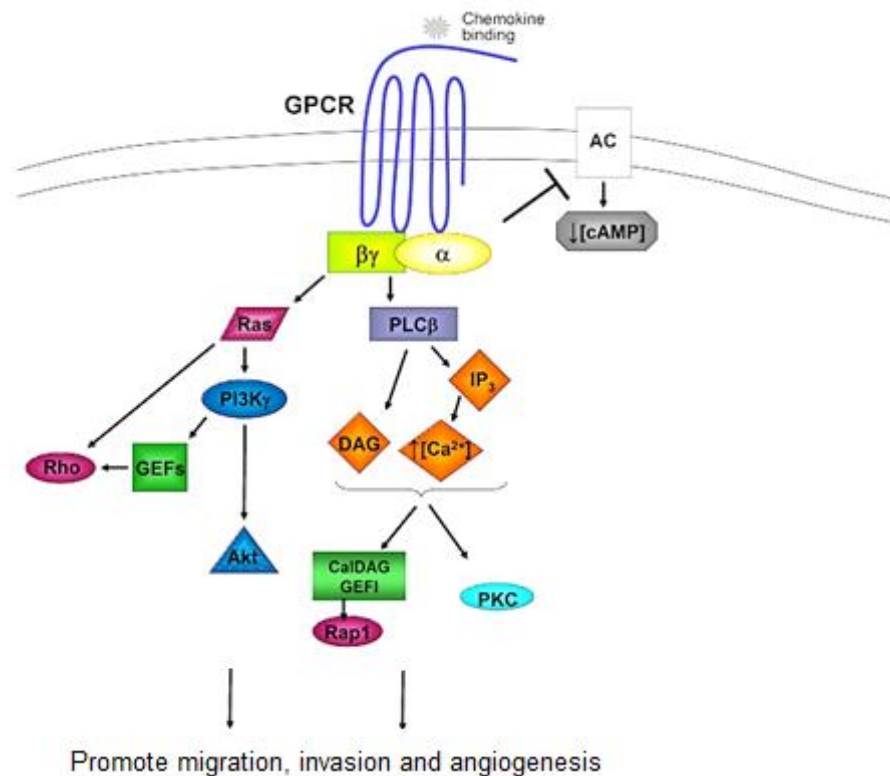


Figure 3 Downstream signalling pathways activation followed by binding between chemokine and its receptor ⁵¹.

The activation and enhancement of cancer cell tumorigenesis and neovascularization by chemokines can be indirect, by modulating leukocyte recruitment. In cancer, soluble factors are produced by epithelial cells and these in turn induce infiltration of CXC chemokines ⁵². The CXC chemokines can attract tumour-associated macrophages (TAMs) and tumour associated neutrophils to the tumour cells. These cells are the source of many other growth factors such as cytokines and enzymes such as proteolytic enzymes that are involved in angiogenesis, growth and migration of tumour cells ⁵³. The tumour microenvironment can also activate chemokines to produce their action. The tumour microenvironment is very rich with cancer associated fibroblasts (CAFs) which promote carcinogenesis by secreting different types

of chemokines that promote and enhance cancer cell growth and metastasis⁵⁴ (Figure 4).

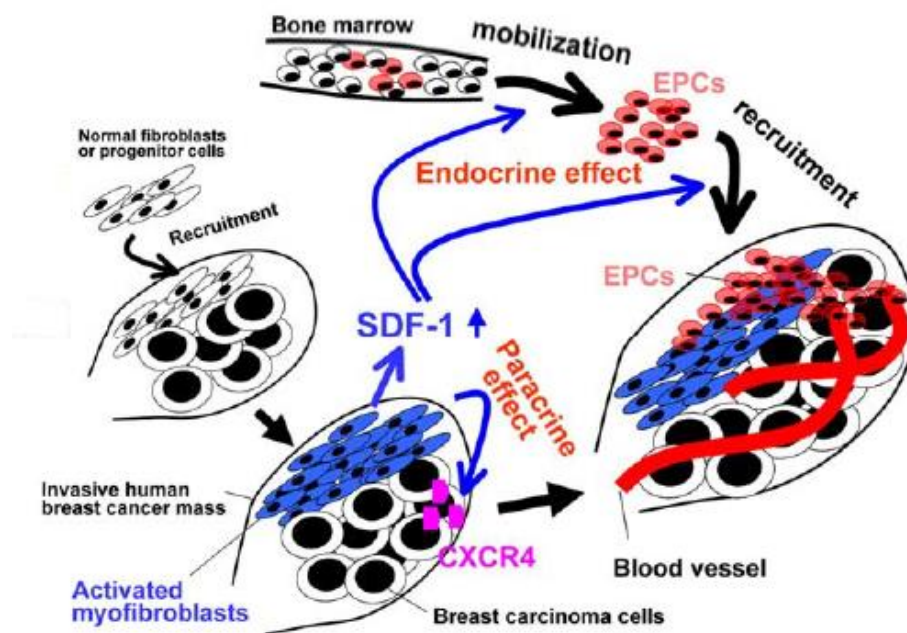


Figure 4 Schematic diagram of Tumour-Promoting Effects initiated by Stromal Fibroblasts within Invasive Human Mammary Carcinomas⁵⁵.

1.5. The CXC Chemokine Receptor Type 4

Recent studies have suggested the importance of the CXCR4 receptor along with CCR7 receptor as major receptors found to be expressed in different types of tumour cells and high level of these receptors were found in breast cancer⁵⁷. Further on in this study, we will investigate the selectivity of the most active compound against both receptors CCR7/CXCR4 using *in vitro* assay which we have called “agarose spot assay”.

Many of the C-X-C chemokines have been identified, including platelet factor 4 (PF4), Interleukin 8 (IL-8) and interferon- γ -inducible protein-10 (IP-10)⁵⁸. A number of the C-X-C chemokines were first detected based on their biological understanding of their ability to be expressed based on a particular

induction ⁵⁹. For instance, based on their melanoma growth stimulatory activity, the growth-related oncogene α , β , and γ (GRO) family of C-X-C chemokines were primarily described ⁶⁰. The chemokine receptor CXCR4 is one of the best studied chemokine receptors, primarily because of its role as a co-receptor for HIV entry and also its ability to mediate metastasis of many different types of cancer ⁶¹. CXCR4 was first cloned by many different laboratories and known as the orphan receptor because its endogenous ligand had not yet been recognised at that time. This receptor was then identified as fusin which was known as the co-receptor with CD4 for inducing HIV-1 virus infection. Then it was characterised as the SDF-1 / CXCL12 receptor and subsequently named CXCR4 ⁶². The chemokine CXCR4 receptor activates migration of human stem cells to bone marrow and peripheral blood cells to lymph nodes by interaction with its ligand, CXCL12 ⁶³. The receptor plays many different roles in B and T lymphocyte and activates and induces thymocyte migration ⁶⁴. It is important in the earliest stages of B-cell lymphopoiesis, colonisation of bone marrow by multipotential haematopoietic cells, cardiac septum formation and in cerebellar neuronal layer formation ⁶⁵.

The activation of the CXCR4 receptor by its ligand leads to a rapid intensification of the affinity of the β 1 integrin for the vascular cell adhesion molecule-1 (VCAM-1) which results in a greater than ten fold adhesion of the leukocyte to the place of inflammation ⁶⁶. Integrins are receptors that attach cells to the extracellular matrix proteins. However, chemokine receptor CXCR4 has many other significant roles in addition to enhancing leukocyte chemotaxis such as embryogenesis, organogenesis, and vasculogenesis ⁶⁷.

CXCR4 is crucial throughout the embryologic development, knocking out the CXCR4 receptor led to several vascular development defects of mice that eventually lead to death ⁶⁸. CXCR4 receptor consists of 352 amino acids which is selectively bind to stromal cell derived factors (SDF-1) ⁶⁹. SDF-1, which is also called CXCL12 was first isolated by Tashiro et al. from a murine bone marrow stromal cell line and was shown to have good inhibitory effect on infection by T-tropic HIV of HeLa-CD4 cells, human cervical epithelial carcinoma. ²⁰. The CXC chemokine SDF-1 was found to encourage the proliferation of bone marrow B-cell progenitors in the presence of interleukin (IL)-7. Its amino acid sequence is notably similar species; nearly 99 % of them are identical between murine and human, assuming that the chemokines may play an essential role in animal physiology ⁷⁰. Lately, there have been studies that revealed the involvement of CXCR4 in cancer growth progression and metastasis ⁴³. Expression of CXCR4 in cancer metastasis appears to be due to Stromal Cell Derived Factor (SDF-1) secretion via stromal cells. SDF-1 binds to CXCR4 receptor and induces migration of cancer cells into distant tissue where tumour cells can grow and metastasis again. High levels of SDF-1 are available in the surrounding stromal cells that are commonly invaded by metastasising cells, like the bones ⁷¹. These high levels of SDF-1 attract CXCR4 which is expressed indifferent types of cancer, including breast cancer, ovarian cancer and melanoma cancer. It has been shown that following CXCR4/SDF-1 interaction, the transmembrane helices of the GPCR is enhanced and activated causing a change in the position on the intracellular part of the receptor, specifically the third intracellular loop, which is connected to the G protein ⁷¹. The G_{α} subunit

exchanges its guanosine diphosphate (GDP) for guanosine triphosphate (GTP) allowing dissociation of G_{α} subunit from $G_{\beta\gamma}$ subunits ⁷². Then phosphoinositide-3 kinase (PI3K) is activated and generates phosphatidylinositol 3, 4, 5-triphosphate (PIP3). PI3K and PIP3 localise in the leading edge of the cell in association with Rac protein ⁷³. These downstream signalling pathways are in turn playing a critical role in promoting cell movement and metastasis (**Figure 5**).

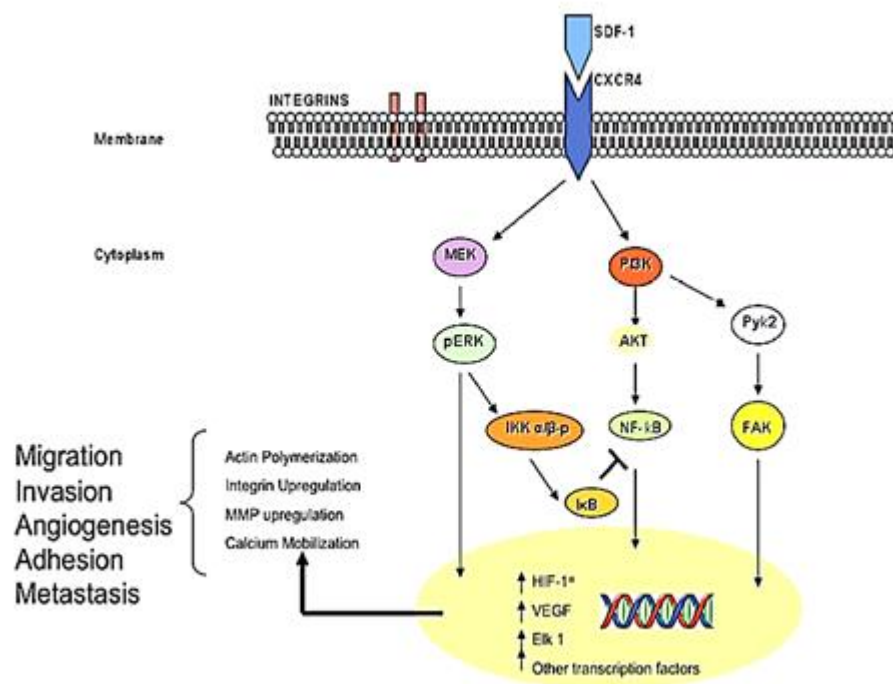


Figure 5 downstream signalling pathways of CXCR4 and its ligand, CXCL12 ⁷⁶.

At the leading edge of the cell, the Rho GTPase plays the main role in activation of myosin, which in turn leads to produce actin–myosin complexes and pulls back the end side of the cell. RhoA belongs to the Ras superfamily of small GTP binding proteins that control configuration of actin stress fibers and focal adhesions ⁷⁴. Migration and metastasis of either normal or malignant stem cells is a multi-step process. CXCR4 enhances a cell ability to migrate, enter blood circulation and arrive at the distant site, which

contains high expression of the CXCR4 ligand, SDF-1. At the end, the migrating cells adhere to the endothelium, invade new tissue and start proliferation ⁷⁵.

1.6. The C-C Chemokine Receptor Type 7

Tumour metastasis resulted from lymphatic and haematogenous dissemination is one of the major causes of death in the world. The new tumour destination can be supported by many different factors, genetic, epigenetic and microenvironment factors ⁷⁷.

Recently, the C-C chemokine receptor model has been suggested to explain the migration of tumour cells to particular organs. They are part of Class I in the rhodopsin-like G-protein coupled receptor (GPCR) superfamily ⁷⁸. The C-C chemokine receptors are small proteins that have been recognised in mammals, but they have also been detected in many other different species like chicken, shark and possibly in nematodes ⁷⁹. Their receptors are characterised by small proteins that induce cytoskeletal reorganisation and adhesion to endothelial cells ⁸⁰. They are small pro-inflammatory receptors which participate in the selective mobilization and migration of leukocytes to their inflammatory location. The significant value of these chemokine receptors has brought considerable attention in recent years, since it has become known that they play major roles in a number of different disease development, such as inflammation, autoimmune disease, infectious diseases (HIV), and lately, cancer (especially in controlling metastasis) ⁸¹. The C-C chemokine system is very important in the growth and maturation of the B-cell lymphocytes, in particular CCL2 (MCP-1). Others such as CCL3 (MIP-1 α), CCL5 (RANTES) and CCR5 were reported to regulate T-cell

growth and progression. They play a major role in the maturation and migration of the dendritic cells (DCs) to tissues and lymph nodes. CCR1, CCR2, CCR5, CCR6 and CCR7 were found to have a critical role in migration of the monocytes toward lymph systems. Following activation of these receptors by their ligands dendritic cells become mature and leave tissues and travel to areas where antigens are available ²⁷. The C-C Chemokine receptors play a major role in ruling the trafficking of many different types of leukocytes to secondary lymphoid organs like peripheral lymph nodes. They control leukocytes cellular composition, maturation, and migration ⁶⁹. As well as maturation and support of secondary lymphoid organs. They are also associated with many immunological activities for instance the production of thymocytes ⁸² central and peripheral tolerance ⁸³.

The C-C chemokine receptor type 7 is a protein that belongs to the C-C chemokine receptors and normally consists of 340–370 amino acids. It is found in many different places throughout the human body in plasma membrane. The seven transmembrane helical domain cross the cellular membrane inside and outside. The N-terminus is located in the extracellular domain while the C-terminus is located in the intracellular region ⁸⁴. The intracellular terminus is enriched with the multiple serine and threonine amino acids which become phosphorylated upon binding of the receptor with the ligands which play a major role in activation of signal transduction pathway that regulates cell growth, proliferation and migration. The extracellular region consists of highly conserved cysteine residue which upon activation upon binding with ligand forms disulphide bridges that connect N-terminal with the extracellular loops and making the receptor conformation ⁸⁵.

The only known ligands for CCR7 receptor are, CCL19 and CCL21. CCL21 and CCL19/ELC are small cytokines which trigger their effect by binding to CCR7 receptor located on the cell surface. Their main function is in the migration of cancer cells to secondary lymphoid organs ⁸⁶. They are originated by stroma cells inside the T cell zone of lymph node cortex ⁸⁶. CCL21 is distinct from CCL19 in term of C-terminal tail. CCL21 consists of a uniquely long C terminal tail that has 32 amino acids, 12 of those are basic residues which permit strong binding to glycosaminoglycan and other molecules ⁸⁷. CCL21 is small chemokine located in human chromosome 9 and known as exodus-2, secondary lymphoid-tissue chemokine (SLC) and 6Ckine because of the six conserved cysteine amino acids. The C-C motif chemokine 19 is small protein also located in the chromosome 9 and known as EB11 ligand chemokine (ELC) ⁸⁸.

1.6.1. Expression and activation of CCR7 and its ligands.

CCR7 receptor is expressed in many different cells but exclusively in mature and semi mature dendritic cells (DCs) ⁸². Resting and inactivated dendritic cells don't express CCR7 until they become activated upon tissue injuries or activation by cytokines such as tumour necrotic factors TNF. Other cells that mainly express CCR7, are naive and central memory T cells, CD4, CD25, T regulatory cells and many other cells ⁸⁹. The CCR7 ligands, CCL19 and CCL21, are together expressed on the high endothelial venules (HEVs) which are post-capillary venules available in lymph nodes that enable lymphocytes to extravasate from blood toward lymph nodes., aggregated lymphoid nodules, fibroblastic reticular cells, stromal cells in T-cell areas of

LNs, thymus ⁹⁰, spleen ⁶⁹ and follicular dendritic cells which make the channels that direct T-cell movement in the lymphatic nodes.

Many studies have been conducted in order to understand the underlying mechanisms of how C-C chemokine receptor type 7 signalling could manage leukocyte propulsion and migration. The chemokine receptor CCR7 plays an important role in Dendritic cells (DCs) and lymphocytes trafficking and homeostasis ⁹¹. The CCR7 receptor is highly expressed in DCs and lymphocytes. The chemotactic migration is controlled by G protein-coupled receptors like CCR7 that initiates and stimulates downstream signalling of mitogen-activated protein kinases (MAPKs). In response to CCL19 and CCL21 binding, MAPKs p38, extracellular signal regulated kinase 1/2 (ERK1/2), and c-Jun N-terminal kinase (JNK) play major and significant part in CCR7-dependent travelling. Furthermore, the actin cytoskeleton is fundamental in chemotaxis organization. The adjustment of actin is organized by Rho guanosine triphosphatases and their downstream signalling, including serine/ threonine kinase Rho-associated kinase (ROCK) ¹⁰³. According to Riol-Blanco ⁹⁸ CCR7 downstream signalling stimulates the mitogen activated protein kinase signalling module which starts to initiate trafficking, while the speed of leukocytes migration is controlled by Rho-cofilin signalling axis.

The travelling and migration of naive T cells toward peripheral lymph nodes from the blood stream consists of multiple steps. Starting from tethering and rotating, CC-chemokine receptor 7 (CCR7) - mediated activation, stopping and trans-endothelial migration ⁹³. Binding of the CCR7 ligands through their receptor leads leukocytes to go from rotation stage to arrest stage on the

surface of endothelial cells. The initial step involves attachment of lymphocyte L-selectin to peripheral node addressins (PNAD), which are collections of sialomucins with sialyl-LewisX-linked group that exist on high endothelial venules (HEVs) ⁹⁴. As a result of this attachment of T cells to HEVs, cells are rotated to make CCR7 receptor available for the ligands. Next, the glycosaminoglycan (GAGs) on the luminal surface of HEVs immobilize CCL21 and CCL19 which make it available for binding to the rotating lymphocytes. Following this stage the integrins, which are transmembrane receptors, become active and re-allocated to lead the lymphocyte trans-endothelial migration. The conformational changes of $\alpha_1\beta_2$ -integrins subunit on lymphocytes permit strong binding to it's ligands, intercellular adhesion molecule 1 (ICAM1) and ICAM2. Also $\alpha_4\beta_7$ -integrins subunit binds to it's ligand, mucosal addressin cell-adhesion molecule 1 (MAdCAM) that is expressed on the surface of HEVs which finally lead the lymphocytes to perform lateral locomotion on the endothelial surface followed by trans-endothelial migration (**Figure 6**) ⁹².

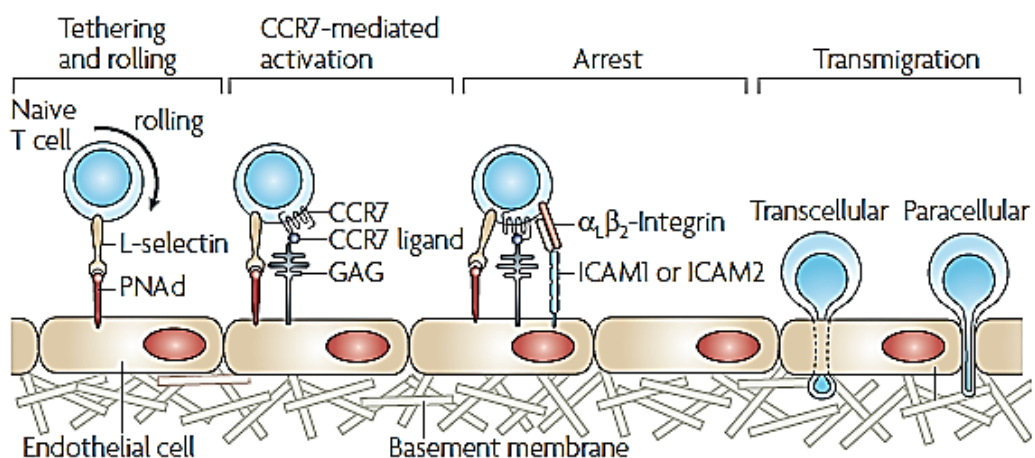


Figure 6 Process of lymphocyte migration to lymph nodes ⁹².

The CCR7 receptor and its ligands, CCL21 and CCL19, plays a critical role not only in homing cells to distant organs, but also work to mediate effects on B lymphocytes during inflammation ⁹⁴. They play very essential roles in many different immunological regulations which are carried out through the process of immune response like, production of thymocytes ⁹⁵.

The CCR7 receptor exerts its effect through its ligands, but the effect may vary based on the type of ligand itself. The CCL21 ligand appears to have higher affinity to bind with its receptor than CCL19. This affinity is up to 10 fold higher than CCL19 which makes the CCL21 a better candidate to produce an effect and form greater immobilized chemokine gradient ⁹⁶. The different binding among the two ligands may also have a significant influence on the location of lymphocytes and DCs in the LN and spleen tissue microenvironment. The CCL19 is a very soluble ligand, while CCL21 stays membrane-bound due to the binding domain of the glycosaminoglycan. Because of differences between the two ligands, CCL21 and CCL19, they induce varied response although they act through the same receptor ⁸².

They have special correlation to the G-proteins coupled receptor kinase (GRK)/ β -arrestin system and therefore differentially phosphorylate CCR7 (GRK)/ β -arrestins are a small family of proteins that desensitize receptor to its ligand. Following binding between CCR7 receptor and its ligands, the receptor becomes active and simultaneously activates G proteins and arrestin-dependent signalling pathways via different biochemical steps. Receptor activation leads to dissociation of heterotrimeric G proteins into free G_{α} and G_{β} subunits and undergoes phosphorylation by G protein-coupled receptor kinases (GRKs), and this boosts the binding of β -arrestins ⁹⁷.

CCL19 but not CCL21 induced strong phosphorylation, β -arrestin-2 recruitment, and CCR7 desensitisation ⁹⁹. CCL19 initiates powerful CCR7 phosphorylation and β -arrestin2 mobilisation, which is stimulated by both GRK3 and GRK6 while CCL21 stimulates GRK6 alone. The differences between the two activations lead to the distinctive ability of CCR7 ligands to stimulate clathrin-dependent receptor endocytosis (**Figure 7**).

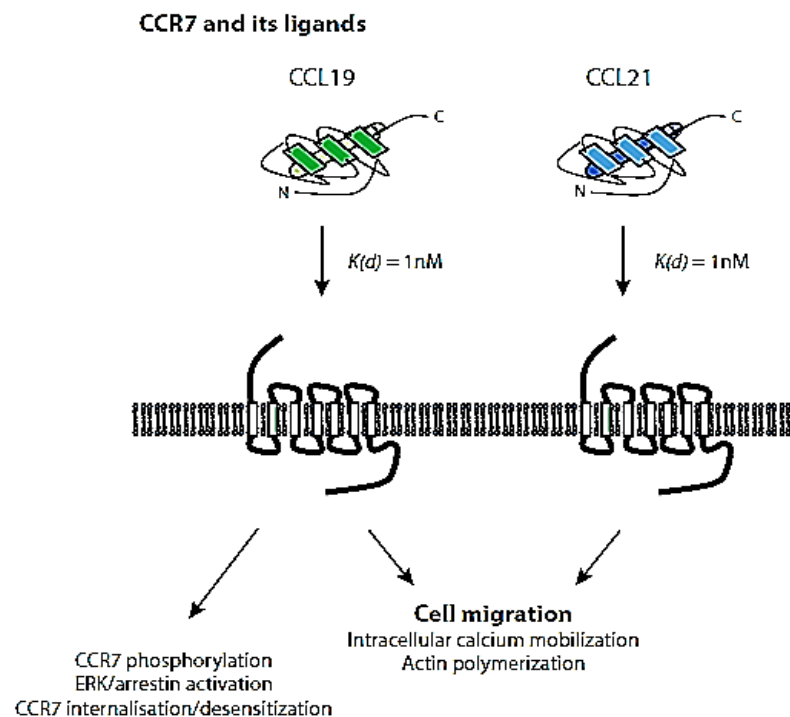


Figure 7. Graphical interaction between CCR7/CCL19/CCL21. CCL19 and not CCL21 induces CCR7 receptor desensitisation ¹⁰⁰.

However, these ligands are both able to signal through GRK6 and β -arrestin2 to ERK kinases ¹⁰¹. One hypothesis described the differences in response to phosphorylation, β -arrestin-2 recruitment, and CCR7 desensitisation are because CCL21 is unable to recognise these cells, because of the active role of the CCL21 in supporting trafficking and migration of the CCR7 into lymphatic vessels in contrast to CCL19 which is produced locally in the T cells ¹⁰².

1.6.2. Cancer and CCR7 expression

Recent studies have shown the ability of the CCR7 receptor to play a major role in cancer progression and metastasis. There are a lot of investigations where researchers have looked into the correlation between high expression of CCR7 receptor and cancer progression and metastasis. In 2001, Muller ⁴⁰ compared expression of different types of chemokine receptors including CCR7 on patients who were diagnosed with primary and invasive breast cancer. The tissues were collected from both groups and found that CCR7 receptor was highly expressed in invasive breast cancer compared to primary breast cancer using real-time polymerase chain reaction (RT-PCR).. In the same study, the regional lymph node (axillary lymph nodes) tissues from both groups were collected and exhibited stronger CCR7 receptor expression in invasive breast cancer than primary breast cancer. CCR7 receptor plays a crucial role in facilitating and directing tumour cells from breast cancer toward lymph nodes. This is logical since CCR7 receptor is highly expressed in breast cancer tissue and its ligands (CCL21 and CCL19) are highly expressed in the lymphatic vessels which will increase the probability of tumour metastasis ¹⁰⁴. Wiley ¹⁰⁵ have confirmed the correlation between CCR7 receptor tumour expressions and metastasise toward lymph nodes in mouse model through introducing the CCR7 gene into B16 melanoma cells. The expression of CCR7-B16 cells at lymph node region was highly recognized using real-time polymerase chain reaction (RT-PCR). To demonstrate the metastasis of B16-CCR7 cells is mediated through CCL21, the CCR7 receptor was blocked with an anti-CCR7 antibody. The result showed less B16-CCR7 cells expression in the regional lymph nodes

which indicates the CCR7-mediated metastasis was blocked ¹⁰⁵. The underlying mechanism which promotes involvement of CCR7 receptor in cancer cell metastasise to lymph nodes is very similar to leukocyte trafficking. The CCR7 receptor activates and initiates different downstream signalling following interaction with its biological ligands. $G_{\alpha\beta\gamma}$ subunits of the GPCR are dissociated following CCR7 receptor binding and induce release of G_{α} subunits and $G_{\beta\gamma}$ subunits. $G_{\beta\gamma}$ subunit stimulates and activates phospholipase C (PLC) and phosphatidylinositol 3 kinase (PI3K) pathways, while G_{α} subunit activates mitogen-activated protein kinase (MAPK) ¹⁰⁶. The activated pathways in turn prompt intracellular actin polymerization and initiates cell survival and migration (**Figure 8**).

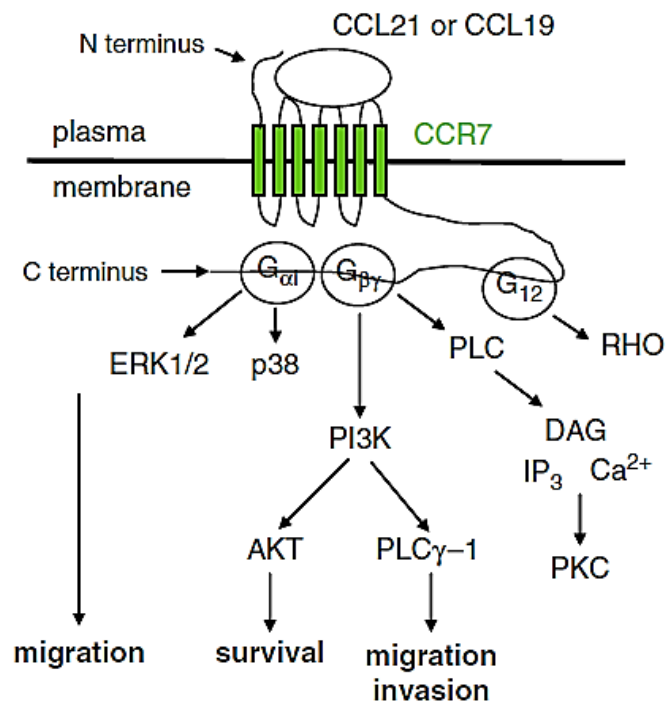


Figure 8 downstream signalling pathways of CCR7 receptor and its ligands ¹⁰⁷.

Sanchez ¹⁰⁸ has shown the effectiveness of CCR7 receptor in stimulation and activation of the intracellular signalling downstream that blocks apoptosis of mature dendritic cells ¹⁰⁸. The activation of the receptor followed by

binding of the CCL21 and CCL19 ligands leads to inactivation and blocking of the well-known apoptotic signal of serum-starved DCs. These signals are due to high phosphatidyl exposure on the membrane, nuclear changes, and loss of mitochondria potential. CCR7 receptors initiate and activate intracellular signals that inhibit apoptosis of DCs, including, phosphatidylinositol 3-kinase/Akt1 (PI3K/Akt1), with a prolonged and persistent activation of Akt1. **Figure 9** describes the use of scanning electron microscopy to highlight the reduction of the apoptotic cells when treated with CCL21 and CCL19 compared to control. The picture shows reduction of the cells that contain blebs or protrusion on the membrane of the cells by almost half in cells which treated with chemokines. Blebs are typically produced during apoptosis which is a physiological process involved in the normal development of tissue homeostasis ¹⁰⁸.

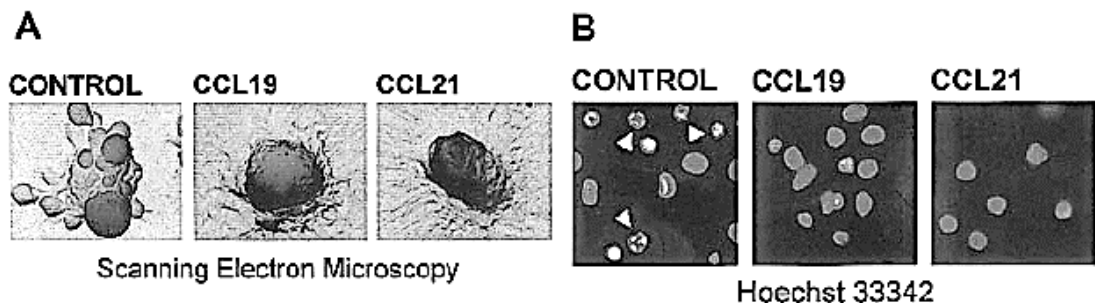


Figure 9 (A) Activation of CCR7 receptor by treating dendritic cells for 6 hours with CCL19 and CCL21 reduced the apoptotic blebs. However control cells showed increase in the apoptotic blebs, (B) Cells were stained with Hoechst 33342 which is used to visualize apoptotic nuclear morphology ¹⁰⁸.

Even though many studies have been conducted and determine many factors that affect the process of cell migration and trafficking, the underlying mechanism of metastasis of cells to lymph nodes is still not fully characterised. There are many different changes that occur inside cells in

order to enable migration or trafficking throughout and to the extracellular barriers, including the change in the cell-cell adhesion and initiation and activation of a number of proteolytic enzymes ¹⁰⁸.

1.6.3. Molecular basis of interaction between CCR7 and its ligands

The extracellular portion of CCR7 is believed to be responsible for binding to heparan and other extracellular molecules which interact with the receptor but more importantly as a “beacon” to initially seek and bind to the chemokine protein which result in conformational changes of the receptor internal loops that initiate the signal. . Although, there is significant promiscuity between chemokines and chemokine receptors, CCL21 and CCL19 bind only to CCR7. In turn, the receptor itself has no other recognized endogenous activating ligands ¹⁰⁹. It has been mentioned earlier in this chapter that both ligands exert their effect on CCR7 receptor differently.. In order to highlight the structure differences between two ligands, an alignment was made using an online resource, the clustalW2 algorithm. The alignment shown between CCL21 and CCL19 (**Figure 10**) illustrates the differences in the amino acid sequences. In contrast to CCL19, CCL21 consists of 111 amino acids as a result of the uniquely extended C-terminus tail while CCL19 typically contains 77 residues. This elongated tail at CCL21 C-terminus bind to heparan sulfate glycosaminoglycan (GAG) at the receptor surface hence, making a local concentration of CCL21 chemokine to be presented to the receptor ¹¹⁰. Also, CCL21 contains six cysteine residues compared to the regular four residues which are available in CCL19. Cysteine residues are sterically smaller and much more reactive than other amino acids. They

contain a sulphur atom which are very important in making covalent bond with cysteines. Hence, availability of more number of cysteine is essential for stabilization of the ligand-receptor binding. In addition to this, the N-terminus which is responsible for binding with the receptor is different between the two ligands (**Figure 10**). As a result of these variations, both ligands bind to the receptor differently and hence the affinity and effect will be different.

```

000585 CCL21_HUMAN   1  SDGGAQCCCLKYSORKIPAKVVRYSYRKQEPSLGCISIPAILFLPRKRSQAEICADPKELWV   60
Q99731 CCL19_HUMAN   1  GTNDAECCCLSVTQKPIPGYIVRNFHYLLIKDGC RVPVAVFTTLR--GROLCAPPDQPWV   58
      .  ***** . : * : * : * : * : * : * : * : * : * : * : * : * : * : * : * : *
000585 CCL21_HUMAN   61  QQLMQHLDKTPSPQKPAQGC RKRDRGASKTGKKKGSKGC RRTERSQTPKGP   111
Q99731 CCL19_HUMAN   59  ERIIQRLQRTSAKMKRRSS-----
      : : : * : * : * : * : * : * : * : * : * : * : * : * : * : * : * : *

```

Figure 10 CCL-19 and CCL-21 Alignments using clustalW2 algorithm

It has been reported that the elimination of the N-terminal of the CCL19 results in a deterioration of binding to the receptor. This impairment is a result of the deletion of the Glu₆ and Asp₇ which play a key role and are responsible for the activation of the receptor and affinity bindings¹¹¹. Ott¹¹² has evaluated the underlying mechanism by which these ligands produce their effects on the CCR7 receptor. The first six amino acids of the CCL19 were successfully replaced with the equivalent residues of the CCL21 in order to measure the tendency of the chimeric ligand to stimulate and activate CCR7. The N-terminal of the CCL21 (SDGGAQ) were substituted with identical N-terminal domain of CCL19 (GTNDAE) and resulted in activation of the CCR7 receptor¹¹². Sasaki¹¹³ investigated the antagonist properties of the deleted N-terminal of the CCL21 ligand. The few modifications in the amino acids at the N terminal are reported to have resulted in significant changes. Truncation of the pyroglutamate residue at the N terminus of the CCL21 results in nearly 50-fold decrease of agonistic

activity on monocytes. Removal of the first two amino acids resulted in nearly entire loss of the activity. However, the activity is recovered when further deletion is obtained ¹¹³. Site-directed mutagenesis studies by Ott ¹¹⁴ have identified two residues in the CCR7 receptor , Lys3.33 (137) and Gln5.42 (227) (the two numbers given for each residue represent the transmembrane domain (TMD) and the number of the residue in the helix respectively) as an important residues for binding with CCL21 ligand, (**Figure 11**). Site-directed mutagenesis is a technique used to create specific, targeted modifications in amino acids. The technique used to generate specific change in the amino acid sequence of the receptor or ligand to understand the significance of specific amino acid in binding. Normally, alanine amino acid is used to replace other amino acids because it is not bulky and chemically inert (unable to make bonds) ¹¹⁴.

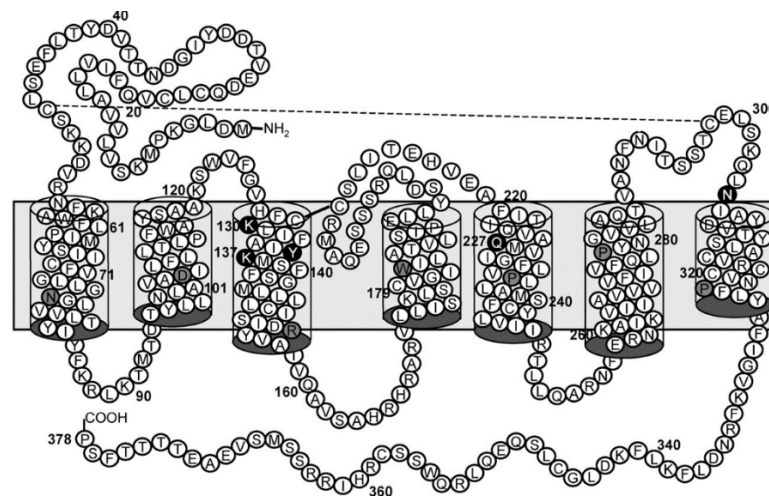


Figure 11 Schematic diagram of CCR-7 receptor shows mutated residues in black colour and most conserved amino acids are shown in grey colour. The residues were replaced with alanine amino acid which is chemically inert. The binding affinity with the ligand of each mutated residue was assessed using binding assay. ¹¹⁴.

Ott ¹¹¹ in a different study also showed the crucial effect of the N terminus as both responsible for the high attraction of the ligand binding and receptor

activity. The side chain of these residues, Asn3, Asp4, and Asp7, are important for high-affinity binding of CCL19 to CCR7, while the acidic amino acids Glu6 and Asp7 were shown to have a significant effect on agonist activity ¹¹¹. Otero ¹¹⁵ have further demonstrated that the Ser/Thr motif at the tip of the intracellular tail of the CCR7 receptor is essential for binding and activation ¹¹⁵. CCL19 and CCL21 are both activators for the CCR7 receptor that promotes the ERK1/2 mitogen-activated protein kinase signalling pathway. CCL19 promote phosphorylation by 4-fold more than CCL21. Site-directed mutagenesis of the CCL19 has been used to determine the residues which are responsible for inducing phosphorylation. Replacing specific residues with alanine, it was shown that Thr-373–376 and Ser-378 are essential for CCL19-receptor phosphorylation, whereas amino acids serine 356, 357, 364, and 365 are crucial for basal receptor phosphorylation by protein kinase C (PKC) ¹¹⁶. CCL21 seems to be found in all interactions with CCR7, which makes it the primary ligand involved in all metastasis of solid tumour to lymph nodes. Love ⁸⁴ solved the solution structure of CCL21 and identified its oligomeric state, and specified CCL21 amino acids putatively participated in binding to the N-terminus of CCR7 using nuclear magnetic resonance spectroscopy (NMR). The figure below shows the solution structure of the residues 8-70 of CCL21 with its unsaturated N-terminus linked by the N-loop, a three-stranded β -sheet, α -helix and unstructured C-terminus (**Figure 12A**). The figure also shows the chemical shifts mapping onto the surface of CCL21 which indicates the regions responsible for CCR7 binding (**Figure 12B**). Chemical shift mapping or perturbation is an experimental technique used to determine the binding affinity site between

ligand and receptor using NMR spectroscopy. Chemical shifts are peaks obtained in NMR due to the change in energy resulted from binding between ligand and receptor in specific region. If there is no binding affinity between ligand and the receptor, there will be no chemical shifts. CCL21 ligand was titrated with CCR7 peptide (responsible for binding with the ligand) and the chemical shifts were monitored by NMR spectroscopy ⁸⁴.

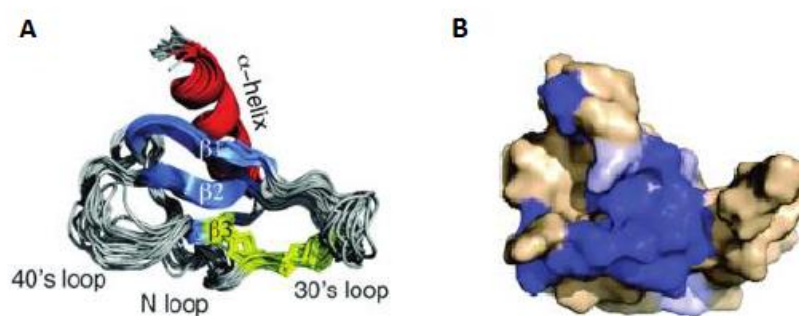


Figure 12 Solution structure of CCL21 using NMR spectroscopy. (A) CCL21 solution structures (B) Chemical shift mapping onto the surface of CCL21 which suggests binding site responsible for binding with the CCR7 receptor. Dark blue indicates region with high chemical shift perturbations or high binding affinity to the receptor while regions in light blue and white have less binding affinity and no binding affinity to the receptor respectively. ⁸⁴.

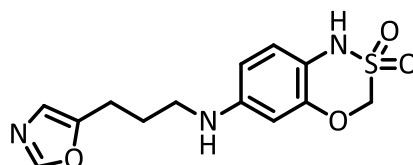
1.6.4. Discovery of a lead CCR7 receptor antagonist.

In the early 80's, cytokines were isolated which allowed immune cells to communicate between each other and destroy pathogens. They have been identified and validated as potentially drugable and can be antagonised by small molecules ¹¹⁷. Although cytokines such as interleukin 1 (IL-1) and tumour necrotic factor (TNF) as proinflammatory were first defined as good targets, few molecules have been discovered which have the ability to block these receptors ¹¹⁷. Also the number of small molecules that were detected

as blockers for the growth factors in the past was very few. Most of these antagonists which block pro inflammatory cytokines are peptide based antagonist or monoclonal antibodies. This gave the perception that the chance of discovering a small molecule that antagonises chemokine receptors was very slight. However, nowadays the vast majority of the companies and academics undertake research on chemokines focus on small molecules that inhibit or block these receptors. Because the chemokine receptors belong to the G-protein-coupled receptors (GPCRs), they possess the best targets for therapeutic interference amongst the other receptors. The GPCRs are widely spread throughout the human body and are involved in many different types of diseases. Chemokines are very important targets for drug development due to their roles in different disease like functions in acute and chronic inflammation, HIV and lately in cancer. Fortunately, in the past six years the number of patents for small molecule inhibitors has increased quickly due to involvement of these chemokines in HIV progression. The majority of these antagonists contain piperidine, piperazine quaternary nitrogen or bicyclam groups with two or more aromatic rings ¹¹⁸. The similarity in the chemokine inhibitor structures could be a result of the availability of the highly conserved binding pocket within the transmembrane region. The structure similarity of the antagonists gives a clear indication of the structure similarity of chemokine receptors. Because chemokine receptors are GPCRs, they are closely related to other classes of GPCRs. Some of these blockers might cross-react with several biogenic amine receptors. For instance a small molecule piperazine based structure which inhibits chemokine receptor CCR5 is found to cross-react with muscarinic

acetylcholine receptors. Also, The CCR2 spiropiperidine based structure antagonist was detected to have an effect on 5-HT_{1A} receptors. Blocking the CCR7 receptor with antagonist can inhibit migration of cancer cells to their common destination ⁴⁰. Glycosaminoglycan (GAG) is believed to be the most important target that plays an important role in the spatial distribution of chemokines. The binding site of GAG with chemokine ligands is called heparan sulfate which make the chemokine ligands available for the CCR7 receptor. Even though chemokines have high structural similarity with each other, there are differences in the specific GAG binding sites between chemokines that are not conserved amongst the classes. Thus interfering with the crucial interaction, between chemokines and GAGs, is maybe one intervention point for inhibition of the system ¹¹⁹. The other possible strategy that inhibits the chemokines effect is by targeting chemokine receptor complex downstream signalling which leads to cell survival and migration ¹²⁰. In order to identify a CCR7 receptor antagonist, the structure of the receptor has first to be modelled using a homology modelling. The accuracy of the structural characterization of the chemokine receptor CCR7 is essential to understand and determine the binding of the receptor with its ligand. Homology modelling is a technique used in this study to create 3D structure of the human chemokine receptor CCR7 based on availability of 3D model of similar protein structure, this work was carried out with help from Professor Colin Fishwick at the University of Leeds. The homology model of CCR7 receptor was built from bovine rhodopsin GPCR-7TM. The CCR7 primary sequence was initially aligned to the bovine rhodopsin sequence (PDB code 1U19) and CXCR4 both of which belong to the GPCRs family of proteins.

Each homology model was subjected to Maybridge screening library, and the top-scored ligands were chosen for *in vitro* screening. The top selected hits obtained from the modelling were tested by using calcium flux assay, this work was conducted at the University of Bradford by Dr Victoria Vinader. However, none of these molecules were active against CCR7 receptor. At this stage, survey of the literature was undertaken and we found a patent, in which a method for assessing ligand affinity for the CCR7 receptor was revealed ¹²¹. The patent described methods for screening for therapeutic compounds valuable in the treatment of CCL21 mediated and CCR7 receptor mediated disorders. To demonstrate the application of the method, the patent describes two compounds which bind to the CCR7 receptor and prevent binding of CCL21 ligand. One of these, compound **1** (ICT5189) was amenable to chemical synthesis (**Figure 13**).



Lead compound **1** (ICT5189)

Figure 13 lead compound **1** (ICT5189) as described in the literature

The method described in the patent does not reveal if compound **1** is an agonist or an antagonist, so we decided to prepare this compound and assess its activity in a calcium flux assay. As will be discussed shortly, the molecule was successfully synthesised (see chapter 2) and was shown to be an antagonist of CCR7. Hence, the molecule was taken as a lead compound and different analogues were then synthesised to study the structure activity relationship of the desired molecule.

1.7. Aims and Objectives

As discussed in this section the CCR7 receptor is involved in promoting and regulating cancer cells metastasis toward lymph nodes. Therefore the aim of this project is to prepare a novel CCR7 chemokine receptor antagonist using ICT5189 as a lead to reduce cancer progression and metastasis.

This will be achieved as follows:

1. Synthesis of novel analogues of ICT5189, a compound identified as having CCR7-binding potential.
2. Characterisation of CCR7 expression in a panel of cell lines to identify a suitable cell line for antagonist screening using immunodetection techniques such as Western blot and flow cytometry
3. Development & validation of assays to evaluate the novel compounds including calcium flux assay and under agarose assay.
4. utilisation of the assays developed & validated in 3 to screen for CCR7 antagonistic activity of the novel analogues & develop improved analogues based on SAR information

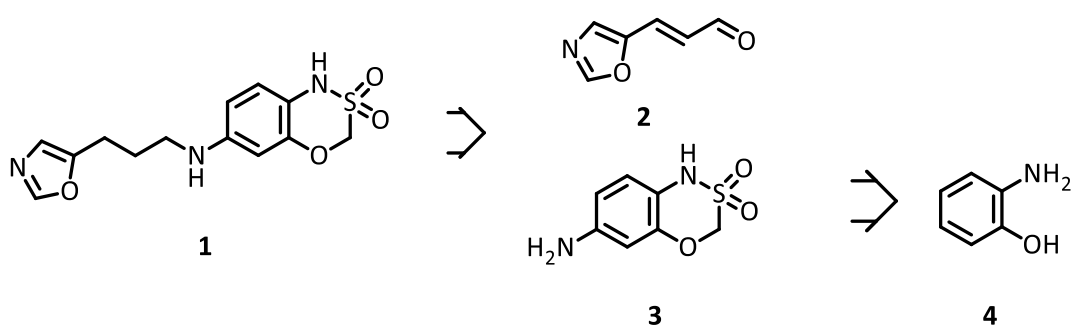
2. Chapter 2: Synthesis of CCR7 receptor antagonists.

2.1. Introduction

We described in chapter 1 the origins of compound **1**, ICT5189, as a lead. To confirm that compound **1** not only binds to the receptor CCR7 but that it can also antagonise it, we set out to synthesize and pharmacologically characterise it. Note that the lead optimisation described in this chapter involves synthesis of the compounds followed by determining the value of antagonist potency using a calcium flux assay. These values inform the next cycle of synthesis and so in this chapter, IC_{50} values for antagonist activity of compounds are given. However, methods for biological testing and the related discussions are given in chapter 3.

2.2. Synthesis of compound **1**, ICT5189.

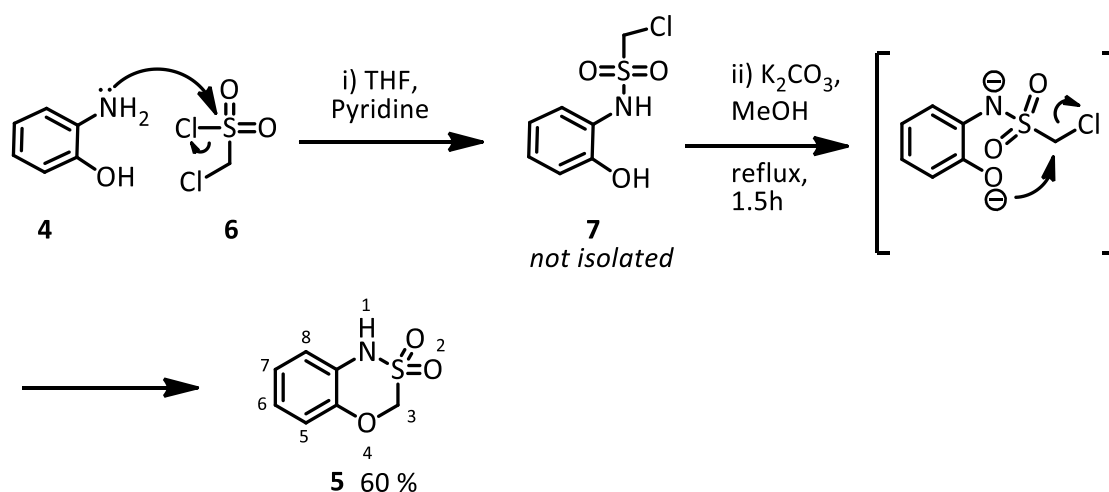
A retrosynthesis of the lead compound **1** is proposed below (**Scheme 1**). We envisaged that compound **1** can be synthesised from reductive amination between aldehyde **2** and 6-amino-1H-benzo[e][1,3,4]oxathiazine 2,2-dioxide, **3**, which in turn can be prepared from 2-aminophenol, **4**.



Scheme 1 Proposed retrosynthesis of compound **1**

2.2.1. Synthesis of compound 3, ICT5888

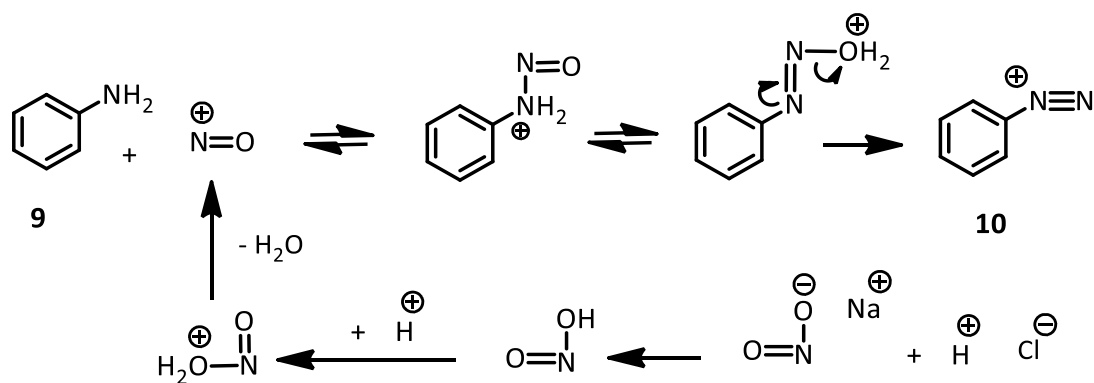
The preparative work begun with the synthesis of compound **5**, ICT13001, using a route described in the literature,¹²¹ by condensation of 2-aminophenol **4** with chloromethanesulfonyl chloride **6** (**Scheme 2**). The electrophilic sulfonyl group is attacked by the lone pair of electrons on the nitrogen atom to initially form intermediate sulphonamide **7**. The second step was a cyclisation that involves the addition of strong base, K_2CO_3 , in methanol. Under these conditions, the hydroxyl group was deprotonated and the corresponding nucleophilic phenoxide anion displaces the chloride to afford compound **5** in 60% yield.



Scheme 2 condensation and cyclisation step mechanism

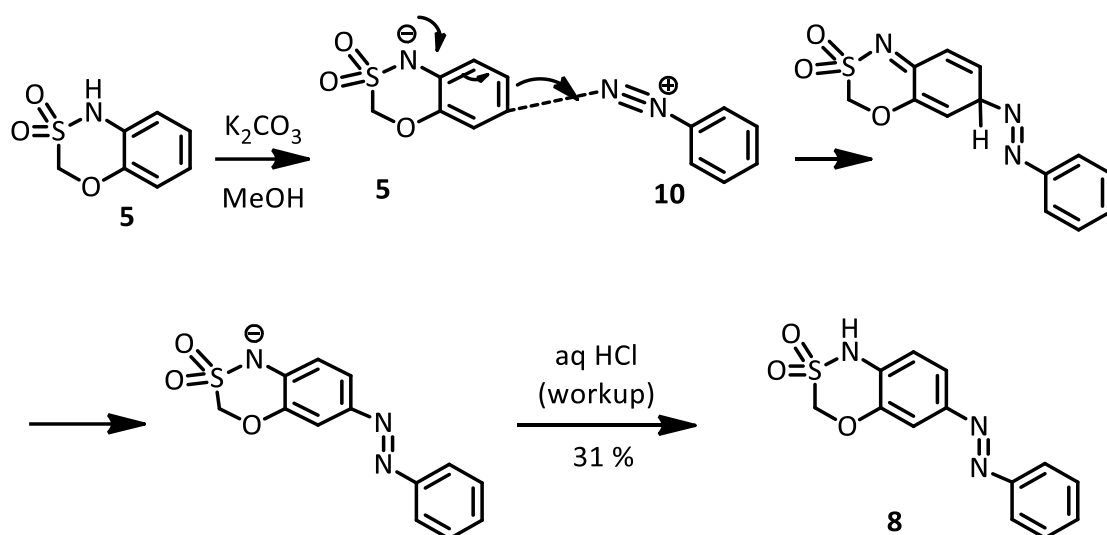
The product from this reaction was purified by flash column chromatography on silica gel and analysed by mass spectroscopy to confirm cyclisation and displacement of the chlorine atom. Proton and carbon NMR was also used to confirm molecular structure. The two single peaks at 10.59 ppm and 5.20 ppm in proton NMR represent hydrogen atoms in NH and CH_2 respectively. Hydrogen atom of the NH is de-shielded and its resonance frequency rose to

give signal appearing downfield. The de-shielding effect of hydrogen atom is a result of the sulfonyl group which has high electronegativity. Chemical shifts obtained centring at 6.83 ppm and 7.07 ppm correspond to aromatic hydrogen atoms at positions 6 and 7, and positions 5 and 8 respectively. Also ^{13}C NMR shifts at 141.91 ppm, 127.09 ppm and 76.39 are assigned for quaternary ArC-O, ArC-N, and CH_2 respectively. Chemical shifts at 123.5 ppm are assigned for C-6 and C-8, and shifts at 119.9 ppm and 118.1 ppm are assigned for C-5 and C-7 respectively. The proton and ^{13}C data were in agreement with previously published data ¹²². The compound was sent to mass spectroscopy for characterization and gave a peak at 186.83 which represent the $[\text{M}+\text{H}]^+$ ion. The next step in the preparation was to form azo compound **8**, ICT13003 using aniline **9** as a building block. This involves a coupling between diazonium salt **10** and aromatic sulphonamide **5**. To form the diazonium salt, concentrated hydrochloric acid was added dropwise to the stirred solution of aniline **9** and sodium nitrite in water (**Scheme 3**). The diazonium ion was formed as a result of the reaction between nitrous acid, (generated *in situ* from hydrochloric acid and sodium nitrite), and aniline, according to the mechanism shown in **Scheme 3**.



Scheme 3 mechanism of diazonium salt formation

The resulting diazonium salt **10** is used immediately for the next reaction due to its instability. Diazonium salts tend to be unstable in presence of water and temperatures higher than 10 °C, and decompose to form nitrogen gas. The azo compound **8** was formed by adding freshly prepared solution of diazonium salt **10** to a solution of compound **5** and K₂CO₃ in MeOH. The mixture was filtered and the filtrate was purified by chromatography on silica gel to give compound **8** in 31 % yield as a dark red-brown solid (**Scheme 4**).

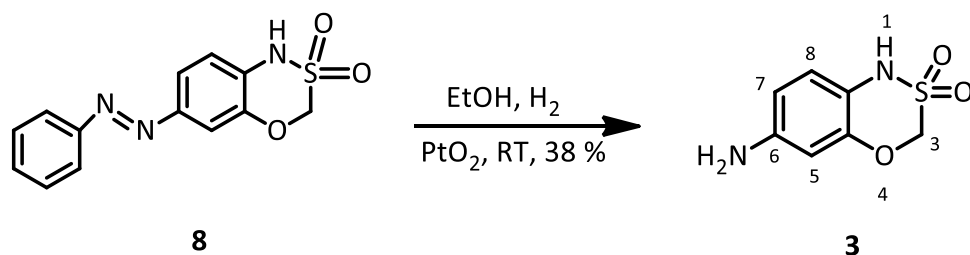


Scheme 4 Mechanism of compound **8** formation

As shown in the proposed mechanism (**Scheme 4**), the azo bond is formed on the carbon atom which is in the *para* position to the NH atom, as this is the position favoured electronically under reaction conditions (*vide infra*). Presumably, whilst sulfonylamino group is not as electron donating as the oxygen atom, under basic reaction conditions it is deprotonated so it becomes more electron donating than oxygen. Hence the electrophilic substitution occurs at the position *para* to the nitrogen rather than the

position *para* to oxygen. The newly formed azo compound was submitted for the proton and carbon NMR and mass spectrum to confirm its formation. Peak obtained at ^1H NMR δ 11.28 ppm represent the hydrogen atom at NH and peaks at 7.86 ppm, 7.59 ppm represent hydrogen atom at phenyldiazene. Chemical shifts obtained centring at 7.67 ppm, 7.56 ppm and 7.00 ppm correspond to aromatic hydrogen atoms at positions 7, 8 and 5 respectively. Also ^{13}C NMR shifts at 147.1 ppm 129.9 ppm 79.4 ppm are assigned for quaternary ArC-O, ArC-N, and CH_2 respectively. ^{13}C NMR shifts at 143.5 ppm and 117.8 ppm are assigned to C-6 and C-7 respectively, and shifts at 119.0 ppm and 108.1 ppm are assigned for C-8 and C-5 respectively. However, because the signals in the aromatic region of the NMR spectra were complex, it was not possible at this stage to confirm the position of the azo substitution.

The last step in the synthesis of compound **3** was catalytic hydrogenation of the azo compound **8**, to form the required aromatic amine **3**. The reaction was carried out in ethanol with platinum oxide added as a catalyst. The reaction mixture was stirred overnight under hydrogen gas. The resulting product was purified by flash column chromatography on silica gel to afford compound **3** in 38 % as a light brown solid (**Scheme 5**).



Scheme 5 Last step in synthesising compound **3**

The newly installed NH₂ was identified using infra-red spectrum with two bands appeared around 3394 cm⁻¹ and 3345 cm⁻¹. The NH₂ group was also identified by proton NMR as a broad peak at around 5.07 ppm. At this stage, we wanted to prove that the substitution of amine was at position C-6 as proposed in **Scheme 4**, and not on C-7. To illustrate successful synthesis of the desired compound, we used cambridgesoft's ChemDraw ultra v 12 software to simulate the chemical shifts of both possible substitutions and compare it to the NMR spectrum of the compound we obtained. **Figure 14** below shows three different spectra. The two spectra to the right side of the picture are predicted by chemdraw software which represent *para* (C-6) and *meta* (C-7) substitution of the amine group. The spectrum at the left side represent the aromatic region of compound **3**. In the case of substitution at C-6, the predicted proton chemical shift of H-5 and H-7 appeared upfield and close together (5.94 and 5.93 ppm), and proton chemical shifts of H-8 appeared downfield (6.27 ppm) due to the effect of amine substitution, which is an electron donating group. Although the actual values of chemical shift are different, this pattern closely resembles the actual chemical shifts in compound **3** where proton chemical shift of H-5 and H-7 appeared upfield and close together (6.22 and 6.26 ppm), and proton chemical shifts of H-8 appeared downfield (6.54 ppm) In contrast, when amine group is substituted at C-7 position, predicted proton chemical shifts of H-5, H-6 and H-8 are all different.

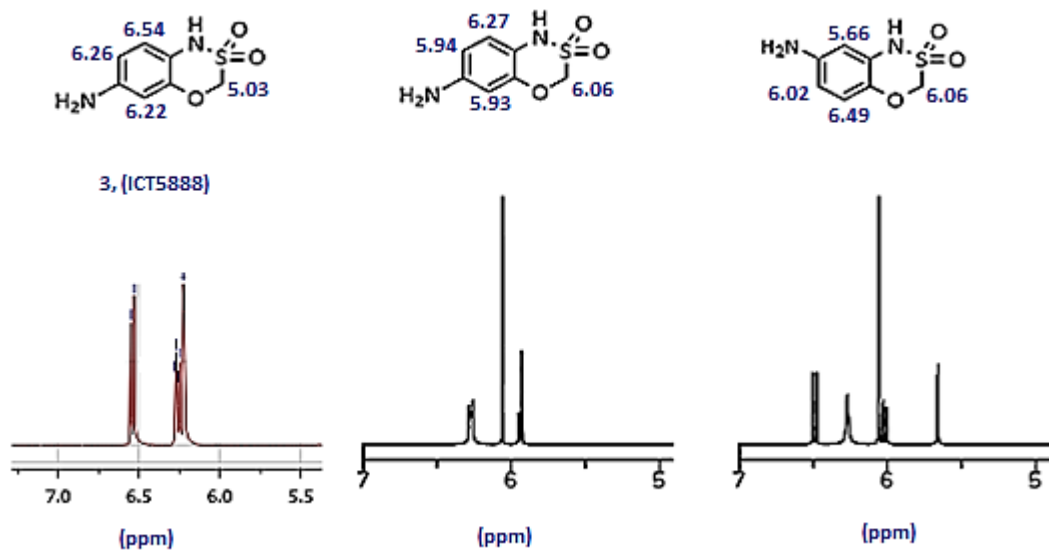
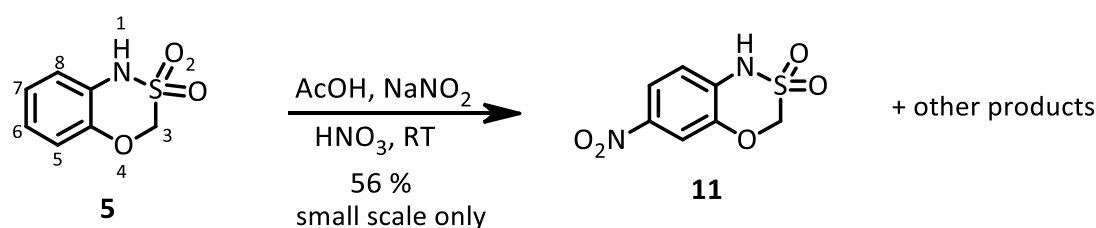


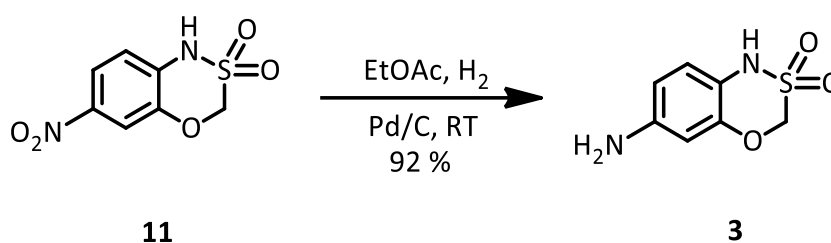
Figure 14 comparison between aromatic proton chemical shifts of compound **3**, and simulated spectra of 6- and 7-substituted amino 1H-benzo[e][1,3,4]oxathiazine 2,2-dioxide.

The synthetic route to compound **3** using the literature process was successful, although difficulties were experienced in making the azo compound **8**, as it is not stable. In addition to this, extensive purification was required during the synthesis and yields in general were not satisfactory. Therefore, we devised an alternative synthesis of compound **3** by the direct nitration of compound **5** to yield compound **11**, ICT13031 (**Scheme 6**).



Scheme 6 Synthesis of compound **3** in different pathway.

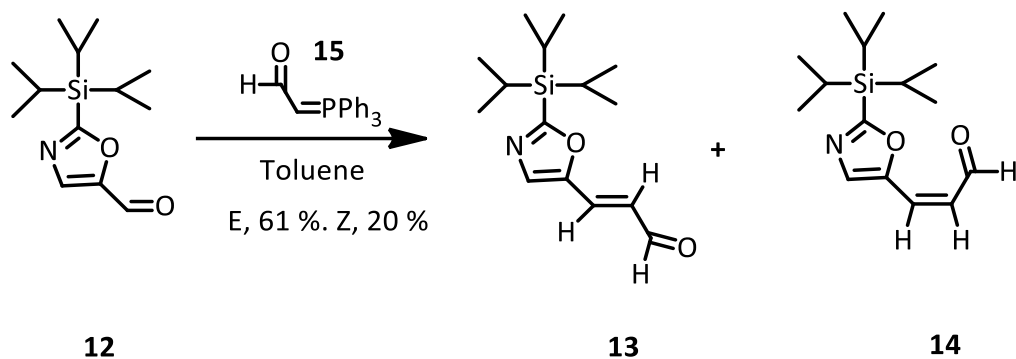
The required nitro-compound was successfully made by the addition of a mixture of glacial acetic acid and one equivalent of 70% nitric acid to a solution of compound **5** and sodium nitrite dissolved in glacial acetic acid. The amount of nitric acid was found to be critical, as any excess of the nitric acid will afford a compound with two nitro groups at *para* positions to NH and O atoms (C-6 and C-7). The nitration step also yielded an isomer of **11** where the nitro was substituted at C-7 (the *para* position to oxygen), nevertheless, the desired compound **11** could be isolated by chromatography in sufficient quantity for us to complete the synthesis of compound **3**. Catalytic amount of palladium on charcoal was added to the compound **11**, in ethyl acetate under hydrogen atmosphere to afford the desired amino-compound **3** cleanly and in good yield (**Scheme 7**).



Scheme 7 Reduction of the compound **11** to give compound **3**.

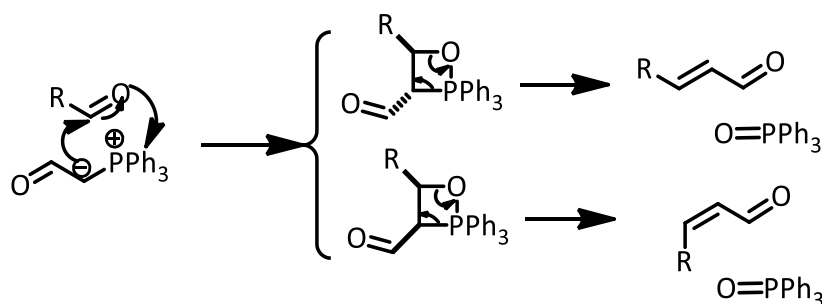
2.2.2. Synthesis of Aldehyde, **2**.

With compound **3** at hand, we set out to prepare aldehyde **2**. The 2-position of oxazole is chemically sensitive, so we decided to start from commercially available protected aldehyde **12** as starting material and react this aldehyde with a Wittig reagent, (**Scheme 8**).



Scheme 8 synthesis of compounds **13** and **14**.

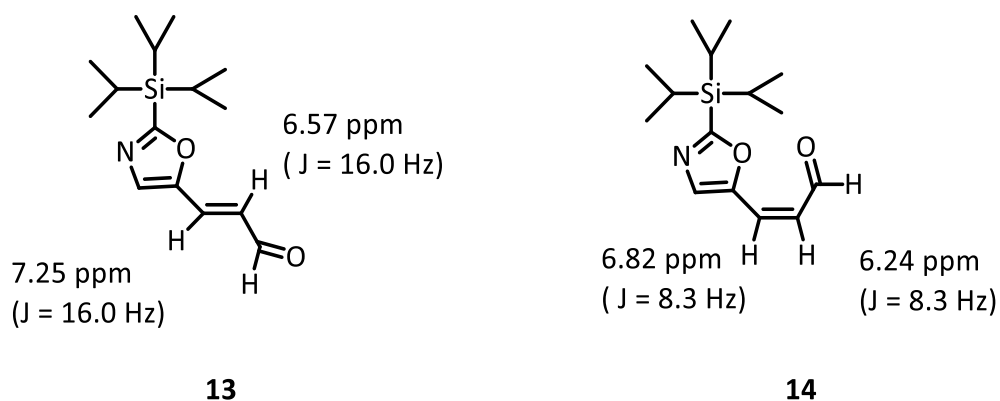
Wittig reagents are very important in chemistry especially in making alkenes. The synthesis of compounds **13**, ICT13040 and **14**, ICT13041 was started by refluxing the protected oxazole **12** with commercially available phosphorane **15**, the reaction mechanism is explained in **Scheme 9**. The phosphorane attacks the carbonyl atom and initially yields a betaine intermediate which undergoes ring closure to form *cis* or *trans* oxaphosphetane intermediate that breaks down to yield the corresponding *cis* and *trans* alkene and triphenylphosphine oxide.



Scheme 9 reaction mechanism of coupling Wittig reaction with aldehyde

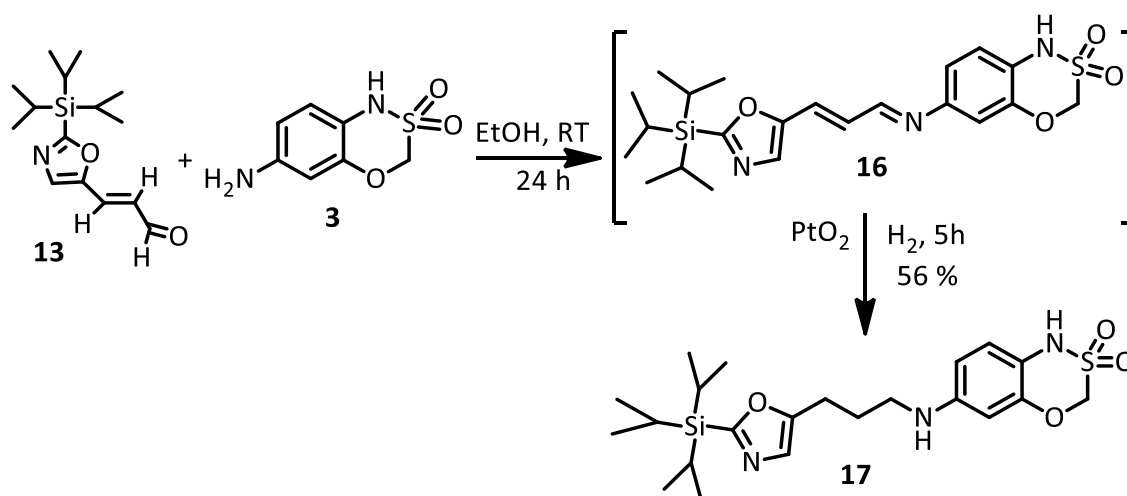
In this reaction, two isomers were obtained with, E, **13** and Z, **14** geometry, after purification using flash chromatography (1:9 EtOAc:PE). The assignment of the geometric isomers was done by ¹H NMR coupling

constants of *trans* isomer which are higher than the coupling constants of *cis* isomer (**Scheme 10**).



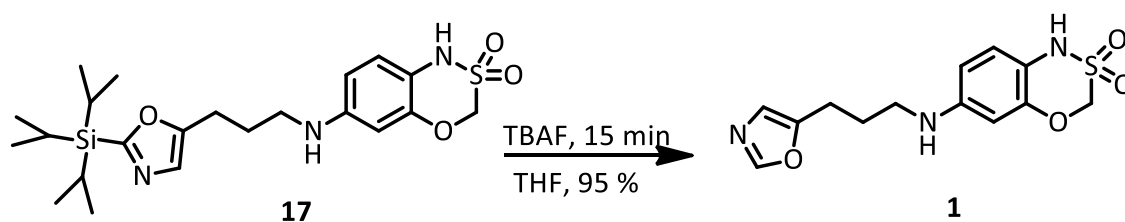
Scheme 10 chemical shifts and coupling constant of isomers **13** and **14**

The synthesised aldehyde **13** and amine **3** were then coupled together. Compound **13** and compound **3** were dissolved in ethanol and stirred overnight at room temperature in order to make imine **16** (**Scheme 11**). The imine formed was then reduced under hydrogen in the presence of platinum oxide to facilitate reduction of the double bond. The reduction step was successfully achieved, and confirmed by ^1H and ^{13}C NMR analysis as well as mass spectrum, to form compound **17**, ICT13042.



Scheme 11 Synthesis diagram of compound **17**.

Proton chemical shifts obtained at 3.06 ppm, 2.72 ppm and 1.88 ppm represent hydrogen atoms at propyl amino carbons. Carbon-13 chemical shifts at 30.92 ppm, 29.69 ppm and 23.07 ppm confirmed formation of propyl amino carbons. Mass spectrum was also obtained showing a peak at 466.7 which corresponds to the $[M+H]^+$ ion. Isomer **14** was also coupled with compound **3** and reduced in a separate reaction and was found to give the same result obtained from isomer **13**. The final step in the synthesis is the deprotection of the triisopropylsilane group. The protection group was removed by dissolving compound **17** in tetrahydrofuran (THF) and treatment with a solution of tetra-butyl ammonium fluoride (TBAF) in THF for 10 to 15 minutes at room temperature under nitrogen atmosphere (**Scheme 12**).

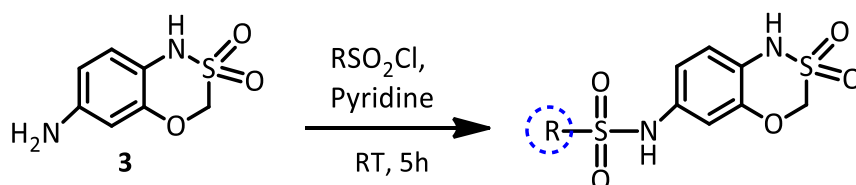


Scheme 12 De-protection step of compound **1**.

The completion of the reaction was monitored by thin layer chromatography (TLC). The reaction mixture was directly impregnated on silica and purified by flash chromatography to give compound **1** as dark brown solid. The formation of compound **1** was proved by proton and carbon NMR. A peak obtained at 7.86 ppm in proton NMR and 153.38 ppm in ^{13}C NMR represent the hydrogen and carbon atoms at the 2-position of the oxazole ring in which the silyl protecting group was replaced by a hydrogen.

The synthesised compounds, **3** and **1** were tested to check their activity as antagonists of CCR7 receptor using calcium flux assay. We found that both

compounds, **3** and **1** reduced the amount of fluorescence released from calcium flux assay with IC_{50} around $10 \pm 2.5 \mu\text{M}$ and $8.2 \pm 1.2 \mu\text{M}$ respectively. The results confirmed that both compounds, which were previously shown to bind CCR7, were antagonists. Compound **1** showed small enhancement against CCR7 receptor over compound **3** which is relatively insignificant. So, we concluded that the elongation at the amino side chain might not be important for activity. However, we decided to do further investigation by making different side chains elongated at the amine position. It was decided to determine if having sulphonamide as a different group at amino group side chain will improve the activity against CCR7 receptor or not, so we made compounds **18**, ICT13081 and **19**, ICT13088. The preparative work simply started by condensation of sulfonyl chloride with the primary amine. Compounds **18** and **19** were synthesised by dissolving compound **3** in 10 ml of pyridine and the corresponding sulfonyl chloride was then added at 0 °C. The reaction mixture was left stirring at room temperature for six hours under nitrogen atmosphere and then was poured over ice and water. A solid was formed and collected by filtration, yielding the corresponding sulphonamides in very good yields (**Table 1**).



Compound	R	Yield (%)
18 , ICT13081		80%

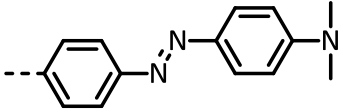
19, ICT13088		70%
--------------	--	-----

Table 1 amino side chain analogues as part of compound **3** SAR

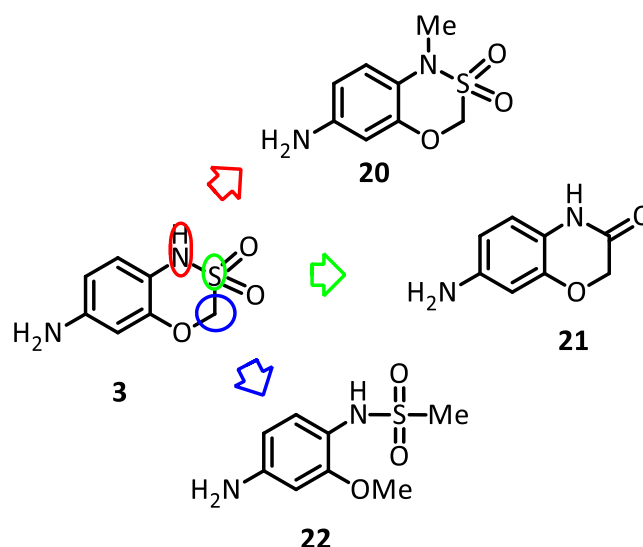
The synthesised compounds, **18** and **19** were tested to check their activity as antagonists of CCR7 receptor using calcium flux assay. Both analogues showed no enhancements in the activity with IC_{50} values around 12.6 ± 2.1 μ M and 11.6 ± 3.0 μ M respectively compared to compound **3** which showed activity against CCR7 receptor with IC_{50} value around 10 ± 2.5 μ M. Therefore, we assured that the amine tail side chain is not important for activity against CCR7 receptor. Taking into account the difficulties and time consuming of synthesizing compound **1**, It was decided to continue on using compound **3** as our lead compound to investigate structure activity relationship. We then wanted to make sure if the amino group (NH_2) is important for activity or not. We tested compounds **5** and **11** where the amine group was replaced with hydrogen and nitro group respectively. The activity of compound **5** was lost against the CCR7 receptor which indicated that the amine group of compound **3** itself is crucial for activity, removal of this group has lost the activity with $IC_{50} > 10$ μ M (9.6% inhibition at 14.2 μ M), **Appendix I**. Compound **11** was also tested using full dose dependant response and again the activity was dropped with IC_{50} around 16.4 ± 3.0 μ M. We concluded that whilst the chain elongation might not contribute to the activity, a polar group at position C-6 would. **Table 2** summarizes IC_{50} values obtained from different analogues tested using calcium flux assay.

Compound	IC ₅₀
5 , ICT13001	>10 μM (n = 3)
1 , ICT5189	8.2±1.2 μM (n = 4)
18 , ICT13081	12.6±2.1 μM (n = 3)
11 , ICT13031	16.4±3.0 μM (n = 3)
19 , ICT13088	11.6±3.0 μM (n = 4)
3 , ICT5888	10±2.5 μM (n = 4)

Table 2 IC₅₀ values of different compounds

2.2.3. Synthesis of analogues of compound **3**, ICT5888

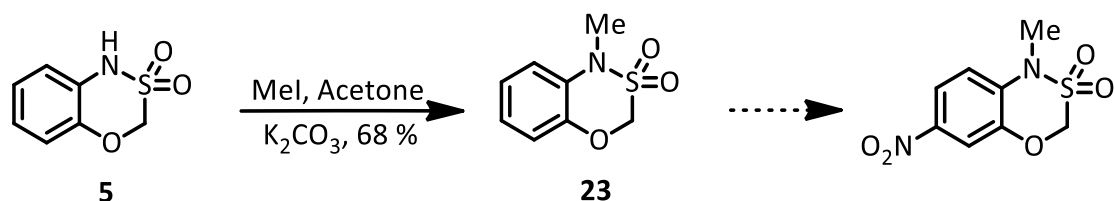
Following the biological evaluation of compound **3** as a weak CCR7 antagonist, we set out to prepare different analogues of this compound in order to look for structure activity relationships and gain access to more potent antagonists of the CCR7 receptor. We decided to first look at three key structural features of the molecule: the role of NH, the role of sulfonyl group and the cyclic ring (**Scheme 13**). To assess the significance of the NH, we decided to make compound **20**, ICT13047 in which the NH was replaced by an NMe. To assess the significance of the sulfonyl, we decided to make amide **21**, ICT13008 and to assess the role of the ring, to make the ring opened compound **22**, ICT13029. The activity of the resulting derivatives would then be evaluated against CCR7 receptor and compared to that of compound **3**, by calcium flux assay.



Scheme 13 Proposed synthesis of compound **3** analogues

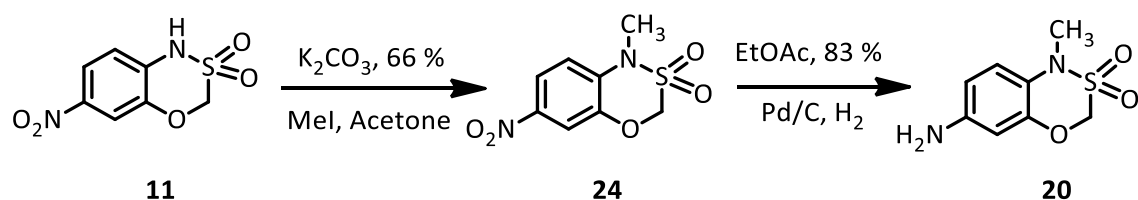
The preparative work towards compound **20** started with a methylation step, which involved the addition of a methyl group to the nitrogen atom of the sulphonamide group. As illustrated in the **Scheme 14** below, methyl iodide and potassium carbonate were added to a solution of compound **5** in acetone. The resulting mixture, was stirred at room temperature for 24 hours under nitrogen. The mixture was then filtered and purified by flash column chromatography on silica gel to afford compound **23**, ICT13006 as white solid material. The compounds were characterised by proton and carbon NMR as well as mass spectrum. A new peak correlating to 3 hydrogens appeared in the proton NMR at 3.19 ppm, confirmed the introduction of an N-methyl group. Also a peak at 32.0 ppm in the carbon NMR represents the newly added methyl group. The next step to prepare compound **20**, was nitration of compound **23** at *para* position to nitrogen. Compound **23** was exposed to the same nitration conditions utilised when synthesising compound **11**. However, the nitration produced a complex reaction mixture

which was very difficult to separate by flash column chromatography (Scheme 14).



Scheme 14 N-methyl synthesis pathway.

Alternatively, it was decided to carry out the reaction the other way around, which is, to methylate compound 11, instead of nitrating compound 23 (Scheme 15). Known amount of iodomethane was added dropwise to a solution of compound 11 dissolved in acetone in presence of potassium carbonate and the mixture was stirred overnight. The mixture was filtered, and the reaction mixture was purified by flash chromatography on silica gel to yield compound 24, ICT13046 as a yellow solid. Compound 24 was then reduced in presence of palladium on charcoal under hydrogen gas to yield compound 20, ICT13047.

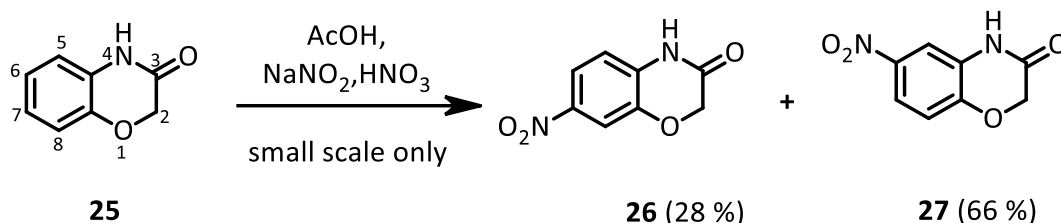


Scheme 15 Synthesis procedure of compound 20

Our next synthesis plan was to prepare the carboxamide analogue of compound 3, nitration of commercially available cyclic amide 25, ICT13007

gave two positional isomers. As illustrated in the scheme below, compounds **26**, ICT13004 and **27**, ICT13011 were synthesised by addition of a mixture of concentrated glacial acetic acid and nitric acid to a solution of 2H-benzoxazin **25** dissolved with sodium nitrate in glacial acetic acid, (**Scheme 16**)

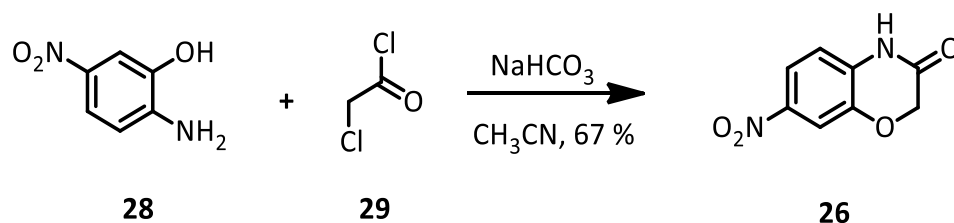
123.



Scheme 16 Synthetic pathway of compounds **26** and **27**.

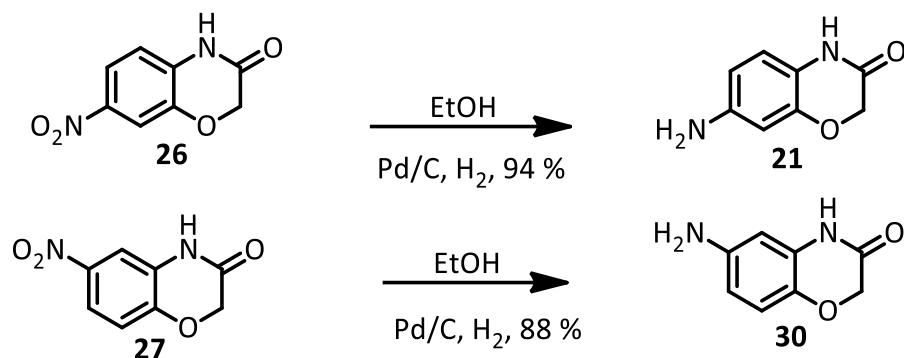
The two isomers were separated by flash chromatography on silica gel and their structure was confirmed by proton and carbon NMR. The major product was assigned as the 6-nitro derivative compound **27**, because the hydrogen signal from position 6 in compound **25** had disappeared, due the hydrogen being substituted. The minor product was assigned as the 7-nitro derivative compound **26**, because the hydrogen signal from position 7 in compound **25** had disappeared, due the hydrogen being substituted with the nitro group to give compound **26**. In both cases, mass spectrometry confirmed the molecular ion mass for the proposed structure. Compounds **26** and **27** were reduced under hydrogen atmosphere to give the corresponding amino compounds and the compounds were assessed for biological activity. The desired isomer, compound **26**, where the nitro group is at position 7 was obtained in lower yield compared to isomer **27**, where the nitro substitution is at position 6. Also, as the reaction was scaled up, there was more of the

undesired isomer. In addition, purification of the two isomers was also an issue, as isomers share similar retention times on TLC, which made the mixture difficult to separate. Therefore, an alternative synthetic procedure that was devised that enables only the synthesis of the desired isomer. As illustrated below, sodium bicarbonate was added to a solution of commercially available 2-amino-5-nitro phenol **28** in acetonitrile which was stirred under reflux (**Scheme 17**). 2-Chloroacetylchloride **29** was then added dropwise and was left stirring on ice bath for 40 minutes. The reaction mixture was then refluxed on an oil bath for 2 h to form compound **26**, which was then purified by recrystallization as brown solid ¹²⁴.



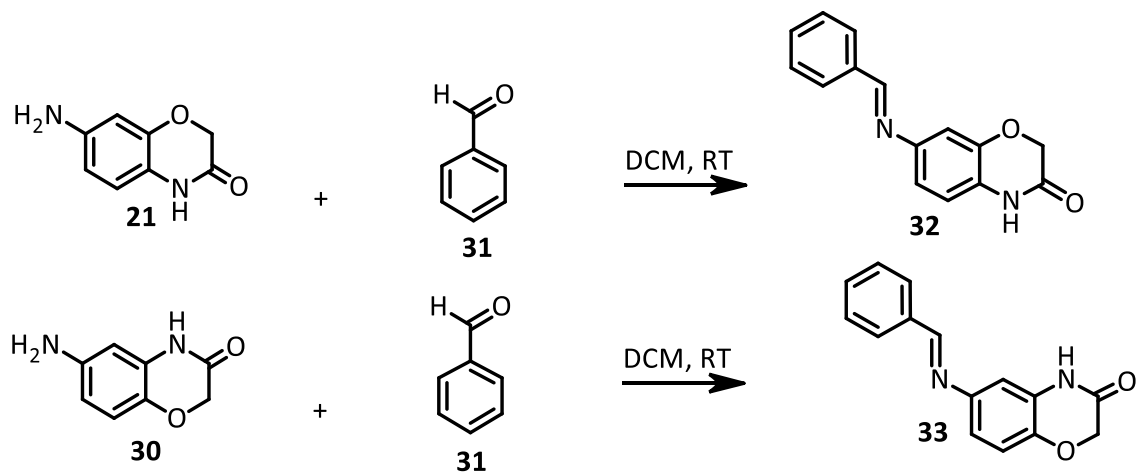
Scheme 17 Synthetic pathway of compound **26**.

Proton NMR chemical shifts of compound **26** was identical with proton NMR chemical shifts of the compound which was synthesised by direct nitration of compound **25**. Mass spectrum was also obtained with a peak at 195.09 which is for (M+H)⁺. The nitro group substituent in compound **26** and **27** was reduced under hydrogen atmosphere in presence of palladium on carbon as a catalyst to yield compounds **21**, ICT13008 and **30**, ICT13010 respectively, (**Scheme 18**). The signals observed by proton NMR at 4.87 and 4.89 ppm represent newly introduced amine for compounds **21** and **30** respectively.



Scheme 18 Synthetic pathway of compound **21** and **30**.

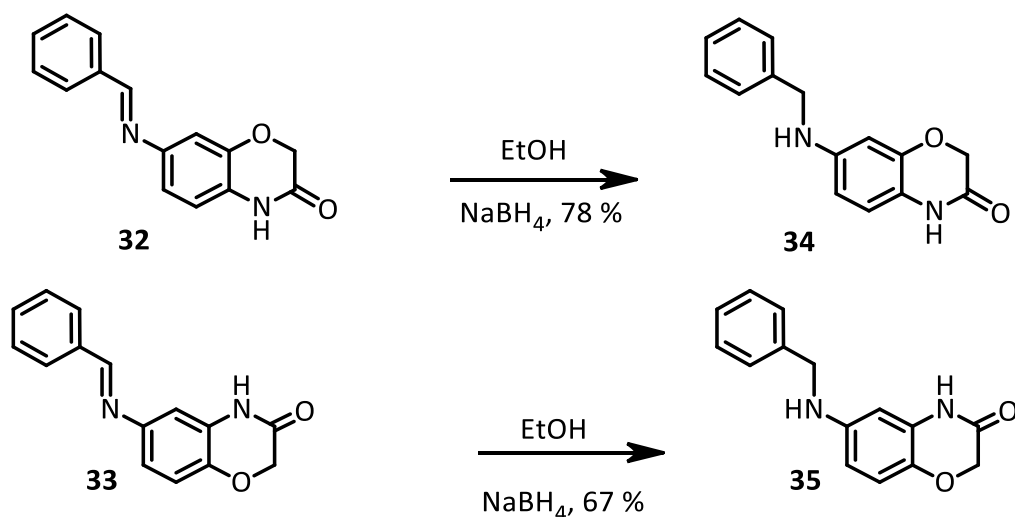
In purpose of making more analogues of the cyclic amide compound, both isomers, compounds **21** and **30** were then coupled with benzaldehyde **31** to give imines **32** and **33** respectively (**Scheme 19**). The nucleophilic addition reaction starts by condensation of aromatic primary amine and aldehyde to form imine. Small quantity of reaction mixture was analysed by proton NMR to characterize formation of imine in both compounds **32** and **33**.



Scheme 19 synthetic pathway of compound **32** and **33**.

Hydrogen atoms at imine moiety was used to characterise the formation of the compound. Peaks obtained from proton ^1H NMR at 8.66 ppm and 8.64 ppm corresponds to the hydrogen atom of imine, of compounds **32** and **33**

respectively. The C-N double bond in compounds **32** and **33** was then reduced by sodium borohydride as reducing agent. The solution of both isomers were separately dissolved in anhydrous ethanol and treated with sodium borohydride, to give compounds **34**, ICT13012 and **35**, ICT13016 as brown solids (**Scheme 20**).

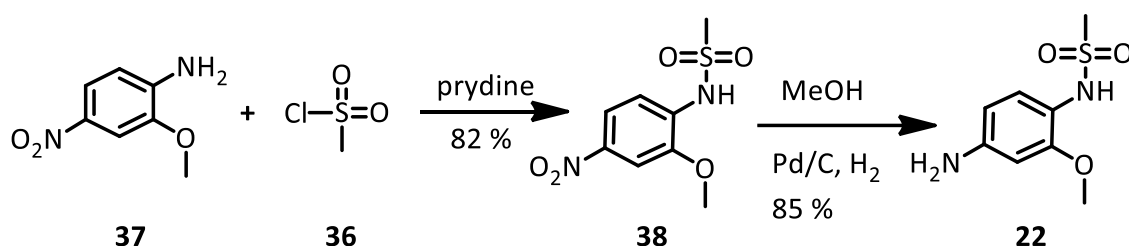


Scheme 20 Synthesis of compounds **34** and **35**.

The appearance of a new CH₂ group peaks at 4.20 ppm and 4.30 ppm in the proton ¹H NMR of compounds **34** and **35** respectively confirms the successful synthesis of the molecules which were tested as CCR7 receptor antagonist by calcium flux assay.

Our next structure activity relationship study was to assess the relevance of the oxathiazine cyclic ring in the potency of the compounds. In particular, would equivalent acyclic compounds retain activity, or is the ring essential for potency? So a number of different analogues were made. A methoxy group replaced O-CH₂- portion of the ring, and different compounds with different sulphonamide substituents were made and assessed for their biological

activity. Compound **22**, ICT13029 was made by addition of methanesulfonyl chloride **36** to a solution of 2-methoxy-4-nitroaniline **37** dissolved in anhydrous pyridine (**Scheme 21**). After the addition was over, the solution was stirred for 5h at room temperature and then poured over ice and water. Solid was formed and then was recrystallized from acetone-hexane to give compound **38**, ICT13019 as yellow crystals. Compound **38** was reduced under hydrogen in the presence of catalytic amounts of palladium on carbon over 24 hour at room temperature to give compound **22**, ICT13029. The proton and carbon NMR of SCH₃ group was detected at 3.31 ppm and 43.4 ppm respectively. Mass spectrum was also used and obtained at 217.0 which is for (M+H)⁺ which proves formation of the analogue.



Scheme 21 Synthesis pathway of compound **22**

The synthesised compounds were tested and compared with our lead compound **3** to check their activity as antagonists of CCR7 receptor using calcium flux assay. Results obtained indicated the importance of NH substitution for the activity of this series of compounds. Methylation of the N atom in presence and absence of amine group exemplified by compounds **20** and **23** respectively has reduced the efficacy as antagonists of CCR7 receptor with IC₅₀ >10 μM (26% and 15% inhibition at 14.2 μM respectively).

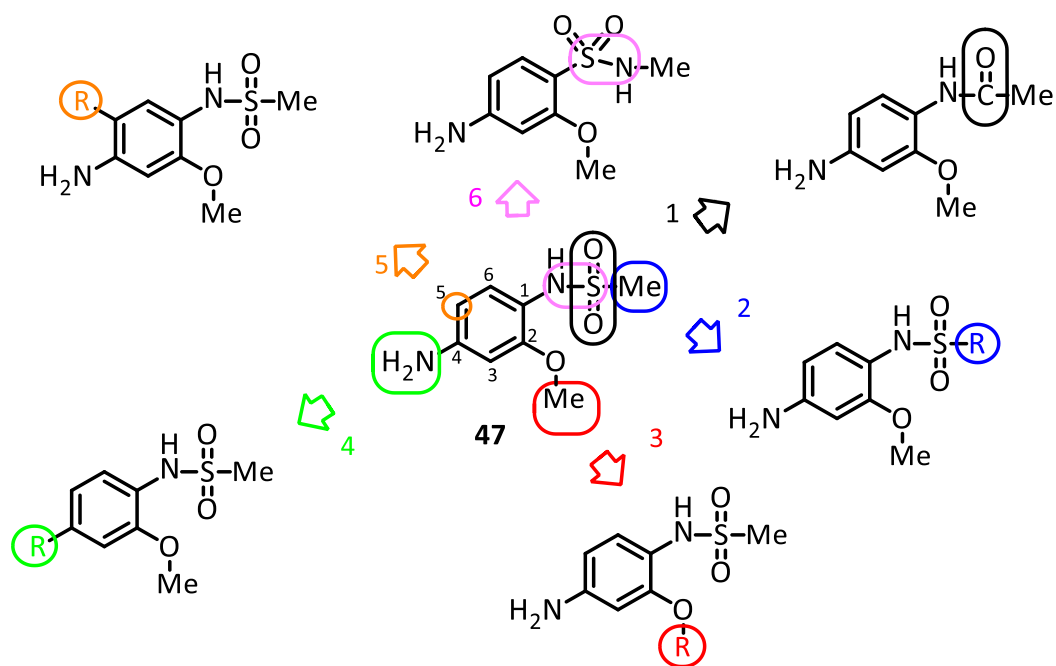
So, we thought that the NH position should not be substituted to retain its activity. The first synthesised amide analogue was compound **21** which was tested and compared to compound **3**. The activity of compound **21** was lost with $IC_{50} > 10 \mu\text{M}$ (11% inhibition at $14.2 \mu\text{M}$) compared to compound **3** which showed activity with IC_{50} around $10 \pm 2.5 \mu\text{M}$ (44% inhibition at $14.2 \mu\text{M}$). This reflects the importance of having sulphonamide group at this position in order to elicit antagonistic activity. We tried to make different analogues of compound **21** just to check if the activity will increase or not. Compounds **30**, **34** and **35** were all made in purpose of making sure the activity we saw previously is related to the cyclic sulphonamides. The activity of these analogues were lost as a result of changing the cyclic sulphonamide group to amide. All of these analogues were analysed with IC_{50} value higher than $10 \mu\text{M}$ (8%, 9% and 17% inhibition at $14.2 \mu\text{M}$ respectively). The activity was lost obviously due to the lack of sulphonamide group at compound **21** compared to compound **3** which altered the nature of interaction between compound and receptor. So, based on these findings we can conclude that in this cyclic series, the sulfonyl group is important for the activity of the molecules. Interestingly compounds **38** and **22** were tested and showed comparable effect to compound **3**. Compound **38** which has nitro group showed 39% inhibition at $14.2 \mu\text{M}$ with low solubility in aqueous medium. However, Compound **22** showed activity with IC_{50} around $11.6 \pm 1.3 \mu\text{M}$ (40% inhibition at $14.2 \mu\text{M}$) which is comparable to compound **3** with better solubility. We decided to make more of the open chain sulphonamides analogues which are considerably easy to synthesise multiple derivatives.

Compound	IC ₅₀
20 , ICT13047	>10 μM (n = 3)
21 , ICT13008	>10 μM (n = 3)
22 , ICT13029	11.6±1.3 μM (n = 3)
23 , ICT13006	>10 μM (n = 3)
30 , ICT13010	>10 μM (n = 3)
34 , ICT13012	>10 μM (n = 3)
35 , ICT13016	>10 μM (n = 3)
38 , ICT13019	>10 μM (n = 3)

Table 3 IC₅₀ values of compound **3** analogues

2.2.4. Synthesis of analogues of compound 22, ICT13029.

Following the discovery that ring open compounds, for example compound **22** are active, we started to prepare different analogues of this compound in order to investigate structure activity relationships and look for more potent antagonists of the CCR7 receptor. We decided to look at modifications to the main structural features of the molecule, as illustrated in **Scheme 22**.



Scheme 22 Proposed synthesis of compound **22** analogues

Our first structure activity relationship investigation in this synthesis plan was to assess the significance of sulphonamide group at position 1, we decided to convert it to amide. The activity of the resulting compound was evaluated against CCR7 receptor and compared to compound **3** by calcium flux assay. We explored the importance of having sulphonamide at position 1 by making compound **39**, ICT13138 which was synthesised by Mr Nile Saunders as part

of his MChem project whilst in our research group and tested on calcium flux assay (**Figure 15**).

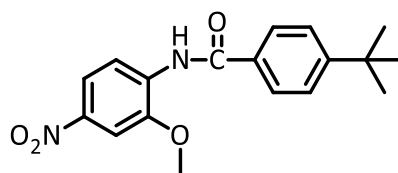
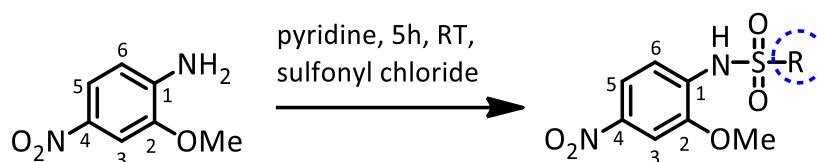


Figure 15 Structure of compound **39**

The activity of this compound was compared with the activity of compound **40**, ICT13062 (synthesised below) which have the same structure but with a sulphonamide group at position 1 instead of a carboxamide. The activity of compound **39** was dropped with $IC_{50} > 10 \mu M$ (25% inhibition at $14.2 \mu M$), however compound **40** showed activity with IC_{50} around $9.5 \pm 1.1 \mu M$. this confirms the previous findings when we discussed the importance of having sulphonamide group on the cyclic compounds. We had previously shown that the activity of compound **3**, which has a cyclic sulphonamide group, was recorded an IC_{50} around $10 \pm 2.5 \mu M$; however the activity of compound **21**, which has the cyclic amide group was dropped as shown previously. Both observations confirm the importance of having sulphonamide group over the amide group for CCR7 antagonism.

Our next investigation plan was to assess the significance of the R group in $NHSO_2R$, we decided to make different analogues starting from small aliphatic group exemplified by methyl and butyl group and then move on to try different aromatic groups like phenyl and methylbenzene group and then more lipophilic groups like tert-butylbenzene and biphenyl group. We prepared different analogues at position 1 where the sulphonamide group is attached, whilst keeping the methoxy group and amino group at position 2

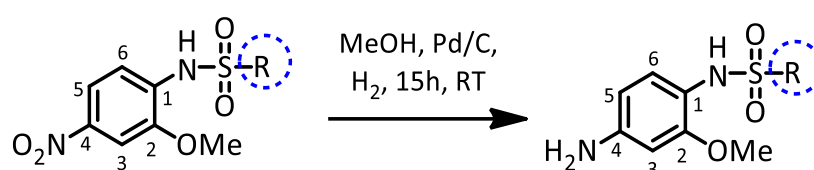
and 4 respectively. This will enable us to directly compare SAR of different analogues. As illustrated below different compounds namely **41**, **42**, **43**, **44**, **45**, **46** and **47** were made and characterised by NMR and mass spectrum analysis (**Table 4**).



Compound	R	Yield (%)
38 , ICT13019	CH ₃	82%
41 , ICT13018	CH ₂ -Cl	90%
42 , ICT13022	Bu	70%
43 , ICT13060	CF ₃	78%
44 , ICT13021		81%
45 , ICT13020		62%
40 , ICT13062		77%
46 , ICT13133*		NS
47 , ICT13135*		NS
* These compounds were prepared by Mr Nile Saunders as part of his MChem project and are included here so that the role of the sulphonamides are more fully explained		

Table 4 N-(2-methoxy-4-nitrophenyl) sulphonamide derivatives

The successfully synthesised compounds in **Table 4** were dissolved separately in ethanol and reduced using a catalytic palladium on carbon to yield the corresponding aniline derivatives. **Table 5** below summarizes successfully reduced compounds namely **48, 49, 50, 51, 52, 53, 54, 55** and **56** which were characterised by NMR and mass spectrum and then tested for their biological activities as antagonists of CCR7 receptor using calcium flux assay.



Compound	R	Yield %
22 , ICT13029	CH ₃	85%
48 , ICT13036	Bu	89%
49 , ICT13063	CF ₃	89%
50 , ICT13035		88%
51 , ICT13034		83%
52 , ICT13070		73%
53 , ICT13119*		NS
54 , ICT13134*		NS

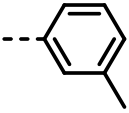
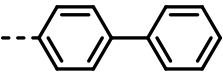
55, ICT13137*		NS
56, ICT13136*		NS
<p>* These compounds were prepared by Mr Nile Saunders as part of his MChem project and are included here so that the role of the sulphonamides are more fully explained.</p>		

Table 5 N-(4-amino-2-methoxyphenyl) sulphonamide derivatives.

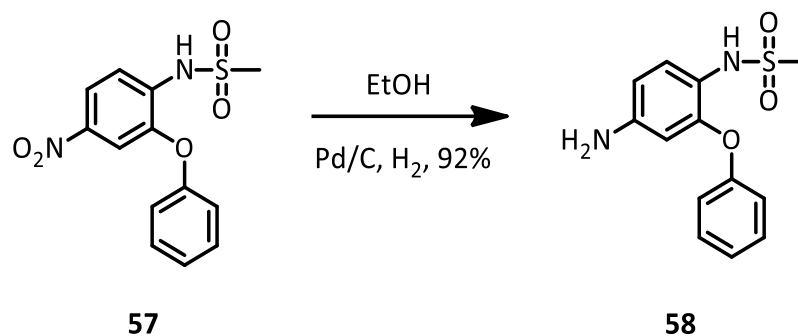
Following biological data analysis, we found that compound **40** has similar activity, with IC_{50} around $9.5 \pm 1.1 \mu M$, to compound **3** which showed activity with IC_{50} around $10 \pm 2.5 \mu M$. Unfortunately compound **40** with nitro group attached at position 4 was sparingly soluble in aqueous medium. Compound **52** activity was improved with IC_{50} around $5.7 \pm 1.3 \mu M$ compared to the activity of compound **22** (IC_{50} around $11.6 \pm 1.3 \mu M$), this enhancement is due to substitution of tert-butylbenzene group at position 1 instead of methyl group. We decided at this point to keep this group at this position and further investigate the importance of other positions. Interestingly compounds **49** showed significant activity against CCR7 receptor with IC_{50} around $1.7 \pm 1.5 \mu M$ which may reflect increased acidity of the sulphonamide NH. Hence further investigation on the role of acidity of the NH on potency of compounds is merited. Most of the other synthesised compounds in this series were tested and showed no improvement in the activity compared to compound **3** (**Table 6**).

Compound	IC ₅₀
38 , ICT13019	>10 μ M (n = 3)
40 , ICT13062	9.5 \pm 1.1 μ M (n = 3)
46 , ICT13133	>10 μ M (n = 3)
47 , ICT13135	>10 μ M (n = 3)
22 , ICT13029	11.6 \pm 1.3 μ M (n = 3)
48 , ICT13036	15.5 \pm 1.1 μ M (n = 3)
49 , ICT13063	1.7 \pm 1.5 μ M (n = 3)
50 , ICT13035	12.1 \pm 2.1 μ M (n = 3)
51 , ICT13034	11.6 \pm 1.6 μ M (n = 3)
52 , ICT13070	5.7 \pm 1.3 μ M (n = 3)
53 , ICT13119	12.6 \pm 1.3 μ M (n = 3)
54 , ICT13134	>10 μ M (n = 3)
55 , ICT13137	>10 μ M (n = 3)
56 , ICT13136	>10 μ M (n = 3)

Table 6 IC₅₀ values of different compounds

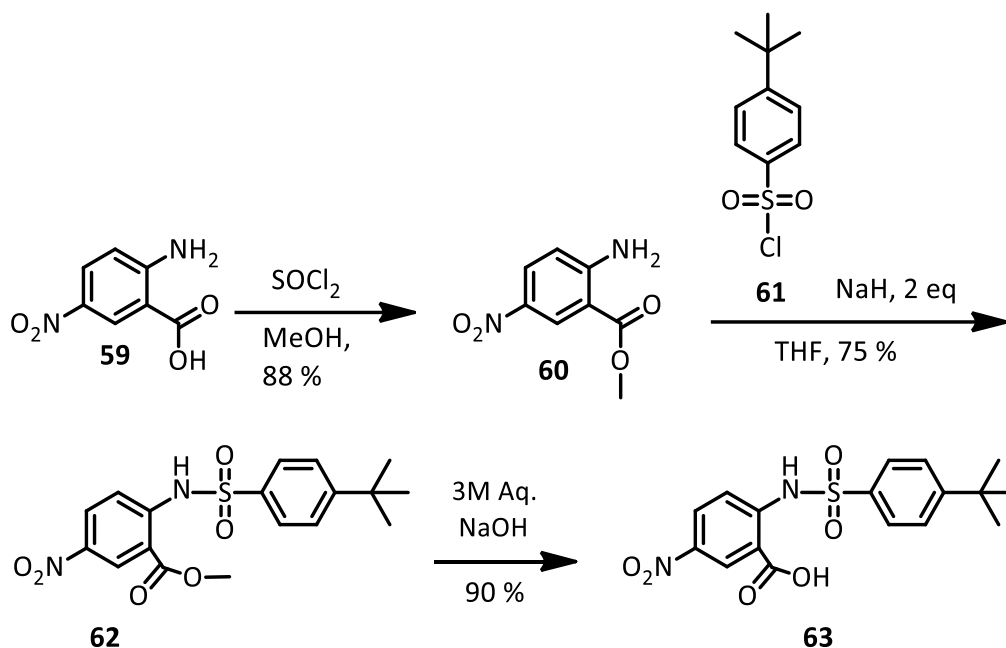
The next modifications were targeted towards the methoxy group at position 2, whilst keeping the methylsulphonamide and nitro groups at positions 1 and 4 respectively unchanged. The commercially available compound, **57**, ICT13052 that has phenoxy group at position 2 was tested on our calcium flux assay and compared with the activity of compound **3**. Compound **57** was then dissolved in ethanol and nitro group was reduced under hydrogen in presence of palladium on charcoal to give compound **58**, ICT13050

(Scheme 23). Compound **58** was tested on calcium flux assay to assess the effect of substitution at methoxy position (see below).



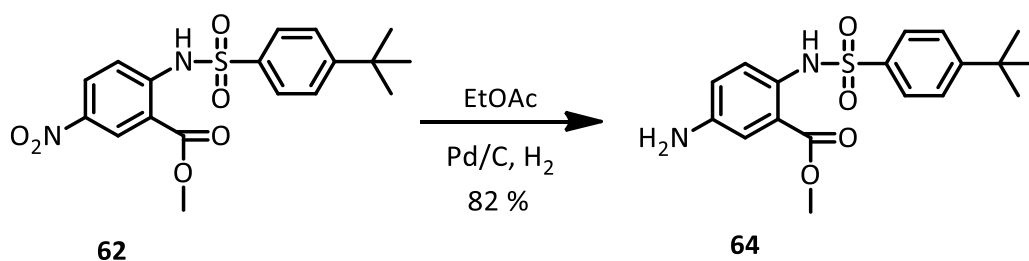
Scheme 23 Nitro-Reduction of compound **57**

Further to this investigation, we explored the importance of having other substitutions at positions 2 whilst keeping tert-butylbenzene group at position 1 unchanged. Commercially available 2-amino-5-nitrobenzoic acid **59** was dissolved in methanol and treated with thionyl chloride and refluxed overnight to obtain the corresponding methyl ester, **60**. The amine function in aniline compound **60** is considerably less nucleophilic due to the presence of two electron withdrawing substituents and this molecule was found not to undergo a reaction with sulfonyl chlorides using pyridine as base. Therefore, compound **60**, ICT13064 was dissolved in tetrahydrofuran THF and treated with sodium hydride before addition of commercially available sulfonyl chloride, **61** to give compound **62**, ICT13067 (**Scheme 24**).



Scheme 24 Synthesis of compound **62** and **63**

The methyl ester of compound **62** was then hydrolysed to carboxylic acid by reflux heating with a solution of sodium hydroxide for one hour to give the corresponding acid compound **63**, ICT13074 (**Scheme 24**). Reduction of the nitro group at position 4 of the compound **62** was then carried out under hydrogen in presence of palladium on charcoal overnight to give compound **64**, ICT13089 (**Scheme 25**).



Scheme 25 Reduction of compound **62**

To assess the importance of having methoxy group at position 2 of compound **52** we have tested the commercially available compound **65**, ICT13055, which has OH group at position 2 instead of methoxy group, using our calcium flux assay and compared its activity with the activity of compound **52** (**Figure 16**).

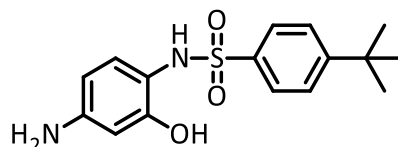


Figure 16 commercially available compound **65**

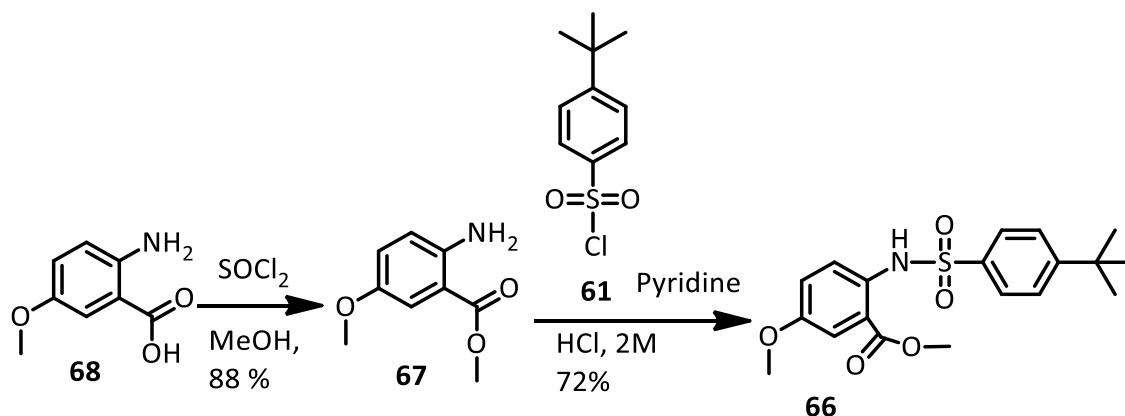
The activity of different analogues which targeted methoxy group at position 2 in calcium flux assay were determined. The substitution of methoxy group at position 2 with phenoxy group reduced the activity against the CCR7 receptor. Hence, compounds **57** and **58** had IC_{50} around $15.1 \pm 2.4 \mu\text{M}$ and $>10 \mu\text{M}$ (4% inhibition at $14.2 \mu\text{M}$) respectively. This is in comparison to compound **22** which showed activity against CCR7 receptor with IC_{50} around $11.6 \pm 1.3 \mu\text{M}$. Also, substitution of methoxy group with hydroxyl group has dropped the activity. Compound **65** has IC_{50} of $16.3 \pm 2.1 \mu\text{M}$. This is in comparison with compound **52** which has methoxy group attached at position 2, IC_{50} around $5.7 \pm 1.3 \mu\text{M}$. this indicated the significance of methoxy group substituted at position 2 over the phenoxy or hydroxyl group. Substitution of methoxy group at position 2 with methyl ester exemplified by compound **62** has increased activity against CCR7 receptor with IC_{50} around $3.4 \pm 0.9 \mu\text{M}$. this is in comparison with compound **40** which has methoxy group substituted at position 2, and an IC_{50} of $9.5 \pm 1.1 \mu\text{M}$. However, solubility of this compound, which have nitro group, in the aqueous medium is still an

obstacle to testing. Luckily, the solubility of compound **64** were enhanced yielding our first analogue with activity below 1 μM , IC_{50} was around 0.8 ± 1.0 μM .

Compound	IC_{50}
57 , ICT13052	15.1 ± 2.4 μM (n = 3)
58 , ICT13050	> 10 μM (n = 4)
62 , ICT13067	3.4 ± 0.9 μM (n = 3)
64 , ICT13089	0.8 ± 1.0 μM (n = 4)
65 , ICT13055	16.3 ± 2.1 μM (n = 4)

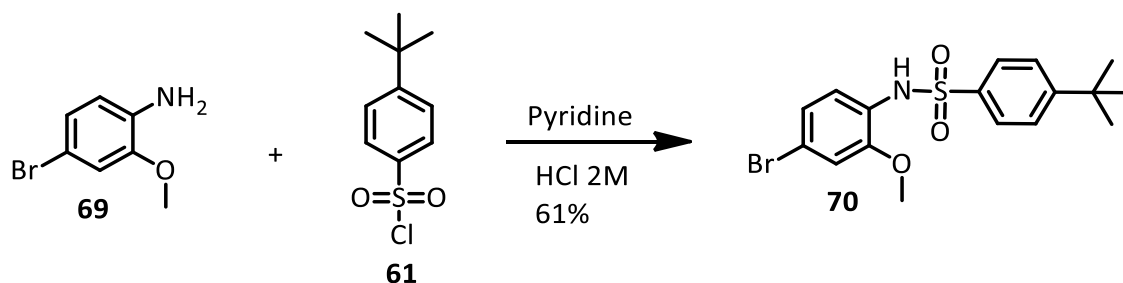
Table 7 IC_{50} values of different compounds

For further investigation for the structure activity of compound **22**, position 4 was also substituted to explore the effect of this position on CCR7 receptor. We first introduced methoxy group at position 4 and compared it with compound **64**. Compound **66**, ICT13108 was made by making the corresponding methyl ester **67**, ICT13093 of commercial available compound **68** which was then treated with commercially available compound **61** to give compound **66** (**Scheme 26**).



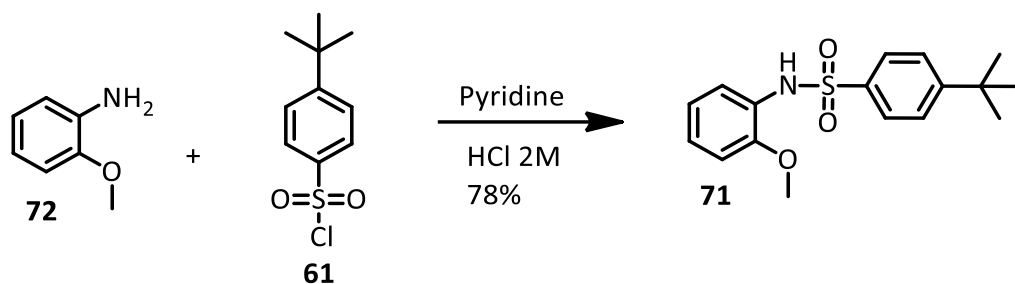
Scheme 26 synthesis of compound **66**

Commercially available 4-bromo-2-methoxyaniline **69** was dissolved in anhydrous pyridine, the reaction mixture was cooled down to 0 °C, and 4-(tert-butyl) benzene-1-sulfonyl chloride **61** was added dropwise and was left stirring for 5h under nitrogen atmosphere. Diluted hydrochloric acid was added to the solution mixture to neutralize the base and then extracted with ethyl acetate to afford a crude material which was purified by flash column chromatography to give compound **70**, ICT13122 as white crystals (**Scheme 27**).



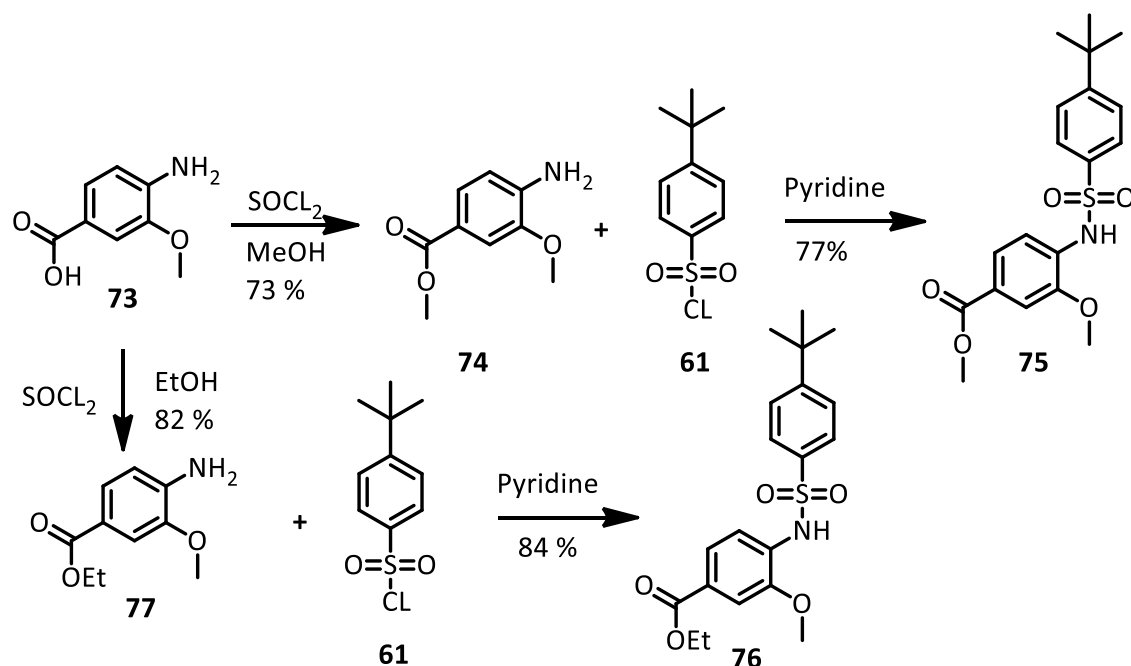
Scheme 27 synthesis of compound **70**.

Compound **71**, ICT13078, where no group on position 4 is present, was made by reacting 2-methoxy aniline **72** with 4-t-butylbenzenesulfonyl chloride **61**, same method mentioned previously (**Scheme 28**). If the IC₅₀ of the compound was increased, which means the efficacy was reduced, this will give a clue that substitution at this position is important to make interaction with the function group of the amino acid of the receptor.



Scheme 28 synthesis of compound **71**.

We then attempted to prepare an analogue with a methyl ester at position 4. 4-amino-3-methoxybenzoic acid **73** was dissolved in methanol and the reaction mixture was treated with thionyl chloride dropwise and refluxed overnight. The resulting methyl ester **74**, ICT13084 was then dissolved in pyridine and treated dropwise with 4-*t*-butylbenzenesulfonyl chloride **61** dissolved in dichloromethane to give compound **75**, ICT13069 (**Scheme 29**).

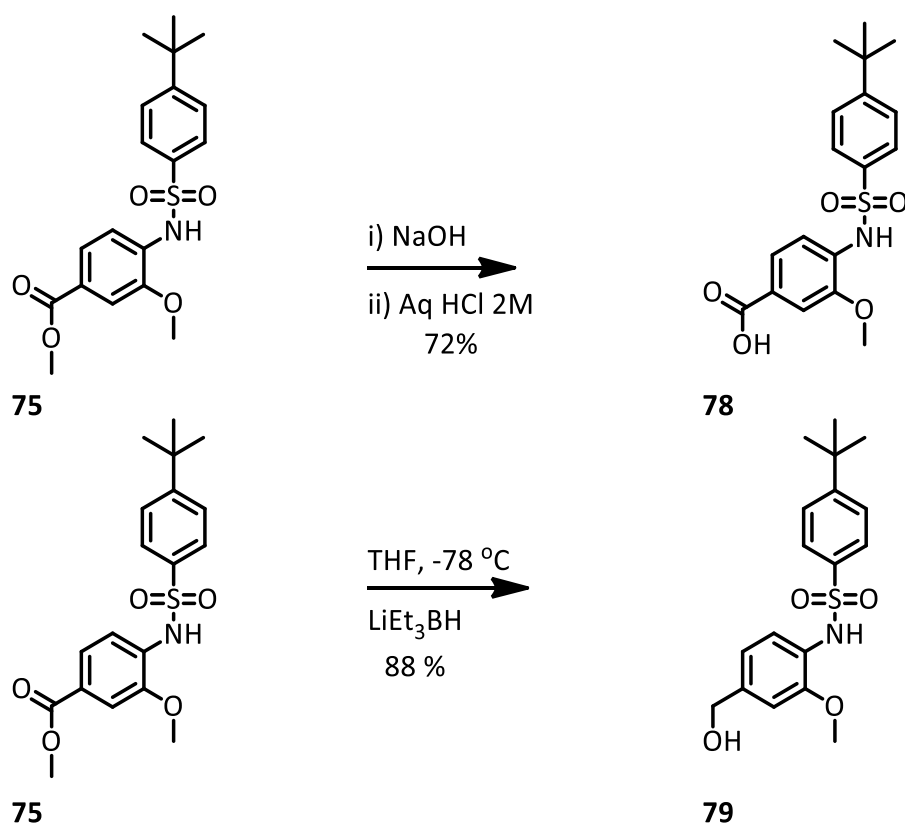


Scheme 29 Synthesis of compound **75**.

We also made compound **76**, ICT13113 which was simply synthesised by making the ethyl ester **77**, ICT13111 of commercially available compound **73**

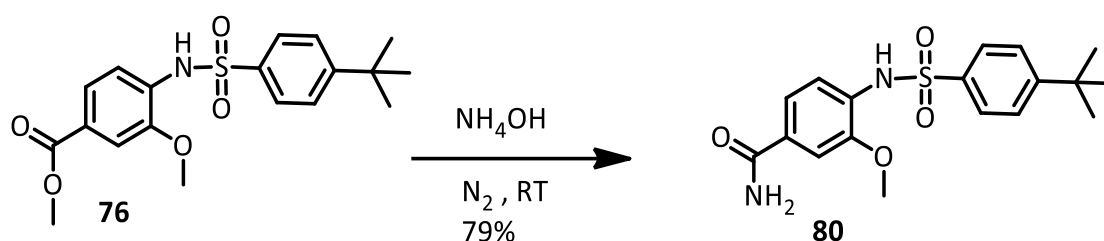
which was then treated dropwise with 4-*t*-butylbenzenesulfonyl chloride **61** to give compound **76**.

Compound **75** was then hydrolysed to its corresponding acid by treating the parent ester with a solution of sodium hydroxide and heating under reflux for an hour to afford compound **78**, ICT13072. Compound **75** was also reduced to alcohol. Compound **75** was dissolved in anhydrous THF and cooled down to -78 °C using dry ice and acetone bath. Lithium triethylborohydride (super hydride) in THF was added carefully and the resulting solution was left stirring for 5 hour under nitrogen atmosphere until the reaction was completed. The reaction was then warmed to room temperature and quenched with methanol and water and then was extracted with ethyl acetate. The resulting crude material was then purified by flash column chromatography to give compound **79**, ICT13091 (**Scheme 30**).



Scheme 30 synthesis of compounds **78** and **79**

The methyl ester of compound **76** was further investigated and converted to amide to find out the effect of this substitution if it would change the efficacy of the compound or not. So, compound **75** was dissolved in ammonium hydroxide under nitrogen atmosphere and was left stirring at room temperature for 5 days. The reaction mixture was then extracted with ethyl acetate to give a crude material which was purified using flash column chromatography to give compound **80**, ICT13092 (**Scheme 31**).



Scheme 31 synthesis of compound **80**.

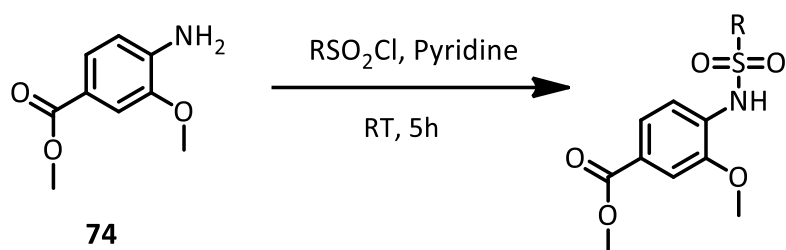
The synthesised compounds were tested to check their activity as antagonists of CCR7 receptor using calcium flux assay. The IC₅₀ obtained for compound **66** was around 2.9±1.0 μM, which is poorer than that for compound **64** with IC₅₀ around 0.8±1.0 μM. In compound **71** which has no substitution at position 4, the activity was lost against CCR7 receptor with IC₅₀ around 31.9±3.2 μM. We concluded from this, that a substituent at the 4-position is crucial for activity and its nature also impacts on potency. This was confirmed previously when testing the role of amine group of cyclic compounds **3**. Compound **5** which has hydrogen atom instead of amine group has abolished the activity with IC₅₀ >10 μM compared to compound **3** which showed activity with IC₅₀ around 10±2.5 μM. Substitution of position 4 with bromine or amide exemplified by compounds **70** and **80**, has shown

good activity against CCR7 receptor with IC₅₀ around 1.0 μM. However, when carboxylic acid or benzyl alcohol was introduced, the activity was reduced. Compounds **78** and **79** showed activity with IC₅₀ around 6.8±2.7 μM and 9.5±2.8 μM respectively. Interestingly, the most active compound was observed when the amine group was substituted with methyl ester or ethyl ester. Methyl ester substitution activity which is exemplified by compound **75** was recorded with IC₅₀ around 0.19±0.2 μM which represent significant improvement compared to our lead compound. Also compound **76** which is the ethyl ester of compound **75** showed comparable activity with IC₅₀ around 0.24±0.3 μM. Based on these findings, compound **75** was identified as our most active compound and its activity was confirmed using another *in vitro* assays, “agarose spot assay”, (see chapter 3) and also in scratch assay which was done within our research group. **Table 8** below summarizes IC₅₀ values obtained from different analogues tested using calcium flux assay.

Compound	IC ₅₀
66 , ICT13108	2.9±1.0 μM (n = 3)
71 , ICT13078	31.9±3.2 μM (n = 3)
70 , ICT13122	1.0±0.9 μM (n = 3)
80 , ICT13092	0.8±0.9 μM (n = 3)
78 , ICT13072	6.8±2.7 μM (n = 3)
79 , ICT13091	9.5±2.8 μM (n = 3)
75 , ICT13069	0.19±0.2 μM (n = 4)
76 , ICT13113	0.24±0.3 μM (n = 4)

Table 8 IC₅₀ values of different compounds

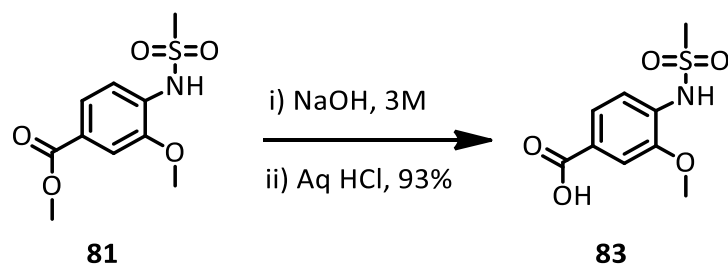
The methyl ester at position 4 appears to be important for activity and its better than other substitutions so far. It is apparent that we no longer need the aniline functionality present in compound **52**. So, it was decided to keep this ester group at this position and do more investigations. We prepared a number of ICT13069 analogues, where the sulphonamide moiety (NSO₂R) is decorated with different substituents, while keeping the methoxy and the methyl ester groups unchanged. **Table 9** below shows different analogues to compound **75** namely, compounds **81** and **82**.



Compound	R	Yield %
81 , ICT13073	CH ₃	73%
82 , ICT13085		89%

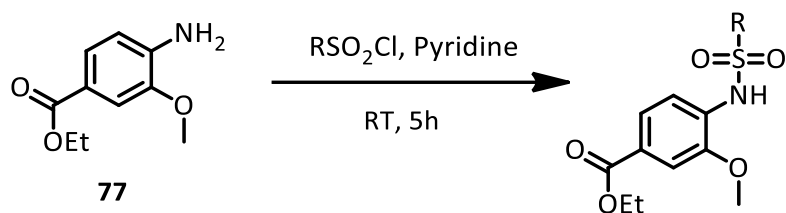
Table 9 compound **75** analogues

The analogues were made by addition of the corresponding sulphonyl chloride compounds to a solution of compound **74** in pyridine. The mixture was left stirring at room temperature for 5 hours. All compounds were purified using flash chromatography on silica gel to afford the analogous **81** and **82**. Compound **81** is further hydrolysed to its corresponding acid by treating the parent ester with a solution of sodium hydroxide and heating under reflux for an hour to afford compound **83**, ICT13071 (**Scheme 32**).



Scheme 32 synthesis of compound **83**

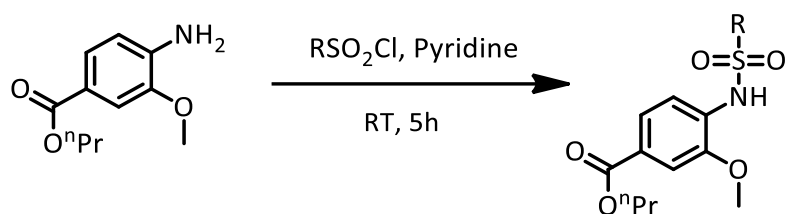
We mentioned earlier that compound **76**, which is the ethyl ester of compound **75**, also displayed similar activity obtained from biological results to compound **75** with IC_{50} around $0.24 \pm 0.31 \mu\text{M}$. So, more substitutions to compound **76** at position 1 (NSO₂R) while keeping the ethyl ester at position 4 were prepared out and summarized in the table below which describes the synthesis of analogues **84**, **85** and **86**.



Compound	R	Yield %
84 , ICT13114		60%
85 , ICT13130		96%
86 , ICT13126		95%

Table 10 compound **76** analogues

Because of similarity of enhancement of the activity which resulted from the elongation of the side chain of the methyl ester of compound **75**, it was then decided that it might be worthy to elongate this side chain a bit more. Making the propyl ester of the compound or isopropyl ester could reach out the function groups at the receptor amino acids and interact with them. More substitutions illustrated in the table below namely analogues **87** and **88**.



Compound	R	Yield %
87 , ICT13143		91%
88 , ICT13144		85%

Table 11 compounds **87** and **88**

The synthesised compounds were tested using our calcium flux assay. Substitution of tert-butylbenzene with methyl group (compound **81**) reduced the activity of the compound tremendously. The activity of compound **81** was recorded with IC_{50} around $37.7 \pm 3.2 \mu\text{M}$, this is in comparisons with compound **75** which showed activity with IC_{50} around $0.19 \pm 0.2 \mu\text{M}$. We can conclude that the tert-butylbenzene is important for activity. Also compound **83** which is the corresponding acid of compound **81** was tested and activity was dropped with IC_{50} around $74.4 \pm 4.0 \mu\text{M}$. This reflects the significant of

methyl ester substitution group over the carboxylic acid group. This was confirmed previously when testing compounds **75** and **78**. We compared the activity of methyl ester, ethyl ester and propyl ester of compounds **82**, **84** and **88**, which all have the same substitution group at position 1 and 2, to check the importance of elongated ester at position 4. The activity of those compounds was reduced toward more elongated ester with IC₅₀ around 4.1±1.3 µM, 4.8±1.2 µM and 6.2±2.6 µM respectively, this was also proved when testing compound **75** and **76**. Substitution of tert-butylbenzene of compound **76** with biphenyl group exemplified by compounds **86** has reduced the activity of the compound with IC₅₀ around 5.2±1.2 µM. However, substitution with Dansyl chloride **85** group has shown to improve the activity of the compound. We think the activity of the compound has increased tremendously, the IC₅₀ obtained from testing on calcium flux assay reached 50nM which marks a significant enhancement in the activity. It is worth to mention that this molecule was synthesised at the very end of the project, so most of the *in vitro* assays (agarose and scratch assay) were taken place using compound **75**. **Table 12** below summarizes different IC₅₀ values of different analogues.

Compound	IC ₅₀
81 , ICT13073	37.7±3.2 µM (n = 3)
83 , ICT13071	74.4±4.0 µM (n = 3)
82 , ICT13085	4.1±1.3 µM (n = 3)
84 , ICT13114	4.8±1.2 µM (n = 3)
86 , ICT13126	5.2±1.2 µM (n = 3)

85 , ICT13130	0.05±0.1 μ M (n = 4)
88 , ICT13144	6.2±2.6 μ M (n = 3)

Table 12 IC₅₀ values of compound **75** analogues

Our next synthesis plan was to investigate the significance of position 5, we first attempted to check the importance of having methoxy group at position 5 instead of position 2 and compared it with compound **22** which has methoxy group at position 2. The commercial available compound **89**, ICT13053 (**Figure 17**) was tested on our calcium flux assay.

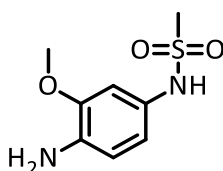
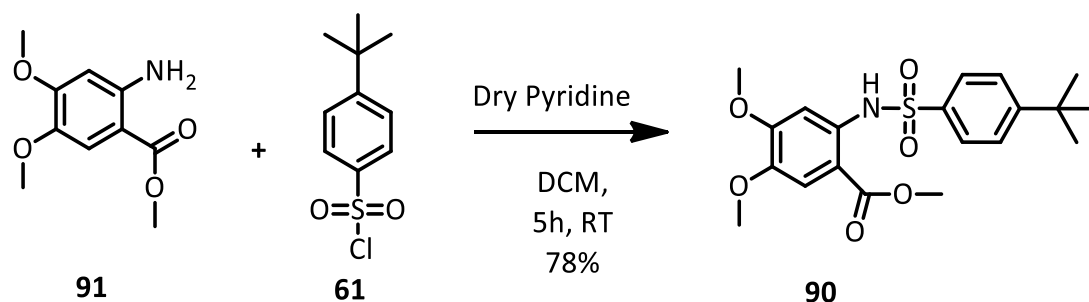


Figure 17 structure of commercial available compound **89**

We next decided to make compound **90**, ICT13068 and compare it with compound **66** to determine if any changes at that position 5 would affect the activity of this molecules against CCR7 receptor or not. We started with commercially available methyl 2-amino-4,5-dimethoxybenzoate **91**, which was dissolved in anhydrous pyridine to this solution, solution of (4-tert-butylbenzene)-1-sulfonyl chloride **61** in anhydrous dichloromethane was added and was left stirring at room temperature for 5 hours to give compound **90** (**Scheme 33**).



Scheme 33 synthesis of compound **90**

We also evaluated commercially available compound **92**, ICT13123 to assess the importance of position 5 again by having carboxylic acid attached at this position in a compound where the sulphonamide group is reversed and has methoxy group at position 2. (**Figure 18**). Unlike the other compounds hitherto synthesised, compound **92** is a reverse sulphonamide.

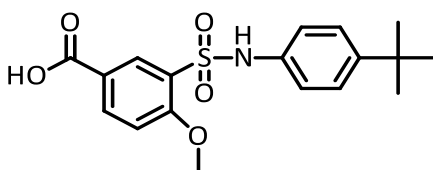


Figure 18 commercial available compound **92**

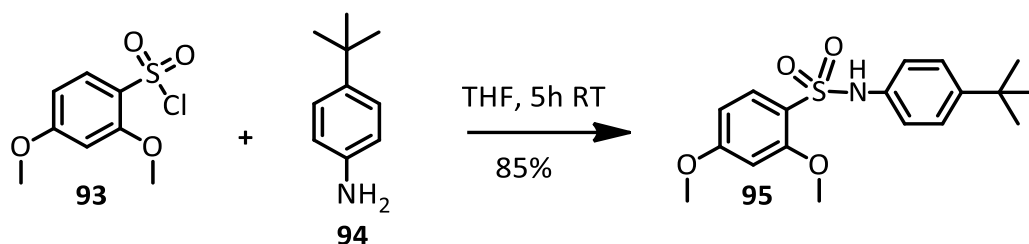
The activity of investigated position 5 analogues against CCR7 receptor was assessed using our calcium flux assay. The activity of compound **89**, which has methoxy group at position 5, was compared with the activity of compound **22**, which has methoxy group at position 2. We found that, the activity of compound **89** was reduced tremendously with IC_{50} value $>10 \mu M$ (6% inhibition at $14.2 \mu M$), however the activity of compound **22** was recorded with IC_{50} around $11.6 \pm 1.3 \mu M$ (40% inhibition at $14.2 \mu M$). This indicates the importance of having methoxy group at position 2. The activity of compound **90** which has methoxy group at position 5 was directly

compared with the activity of compound **66**. The activity of compound **90** was reduced with IC_{50} around $11.5 \pm 2.0 \mu\text{M}$, however the activity of compound **66** was recorded with IC_{50} around $2.9 \pm 1.0 \mu\text{M}$. The activity was also lost with IC_{50} around $32.1 \pm 3.0 \mu\text{M}$ when position 5 of the reverse sulphonamide was substituted with carboxylic acid moiety, compound **92**. We concluded from this investigation that substitution at, position 4 is favoured to potency, however further investigation is needed to confirm this since the range of compounds we used was limited. **Table 13** below summarizes different IC_{50} values of different analogues.

Compound	IC_{50}
89 , ICT13053	$>10 \mu\text{M}$ (n = 3)
90 , ICT13068	$11.5 \pm 2.0 \mu\text{M}$ (n = 3)
92 , ICT13123	$32.1 \pm 3.0 \mu\text{M}$ (n = 3)

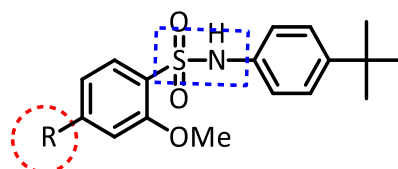
Table 13 IC_{50} values of different compounds

The last stage in our structure activity relationship investigation was to synthesise reverse sulphonamides in which the nitrogen and sulphonyl are juxtaposed. The preparative work started by dissolving commercially available 2,4-dimethoxybenzene-1-sulfonyl chloride **93** in THF and 4-t-butylaniline **94** was added to the solution and stirred under nitrogen for 5h. Diluted hydrochloric acid was added and the solution extracted with ethyl acetate. The crude material was purified by flash column chromatography to give compound **95**, ICT13121 as white powder (**Scheme 34**).



Scheme 34 synthesis of compound **95**.

We then synthesised different analogues namely, compounds **96**, **97**, **98** and **99** in purpose of investigating the importance of reverse sulphonamide as CCR7 receptor antagonist which is summarizes in the figure below.



- 96**, ICT13120* R = NH₂
- 97**, ICT13124* R = NO₂
- 98**, ICT13145[§] R = H
- 99**, ICT13146[§] R = CONHCH₃

Figure 19 number of reverse sulphonamide analogues synthesised. * These compounds were prepared by Mr Nile Saunders, and [§] These compounds were prepared by Mario Izidro as part of their projects and are included here so that the role of the sulphonamides are more fully explained.

We also tried to have methyl ester at position 2 instead of methoxy group, compound **100**, ICT13147 was synthesised by Mr Mario Izidro as part of his master project (**Figure 20**).

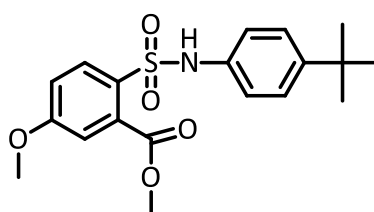


Figure 20 Structure of compound **100**.

The synthesised analogues were tested using our calcium flux assay and compared with the most active compound, **75**. Compound **97** showed a significant improvement in activity with IC_{50} around $0.10 \pm 0.3 \mu\text{M}$ compared to sulphonamide compound **40** (IC_{50} around $9.5 \pm 1.1 \mu\text{M}$). However we thought because of the poor solubility of this compound in aqueous medium this result should be treated cautiously and more investigation required to confirm its activity. The activity of the reversed sulphonamide compound **96** with IC_{50} of $0.7 \pm 0.08 \mu\text{M}$ was also better than corresponding sulphonamide compound **52**, IC_{50} around $5.7 \pm 1.3 \mu\text{M}$. The activity of compound **96** is more reliable than the activity of compound **97** because of the better solubility in aqueous media. We also tried to have no substitution at position 4 exemplified by compound **98** which was compared with the activity of normal sulphonamide compound **71**. Both compound have the same substitution groups at position 1 and 2 whilst no substitution group was at position 4, the only differences is in the reversed sulphonamides. The activity of compounds **98** and **71** was tremendously reduced with IC_{50} around $26.6 \pm 3.7 \mu\text{M}$ and $31.9 \pm 3.2 \mu\text{M}$ respectively due to the lack of position 4 substitution. Methyl amide substituted at position 4 of compound **99** showed activity with IC_{50} around $2.7 \pm 1.3 \mu\text{M}$. We can compare activity of this compound with the activity of compound **79**, the normal sulphonamide that has amide at position 4, which showed activity with IC_{50} around $0.8 \pm 0.9 \mu\text{M}$. So, we thought substitution of methyl group at amide probably is behind the modest reduction in the compound activity. Substitution of methoxy group at position 4 on the reversed sulphonamide also showed some activity with IC_{50} around $4.5 \pm 1.8 \mu\text{M}$, exemplified on compound **95**. We then tried to have methyl ester group

at position 2 and methoxy group at position 4 in order to make direct comparison with compound **66**. Compound **100** was synthesised by Mr Mario Izidro as part of his master project and tested to find the activity of the compound was recorded with IC₅₀ around 3.5±1.9 µM. There was no significant differences between the activity of this compound and compound **66** which showed activity IC₅₀ around 2.9±1.0 µM. We concluded reversed sulphonamide seems to have significant effect on CCR7 receptor. Further investigation needs to be carried out in order to explore the importance of having reverse sulphonamide on many other compounds especially the most active compound, **75**. **Table 14** below summarizes different IC₅₀ values of different analogues.

Compound	IC ₅₀
97 , ICT13124	0.10±0.3 µM (n = 3)
96 , ICT13120	0.7±0.08 µM (n = 3)
98 , ICT13145	26.6±3.7 µM (n = 3)
99 , ICT13146	2.7±1.3 µM (n = 3)
95 , ICT13121	4.5±1.8 µM (n = 3)
100 , ICT13147	3.5±1.9 µM (n = 3)

Table 14 IC₅₀ values of different analogues

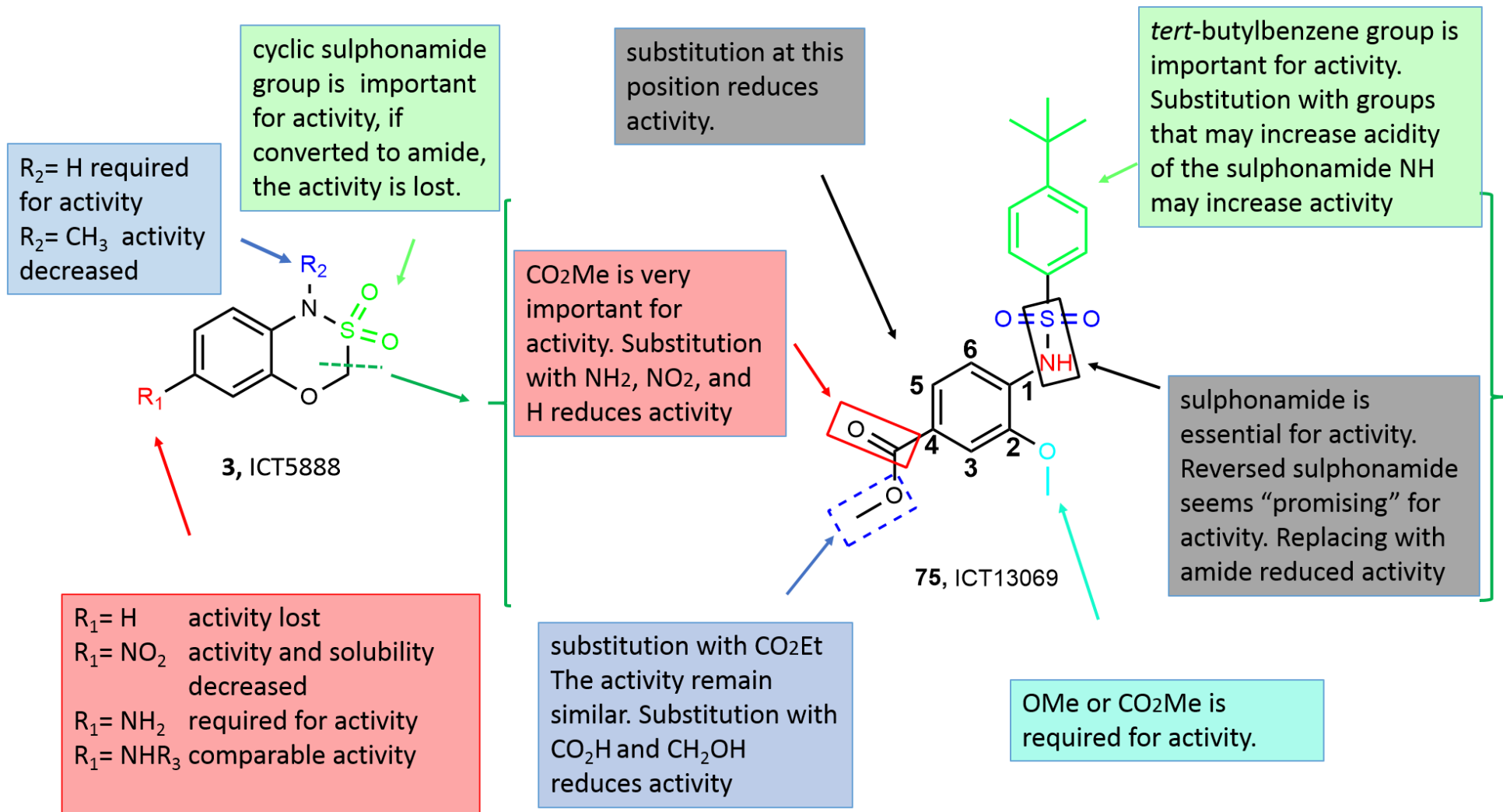


Figure 21 structure activity relationship scheme of the newly discovered CCR7 receptor antagonist

2.3. Structure activity relationship: summary of findings

The conclusions of structure activity relationship of CCR7 receptor antagonist starts with compound **1**. During the synthesis process of this molecule, the tailless compound **3** was discovered and tested on calcium flux assay which proved to be as active as compound **1**. The IC₅₀ of compound **3** and **1** was obtained around 10±2.5 µM and 8.2±1.2 µM respectively (**Table 2**). In order to confirm the NH₂ elongated side group is not contributing to activity, we tried different group such as sulphonamide and hence the activity remained the same. This confirms the result obtained from compound **1**, so we abandoned further investigation at this amino position. Taking into account time consuming and synthesis difficulties of making compound **1**, the newly discovered compound **3** was considered to be our new lead compound. Investigation of structure activity relationship of this compound started by making substitution at R₂ position, illustrated in the **Figure 21** above. Methyl substitution at this position reduced the activity against CCR7 receptor. This illustrates the importance of the cyclic NH for the activity. We then looked at R₁ position. The activity was lost when this position has no substituted group. The sulphonamide group is also found to be required for activity. When this functional group was replaced with amide, we found the activity was lost. Different analogues were synthesised in regard to improve the cyclic amide activity, however all molecules were shown to lose their activity against the CCR7 receptor. A number of different analogues were also made in order to understand the relevance of the oxathiazine cyclic ring in the potency of the compounds. The cleavage of the ring at the bond highlighted in green, **Figure 21**, afforded non cyclic analogues. A number of different analogues in this series were

synthesised and tested to find the activity reduced, with exception to compound **22**, IC_{50} around $11.6 \pm 1.3 \mu\text{M}$, where the activity remained the same. We decided to make more of the ring open analogues, particularly as it is easy to make many different derivatives in this series of compounds. So, different analogues were made to explore different variations to compound **22**. This new configuration to the lead compound, **3**, has led us to discover the most active compound in the series, compound **75** which is described in the figure above. The IC_{50} value for compound **75** was recorded around $0.19 \pm 0.2 \mu\text{M}$ which marks significant enhancement compared to our starting point compound **3**. The structure activity relationship of the newly discovered CCR7 receptor antagonist, **75**, has revealed the importance of different positions. Firstly, position 1, is very important and essential for the activity, the substitutions at this position started from small group such as methyl group and then with many different aromatic and highly lipophilic group. Most of these different groups were tested using calcium flux assay and the optimum activity was shown when tert-butylbenzene group is substituted at this position. Sulphonamide group is crucial for the activity, substitution of this group with amide has dropped the activity. So, in order to get optimum activity, tert-butylbenzene group and sulphonamide group has to be substituted at position 1. Secondly, position 2 is also very important for activity, substitution in this position with phenoxy or hydroxyl group has reduced the activity. However, substitution with methoxy or methyl ester group has improved the activity. Methyl ester group seems to have promising activity, however additional investigation has to be done to further explore other positions whilst keeping methyl ester group substituted at position 2. Thirdly, position 4 is also crucial for activity, having no substitution group at

this position dropped the activity. However, when this position was substituted with many different groups, better enhancement in the activity was observed. The activity of this position was varied depending on the substituted group, the greatest potency was achieved when this position was substituted with methyl ester, **75**. Ethyl ester of compound **75** showed comparable activity to compound **75**, so different analogues were made in purpose to look for better activity molecules. Compound **85**, which has dansyl group substituted at position 1 showed significant activity with IC₅₀ around 50nM, so more investigation has to take place to explore activity of this compound. Fourthly, substitution at position 5 seems not to be important for the activity, different groups substituted at position 5 reduced the activity against CCR7 receptor tremendously. So, we thought position 5 should not be substituted in order to retain compound activity. Finally, reverse sulphonamide group substituted at position 1 showed significant increase in the activity. We thought the reverse sulphonamide group substituted at position 1 has an important activity against the CCR7 receptor, further investigation has to take place to explore the importance of having reverse sulphonamide on compound **75**.

Compound **75** is the most active compound we have synthesised against the CCR7 receptor. The activity of this compound is confirmed by calcium flux assay and different *in vitro* assays like scratch assay and “agarose spot assay” (**chapter 3**). The compound is novel and fairly soluble in aqueous medium. The partition coefficient (cLogP) of the compound was calculated using National Chemical Database and was determined around 4.37 which is less than 5 and hence compliant to the Lipinski's Rule of Fives. Also the molecule has a molecular weight of 377.45 g/mol which is below the 500 mark set by the Rule.

So further modifications including adding more groups to this molecule to increase its potential interaction at the binding site, may be carried out. To conclude, compound **75** is a novel molecule with significant inhibitory effect against CCR7 receptor, and with good solubility in aqueous medium.

3. Chapter 3: Pharmacological characterization of CCR7 receptor antagonists

3.1. Introduction

In the previous chapter, we discussed the potency optimisation of CCR7 small molecule antagonists. The potency of the antagonists was measured by a calcium flux assay and later by another functional assay, which we have termed “agarose spot assay”. In this chapter, we first describe the development of the calcium flux method and will then describe the “agarose spot assay” which was used as a secondary assessment of potency and selectivity for CCR7 antagonist.

Chemokine receptor CCR7 belongs to the transmembrane G protein-coupled receptor (GPCR) superfamily. GPCRs are involved in binding with many different signalling molecules, including neurotransmitters, hormones, and peptides¹²⁵ and play decisive roles in managing and controlling many different physiological functions. Small molecules that modulate the interaction of GPCRs, such as CCR7, with their endogenous ligands are therefore medically important and a number of methods are developed for measuring the level of this modulation. GPCRs are very sensitive to their ligands which once bound to the receptor, initiate and activate different intracellular signalling pathways which include mobilisation of calcium ions inside cells. Hence, a key outcome of GPCR activation is an increase in cytoplasmic concentration of calcium ions released from endoplasmic reticulum (ER). Hence, calcium mobilisation assays are one of the most important screening methods used in the field of GPCR drug discovery¹²⁶. There are of course, a number of other methods used to screen for small molecules which have the ability to modulate GPCR signalling. One of these methods is ligand binding assay which is used to determine the binding affinity of compounds to a GPCR compared with that of the natural

ligand. However, the ligand binding assay can't be used to determine if the compound is agonist or antagonist and also it is restricted to the availability of the radio labelled ligand. Therefore, calcium flux assay is one of the favoured functional assay used as a screening platform to evaluate and measure activity of compounds against GPCR. The assay has the ability to measure activity of both agonist and antagonist which makes it a better technique to use over ligand binding assay. In order to assess and evaluate the potency of different CCR7 receptor antagonists using calcium flux assay, we first needed to identify suitable cell line models which express CCR7 receptor and efficiently respond to it. We used Western blot assay to qualitatively determine expression of CCR7 receptor in number of cell lines in our cell bank. Western blot assay determines expression of protein but it does not tell if the protein is cytoplasmic or membranous. In order to have full picture of CCR7 receptor expression on these cell lines, we used flow cytometry assay to determine expression of CCR7 receptor on cell surface. The ability of cancer cell to mobilize calcium ions from internal stores differs from cell line to another. Hence, we lastly required to assess the aptitude of those cancer cells, which were shown to express CCR7 receptor using calcium flux assay. Cells which responded to the ligand and mobilized calcium ions perfectly were used to measure compounds activity against CCR7 receptor. We then assessed and evaluated the most active compound obtained from calcium flux assay *in vitro* using "agarose spot assay" and scratch assay.

3.2. Characterization of CCR7 receptor antagonists potency using calcium flux assay

Calcium ions play an essential part in GPCR mediated cell signalling transduction pathway. In order for cells to survive and function properly, the intracellular Ca^{2+} concentration must be controlled ¹²⁷. The resting concentration of calcium in the cytoplasm is normally between 10–100 nM. This concentration is maintained through balanced processes involving release of the ions from reservoirs such as endoplasmic reticulum (ER) to the cytoplasm, and active transport of the ions to and from the extracellular space. When an external signal, for instance binding of a ligand to GPCR occurs, a transient 10 fold increase in cytoplasmic calcium concentration is observed ¹²⁸. Hence, the interaction between chemokines and their receptors leads to activation and initiation of a complex set of downstream signalling pathways which will include calcium mobilization from internal calcium stores. Calcium flux assay is based on measurement and detection of fluorescent light that is emitted by a calcium sensitive fluorescence dye, upon binding with calcium ions released into the cytoplasm. The effective concentration of ligand (see below) was used to treat cells with and without antagonists. In order to measure the activity of small molecules, serial dilution of antagonist concentrations was added to cells containing dye taking into account some wells were left as control. Calcium ions are mobilized as a result of interaction between CCL21 or CCL19 ligands (which are discharged from Fluoroskan Ascent FL instrument) and their receptor CCR7 on cell membrane. Calcium ions released upon interaction binds with the dye used in the assay (Fluo-4 NW) and emits fluorescence. **Figure 22** below explains how fluorescence is produced upon binding of ligand with its

receptor. The amount of fluorescence obtained in response to the addition of the ligand is measured at Ex 485 nm, Em 538 nm wave length using Fluoroskan Ascent FL instrument at room temperature (see experimental). The principle of this assay is based on inhibition of calcium channel opening mediated through G-protein coupled receptor (GPCR) followed activation of CCR7 receptor upon binding to its ligand. The amount of fluorescence measured in presence of antagonist should be reduced if the antagonist is potent.

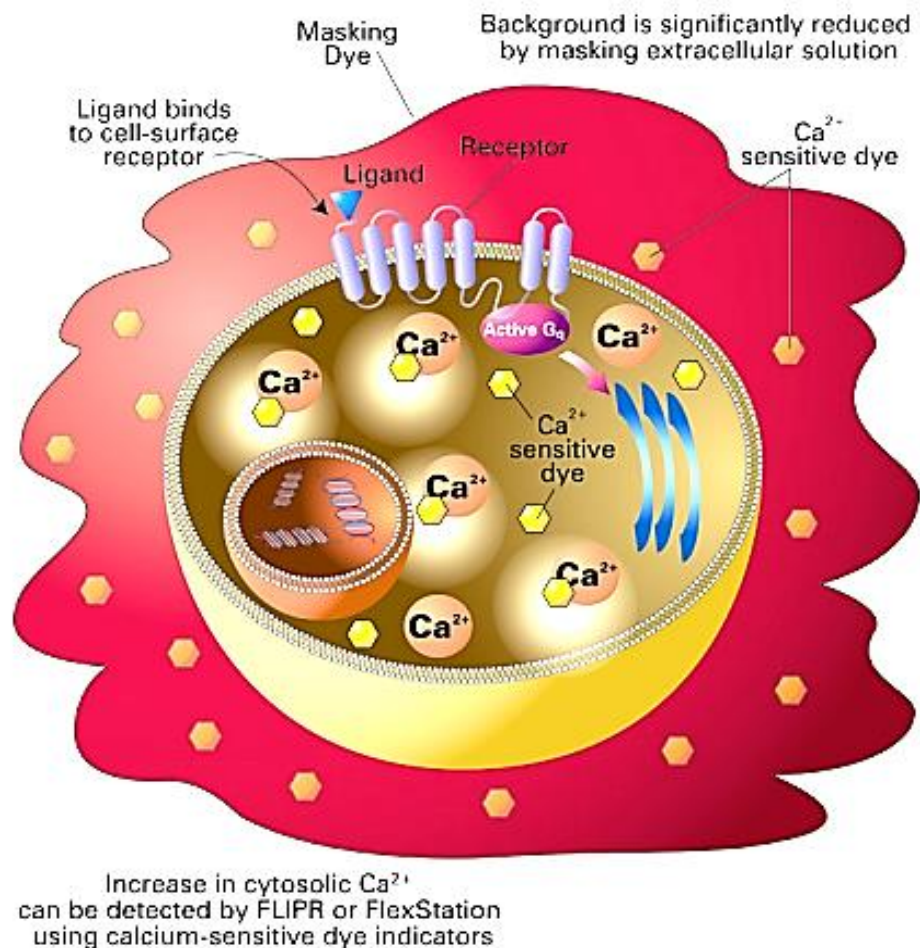


Figure 22 basic principle of calcium flux assay. Picture adopted from www.moleculardevices.com

3.3. Characterization of CCR7 Receptor expression using Western blot.

Western blot or immunoblotting is a powerful technique used in cell and molecular biology to identify, in qualitative and semi quantitative way, specific proteins in a given sample based on their size ¹²⁹. Western blotting is different from Southern and northern blotting which are based on detecting specific fragments of DNA and RNA sequences respectively. Western blot technique uses electrophoresis to identify mixtures of proteins based on their molecular weight ¹³⁰. In this study, we used Western blot in order to investigate and evaluate expression of CCR7 receptor in a panel of in house tumour cell lines and to compare our result with those reported in literature to have CCR7 receptor expression. So, human caucasian colon adenocarcinoma (SW620) ¹³¹, human breast cancer cell line (MDA-MB-231) ¹³², human primary glioblastoma cell line (U-87 MG) ¹³³, human prostate cancer cell lines (DU-145) ¹³⁴, human prostate cancer cell lines, (PC-3) ¹³⁵, human colon adenocarcinoma (DLD-1) ¹³⁶, human breast cancer cell line (MCF-7) ^{137 138}, Drug resistant human breast cancer cells (MCF-7/ADR) human colorectal adenocarcinoma cell line (HT-29) ¹³⁹ and human umbilical vein endothelial cells (HUVECs) ¹⁴⁰ were selected and screened for CCR7 receptor expression. β -Actin was used as loading control, which is commonly used for western blot. If the expression of β -actin shows an equal loading, we can assume the equal loading of protein and hence we estimate the comparative expression of CCR7 receptor on these cell lines. Results obtained from cell lines screening for CCR7 receptor expression and β -Actin were broadly in agreement with literature findings. **Figure 23** below shows cell lines with CCR7 protein expression. The amount of CCR7 protein expressed was determined based on the intensity of the band obtained. MCF-7

and DU-145 cell lines appear to have high expression of CCR7 receptor compared to the rest of the cells. The assay was repeated at least three times to confirm results. These findings were also confirmed in a different study using knocked down CCR7 receptor in human oral squamous cell carcinoma cells (OSC-19) as a negative control to make sure the antibody used in the assay is specific for CCR7 receptor. With exception of knocked down OSC-19 cells, all other tested cell lines showed CCR7 receptor expression. This was carried out by Mrs Haneen Basheer as part of her PhD project whilst in our research group.

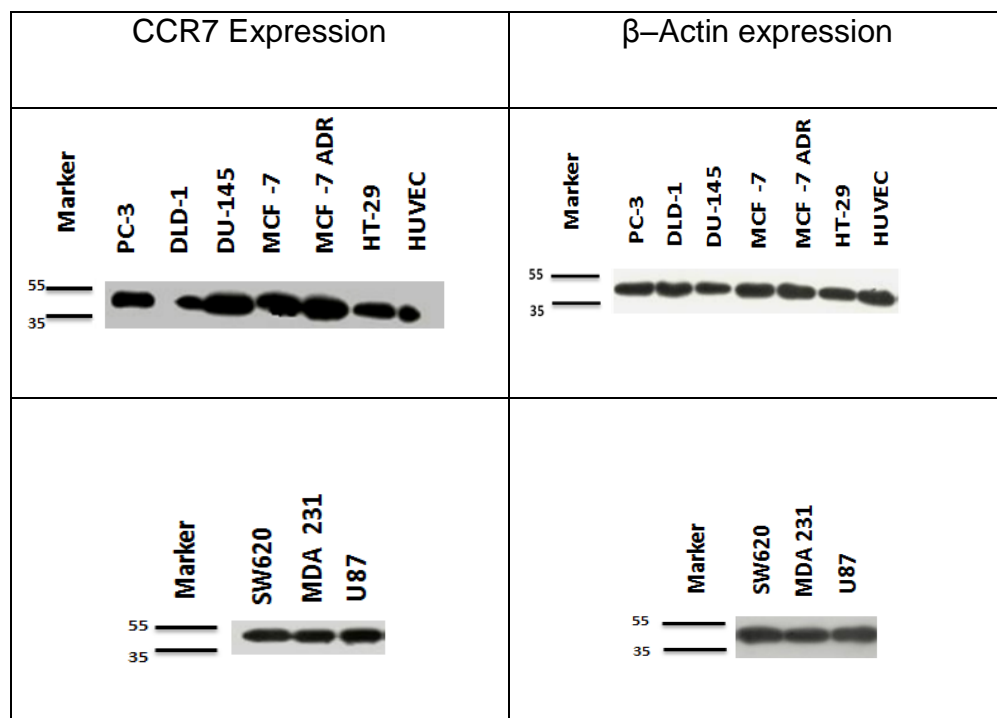
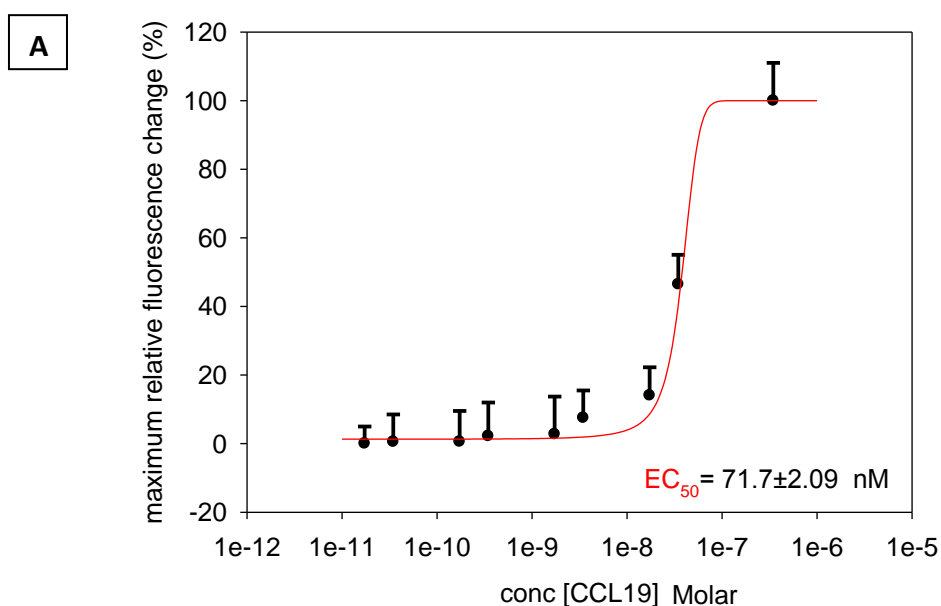


Figure 23 Expression of CCR7 receptor protein in a panel of human cancer cell lines by western blot. β -Actin was used as loading control. (We thank Dr Hanadi Talal for help in the execution of this experiment)

3.4. Determining the efficacy of the agonist

Initially, we wanted to determine from results obtained above which cell line has good response to ligand and hence mobilize calcium efficiently from internal stores. We also wanted to determine the effective concentration of the ligand required for optimum performance of the assay. The reason this is practically important is that in determination of potency of an antagonist, the assay detects absence of fluorescence. Therefore, we wanted to use a cell line in which the fluorescent response to the chemokine ligand is high so that changes can be more accurately determined. We decided to choose cell lines which were confirmed expression of CCR7 receptor using Western blot. The ability of these cells to release calcium ions upon interaction between receptor and ligand is measured by calcium flux assay. Functional assay is always a way to determine the involvement of the receptor in response to cellular pathway. CCL21 and CCL19 are both ligands for the CCR7 chemokine receptor. We decided to determine the effective concentration EC_{50} of both ligands, CCL21 or CCL19, to be used during the assay. Different serial dilution of both ligands were applied to cells containing dye using Fluoroskan Ascent FL instrument (ThermoScientific) in order to obtain dose dependant curve (see below). Cells were first optimized at 5×10^5 cells per well just to cover the well bottom as a monolayer. Cells were left to attach overnight in 10 % FCS containing medium at 37 °C. Medium was removed completely so that we make sure the ligand will not be diluted as this will affect the whole analysis. The dye was then added per well and the plate incubated half an hour before using the Fluoroskan Ascent FL instrument (ThermoScientific) to measure fluorescence emitted. Serial dilution of both ligands were prepared and applied to the plate respectively. The

fluorescence emitted as a result of calcium mobilization upon binding of the ligands with their CCR7 receptor is measured and plotted (**Figure 24**). All EC_{50} obtained are calculated automatically using sigmaplot software. Although the intensity of Western blot bands obtained for both cell lines, MCF-7 and DU-145, are higher than the intensity band of U87-MG cell line, U87-MG cells were found to have better response to the ligand than MCF-7 and DU-145. This might be due to that although these two cell lines have high expression of CCR7, the protein is mostly present in the cytoplasm rather than cell membrane. Western blot assay based on disruption of the outer cell membrane and hence the expression measures both proteins inside the cells and cell surface. U87-MG cells, showed good responses to both ligands, CCL21 and CCL19. It was reported in literature that CCL21 ligand appears to have higher affinity to bind with its receptor than the CCL19⁹⁶. This was confirmed in our assay as illustrated from **Figure 24** below, CCL21 showed higher activity than CCL19.



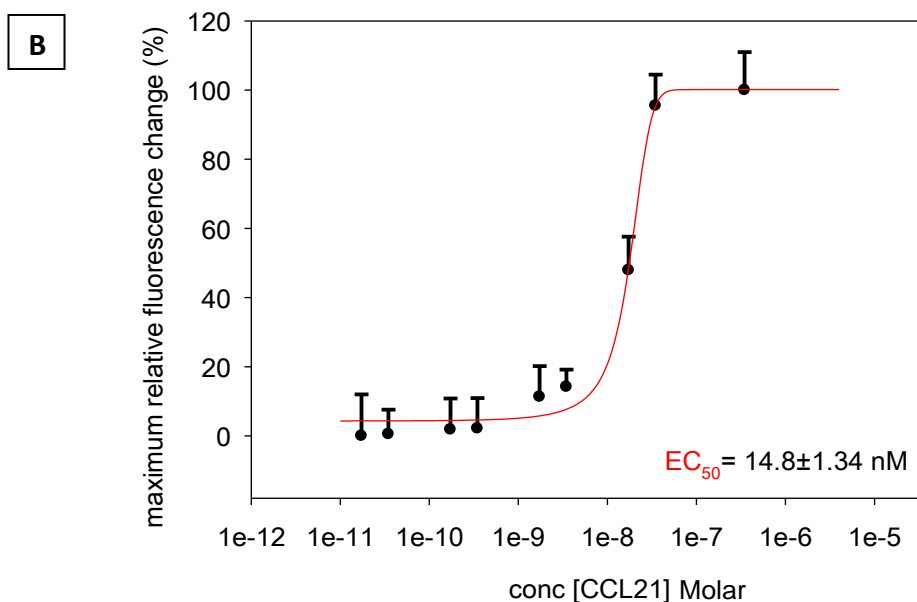
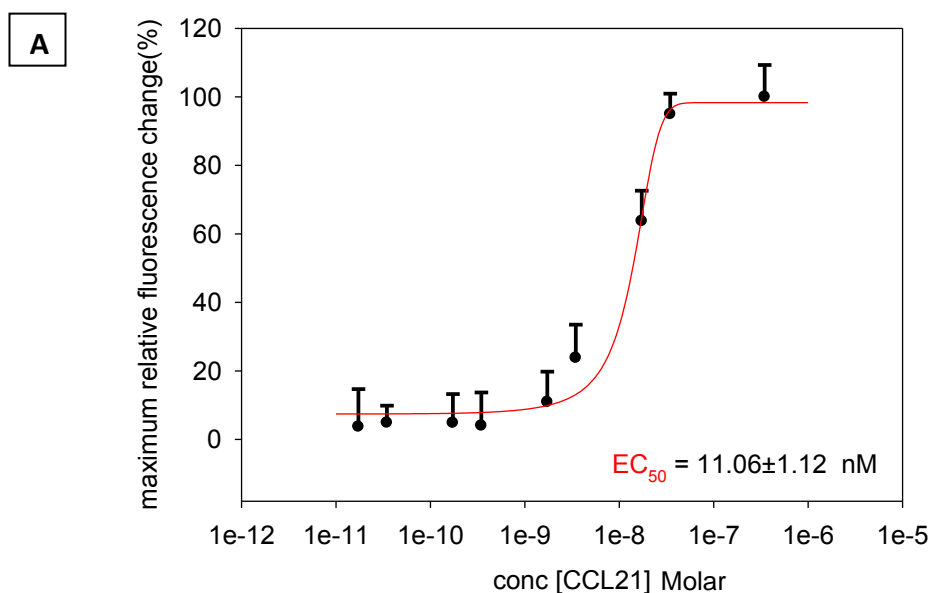


Figure 24 CCL19 (A) and CCL21 (B) Dose Response Curve using U-87 MG. The curves were obtained by three *in vitro* experiments. Mean \pm SD of triplicate determination is given.

The CCL21 EC_{50} was at $14.8 \pm 1.34 \text{ nM}$ compared to CCL19 which was $71.7 \pm 2.09 \text{ nM}$. It was therefore decided to use CCL21 instead of CCL19 through all our assays. However, we observed that there was variability of the fluorescent obtained from one well to another. U87-MG cells are astrocyte and we felt that some of the problems we experienced in result variability were due to the lack of a uniform monolayer of the cells. To provide a robust assay for evaluating our antagonists, we tested a number of other cell lines. At this stage, it was decided to use flow cytometry techniques which can be adapted to detect expression of proteins on the cell surface. Therefore, flow cytometry is advantageous over Western blot and would avoid problems we had. Concurrent studies in our research group using flow cytometry, indicated that the CCR7 receptor is highly expressed in human pancreatic carcinoma, epithelial-like cell line (Panc-1) and human oral squamous cell carcinoma cells (OSC-19)

(Appendix II). Also, a review of the literature, indicated that, human T cell lymphoblast-like cell line (CCRF-CEM) ¹⁴¹ showed high expression of the CCR7 receptor. These cell lines were also tested by Mrs Haneen Basheer using Western blot assay which confirmed expression of CCR7 receptor. Initially, we tested Panc-1 and CCRF-CEM cell lines to determine whether the response of those two cell lines are better than U-87 MG, or indeed that the fluorescence variation was less pronounced. So, serial dilution of CCL21 ligand concentrations were used as before and the response curves obtained from both cell lines were similar to ones obtained with the U-87 MG. We only used CCL21 ligand in this assay because it's more potent than CCL19 as described in previous result. As illustrated in **Figure 25** below, the half maximum effective concentration (EC_{50}) was obtained around at 11.06 ± 1.12 nM and 15.03 ± 1.89 for CCRF-CEM and Panc-1 cell lines respectively.



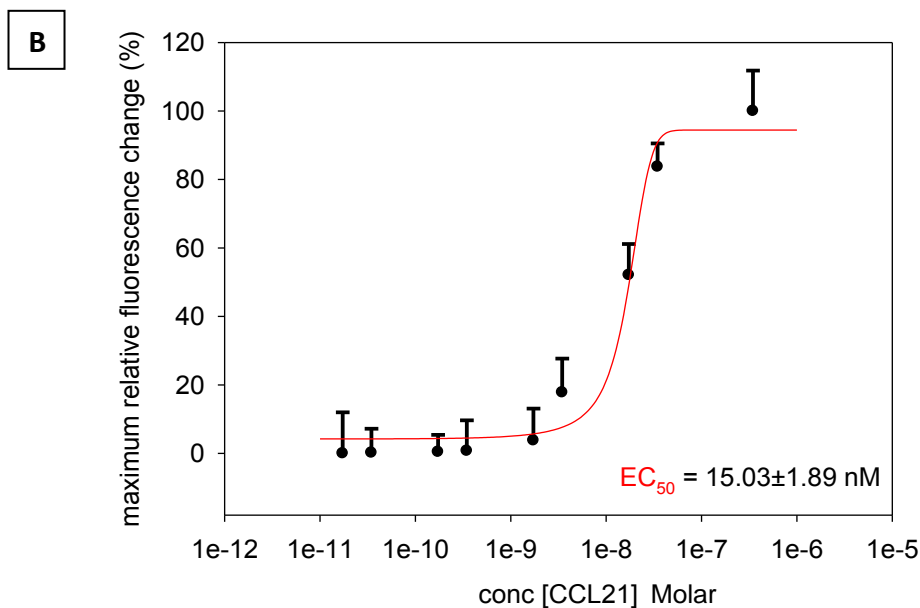


Figure 25 CCL21 Dose Response Curve using (A).CCRF-CEM and (B). Panc-1 cells. The curves were obtained by three *in vitro* experiments. Mean \pm SD of triplicate determination is given.

However, after analysis of the data, there was still some variations in fluorescence obtained and hence make different response from one well to another. The fluorescent variation was not that significant but we wanted to make sure the variations as small as possible. Further investigations took place using OSC-19 cells to ascertain if it would afford less fluorescent variability in our results. OSC-19 cells produce a very consistently uniform monolayer, which covers the wells completely; so we decided to try these cells and determine if we could reduce the variability we experienced with previous attempts. Full dose response curve were performed for both ligands CCL21 and CCL19, and we were satisfied that we obtained the most consistent results, with little variability. **Figure 26** below shows the full dose response curve of both ligands using OSC-19 cell lines.

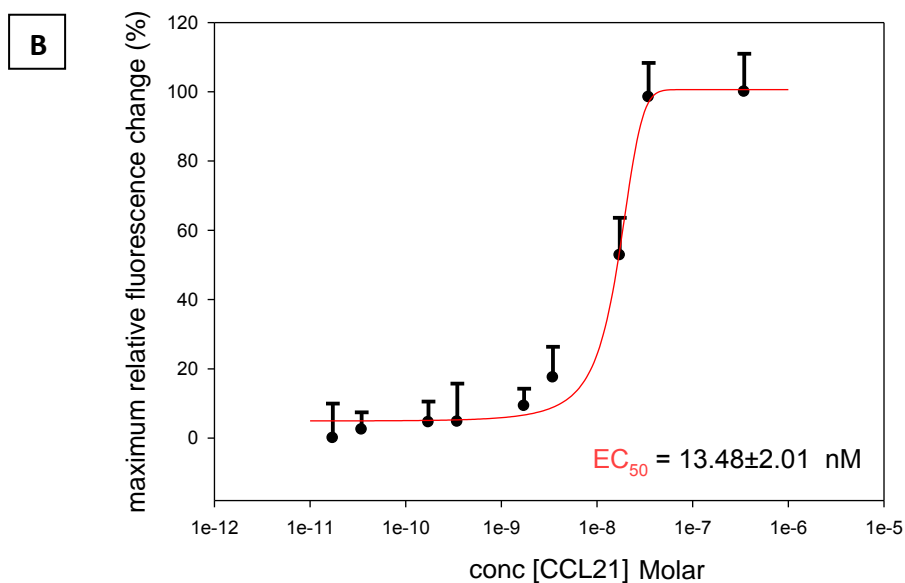
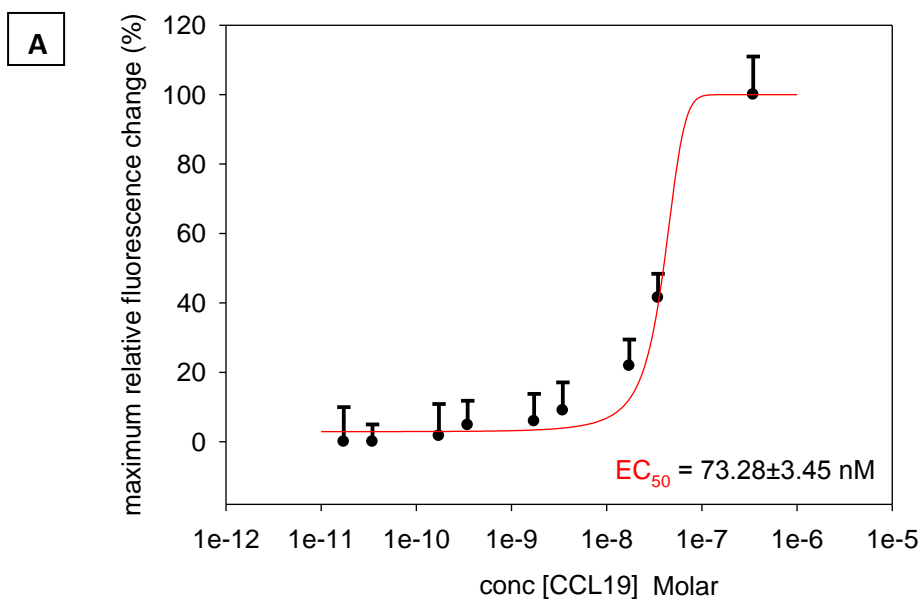


Figure 26 CCL19 (A) and CCL21 (B) Dose Response Curve using OSC-19 cells. The curve were obtained in three *in vitro* experiments. Mean \pm SD of triplicate determination is given.

The EC_{50} obtained from treating OSC-19 cells with CCL21 and CCL19 ligands were around $13.48 \pm 2.01 \text{ nM}$ and $73.28 \pm 3.45 \text{ nM}$ respectively, which were comparable with previous results. It was concluded from the results obtained

above that CCL21 is more active and potent than CCL19, so CCL21 was considered as a ligand to be used for further analysis. The minimum concentration required to achieve maximum response in the assay was estimated at 100nM. It was therefore decided that OSC-19 cell line will be used to test the efficacy of compounds because these cells showed the least variation obtained from the data analysis. So far, we have the cells, we know what ligand to use and we know the effective concentration to be applied in the assay. The next aspect to investigate was if the percentage of the Foetal Calf Serum (FCS) in the medium used would have an effect on the ability of the cells to respond in the calcium flux assay. According to the manufacturer's instructions for Fluo-4 NW calcium flux assay protocol, 10% FCS is used when culturing cells into 96-well plate ¹⁴². However, we felt it worthy to try if culturing these cells with 0% FCS, would stress the cells into producing more CCR7 and thus improve the response toward the ligand, CCL21. 96-well plate was cultured with OSC-19 contain 10% and 0% FCS and left over 24 hours in the incubator. The next day medium was removed, dye added and the ability of cells to mobilize calcium ion were tested using 100nM CCL21 ligand. The test was repeated at least three times to confirm findings. The result shown below illustrates that the response of OSC-19 cells toward the CCL21 ligand did not change **(Figure 27)**. So, it was decided to use 10% FCS during the whole process to follow the manufacturer's instructions and also to make sure the cells were attached perfectly to the bottom of the wells. So, CCL21 ligand was used at 100nM concentration using OSC-19 cell line, which express CCR7 receptor, and the medium should contain 10% FCS.

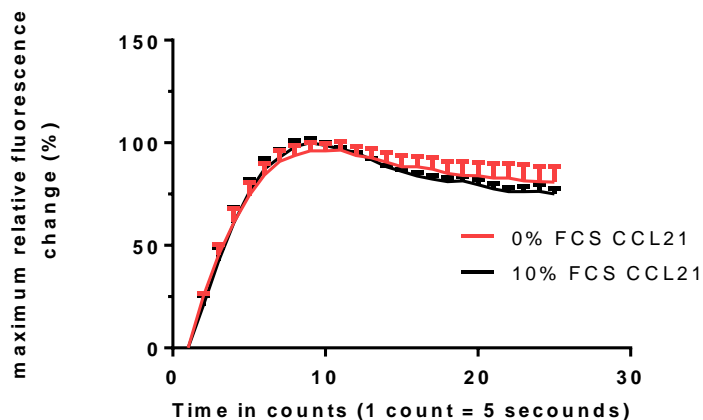


Figure 27 Calcium mobilization using OSC-19 cells contain 10%FCS and 0% FCS. The curves were obtained in three *in vitro* experiments. Mean \pm SD of triplicate determination is given.

3.5. Determining the efficacy of the antagonists

The optimised calcium flux assay, described above, was used to determine the efficacy of the antagonists described in chapter 2 to examine their ability to block CCR7 receptor. If the antagonist is potent, it will block the effect of the ligand (CCL21) on the receptor, so the amount of fluorescence emitted would be reduced. With this in mind, the first synthesised compounds, **3**, ICT5888 and **1**, ICT5189 were tested to check their activity against CCR7 receptor. (Note: all antagonist data and IC_{50} curves are available in the **Appendix I**). Different antagonist concentrations were prepared in order to have full dose dependent concentration and hence we could conclude the half maximal inhibitory concentration (IC_{50}) which measures how effective the drug is. A stock solution of each compound was prepared by dissolving known amount of compound in DMSO which was then diluted so that the amount of DMSO is not toxic to the cells in the top concentration of antagonist. The top concentration of the antagonists used in the well after addition of the ligand was 142 μ M. We wanted

to make sure the effect that we got is actually directly from the antagonist used and not because of the toxic effect of DMSO. The final percentage of DMSO used in our top concentration (142 μ M) was 0.14% which gets even more diluted in the next serial dilution. Some cells are too sensitive and respond differently toward DMSO. To confirm that the response we got from OSC-19 cells (which express CCR7 receptor) was not affected by DMSO, control wells were used containing corresponding quantities of DMSO and buffer without the antagonist, which then were treated with the cognate ligand. No reduction of fluorescence was observed with all wells which contain the same percentage of DMSO and have no antagonist. This reflects the amount of DMSO used in our top antagonist concentration is not toxic to the cells especially we only incubate the antagonists solution with the cells for half an hour at 37 °C which is relatively short period. Since the assay looks for absence of fluorescence, an important consideration in interpreting any reading in this assay is purely derived from antagonism and not from other factors that can lead to absence of fluorescence, such as cell death at the concentrations used. Therefore, a chemosensitivity assay (MTT based method) was carried out for different molecules and our top active molecules. The MTT based assay is the most commonly used assays for the detection of cytotoxicity following exposure to toxic compounds ²⁶. The results obtained from the MTT cytotoxicity assay was done on dose dependant response. This was carried out by Mrs Haneen Basheer as part of her PhD project whilst in our research group. It was established from these studies that concentrations used in this assay were not toxic to cells (**Appendix III**). Before carrying out the assay, we determined that the compounds were highly pure using Liquid chromatography–mass

spectrometry (LC-MS), melting point and Nuclear magnetic resonance spectroscopy (NMR) (see experimental). All tested compounds must show highly purity otherwise the impurities would have an effect on cells and hence will affect the result obtained. We then prepared the required serial dilutions of antagonists which were similarly prepared from the corresponding stock solutions by adjusting the second dilution by assay buffer as required. OSC-19 cells were first plated into 96-well plate overnight to give enough time for cells to attach to the bottom of the wells, medium was then completely discarded and replaced with Fluo-4 NW dye loading solution and the plate was incubated half an hour. Antagonists serial dilutions were then added to wells whilst some wells were left as control in order to measure the fluorescent obtained from cells in presence and absence of the antagonist. The most potent compound was always included in the assay as a reference to determine the effectiveness of the other tested compounds. The plate was then incubated another half an hour before taking to Fluoroskan Ascent FL instrument (ThermoScientific). After, it was transferred into a Fluoroskan Ascent FL instrument and the fluorescence in response to the addition of 20 μ l CCL21 (100nM) was measured at room temperature. In order to run the calcium flux assay more time efficiently, we first tested compounds using two different concentrations of each compound and compared together with the lead compound, **3**, ICT5888, at identical experiment conditions and if we observe good activity, we carry out full concentration dependant response to get IC₅₀ value. All runs were done at least in triplicate (n \geq 3). All data and IC₅₀ values obtained in this assay was analysed using Prism software.

In order to proof that the most active compound is active against CCR7 receptor, we evaluated its potency using different *in vitro* techniques like “agarose spot assay” (see below) and scratch assay (**Appendix IV**). Initially, we modified the existing under agarose assay to fulfil our demand and then we applied the configured under agarose assay to investigate activity and selectivity of the top active compound toward multiple chemokine receptors. We also applied these modification to compare activity of our top active compound with much less active compound against CCR7 receptor.

3.6. Agarose spot method for *in situ* analysis of chemotactic responses to multiple chemoattractants.

3.6.1. Introduction

As discussed previously, chemokines play vital role in cell migration and invasion. However, the pharmacology of the chemokine system can be complex. The chemokine system comprises almost 50 chemokines divided into four subfamilies (CXCL1-18, CCL1-CCL28, XCL1-2, and CX₃CL1) which bind and activate 18 chemokine cell surface receptors (CXCR1-6, CCR1-10, XCR1 and CX₃CR1) and four atypical receptors (ACKR1-4) ¹⁴³. Although a number of chemokine receptors are selectively activated by a single chemokine (such as CXCR4, which is activated by CXCL12), there is generally speaking a significant degree of promiscuity between ligands and receptors in the chemokine system. In other words, some chemokine receptors are activated by more than one chemokine (for example CCR7 is activated by CCL19 and CCL21), in addition, the same chemokine can activate more than one chemokine receptor (for example CCL2 activates both CCR2 and CCR4) ¹⁴⁴.

These issues highlight the need for protocols to assess the chemotactic responses to multiple chemoattractants, or through multiple chemotactic receptors. There are of course, a number of protocols to study cell migration and chemotaxis in response to a single chemoattractant. They include methods using Boyden chamber ¹⁴⁵, Zigmond chamber ¹⁴⁶, Dunn chamber ¹⁴⁷, Insall chamber ¹⁴⁸ and under-agarose method ¹⁴⁹. However, none of these methods is yet adapted for investigation of cellular migration in response to multiple chemokine axes. Our group previously developed the agarose spot assay. The experimental configuration of the assay is as follows: two agarose drops contain one chemokine ligand and other two drops contain control, phosphate buffered saline (PBS). The drops were applied to a glass bottomed petri dish as a spot which is allowed to solidify and then immersed under media containing cells (Figure 28).

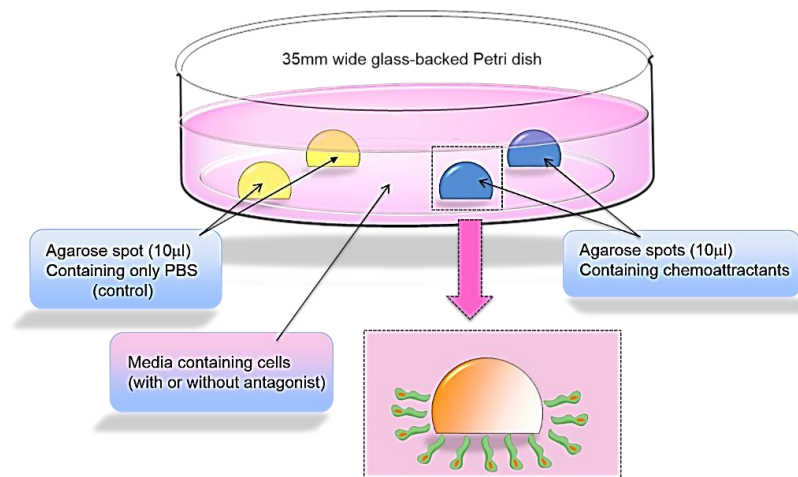


Figure 28 Schematic representations of a glass backed 35 mm petri dish. Two agarose drops containing the same chemoattractant, and two agarose drop as control (original design) ¹⁵⁰. (Picture reproduced courtesy of Dr. Victoria Vinader).

Over time, chemokine molecules slowly leach out from the agarose spot, creating a transient gradient. Cells which contain the cognate chemokine receptors respond to the chemokine and migrate against this gradient towards

the spot and eventually migrate under the spot. The evaluation of the number of cells and the distance they travel under the spot provides quantitative information on the chemotactic aptitude of cells towards chemokines. The media can be supplemented by small molecule antagonists, or other agents, which can modulate this chemotactic response ¹⁵⁰. In this method, we will discuss a modification to the configuration of this assay which permits the time-dependant analysis of cell migration in response to multiple chemokines at the same time. We will study the chemotactic aptitude of different cell lines towards different chemoattractants under identical experiment conditions. We will also evaluate the reduction of cells migration toward agarose spots contain chemoattractants by antagonists. The effectiveness of compound **75** as CCR7 antagonist will be evaluated under agarose spot assay and compared to much less active compound **3**. The selectivity of compound **75** will be investigated against two different receptors, CCR7 and CXCR4. We used CXCR4 receptor in this study because it is very important in dual CXCR4 and CCR7 antagonism. This is evident by clinical observations which support the hypothesis that the CXCR4 and CCR7 axes may work in tandem to promote the dissemination of cancer. For example, co-expression of CXCR4 and CCR7 in breast ¹⁵¹, cervical ¹⁵², thyroid ^{153,154}, and gastric ¹⁴ correlates to poorer prognosis and exacerbated metastasis compared to expression of either receptor alone. These observations highlight that in these cancers, dual CXCR4 and CCR7 antagonism may be more beneficial than antagonism of either alone. Therefore, an experimental setting that allows the investigation of CXCR4 and CCR7 antagonism at the same time is extremely appropriate. This assay can be adapted to other chemoattractants/receptor pairs; however for the purpose of

this research, we have concentrated on CCR7/CCL21, CCL19 and CXCR4/CXCL12. We investigated CXCR4 and CCR7 expression and antagonism using the same experiment condition. In this assay we used four agarose drops per petri dish, however more drops can be applied in order to compare more chemokine receptors at the same time. Four agarose spots were used and each spot contains different chemokine ligand and the last drop was used as control. The experimental configuration of the assay is as follows: the first agarose spot contain CXCL12 (ligand for CXCR4), the second agarose spot contain CCL21 (ligands for CCR7), the third agarose spot contain CCL19 (ligands for CCR7) and the fourth agarose spot contain control, PBS (no chemokine). 100 mg of low-melting point agarose was dissolved into 20 ml of PBS to make a 0.5% agarose solution. This percentage of the agarose used in the assay is very important, higher or lower agarose percentage will make the agarose drop harder or softer and will affect the whole process of cell migration. The agarose solution was heated until complete dissolution and was left to cool down to 40 °C. This temperature is critical, if the temperature was higher than this, the agarose drop will melt down quickly on the glass bottom petri dish and if the temperature is lower than this, the agarose drop will solidify quickly and will not attach properly on the glass bottom petri dish. So once the temperature of the agarose solution is at 40 °C, a stock solutions of the known chemokines concentrations were prepared and mixed with known amount of agarose solution. In this configuration, three different chemokines stock solutions were prepared, CXCL12, CCL21 and CCL19 (see experimental) and then mixed with known amount of PBS contain melted agarose at 40 °C. The chemokine concentration embedded in the agarose spot was optimized by applying

different range of concentration dilution mixed with the agarose drop. The chemokine ligand concentrations used for the optimization process in this assay were 1nM, 100nM, 200nM and 1 μ M. The optimum results obtained when 100nM was utilised. Namely, no migration was noticed using the lowest concentration, and we observed that the drops “exploded” using the highest concentration of 1 μ M in the majority of occasions. So, the chemokine concentration embedded in the agarose spot was used at 100nM for the three ligands used. The fourth spot was used as control, PBS was added instead of using chemokine ligand. The control spot was used in purpose to compare cells migrations between PBS containing spot and chemokine ligands containing spots. The spots can be identified by writing on the backside of the glass, using a marker pen, a cross was drawn on the back of the plate to form four quadrants, one for each of the four spots (**Figure 29**).

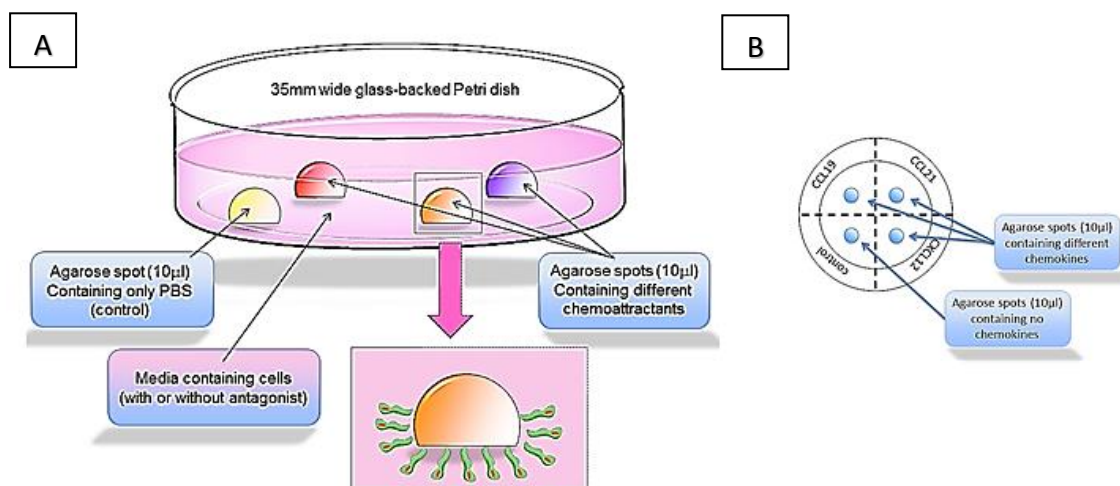


Figure 29 Schematic representations of a glass backed 35 mm petri dish: **(A)** Modifications carried out in this thesis with three agarose drops containing different chemoattractant, and one agarose drop as control. **(B)** A picture of glass back petri dish with agarose drops, showing marking. (Picture reproduced courtesy of Dr. Victoria Vinader).

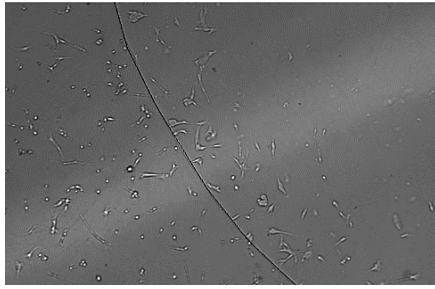
The petri dish containing the spots was then cooled for exactly 5 minutes in a 4 °C fridge to allow the agarose spot to set. Again this step is critical, if the agarose spots left in fridge for more than 5 minutes the drop will solidify harder and this will make it very difficult for cells to crawl under the spot. Once the spots have solidified, 1 ml of cell suspension in 10% FCS media, either containing the antagonist, or control (no agent), was plated into the dishes which were then incubated at 37 °C to allow the cells to adhere. We started our optimization steps using U-87 MG cell line and then different cell lines were utilized for our study, this will be highlighted further in this assay. Cells density used was optimized at 6.0×10^4 /ml as a starting point, but this can be adjusted based on cell type. After 4 hours incubation, the culture media was replaced with 0.1% FCS, either containing the antagonists or no reagent (as control), and the dish was returned to the 37 °C incubator. Initially, we require 10% FCS media, to ensure good cell adhesion, however, after 4hrs, we change to 0.1% FCS, the purpose of the media change is to ensure no cell proliferation during the overnight incubation period, in order to ensure that what we see is cell migration, rather than cell number growth. Cells were originally plated in medium containing 10% FCS without changing to 0.1% FCS medium and found cell number increased tremendously and this would affect the analysis process. So, we introduced the 0.1% FCS medium after the cells were attached, but this step, inherently includes the extra step of changing the media. We attempted to avoid disturbing and moving of petri dish after 4 hour incubation, by plating cells in medium containing 0.1% FCS from the beginning; however, analysis after 16 hours showed that the cells were not properly attached to the plate and this affected the cell migration process. In this experiment, we tried different types of

disposable glass-bottomed plastic, however 35mm petri dishes with lid from iBidi (Glasgow, United Kingdom) were found to be the best for cells to attach and migrate toward agarose spots. After 16 h, the agarose spots were analysed by counting total number of invading cells using LumaScopes 500. Six fields of view of equal size were photographically captured using LumaScopes 500. The edges of the spots are clearly discernible in the photographs and the cells migrating under the spots are easily distinguishable from those which are not. Cells which tend to migrate or travel as group were quantified by measuring the percentage of cell-covered area. This is done by measuring the distance travelled between migrated cells and the edge on the agarose drop using Fiji/ImageJ software ¹⁵⁵. In contrast to cells travelling in group, number of cells moving individually under the spot was determined using the same software. Migrated cells were highlighted and separated from the resting cells using segmented line selection tool, the image was then processed by converting it to a binary. Cells were counted by an automatic particle analysis. The number of cells in each of the six fields were counted and summed up to give the total number of cells under the spot. Cells can also be individually counted but we found no significant improvement to the results compared with the image analysis software. In order to make direct comparison between cells which travel as group and cells which travel as individual, we used relative chemotaxis index (RCI) of cells. This index provides direct comparison between the chemotactic aptitudes towards different chemokines in comparison to the chemotactic aptitudes towards CXCL12. A RCI of 1 correlate to cells with chemotactic aptitudes similar to that towards CXCL12, whereas RCI of 0 correlate to cells with low chemotactic aptitudes. We also recorded a time-lapse

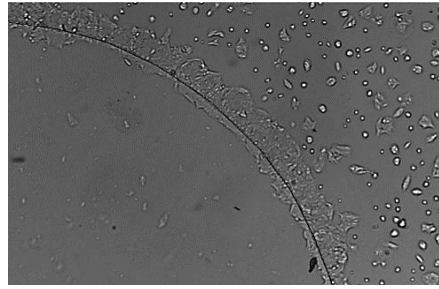
imaging for cells migrating toward the agarose spot overnight using Nikon Eclipse TEZ000-U confocal microscope showing the agarose spot method. Images obtained were analysed by Fiji/ImageJ software. This short film clearly shows the cells moving towards the chemokine containing spot and is included in a CD attached to the thesis. Data is presented as the mean \pm SE of at least 3 independent experiments.

3.6.2. Results and Discussions

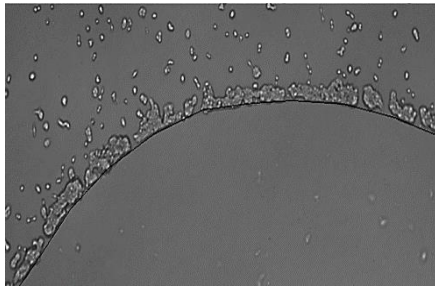
In order to compare the chemotactic aptitude of different cell lines towards chemoattractant, we required cell lines with contrasting expression of the chemokine receptors CXCR4 and CCR7, and responsiveness to their cognate ligands. Cells were screened from our cell bank for the expression of chemokine receptors CCR7 and CXCR4 using Western blot (**Figure 23**) and flow cytometry (**Appendix II**). Based on the results obtained, a number of CCR7 and CXCR4 expressing cell lines were selected and tested under the agarose spot assay. Initially, human primary glioblastoma cell line (U-87 MG), human colon adenocarcinoma cell line (DLD-1) and human colorectal adenocarcinoma cell line (HT-29) cell lines were selected to be used for the agarose spot assay. Cells were allowed to migrate under agarose spots contain CXCL12 (ligand for CXCR4), CCL21 (ligands for CCR7), CCL19 (ligands for CCR7) and control, PBS under identical conditions (**Figure 30**). The spots were visualized and analysed after 16 hours of incubation at 37 °C.



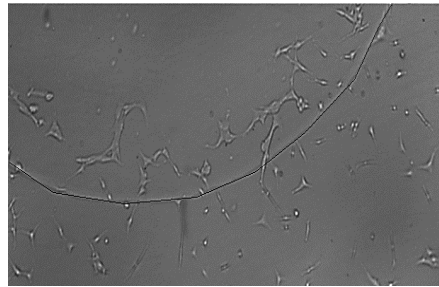
(A) U87-MG cells (CCL21 100nM, 16hr)



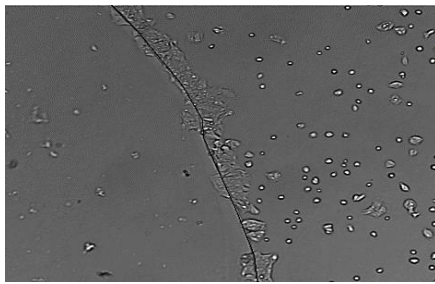
(B) DLD-1 cells (CCL21 100nM, 16hr)



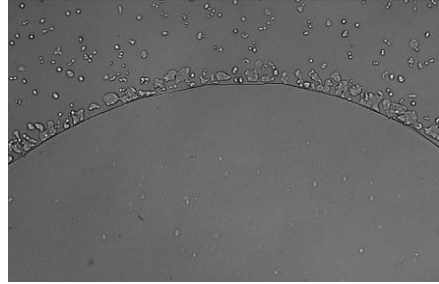
(C) HT29 cells (CCL21 100nM, 16hr)



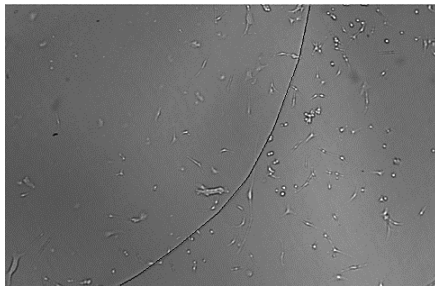
(D) U87-MG cells (CCL19 100nM, 16hr)



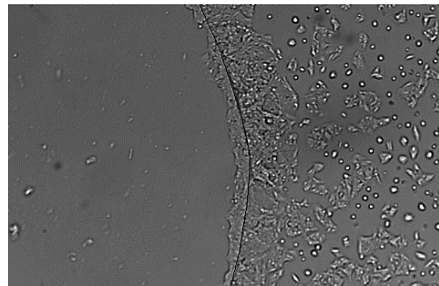
(E) DLD-1 cells (CCL19 100nM, 16hr)



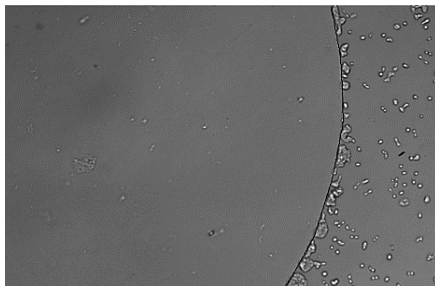
(F) HT29 cells (CCL19 100nM, 16hr)



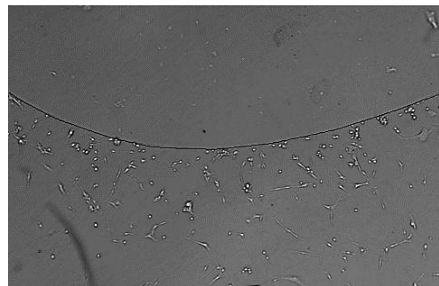
(G) U87-MG cells (CCL12 100nM, 16hr)



(H) DLD-1 cells (CCL12 100nM, 16hr)



(I) HT29 cells (CCL12 100nM, 16hr)



(J) U87-MG cells (PBS, 16hr)

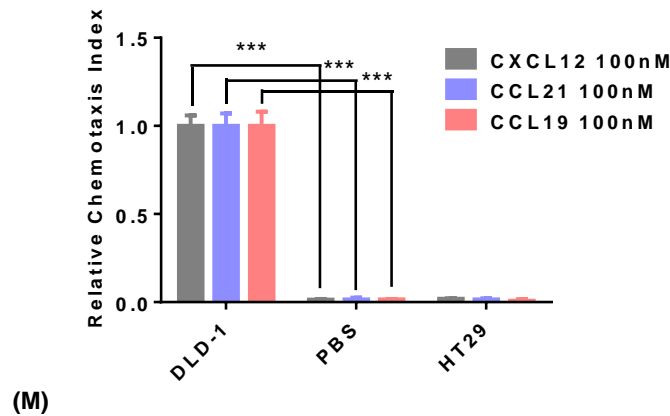
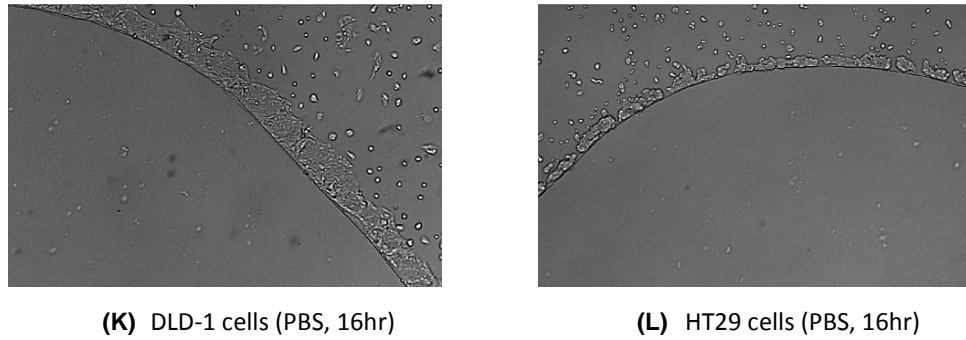


Figure 30 Cells migrate under the agarose spot containing a chemokine (A), (B) and (C) represent U87-MG, DLD-1 and HT29 cells migrating toward drop containing CCL21, 100 nM. (D), (E) and (F) represent U87-MG, DLD-1 and HT29 cells migrating toward drop containing CCL19, 100 nM. (G), (H) and (I) represent U87-MG, DLD-1 and HT29 cells migrating toward drop containing CXCL12, 100 nM. (J), (K) and (L) represent U87-MG, DLD-1 and HT29 cells migrating toward drop containing PBS. (M) Relative chemotaxis index of PC-3, DLD-1 and HT29 cells migration under agarose spots. Data is presented as the mean \pm SE of at least 3 independent experiments.

With the exception of HT29 cell line, cells migrated under the spots which contain the cognate ligands and no migration was observed in the control spot which contain PBS. Although, expressing the receptors, U87-MG and DLD-1 were not included for further investigations. U-87 MG cells are astrocytes and were very challenging to count individually, as it is difficult to tell when one cell finishes and the next one starts without further staining (eg. using DAPI to stain the nuclei) which will inherently include an extra step to the assay. **(Figure 30).**

DLD-1 cells were also excluded from further investigation because we were looking for cells which are able to migrate as individual so it would be easier to count them. HT29 cell line was also excluded from further investigation because no migration was noticed, although they express CCR7 and CXCR4 and this suggests that this cell line has too little migratory activity, which was reported in literature ¹⁵⁶. Further results obtained from our cell bank screen indicated that human prostate cancer cell line, PC-3 express high levels of both CCR7 and CXCR4 (**Appendix II**). PC-3 cells also have the ability to travel and evade individually and not as group. This will allow us to easily count the cells and quantitatively assess the responses for both receptors. In addition, we found human colorectal cancer cell line (SW480) do express CXCR4, however their expression of CCR7 is low or negligible (**Appendix II**). Therefore, we set out an intracellular calcium mobilisation (calcium flux) assay to assess PC-3 respond toward both ligands CCL21, CCL19 and CXCL12 (ligands for CCR7 and CXCR4 respectively). PC-3 cells were plated and left to attach to the 96-well plate bottom overnight incubation with 10% FCS containing medium. Medium was discarded totally the day after, so the ligands will not become diluted, and was replaced with Fluo-4 NW dye loading solution and the plate was incubated half hour before taking to the Fluoroskan Ascent FL instrument (ThermoScientific) to measure fluorescent emitted upon binding ligands with their receptors. Each ligand was added separately and washing buffer was used to remove any ligand traces before addition of the next one. The fluorescence in response to the addition of the chemokine (to give 100nM in-well concentration) was measured at room temperature (Ex 485 nm, Em 538 nm). The ligands concentration used in this assay was 100nM in the well, same calculation used

before in this chapter was applied in this assay. **Figure 31** below illustrates the response of CXCR4 and CCR7 receptor upon interaction with their cognate ligands.

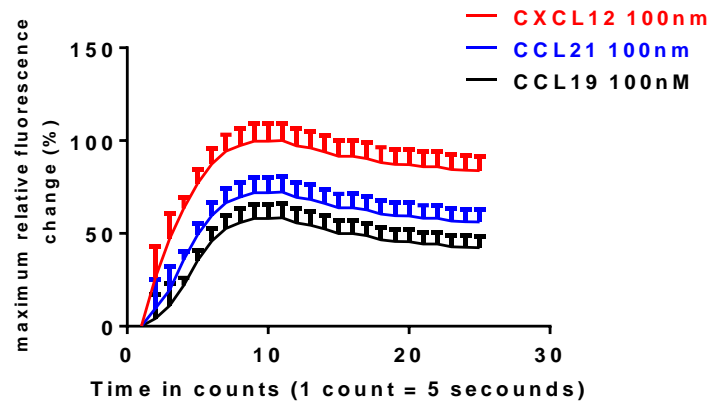
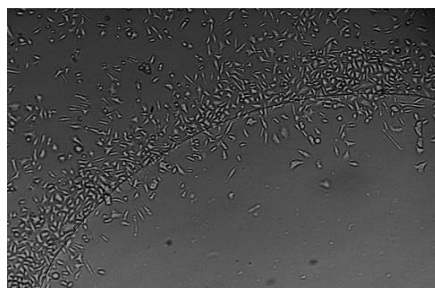


Figure 31 Calcium Flux Mobilization charts comparing response of CXCR4 and CCR7 receptors toward their cognate ligands using PC-3 cells. Data is presented as the mean \pm SE of at least 3 independent experiments.

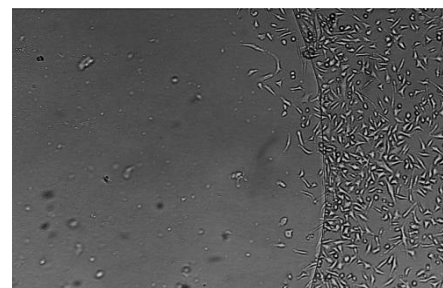
We found that PC-3 cells responded to both CCL21, CCL19 and CXCL12 (**Figure 31**). Interestingly, we observed that PC-3 cells responded with high fluorescence emitted upon interaction with CXCL12 ligand than the response obtained upon interaction cells with CCL21 ligand and the least response was noticed upon interaction cells with CCL19 ligand. We thought this might correlate to the level of chemokine expression. This was confirmed using flow cytometry assay within our research group which revealed higher expression of CXCR4 receptor in PC-3 cells than CCR7 receptor (**Appendix II**).

Migration under agarose spot correlates to the expression level of chemokine receptor

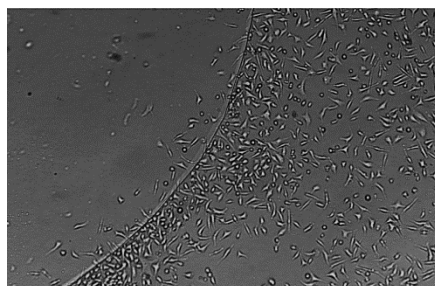
As indicated above, PC-3 cell line was shown to respond to calcium flux assay for both CXCR4 and CCR7 receptors. Therefore we carried out the agarose spot assay experiment with four agarose spots on the same 35-mm dish, with one spot as a control (PBS), and the other three spots containing similar concentrations of CXCL12, CCL19 and CCL21 each. In this experiment, PC-3 cells are allowed to migrate toward CXCL12, CCL19 and CCL21 spots under identical conditions. This experiment will allow us to assess the chemotactic aptitude of PC-3 cells toward different chemokine ligands using same experimental conditions. After 16 hour of incubation time, the spots were visualized and analysed using LumaScopes 500 (**Figure 32**).



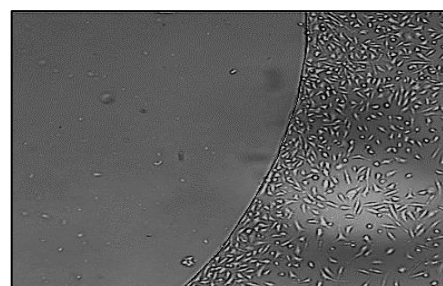
(A) PC-3 cells (CXCL12 100nM, 16hr)



(B) PC-3 cells (CCL21 100nM, 16hr)



(C) PC-3 cells (CCL19 100nM, 16hr)



(D) PC-3 cells (PBS 16hr)

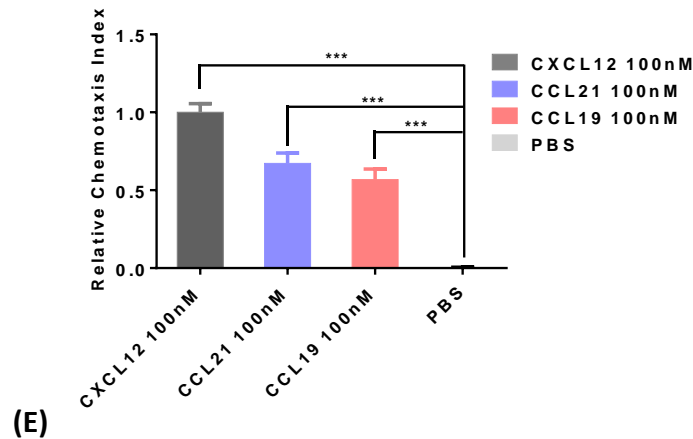


Figure 32 PC-3 cells which express chemokine receptors CCR7 and CXCR4 migrate under agarose spot containing (A) CXCL12 (ligand for CXCR4), and (B) CCL21 and (C) CCL19 (ligands for CCR7), but not under agarose spot containing (D) no chemokine. (E) Relative chemotaxis index of PC-3 cells migration under agarose spots. Data is presented as the mean \pm SE of at least 3 independent experiments.

PC-3 cells do indeed migrate under the agarose spots containing CXCL12, CCL19 and CCL21 (**Figure 32**). However, no migration was observed under the agarose spot containing PBS. It was observed number of cells migrated toward spot containing CXCL12 is more than number of cells migrated toward spots contain CCL21 and CCL19. Interestingly in this experiment, the chemotactic aptitude of PC-3 cells, as measured by the number of migrated cells under the agarose spot, correlates to the response of the same cells in a calcium mobilisation experiment (**Figure 31**). Since cytoplasmic calcium enables cellular motility, this is not surprising. None-the-less, this correlation suggests that the agarose spot is a rigorous functional assay. These findings comply with previous results obtained from flow cytometry and calcium flux assay which indicates availability of high expression level of CXCR4 receptor in PC-3 cells than the expression level of CCR7 receptor. In contrast to PC-3 cells, SW480 cells do not significantly express CCR7, but do express high level of CXCR4.

Therefore, we repeated this experiment and allowed SW-480 cells to migrate under CXCL12, CCL19 and CCL21 spots under identical conditions (**Figure 33**).

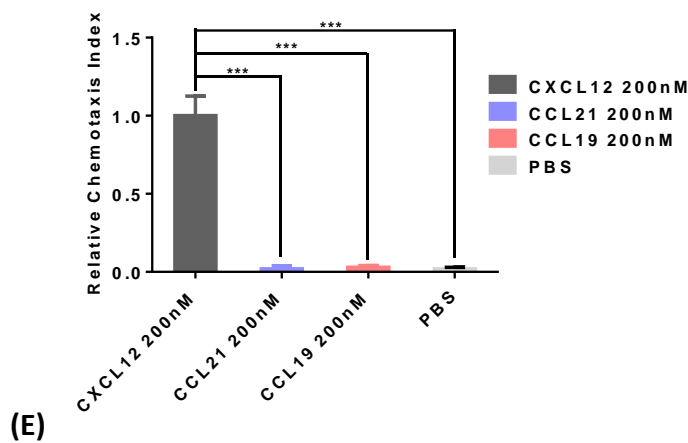
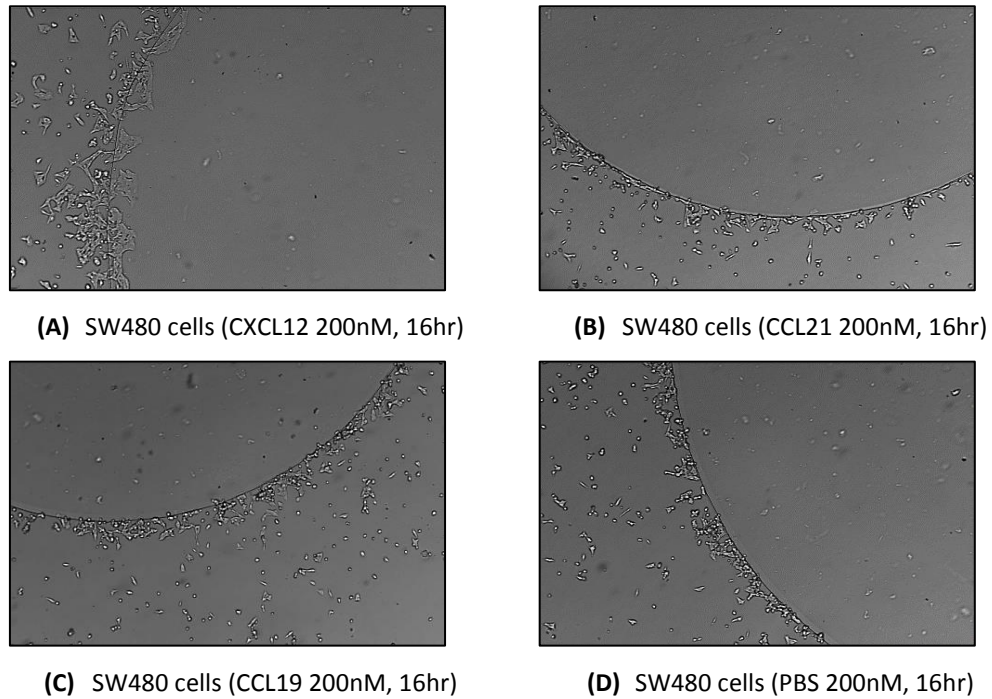


Figure 33 SW480 cells which express chemokine receptor CXCR4 but not CCR7, migrate under agarose spot containing (A) CXCL12 (ligand for CXCR4), but not under agarose spot containing (B) CCL21 and (C) CCL19 (ligands for CCR7), or agarose spot containing (D) no chemokine, (E) Relative chemotaxis index of PC-3 cells migration under agarose spots. Data is presented as the mean \pm SE of at least 3 independent experiments.

After 16 hours of incubation, we observed migration of SW480 cells under the agarose spot containing CXCL12 ligand, but not under agarose spot containing CCL19 nor CCL21 ligand. We first started the experiment using 100nM concentration of each ligand, however we then increased the concentration of each ligands to 200nM to make sure there was no migration under agarose spots containing CCL21 or CCL19. This observation is wholly consistent with the lack of significant expression of CCR7 in SW480 cells. This was also confirmed using scratch assay within our research group (**Appendix IV**). Scratch assay or wound healing assay is an easy-to-perform technique to assess cell migration in vitro. The basic steps include making a "scratch" in a cell monolayer and then monitoring cell migration by taking images at regular intervals and comparing the images to measure the migration rate of the cells.¹⁷⁰ Wound closure is accelerated over control when PC-3 and SW480 cells are treated with CXCL12, showing that activation of the CXCR4 receptor on these cells results in increased cell motility. Although wound closure is accelerated over control when the PC-3 cells are treated with CCL21 or CCL19, no difference was observed when SW480 cells were treated with CCL21 or CCL19.

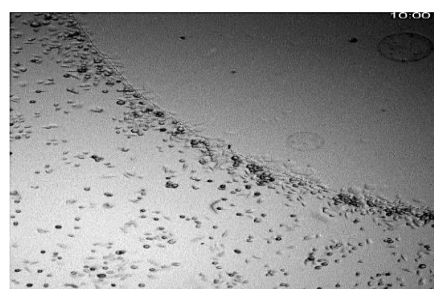
Cells Migration under agarose spot is monitored by confocal microscope

In order to demonstrate and describe PC-3 cells migration and movement under agarose spot assay is chemoattractant directed, we compiled a cell motility short film. Cells were initially incubated with 10% FCS containing medium for 4 hours. Medium was then replaced with 0.1% FCS containing medium and incubated at 37 °C and 5% CO₂ atmosphere over 16 hour time. Time-lapse

imaging was taken for the cells migrating toward the planar surface overnight using Nikon Eclipse TI confocal microscope and cells movement were analysed using Fiji/ImageJ software after 16 hours incubation. **Figure 34** shows pictures which were captured from time-lapse imaging for PC-3 cells migrating toward agarose spot containing CCL21 ligand over 16 hours period. (The time-lapse imaging movie is included in a CD attached to this thesis)



(A) PC-3 cells (CCL21 100nM, 4hr)



(B) PC-3 cells (CCL21 100nM, 10hr)



(C) PC-3 cells (CCL21 100nM, 16hr)

Figure 34 Migration under agarose spot is monitored by confocal microscopy using PC-3 cells;

After 4 hours of incubation (**Figure 34 A**), we found that PC-3 cells settled near the edge of the agarose spot containing CCL21 chemokine. Cells at this stage seem to aggregate near the spot border toward chemoattractant gradient just prior to the migration stage. After 10 hours of incubation (**B**), cells were

migrating toward the drop core which contain higher level of the ligand concentration. After 16 hours of incubation **(C)**, migrated cells moved much further toward the spot core. The key observation in this assay is that we have seen that cells were migrating toward the spot containing chemoattractants. However, no cells movement was observed in all spots which contain no chemoattractants.

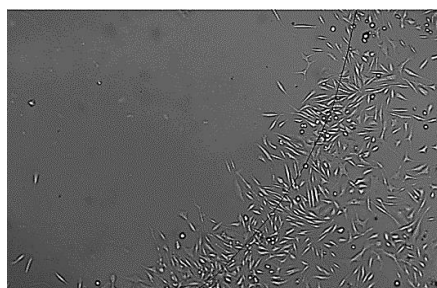
Using Nikon Eclipse TI confocal microscope which detects fluorescently-labelled molecule, we attempted to determine if the chemokine actually leaves the agarose spot. A fluorescently-labelled molecule was embedded in the agarose spot under the same conditions of the assay and the decay of fluorescence intensity in the spot by fluorescence microscopy was measured. As a surrogate for fluorescently labelled CCL21 chemokine, which is commercially available, but extremely expensive, blue dextran 10 kDa was used, which is similar to the molecular weight of the ligand CCL21, and this was tracked using confocal fluorescence microscopy. Unfortunately, the spot did not stay attached to the glass bottom although repeated attempting of making many different conditions like increasing the solidity of the agarose, going from 0.5% to 2%. Cold medium was added to the dextran containing spot in attempt to keep spot in a rigid state, however all efforts failed to keep the spot attached to the petri dish glassed bottom. This is in contrast to the agarose spot containing chemoattractant ligand which properly attached to the glass bottom dish even though the medium was exchanged with 0.1% FCS after 4 hour incubation. This is probably something to do with the structure of the dextran as a polysaccharide which is different from CCL21 ligand as a protein. This

experiment will be repeated again using a fluorescent labelled protein that has similar molecular structure and weight to the CCL21 ligand.

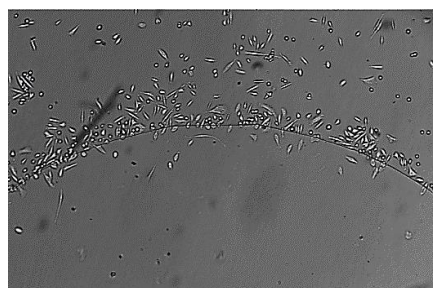
Migration under agarose spot is selectively modulated by small molecule antagonists

Our group has previously shown that migration of cells under an agarose spot containing CXCL12 can be decreased by an anti-human CXCR4 monoclonal antibody (MAB) and small molecule CXCR4 antagonists ICT5040 and AMD3100¹⁵⁰. AMD3100 is a selective CXCR4 antagonist and was previously shown not to antagonise other chemokine receptors including CCR7¹⁵¹. In this experiment we aimed to demonstrate the suitability of the modified agarose spot assay to assess selectivity of small molecule antagonists toward multiple chemokine receptors under identical conditions. PC-3 cells were allowed to migrate under CXCL12, CCL21, and CCL19 spots in the same petri dish, in the presence or absence of CXCR4 antagonist AMD3100 in media. We set out the experiment using four petri dishes, each petri dish contain four agarose spots which contain CXCL12, CCL21, CCL19 and control. The petri dish was used as control in absence of AMD3100 in order to monitor migration of PC-3 cells toward different ligands in absence of AMD3100. The rest of the petri dishes were used in presence of different concentration of AMD3100 to monitor the effect of the antagonist on migration of PC-3 cells toward different receptors. In order to have dose dependant response of compound AMD3100, we used different concentrations including, 50µM, 100µM and 200µM in medium. All petri dishes were prepared at the same time and incubated for 4 hours to make cells attach properly to the glass bottom petri dish. Medium was discarded after 4 hours and replaced with 0.1% FCS and again different concentrations of the

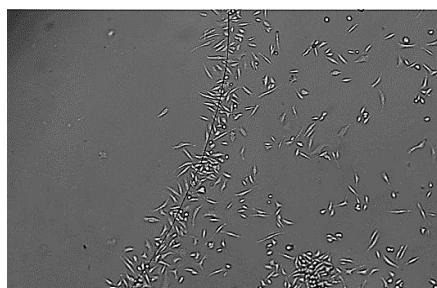
antagonist were prepared and applied to medium for overnight incubation. The figures obtained below demonstrates effectiveness and selectivity of compound AMD3100 against PC-3 cells migration under agarose spot containing CXCL12 (**Figure 35**), CCL21 (**Figure 36**) and CCL19 (**Figure 37**) chemoattractant. The experiment presented herein was repeated at least three times using same conditions and results obtained were consistent.



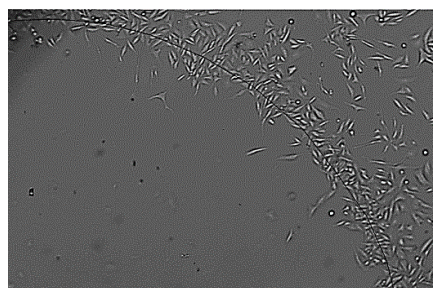
(A) PC-3 cells (CXCL12 100nM, 16hr)



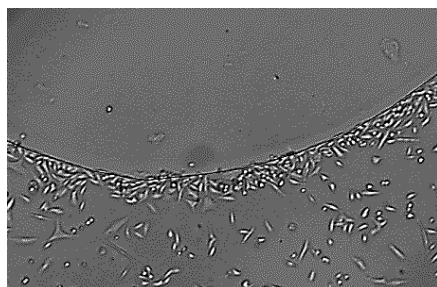
(B) PC-3 cells (CXCL12 100nM, AMD3100 200 μ M, 16hr)



(C) PC-3 cells (CXCL12 100nM, AMD3100 100 μ M, 16hr)



(D) PC-3 cells (CXCL12 100nM, AMD3100 50 μ M, 16hr)



(E) PC-3 cells (PBS, 16hr)

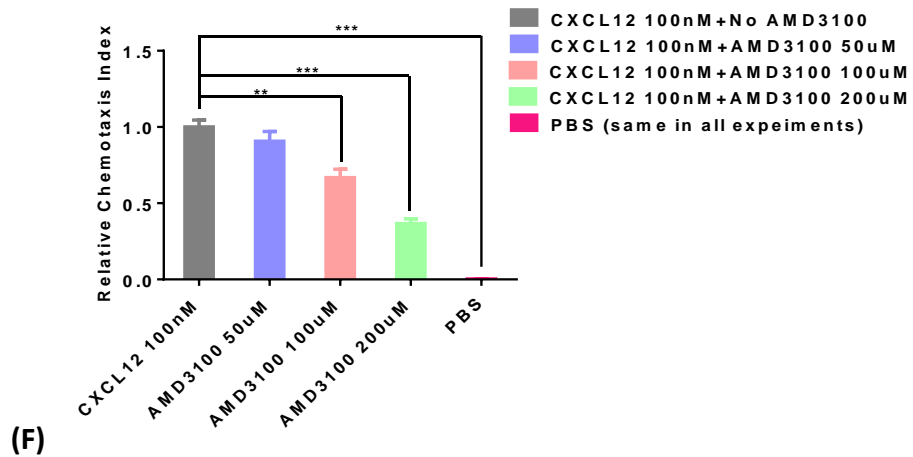
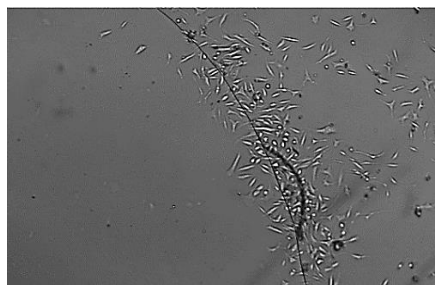
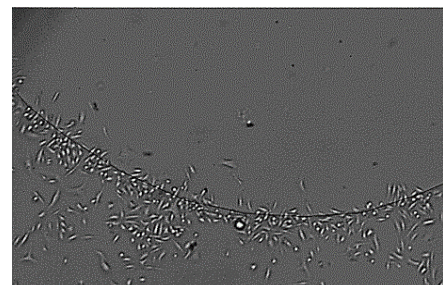


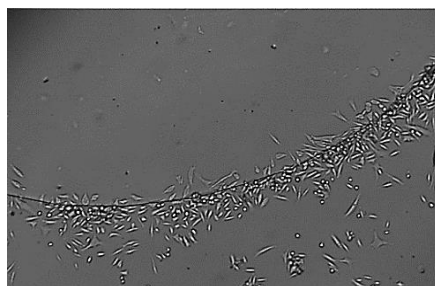
Figure 35 Migration under agarose spot is selectively modulated by small molecule antagonists AMD3100. PC-3 cells migration, which express chemokine receptor CXCR4, is blocked toward agarose spot containing CXCL12 (ligand for CXCR4) by using dose dependant small molecule antagonists AMD3100 (A) CXCL12, (B) 200 uM, (C) 100uM, (D) 50 μ M of AMD3100, (E) PBS, (F) Relative chemotaxis index of PC-3 cells migration under agarose spots. Data is presented as the mean \pm SE of at least 3 independent experiments.



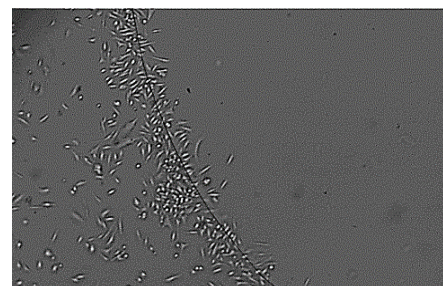
(A) PC-3 cells (CCL21 100nM, 16hr)



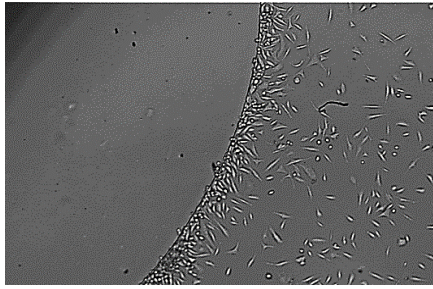
(B) PC-3 cells (CCL21 100nM, AMD3100 200 μ M, 16hr)



(C) PC-3 cells (CCL21 100nM, AMD3100 100 μ M, 16hr)



(D) PC-3 cells (CCL21 100nM, AMD3100 50 μ M, 16hr)



(E) PC-3 cells (PBS, 16hr)

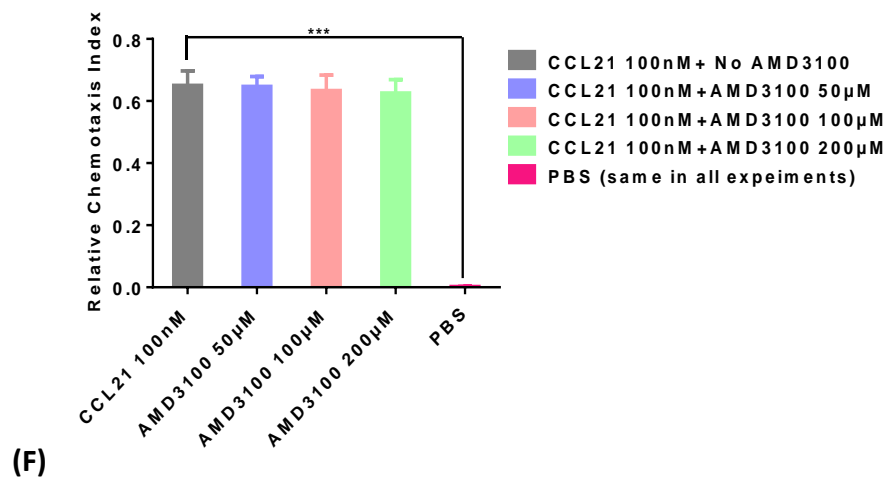
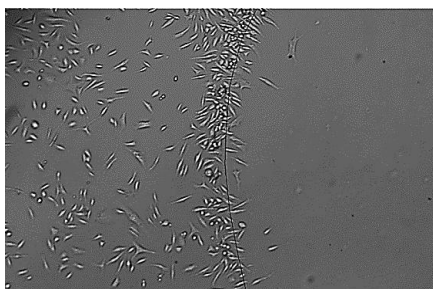
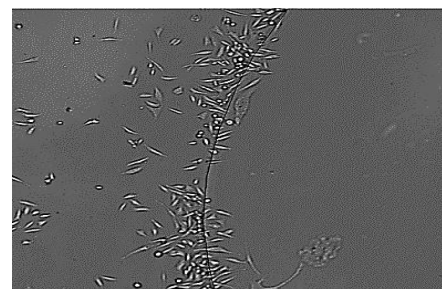


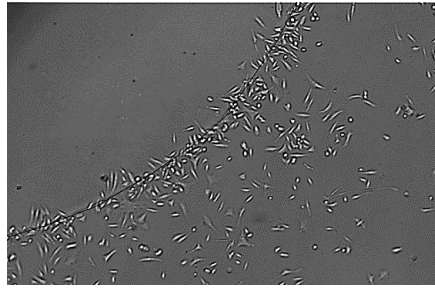
Figure 36 Migration under agarose spot is selectively modulated by small molecule antagonists AMD3100. PC-3 cells migration, which express chemokine receptor CCR7, is blocked toward agarose spot containing CCL21 (ligand for CCR7) by using dose dependant small molecule antagonists AMD3100 (A) CCL21, (B) 200 µM, (C) 100 µM, (D) 50 µM of AMD3100, (E) PBS, (F) Relative chemotaxis index of PC-3 cells migration under agarose spots. Data is presented as the mean ±SE of at least 3 independent experiments.



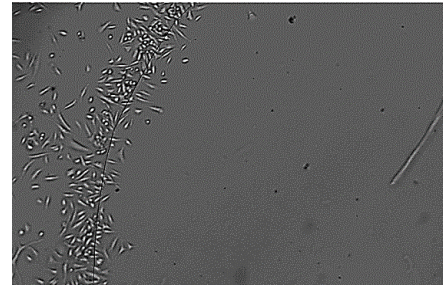
(A) PC-3 cells (CCL19 100nM, 16hr)



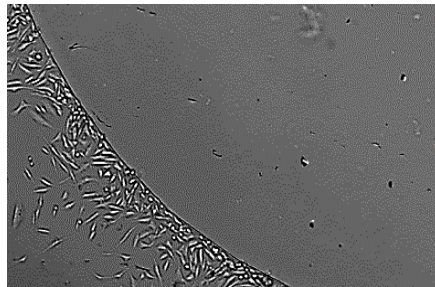
(B) PC-3 cells (CCL19 100nM, AMD3100 200 µM, 16hr)



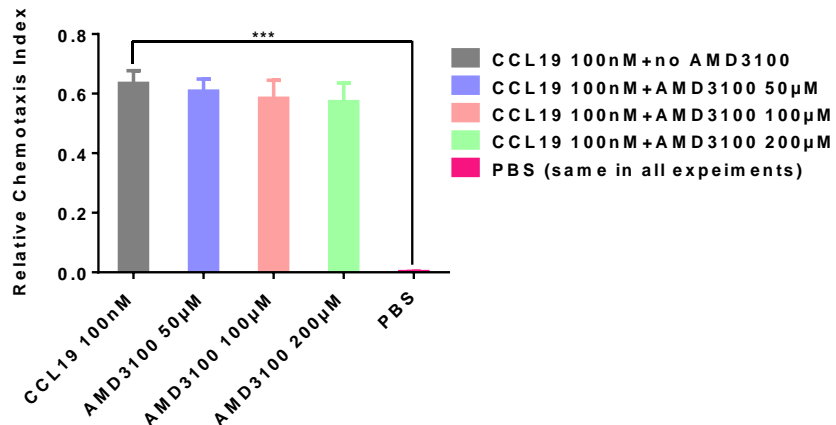
(C) PC-3 cells (CCL19 100nM, AMD3100 100 μ M, 16hr)



(D) PC-3 cells (CCL19 100nM, AMD3100 50 μ M, 16hr)



(E) PC-3 cells (PBS, 16hr)



(F)

Figure 37 Migration under agarose spot is selectively modulated by small molecule antagonists AMD3100. PC-3 cells migration, which express chemokine receptor CCR7, is blocked toward agarose spot containing CCL19 (ligand for CCR7) by using dose dependant small molecule antagonists AMD3100 (A) CCL19, (B) 200 μ M, (C) 100 μ M, (D) 50 μ M of AMD3100, (E) PBS, (F) Relative chemotaxis index of PC-3 cells migration under the agarose spots. Data is presented as the mean \pm SE of at least 3 independent experiments.

The figures above indicate the selectivity of the AMD3100 small molecule in antagonizing the effect of CXCL12 through CXCR4 receptor. In these figures, clearly that show there was a negligible effect on the CCR7. In **(Figure 35)**, we can see the selectivity of AMD3100 toward PC-3 migrated cells expressing CXCR4 receptor in a dose dependant manner. In the presence of 200 μ M AMD3100, we observed significant reduction of migration of PC-3 cells under agarose spot containing CXCL12 ligand. However, no significant reduction of migration was observed under the agarose spot containing CCL21 and CCL19 ligands **(Figure 36 and Figure 37 respectively)**. This observation is consistent with our expectation; a selective CXCR4 antagonist does antagonise the migration against CXCL12, but does not interfere with the migration against CCL19 or CCL21, because it does not antagonise CCR7, the corresponding receptor for these two chemokines. There was no migration seen under the agarose spots which contain no chemoattractant, this confirms that the induction of chemotaxis is caused by the chemoattractant gradient. It was mentioned above that the sensitivity of PC-3 cells toward CXCL12 is more likely to be higher than the CCL21 or CCL19 due to higher level of CXCR4 receptor expressed than the CCR7 receptor. Evidently the migration seen in the images above caused by the chemoattractant CCL21 is less than the migration obtained from the effect of CXCL12. **Figure 38** below shows the direct comparison between PC-3 cells migration toward their cognate ligands CXCL12 (ligand for CXCR4), CCL21 and CCL19 (ligands for CCR7) under agarose spot and selectivity of the antagonist AMD3100 toward CXCR4 receptor but not CCR7 receptor.

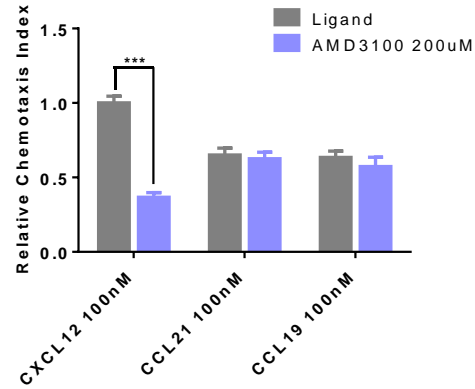
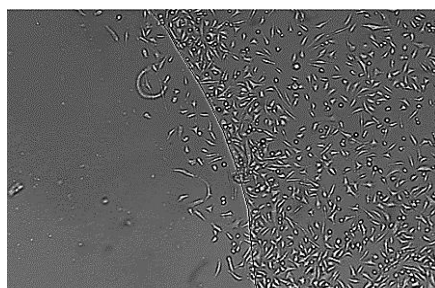
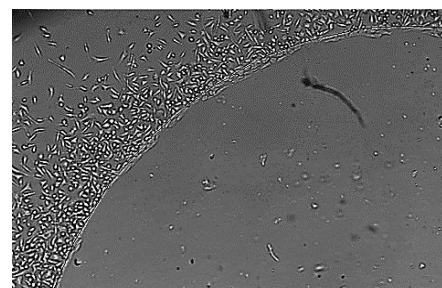


Figure 38 PC-3 cells migration under agarose spot is selectively modulated by small molecule antagonists AMD3100. PC-3 cells migration, which express chemokine receptor CXCR4 and CCR7, is blocked toward agarose spot containing CXCL12 (ligand for CXCR4), but not under agarose spot containing CCL21 and CCL19 (ligands for CCR7). Data is presented as the mean \pm SE of at least 3 independent experiments.

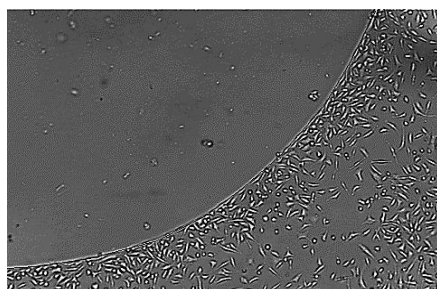
In order to study the effectiveness and selectivity of compound **75**, we set out a parallel experiment to compound AMD3100. PC-3 cells which express both receptors were allowed to migrate under agarose spot containing CCL21 (**Figure 39**), CCL19 (**Figure 40**), and CXCL12 (**Figure 41**) ligands in presence or absence of 10 μ M CCR7 small molecule antagonist compound **75**, ICT13069 in medium. All spots were in the same petri dish and therefore the experiment conditions are identical.



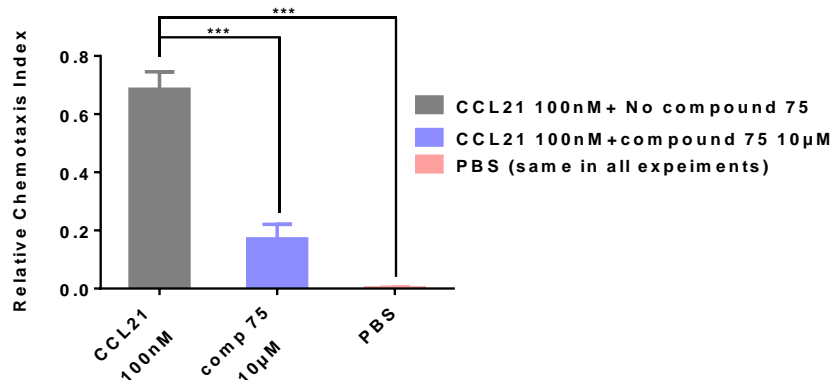
(A) PC-3 cells (CCL21 100nM, 16hr)



(B) PC-3 cells (CCL21 100nM, compound **75** 10 μ M, 16hr)



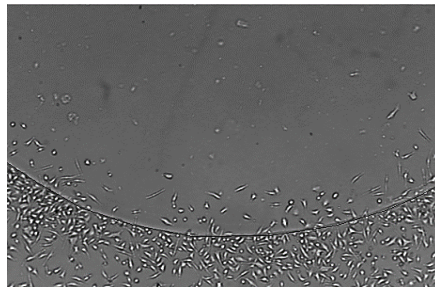
(C) PC-3 cells (PBS, 16hr)



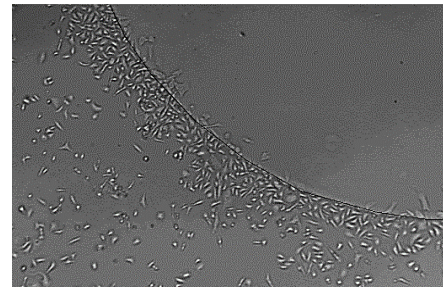
(D)

Figure 39 Migration under agarose spot is selectively modulated by small molecule antagonists, **75**. PC-3 cells migration, which express chemokine receptor CXCR4 and CCR7, is allowed to migrate toward agarose spot containing (A) CCL21 (ligand for CCR7), (B) 10 µM of compound **75** (C) control (PBS) (D) Relative chemotaxis index of PC-3 cells migration toward agarose spots. Data is presented as the mean \pm SE of at least 3 independent experiments.

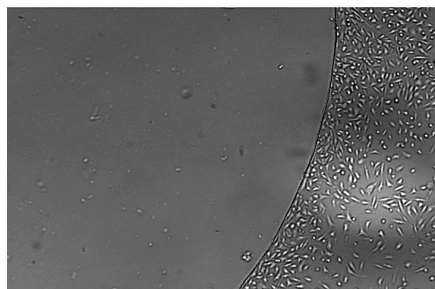
In order to demonstrate the reliability of the newly modified agarose assay, PC-3 cells were also allowed to migrate toward agarose spot containing CCL19 and in presence of 10 µM of CCR7 receptor antagonist, compound **75**. **Figure 40** shows modulation of PC-3 cells migration toward CCL19 spot using CCR7 receptor antagonist.



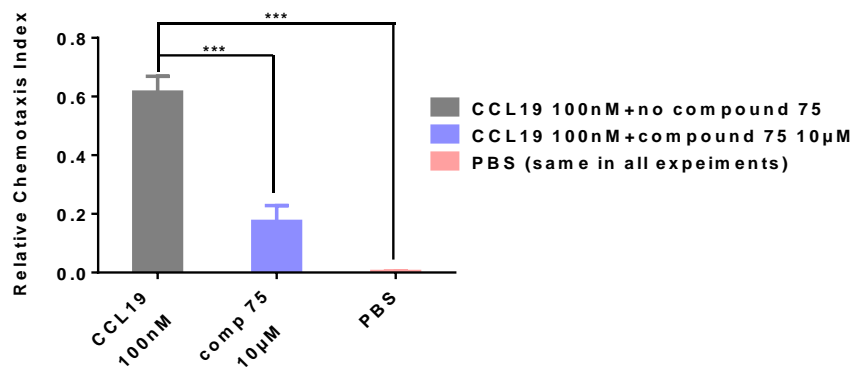
(A) PC-3 cells (CCL19 100nM, 16hr)



(B) PC-3 cells (CCL19 100nM, compound 75 10 μM, 16hr)



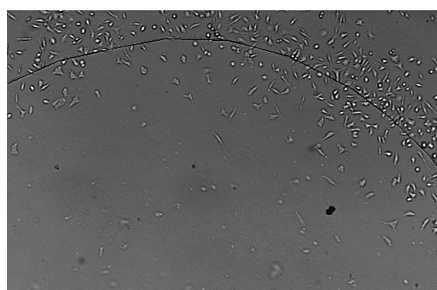
(C) PC-3 cells (PBS, 16hr)



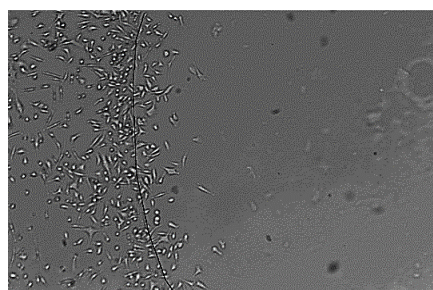
(D)

Figure 40 Migration under agarose spot is selectively modulated by small molecule antagonists **75**. PC-3 cells migration, which express chemokine receptor CXCR4 and CCR7, is allowed to migrate toward agarose spot containing (A) CCL19 (ligand for CCR7), (B) 10 μM of compound **75** (C) control (PBS), (D) Relative chemotaxis index of PC-3 cells migration toward agarose spots. Data is presented as the mean ±SE of at least 3 independent experiments.

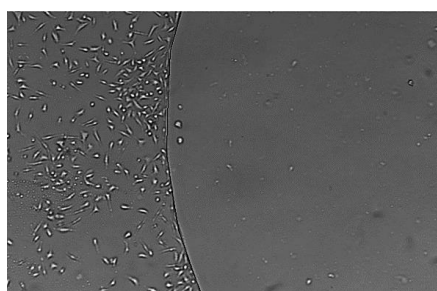
In the same experiment, compound **75** selectivity was determined using different spot containing CXCL12 ligand with same experiment conditions. PC-3 cells were allowed to migrate toward agarose spot containing CXCL12 and in different petri dish, same conditions were applied, yet this time in presence of 10 μ M of CCR7 receptor antagonist, compound **75**. This was done to find out how selective is the newly synthesized molecule is? **Figure 41** shows the effect of the antagonist against CXCR4 receptor using CXCL12 as a cognate ligand.



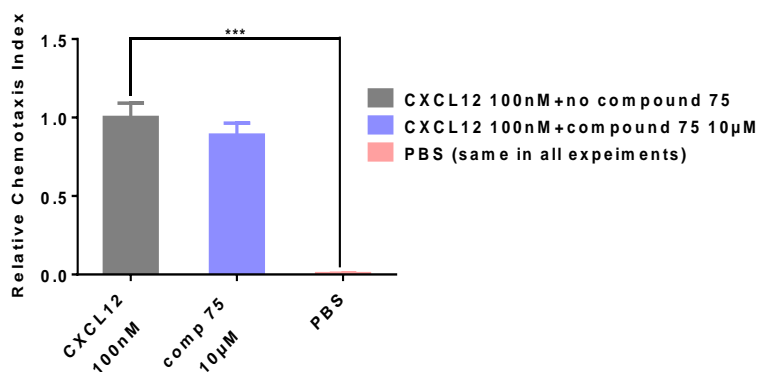
(A) PC-3 cells (CXCL12 100nM, 16hr)



(B) PC-3 cells (CXCL12 100nM, compound **75** 10 μ M, 16hr)



(C) PC-3 cells (PBS, 16hr)



(D)

Figure 41 Migration under agarose spot is selectively modulated by small molecule antagonists **75**. PC-3 cells migration, which express chemokine receptor CXCR4 and CCR7, is allowed to migrate toward agarose spot containing (A) CXCL12 (ligand for CXCR4), (B) 10 µM of compound **75** (C) control (PBS), (D) Relative chemotaxis index of PC-3 cells migration toward agarose spots. Data is presented as the mean ±SE of at least 3 independent experiments.

Figures above demonstrates effectiveness and selectivity of compound **75** against PC-3 cells migration under agarose spot containing CXCL12, CCL21 and CCL19 chemoattractant. In the presence of 10 µM compound **75**, migration of PC-3 cells under the CCL21 and CCL19 spots was significantly reduced. However, the reduction observed with the CXCR4 receptor was not as significant as the CCR7 receptor. This observation is consistent with our expectation, and correlates with the calcium flux assay results. **Figure 42** below shows the direct comparison between PC-3 cells migration toward their cognate ligands CXCL12 (ligand for CXCR4), CCL21 and CCL19 (ligands for CCR7) under agarose spot and selectivity of the antagonist **75** toward CCR7 receptor but less toward CXCR4 receptor.

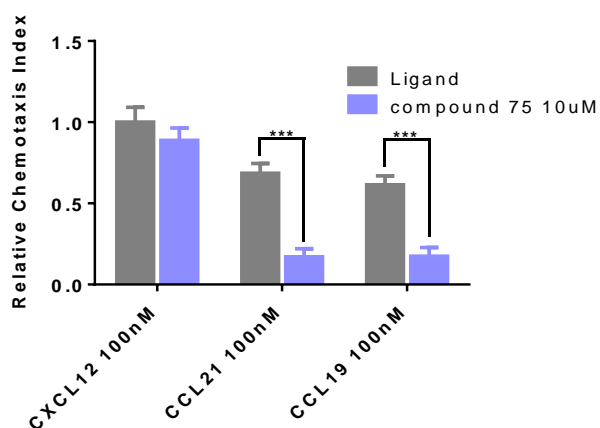


Figure 42 Migration under agarose spot is selectively modulated by small molecule antagonists **75**. PC-3 cells migration, which express chemokine receptor CXCR4 and CCR7, is blocked toward agarose spot containing CCL21, CCL19 (ligands for CCR7) and CXCL12 (ligand for CXCR4). Data is presented as the mean \pm SE of at least 3 independent experiments.

For further confirmation to our results obtained from the selectivity of compound **75** using newly modified agarose spot assay, calcium flux mobilization assay was conducted. PC-3 cells were plated in 96-well plate and tested each time using the three different ligands, CCL21 and CCL19 (ligands for CCR7) and CXCL12 (ligand for CXCR4) without the antagonist to measure the fluorescence obtained upon binding of these ligands with their receptors. PC-3 cells responded to all ligands and this is obviously because of the expression of these receptors in this cell line. Using the same 96-well plate PC-3 cells were incubated with the antagonist, **75** and fluorescence released from the ligands interaction with the receptors was measured. Significant reduction in fluorescent was observed in wells which treated with the antagonist and used CCL21 and CCL19 as a cognate ligand. However, wells which treated with the antagonist and used CXCL12 as cognate ligand showed no significant reduction in the amount of fluorescent released (**Figure 43**). However, still some effect observed

against CXCR4 receptor in compare to the CCR7 receptor. It is also worth to mention that in this assay, as illustrated from the figure below, PC-3 cells showed response to their cognate ligands in relation to the level of expression of these receptors. Fluorescent released upon binding CXCL12 ligand with CXCR4 receptor was higher than the fluorescent released upon binding CCL21 ligand with CCR7 receptor. PC-3 cells showed least release of the fluorescence upon binding of CCL19 ligand with CCR7 receptor. These findings correlated with the previously mentioned results in **Figure 31** regarding chemotactic aptitude of PC-3 cells, as measured by the number of migrated cells under the agarose spot assay.

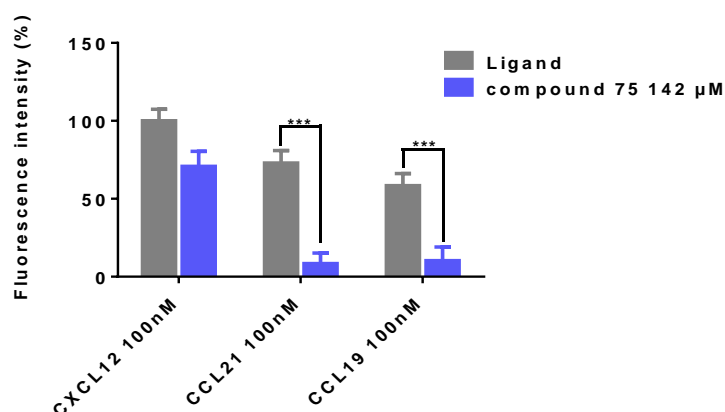
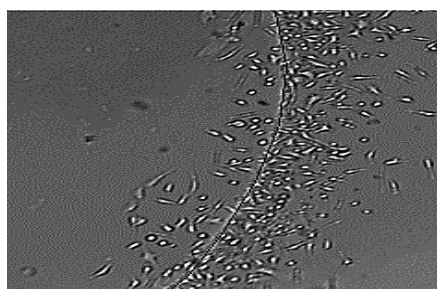


Figure 43 Inhibition of CCL21, CCL19 (ligands for CCR7) and CXCL12 (ligand for CXCR4) mediated response by small molecule antagonists **75** using PC-3 cells. Data is presented as the mean \pm SE of at least 3 independent experiments.

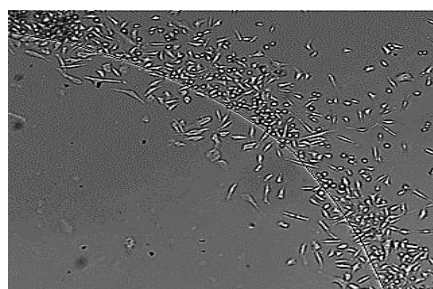
Comparison between compound 75 and compound 3 under agarose spot assay

We have previously shown that migration of PC-3 cells under an agarose spot containing CCL21 or CCL19 can be modulated by small molecule CCR7 antagonist, **75**. We have also shown in chapter 2 that compound **75** showed higher potency as CCR7 antagonist in the calcium flux assay with IC_{50} around

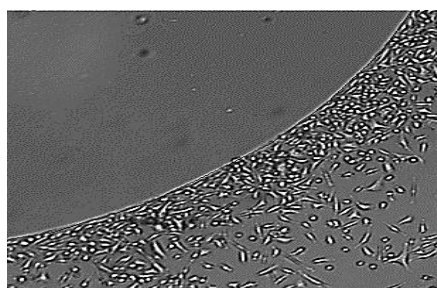
0.19±0.22 μM than compound **3** which showed activity with IC_{50} around 10 ± 2.56 μM . We wanted to draw a direct comparison between assessment of potency using calcium flux and agarose spot method. So, the inhibition of PC-3 cells migration was compared between compound **75** and much less potent compound **3**. PC-3 cells were plated in two small petri dish, each contain two agarose spots containing CCL21 and CCL19 ligands and two spots containing control, PBS. In one petri dish using the same experiment conditions, compound **3** was included in the medium and the other petri dish was used as control, both petri dishes were incubated overnight to be inspected the following day. The concentration of compound **3** used in this experiment is 50 μM which is 5 fold higher than the concentration of compound **75**, 10 μM , which used previously in **Figure 39**. **Figure 44** below shows migration of PC-3 cells toward agarose spot containing CCL21 ligand and in presence of small molecule compound **3** at concentration 50 μM .



(A) PC-3 cells (CCL21 100nM, 16hr)



(B) PC-3 cells (CCL21 100nM, compound **3** 50 μM , 16hr)



(C) PC-3 cells (PBS, 16hr)

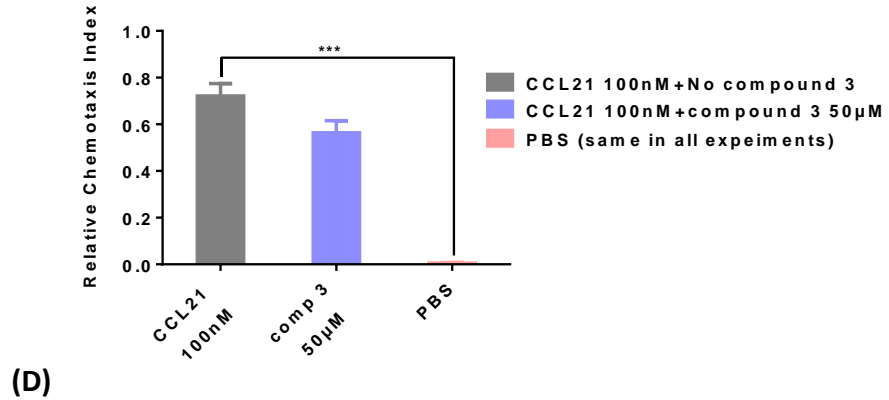
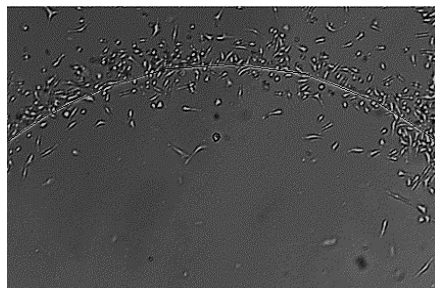
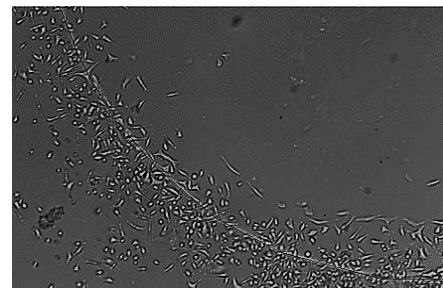


Figure 44 Inhibition of PC-3 migration by CCR7 antagonists **3** in an agarose spot containing CCL21 ligand: PC-3 cells migration, which express chemokine receptor CCR7, is allowed to migrate toward agarose spot containing (A) CCL21 (ligand for CCR7), (B) 50 µM of compound **3** (C) control (PBS), (D) Relative chemotaxis index of PC-3 cells migration toward agarose spots. Data is presented as the mean ±SE of at least 3 independent experiments.

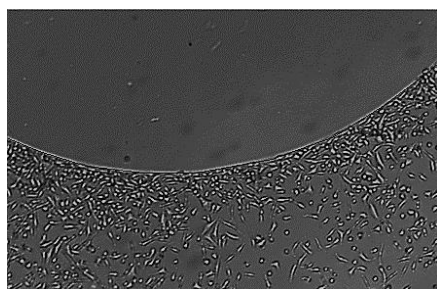
Figure 45 below shows migration of PC-3 cells toward agarose spot containing CCL19 ligand and in presence of small molecule compound **3** at concentration 50µM.



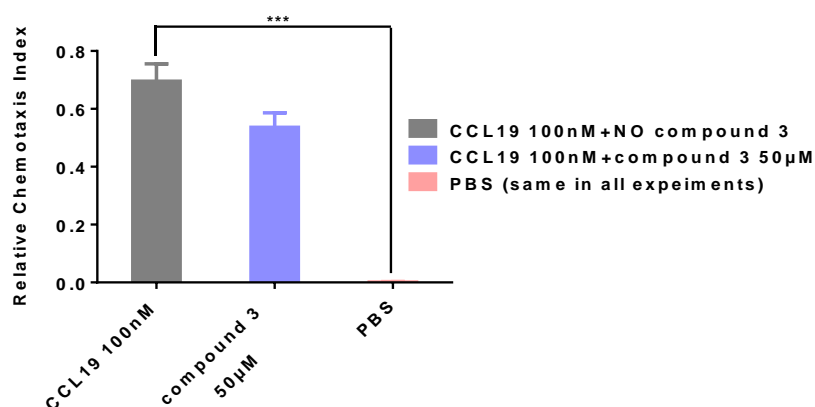
(A) PC-3 cells (CCL19 100nM, 16hr)



(B) PC-3 cells (CCL19 100nM, compound **3** 50 µM, 16hr)



(C) PC-3 cells (PBS, 16hr)



(D)

Figure 45 Inhibition of PC-3 migration by CCR7 antagonists **3** in an agarose spot containing CCL19 ligand: PC-3 cells migration, which express chemokine receptor CCR7, is allowed to migrate toward agarose spot containing (A) CCL19 (ligand for CCR7), (B) 50 µM of compound **3** (C) control (PBS), (D) Relative chemotaxis index of PC-3 cells migration toward agarose spots. Data is presented as the mean ±SE of at least 3 independent experiments.

All experiment were performed on the same day using same cell density and same conditions. **Figure 44** shows migration of PC-3 cells toward agarose spot containing CCL21 ligand in presence and absence of compound **3** as antagonist. When cells were treated with 50 µM of compound **3**, a modest reduction in cells migration toward the drop was observed. This is beyond comparison with the significant reduction observed when these cells were

treated with 10 μ M of compound **75** (**Figure 39**). The figure shows no migration in spots containing no chemoattractant, control. **Figure 45** shows modest effect of compound **3** against PC-3 cells migration toward agarose spot containing CCL19 ligand. However, when compound **75** was used in presence of CCL19 as a ligand, there was a significant decrease in cell numbers (**Figure 40**). The concentration of compound **75** used was 10 μ M which is five times less than the concentration of compound **3**, 50 μ M. This indicates the improvement and enhancement of the antagonizing activity of compound **75** against CCR7 receptor which was carried out in our laboratory department.

To summarize, the modified agarose spot assay described herein provided us with opportunity to examine cells movement toward different chemo-attractants at the same time. We described how different cells responded to different chemo-attractants. Cells are only directing their movement toward agarose spot which contain chemo-attractants. The key observation in this newly configured technique is that we have seen cell which express chemokine receptors migrating toward all the agarose spots which contain chemoattractants through all the experiments. In contrast, we have seen no cells movement toward spots which lack chemo-attractants which proves the migration was mediated by the presence of ligand. We performed time-lapse imaging to study cells movement toward spots contain chemo-attractants, the motility of migrated cells were moving toward the agarose spot core contains ligand in progressive way. In order to prove that cell migration is in response to the receptor expression, we applied this assay using SW480 cells which express only CXCR4 receptor and not CCR7 receptor. SW480 cells migrated only toward agarose spot which contain CXCL12 (ligand for CXCR4) and we have seen no cell migration toward

agarose spots which contain CCL21 and CCL19 (ligands for CCR7). This migration toward CXCL12 drop is obviously in response to CXCR4 receptor which proved to be expressed in SW480 cells using flow cytometry and western blot. We measured and assessed antagonist selectivity between different chemokine receptors under identical experimental conditions. The selectivity of the small molecule AMD3100 was observed to block CXCR4 receptor but not CCR7 receptor. We demonstrated the significant selectivity of compound **75** against CCR7 receptor over CXCR4 receptor. We also compared effectiveness of highly active compound **75** with less active compound **3** against CCR7 receptor which proved the potency of compound **75** to reduce chemotaxis at a given concentration over compound **3**. In summary, we established and generated rigorous and easy to perform assay, which allow us to analyse and assess cells chemotactic aptitude toward multiple chemo-attractants over a period of time. The importance of this modification is to analyse cells movement and to evaluate antagonist's activity of small molecules against migration and invasion of cells through a planner surface in an identical conditions. Results obtained from agarose spot assay was in agreement with results obtained from different functional assays like calcium flux assay, flow cytometry and scratch assay.

3.7. Concluding remarks and future works

The chemokine receptor CCR7 is belonging to the G-protein coupled receptor family which is commonly associated in cancer progression and metastasis. Blocking the activity of this receptor by a small molecule will eventually reduce or prevent cancer growth and metastasis. It is true that blocking the CCR7 receptor means blocking its normal role in attracting immune cells toward

inflammation site. However, there are other types of chemokine receptors and cytokines working as chemo-attractants leading to immune cells migration to the infection site and cancer is resistant to the immune system ¹⁷¹. Although recent studies reported high expression of CCR7 receptor in number of different cancer tissues, limited studies explored interfering of the receptor function using antibody. However, up to date, there is no small molecule discovered or claimed to be an antagonist for this receptor. In this study, we investigated the interference between chemokine receptor CCR7 and its ligands using small molecule antagonist.

This receptor was first modelled using a homology modelling which was constructed by help of Professor Colin Fishwick at the University of Leeds. Compounds obtained from screening library were tested using calcium flux assay in our laboratory department and none of these molecules were active against CCR7 receptor, so they were excluded from further analysis. Additional investigation in literature review, we found a patent describes a technique for screening therapeutic compounds which thought to be useful in the methods for screening for therapeutic compounds that are useful in the recovery from diseases that involves CCL21 and CCR7 interaction. The binding nature of this compound remains unknown and not identified and was not claimed as CCR7 antagonist. We successfully synthesized and characterised this compound in our laboratory department and named compound **1**, ICT5189. We tested the compound using calcium flux assay and confirmed to be an antagonist to the CCR7 receptor. Compound **3**, ICT5888 was discovered during the synthesis process of compound **1** and tested to give activity with comparable result to compound **1**. Following the biological evaluation of compound **3**, different

analogues of these compounds have been synthesised and characterised in order to look for structure activity relationships and improve their potency as antagonists of the CCR7 receptor. Structural activity relationship was carried out and determined the most active compound amongst series of many compounds. Based on calcium flux assay results obtained, compound **75**, ICT13069 was identified as the most active compound. It is a novel small molecule CCR7 receptor antagonist which is never been synthesised or claimed in literature. We evaluated the activity of this compound using different *in vitro* assays like agarose spot assay and scratch assay. The selectivity of the **75** against CCR7 receptor was determined using PC-3 cells, which express both CCR7 and CXCR4. Results obtained showed higher selectivity of the compound toward CCR7 receptor than CXCR4. These findings were confirmed using calcium flux assay and other biological assays. The structure-activity relationship study of compound ICT5888 and development of its analogues has afforded greater understanding of the lead compound pharmacophore which is responsible for binding to the CCR7 receptor. These findings allowed us to identify the important sites in the compound which are amenable to modifications. Consequentially, in future, there will be more investigations towards compounds which showed comparable activity to the top active compound. Compound ICT13069 is now used as a tool to look for a more potent compound. Our first objective is to make the reverse sulphonamide of compound **75**. Also, more studies are required to explore different positions of compounds **85**, ICT13130, **97**, ICT13124 and **49**, ICT13063 which were synthesised in very late stage of my research. Future analogues will address the importance of solubility in an aqueous medium which is an important factor

that may improve compounds efficacy and reduce their side effects. This is can be done by keeping the right balance between hydrophilicity and lipophilicity of the compound. It would also be worth chemically attaching a florescent tag to the most active compound in order to aid in tracking down the process of blocking the receptor using confocal microscope which detects fluorescently-labelled molecule. One of the most important considerations which will take place in future investigations is the selectivity of the top active compound against CCR7 receptor. At this stage, we are looking for a compound that blocks this receptor and has no or less effect on other GPCR receptors. We investigated the selectivity of compound ICT13069 against CXCR4 receptor, which has similar receptor structure, and showed less selectivity. The aim, in future, is to synthesise compounds which are highly activity against CCR7 receptor and send it to companies which target selectivity profiles of any new small molecule. The newly top active synthesised compound will be evaluated and tested using different preclinical studies including *in vitro* and *in vivo* assays in order to prove its potency against CCR7 receptor. Future investigation will also cover all the biological assays that have to be completed. Table 15 below summarises all the cell lines used for each assay in this research, so that future work will cover all the gaps required to have a full picture of the research. Once all of these studies and investigations have taken place and proved the candidate drug as a potent and selective for CCR7 receptor, the next step would be to more towards pre-clinical and clinical trials. The clinical trial is aimed to evaluate drug efficacy and safety in human and eventually to collect data from post marketing.

Cell Lines	CCR7 WB	CCR7 FACS	CXCR4 FACS	CCL19 Agarose S. A.	CCL21 Agarose S. A.	CXCL12 Agarose S. A.	CCL19 Ca ²⁺ Flux	CCL21 Ca ²⁺ Flux	Scratch Assay
SW620	✓								
MDA231	✓	✓	✓						
U87-MG	✓	✓		✓	✓	✓	✓	✓	
DU-145	✓	✓	✓						
PC3	✓	✓	✓	✓	✓	✓			✓
DLD-1	✓	✓	✓	✓	✓	✓			
MCF-7	✓	✓	✓						
MCF-7 ADR	✓								
HT-29	✓	✓	✓	✓	✓	✓			
HUVEC	✓								
Panc-1		✓	✓					✓	
CCRF-CEM								✓	
OSC-19		✓	✓				✓	✓	✓
SW480		✓	✓	✓	✓	✓			

Table 15 summary table of all cell lines used for each assay and gaps which will be covered in future investigation.

4. Chapter 4: Experimental

4.1. Experimental Section

4.1.1. Experimental techniques and materials

All chemical reagents and starting materials used below were commercially available and purchased from Sigma-Aldrich, alfa aesar and tocris. All the reagents were used as purchased without any additional purification unless otherwise stated. All solvents were of reagent grade, suited for general laboratory use. Petroleum ether (PE) refers to the fraction of petroleum spirit boiling in the range of 60 to 80 °C. Where stated, mixtures of solvents are referred to as volume-to-volume (v/v) ratios. All the compounds made were purified by flash chromatography using high-purity silica gel (Merck Grade 9385), pore size 40-63 μm (CAS Number: 112926-00-8). The analytical thin layer chromatography was conducted on Merck silica gel 60 F₂₅₄ glass backed plates (catalogue number 1.05715.0001, Merck Millipore). TLC plates were visualised under ultraviolet light lamp (254 nm), or by dipping in basic potassium permanganate (KMNO₄) solution.

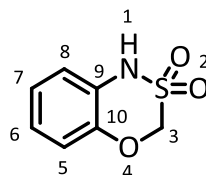
Hydrogen (¹H) Nuclear Magnetic Resonance spectra were recorded in deuterated solvents as stated in individual experimental procedures, using Bruker AMX400 spectrometer operating at 400 MHz. Carbon (¹³C) Nuclear Magnetic Resonance were performed on the same machines operating at 101 MHz. Chemical shifts are reported in parts per million (δ , ppm). ¹H NMR chemical shifts are reported relative to an internal reference (tetramethylsilane) or residual proton signals of the solvent. Coupling constants (*J*) are expressed in Hertz (Hz). The splitting patterns in NMR spectra are reported with the following abbreviations: singlet (s), doublet (d), triplet (t), quartet (q), quintet

(quint.), multiplet (m) and broad (br). ^{13}C NMR chemical shifts are reported relative to the signal of the solvent. Where necessary, correlation spectroscopy (COSY), nuclear Overhauser enhanced spectroscopy (NOESY), heteronuclear multiple quantum correlation spectroscopy (HMQC), and distortionless enhancement by polarization transfer (DEPT) technique were employed to confirm the assignment of NMR spectra. Routine mass spectra was carried out at the Analytical Center of the University of Bradford by Mr Andrew Healey and were run on a Micromass Quattro Ultima spectrometer in the electron impact (EI), chemical ionisation (CI) or positive (+ve) electrospray mode, as stated. All high resolution mass spectrometry (HRMS) was carried out at the ESPRC National mass spectrometry service centre located in Swansea University.

Drying oven was used at $140\text{ }^{\circ}\text{C}$ temperature in order to dry all the glassware. Reactions sensitive to moisture or air, were carried out under inert atmosphere using dry nitrogen or argon. Silicon oil was used to heat up reaction on oil bath and place on top of a hot plate stirrer. Mixtures of ice and water were used to maintain temperature at $0\text{ }^{\circ}\text{C}$.

4.1.2. Experimental procedures for preparation of chemical compounds

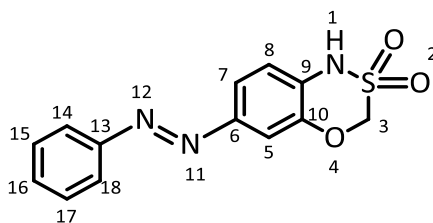
1H-benzo[e][1,3,4]oxathiazine 2,2-dioxide (5, ICT13001).



Chloromethane sulfonyl chloride (10.0 g, 67.1 mmol) was added dropwise to a stirred solution of 2-aminophenol (7.06 g, 64.7 mmol) in anhydrous tetrahydrofuran (40 mL) maintained at room temperature under an inert atmosphere. After 30 minutes, pyridine (7.30 mL) was added and the resulting solution was left stirring overnight at room temperature. Concentrated hydrochloric acid (10 mL, 37 %) was added and reaction mixture was extracted with ethyl acetate (3 x 150 mL). The combined organic extracts were washed with saturated aqueous sodium bicarbonate (200 mL) and brine (200 mL). The organic extracts were dried over magnesium sulphate, filtered and concentrated *in vacuo* to give dark red residue. This residue was re-dissolved in methanol (100 mL) and solid K₂CO₃ (26 g) was added to the solution. The solution was heated under reflux for 1.5 hr, cooled to room temperature, filtered and concentrated to give a black residue. Dichloromethane (3 mL) was added to the residue which resulted in precipitation of a solid identified as the title compound and supernatant which contained the title compound plus impurities. The supernatant was purified by flash column chromatography (EtOAc:PE, 2:8 v/v) to give the title compound as a brown solid (combined 7.22 g, 60%); The proton and ¹³C data were in agreement with previously published data ¹²²; m.p. 123.2-123.9 °C; IR: 3225, 2791, 1606, 1591, 1494, 1467, 1429, 1395, 1331,

1314, cm^{-1} ; ^1H NMR (DMSO-d_6) δ 10.59 (s, 1H, NH), 7.07 (d, $J=7.1$ Hz, 2H, H-5, H-8), 6.83 (d, $J=7.1$ Hz, 1H, H-6, H-7), 5.20 (s, 2H, CH_2); ^{13}C { ^1H } NMR (DMSO-d_6) δ 141.9 (ArC-O), 127.1 (ArC-N), 123.5 (overlapping, C-6, C-8), 119.9 (C-5), 118.1 (C-7), 76.4 (CH_2); LRMS (ESI) m/z : 186.83 ($\text{M}+\text{H}$) $^+$; HRMS (ESI) m/z calcd. for $\text{C}_7\text{H}_7\text{O}_3\text{NNaS}$ [$\text{M}+\text{Na}$] $^+$ 208.0036, found: 208.0036.

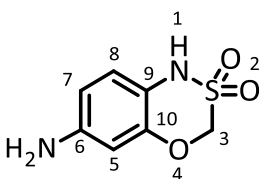
(E)-6-(phenyldiazenyl)-1H-benzo[e][1,3,4]oxathiazine 2,2-dioxide. (8, ICT13003).



Preparation of benzenediazonium salt: To a stirred solution of aniline (4.29 g, 46.00 mmol) in water (25 mL), concentrated hydrochloric acid (10 mL, 37 %) was added drop wise. The solution was left to cool in an ice bath for 15 minutes and then a solution of sodium nitrite (3.32 g) in water (5 mL) was added to give benzenediazonium salt as a yellow solution.

Potassium Carbonate K_2CO_3 (8.40 g, 60.7 mmol) was added to a stirred solution of 1H-benzo[e][1,3,4]oxathiazine 2,2-dioxide **5** (2.80 g, 15.1 mmol) in methanol (25 mL). The reaction mixture left to cool in ice bath and then freshly prepared solution of benzenediazonium salt was added (35 mL). Hydrochloric acid (10 mL, 3M) was then added to the reaction mixture. The mixture was filtered and resultant dark red solid was collected and dried. The crude product was purified by chromatography (EtOAc:PE, 2:8 v/v) to the title compound (1.38 g, 31%) as dark brown solid; 1H NMR (DMSO- d_6) δ 11.28 (s, 1H, NH), 7.86 (d, J = 8.0 Hz, 2H, H-14, H-18), 7.67 (dd, J = 8.5, 2.0 Hz, 1H, H-7), 7.59 (d, J = 8.0 Hz, 2H, H-15, H-17), 7.56 (d, J = 8.5 Hz, 1H, H-8) 7.00-6.98 (m, 2H, H-5, H-16), 5.75 (s, 2H, CH $_2$); ^{13}C { 1H } NMR (DMSO- d_6) δ 151.9 (C-13), 147.1 (C-10), 143.5 (C-6), 130.1 (C-16), 129.9 (C-9), 128.1 (overlapping C-14, C-18), 123.4 (overlapping C-15, C-17), 119.0 (C-8), 117.8 (C-7), 108.1 (C-5), 79.4 (CH $_2$); LRMS (ESI) m/z : 290.1 (M+H) $^+$;

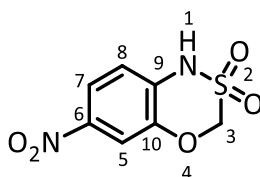
6-amino-1H-benzo[e][1,3,4]oxathiazine 2,2-dioxide. (3, ICT5888).



From Compound **8**: To a stirred solution of compound **8** (0.92 g, 3.17 mmol) in ethanol (50 mL), platinum oxide (70.0 mg) was added. The mixture was left stirring overnight under hydrogen gas. The reaction mixture was filtered, using celite as filtering aid, and concentrated. The product was purified by flash column chromatography (EtOAc:PE, 4:6 v/v → neat EtOAc) to give the *title compound* as light brown solid (0.24 g, 38%);

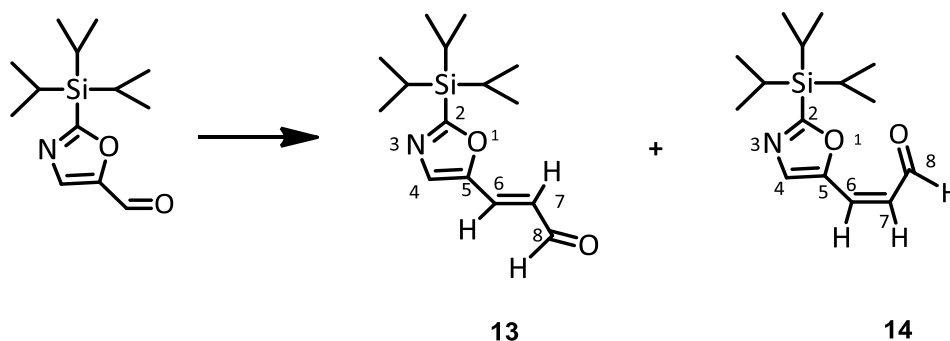
From compound **11** (see next experiment): 250 mL flask was charged with - nitro-1H-benzo[e][1,3,4]oxathiazine 2,2-dioxide **11** (0.28 mg, 1.21 mmol) and EtOAc (40 mL). Palladium on carbon (10% (w/w), 72 mg) was then added carefully. The reaction mixture was stirred at R.T under hydrogen for 24h. The mixture was filtered through celite and concentrated to give (0.27 mg, 92%) of the *title compound* as light brown powder; m.p. 175.1-175.7 °C; IR: 3394, 3345, 3001, 2710, 1624, 1589, 1507, 1423, 1340, 1323 cm⁻¹; ¹H NMR (DMSO-d₆) δ 9.50 (s, 1H, NH), 6.54 (d, *J* = 8.5 Hz, 1H, H-8), 6.26 (dd, *J* = 8.5, 2.5 Hz, 1H, H-7), 6.22 (d, *J* = 2.5 Hz, 1H, H-5), 5.07 (s, 2H, NH₂), 5.03 (s, 2H, CH₂); ¹³C {¹H} NMR (DMSO-d₆) δ 148.4 (C-10), 143.6 (C-6), 122.7 (C-9), 114.9 (C-8), 109.6 (C-7), 102.2 (C-5), 100.8 (CH₂); LRMS (ESI) m/z: 201.83 (M+H)⁺; HRMS (ESI) m/z calcd. for C₇H₉O₃N₂S [M+H]⁺: 201.0328, found: 201.0324.

6-nitro-1H-benzo[e][1,3,4]oxathiazine 2,2-dioxide (11, ICT13031).



To a solution of 1H-benzo[e][1,3,4]oxathiazine 2,2-dioxide **5** (1.00 g, 5.40 mmol) in glacial acetic (8 mL) acid, sodium nitrite (0.45 g, 6.53 mmol) was added. Solution of concentrated glacial acetic acid (4.5 mL) and nitric acid (0.22 mL) was prepared and added drop wise, changes to yellow solution. The reaction solution was left stirring at room temperature for 4 hours. The reaction solution was then poured into a beaker contain mixture of ice and water (50 mL) and the resulted powder was filtered, collected and dried. The crude product was separated and purified by chromatography (EtOAc:PE:Acetic Acid, 2:8:3d) to give the *title compound* (0.70 g, 56%) as yellowish white powder; m.p. 170.5-170.9 °C; IR: 3241, 2947, 1935, 1612, 1529, 1478, 1460, 1432, 1348, 1314, cm⁻¹; ¹H NMR (DMSO-d₆) δ 7.98 (dd, *J* = 8.6, 1.8 Hz, 2H, H-7), 7.94 (d, *J* = 1.8 Hz, 2H, H-5), 7.01 (d, *J* = 1.8 Hz, 1H, H-8), 5.42 (s, 2H, CH₂); ¹³C {¹H} NMR (DMSO-d₆) δ 141.8 (C-10), 140.9 (C-6), 134.5 (C-9), 119.7 (C-7), 118.5 (C-5), 113.9 (C-8), 76.2 (CH₂); LRMS (ESI) *m/z*: 231.4 (M+H)⁺.

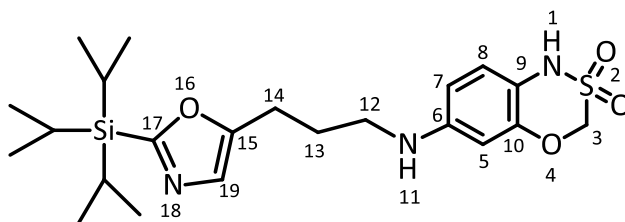
(E) & (Z)-3-(2-(triisopropylsilyl)oxazol-5-yl)acrylaldehyde (13, ICT13040, 14, ICT13041).



A solution of 2-(triisopropylsilyl) oxazole-5-carbaldehyde **12** (0.90 g, 3.5 mmol) in dry toluene (50 mL) was refluxed with 2-(triphenylphosphoranylidene) acetaldehyde **15** (3.23 g, 3 eq.) for 3 hours. The solution was allowed to cool to room temperature and solvent was then reduced under pressure. The crude material was purified by flash chromatography (EtOAc:PE, 1:9 v/v). Which yielded two pure isomers, *compound 13* (0.60 g, 61%) as yellowish orange solid and *compound 14* (0.2 g, 20%) as yellow solid; Compound **13**; m.p. 145.2-146 °C; IR: 3404, 3114, 2942, 2865, 2756, 1666, 1624, 1611, 1548, 1463 cm⁻¹; ¹H NMR (CDCl₃) δ 9.60 (d, *J* = 8.0 Hz, 1H, COH), 7.42 (s, 1H, H-4), 7.25 (d, *J* = 16.0 Hz, 1H, H-6), 6.57 (dd, *J* = 16.0, 8.0 Hz, 1H, H-7), 1.36 (m, 3H, C₃H (CH₃)₆), 1.08 (d, *J* = 7.4 Hz, 18H, C₃(CH₃)₆); ¹³C {¹H} NMR (CDCl₃) δ 192.7 (COH), 172.5 (C-2), 149.4 (C-4), 134.5 (C-6), 131.9 (C-5), 128.1 (C-7), 30.8 (C₃ (CH₃)₆), 18.3 (C(CH₃)₆); LRMS (ESI) *m/z*: 280.1 (M+H)⁺; Compound **14**; m.p. 146.1-146.9 °C; IR: 3405, 3114, 2942, 2866, 2757, 1666, 1624, 1611, 1548, 1463 cm⁻¹; ¹H NMR (CDCl₃) δ 9.56 (d, *J* = 8.0 Hz, 1H, COH), 7.26 (s, 1H, H-4), 6.82 (d, *J* = 8.3 Hz, 1H, H-6), 6.24 (dd, *J* = 8.3, 8.0 Hz, 1H, H-7), 1.26 (m, 3H, C₃H (CH₃)₆), 1.04 (d, *J* = 7.4 Hz, C₃(CH₃)₆); ¹³C {¹H} NMR (CDCl₃) δ 193.3

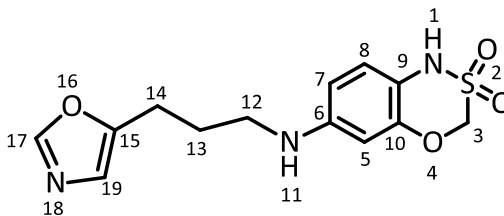
(COH), 150.6 (C-2), 132.4 (C-4), 128.7 (C-6), 126.6 (C-5), 125.4 (C-7), 23.3 (C₃
(CH₃)₆), 17.9 (C (CH₃)₆); LRMS (ESI) m/z: 280.1 (M+H)⁺.

6-((18-(17-(triisopropylsilyl) oxazol-15-yl) propyl) amino)-1H-benzo[e][1,3,4]oxathiazine 2,2-dioxide (17, ICT13042).



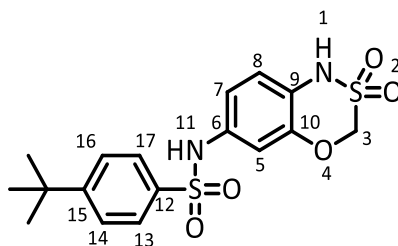
A solution of compound **13** (0.50 g, 1.78 mmol) and compound **3** (0.29 g, 1.49 mmol) in absolute ethanol (9 mL) was left stirring at room temperature overnight. Platinum (IV) oxide (18.0 mg) was then added and the resulting mixture was left stirring under hydrogen for 5 hours at room temperature. The reaction mixture was filtered through celite and concentrated to give dark brown oil. The crude material was purified by flash chromatography (EtOAc:PE 3:7 v/v) to afford the *title compound* as dark brown solid (0.39 g, 56 %); m.p. 171.4-172 °C; ¹H NMR (CDCl₃) δ 6.78 (s, 1H, H-19), 6.63 (d, *J* = 8.6 Hz, 1H, H-8), 6.45 (dd, *J* = 8.6, 2.4 Hz, 1H, H-7), 6.23 (d, *J* = 2.4 Hz, 1H, H-5) 4.98 (s, 1H, CH₂S), 3.06 (t, *J* = 7.2 Hz, 2H, H-12), 2.72 (t, *J* = 7.2 Hz, 2H, H-14), 1.88 (m, 2H, H-13), 1.23 (m, 3H, C₃H (CH₃)₆), 1.10 (d, *J* = 7.4 Hz, 18H, C₃(CH₃)₆). ¹³C {¹H} NMR (CDCl₃) δ 167.8 (C-17), 153.7 (C-10), 122.5 (C-15), 122.2 (C-6), 120.7 (C-19), 116.5 (C-9), 116.2 (C-8) 109.5 (C-7) 104.5 (CH₂S), 94.3 (C-5), 30.9 (C-12), 29.7 (C-14), 23.1 (C-13), 18.4 (C₃ (CH₃)₆), 10.9 (C (CH₃)₆). LRMS (ESI) *m/z*: 466.7 (M+H)⁺, HRMS (ESI) *m/z* calcd. for C₂₂H₃₆N₃O₄SSi [M+H]⁺: 466.0256, found: 466.0254

6-((18-(oxazol-15-yl)propyl)amino)-1H-benzo[e][1,3,4]oxathiazine 2,2-dioxide (1, ICT5189).



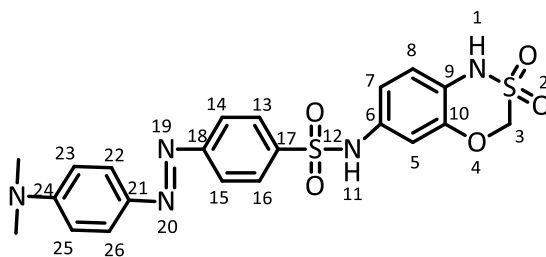
A 1M solution of tetra butylammonium fluoride (TBAF) (0.15 mL, 1 eq) was added to a solution of compound **17** (68.3 mg, 0.14 mmol) in THF (7.35 mL) at room temperature. The reaction solution was left stirring under nitrogen for 15 minutes. The completion of the reaction was monitored by TLC. The reaction mixture was directly impregnated on silica and purified by flash chromatography (EtOAc:PE, 6:4 v/v) to give the title compound as dark brown solid (41.3 mg, 95%); m.p. 160.5-161 °C; IR: 3401, 2929, 2852, 1625, 1588, 1509, 1433, 1392, 1326, 1212 cm^{-1} ; ^1H NMR (Acetone- d_6) δ 7.86 (s, 1H, H-17), 6.71 (s, 1H, H-19), 6.59 (d, J = 8.6 Hz, 1H, H-8), 6.25 (dd, J = 8.6, 2.4 Hz, 1H, H-7), 6.15 (d, J = 2.4 Hz, 1H, H-5), 4.87 (s, 2H, CH_2S), 3.02 (t, J = 7.6 Hz, 2H, H-12), 2.69 (t, J = 7.6 Hz, 2H, H-14), 1.82 (m, 2H, H-13); ^{13}C { ^1H } NMR (Acetone- d_6) δ 153.4 (C-17), 151.4 (C-10), 145.4 (C-10, C-6), 124.5 (C-19), 122.8 (C-8), 116.1 (C-9), 109.3 (C-7), 101.4 (CH_2S), 77.8 (C-5), 43.5 (C-12), 27.9 (C-14), 23.4 (C-13); LRMS (ESI) m/z : 310.1 ($\text{M}+\text{H}$) $^+$; HRMS (ESI) m/z calcd. for $\text{C}_{13}\text{H}_{16}\text{O}_4\text{N}_3\text{S}$ [$\text{M}+\text{H}$] $^+$: 310.0856, found: 310.0858.

15-(tert-butyl)-N-(2,2-dioxido-1H-benzo[e][1,3,4]oxathiazin-6-yl) benzenesulfonamide (18, ICT13081).



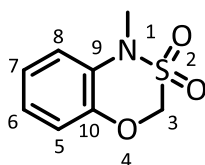
Round bottom flask was charged with 6-amino-1H-benzo[e][1,3,4]oxathiazine 2,2-dioxide **3** (0.10 g, 0.50 mmol) and dry pyridine (7 mL). The solution was treated dropwise with solution of 4-tert-butylbenzenesulfonyl chloride **61** (0.13 g, 0.60 mmol) in DCM with constant stirring and cooling to 0 °C. After the addition was over, the mixture was stirred for 5 hour at R.T and then poured over ice and water. The solid was filtered, washed with water and extracted with ethyl acetate (3x50 mL). The combined organic extracts were dried over anhydrous MgSO₄, filtered and the solvent was removed under reduced pressure. The resultant material was purified by flash column chromatography (EtOAc:PE, 2:8 v/v) to give the *title compound* (0.15 g, 80%) as white powder; m.p: 165.4-165.9 °C; IR: 3274, 2963, 1593, 1507, 1405, 1329, 1306, 1291, 1255, 1196 cm⁻¹; ¹H NMR (Acetone-d₆) δ 7.67 (d, *J* = 8.7 Hz, 2H, H-13, H-17), 7.51 (d, *J* = 8.7 Hz, 2H, H-14, H-16), 6.83 (dd, *J* = 8.5, 2.3 Hz, 1H, H-7), 6.81 (d, *J* = 2.3 Hz, 1H, H-5), 6.72 (d, *J* = 8.5 Hz, 1H, H-8), 4.94 (s, 2H, CH₂), 1.18 (s, 9H, C(CH₃)₃); ¹³C {¹H} NMR (Acetone-d₆) δ 156.9 (C-15), 143.8 (C-10), 137.6 (C-12), 135.2 (C-6), 127.7 (overlapping C-13, C-17), 126.9 (overlapping C-14, C-16), 124.3 (C-9), 124.1 (C-8), 122.5 (C-7), 116.6 (CH₂), 111.1 (C-5), 76.7 (CH₂), 35.6 (C(CH₃)₃), 31.2 (C(CH₃)₃); LRMS (ESI) *m/z*: 395.98 (M-H)⁻; HRMS (ESI) *m/z* calcd. for C₁₇H₂₄O₅N₃S₂ [M+NH₄]⁺: 414.1152, found: 414.1149

17-((17-(dimethylamino)phenyl)diazenyl)-N-(2,2-dioxido-1H-benzo[e][1,3,4]oxathiazin-6-yl)benzenesulfonamide (19, ICT13088).



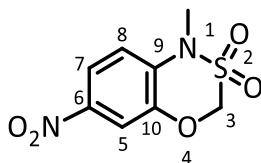
Compound 6-amino-1H-benzo[e][1,3,4]oxathiazine 2,2-dioxide **3** (0.10 g, 0.50 mmol) in dry pyridine (10 mL) was treated dropwise with Dabsyl chloride (0.19 g, 0.60 mmol) with constant stirring and cooling to 0 °C. After the addition was over, the mixture was stirred for 5h at R.T and then poured over ice and water. The solid was filtered, washed with water and extracted with ethyl acetate (3x50 mL). The combined organic extracts were dried over anhydrous MgSO₄, filtered and the solvent was evaporated under reduced pressure. The resultant material was purified by flash column chromatography (EtOAc:PE, 2:8 v/v) to give the *title compound* (0.13 g, 70 %) as a light red powder; m.p: 171.1-171.6 °C; ¹H NMR (Acetone-d₆) δ 7.77 (d, *J* = 9.7 Hz, 4H, H-14, H-15, H-22, H-26), 7.73 (d, *J* = 9.2 Hz, 2H, H-13, H-16), 6.85 (d, *J* = 2.4 Hz, 1H, H-5), 6.81 (dd, *J* = 8.6, 2.4 Hz, 1H, H-7), 6.70 (d, *J* = 8.8 Hz, 3H, H-23, H-25, H-5), 4.88 (s, 2H, CH₂), 3.02 (s, 6H, N(CH₃)₂); ¹³C {¹H} NMR (Acetone-d₆) δ 156.2 (C-18), 153.6 (C-24), 143.9 (C-10), 143.9 (C-21), 139.7 (C-17), 135.3 (C-9), 128.9 (overlapping C-22, C-26), 126.1 (overlapping C-13, C-16), 124.9 (C-6), 123.2 (overlapping C-14, C-15), 122.2 (H-8), 117.4 (C-7), 112.3 (overlapping C-23, C-25), 112.1 (CH₂), 108.4 (C-5), 40.1 (s, N(CH₃)₂); LRMS (ESI) *m/z*: 488.04 (M+H)⁺; HRMS (ESI) *m/z* calcd. for C₂₁H₂₂O₅N₅S₂ [M+H]⁺: 488.1057, found: 488.1050.

1-methyl-1H-benzo[e][1,3,4]oxathiazine 2,2-dioxide (23, ICT13006).



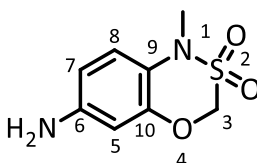
Potassium carbonate (0.24 g, 1.73 mmol) and methyl iodide (3.41g, 24.0 mmol) were added to a solution of compound **5** (0.22 g, 1.18 mmol) in acetone (10 mL). The reaction mixture was stirred at room temperature for 24 hour. Organic components were extracted with DCM (3x50mL). The combined organic extracts were dried over anhydrous MgSO₄, filtered and stripped of solvent under reduced pressure to give brown solid. The resultant material was purified by flash column chromatography (EtOA:PE, 2:8 v/v) to give the *title compound* as white solid material (160 mg, 68%); m.p. 112.1-112.6 °C; IR: 2923,1583, 1488, 1429, 1343, 1319, 1297, 1251, 1223, 1202 cm⁻¹; ¹H NMR (CDCl₃) δ 6.97 (m, 3H, H5, H-6, H-7), 6.87 (d, *J* = 7.8 Hz, 1H, H-8), 4.85 (s, 2H, CH₂), 3.19 (s, 3H, CH₃); ¹³C {¹H} NMR (CDCl₃) δ 143.1 (C-10), 129.9 (C-9), 124.4 (C-7), 123.9 (C-8), 121.3 (C-6), 118.6 (C-5), 76.8 (CH₂), 32.1 (CH₃); LRMS (ESI) *m/z*: 200.23 (M+H)⁺; HRMS (ESI) *m/z* calcd. for C₈H₉O₃NS [M]⁺: 199.0296, found: 199.0295

1-methyl-6-nitro-1H-benzo[e][1,3,4]oxathiazine 2,2-dioxide (24, ICT13046).



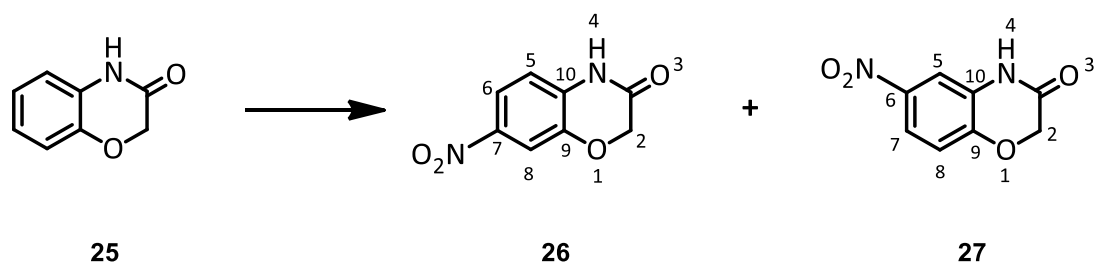
Potassium carbonate (119 mg, 0.86 mmol) and methyl iodate (1.67g, 11.7 mmol) were added to a solution of 2-nitro-1H-benzooxathiazine **11** (0.1 g, 4.34 mmol) in acetone (5 mL). The reaction mixture was stirred at room temperature for 24 hour. Organic components were extracted with DCM (3x20mL). The combined organic extracts were dried over anhydrous MgSO₄, filtered and stripped of solvent under reduced pressure to give yellow solid. The resultant materials was purified by flash column chromatography (EtOA:PE, 2:8 v/v) to give the *title compound* as yellow solid material (0.7 g, 66%); m.p. 165.5-166 °C; IR: 3097, 3011, 2923, 2853, 1729, 1577, 1518, 1466, 1371, 1361 cm⁻¹; ¹H NMR (Acetone-d₆) δ 7.72 (dd, *J* = 8.1, 1.4 Hz, 1H, H-7), 7.52 (d, *J* = 1.4 Hz, 1H, H-5), 7.43 (d, *J* = 8.1, 1H, H-8), 5.48 (s, 2H, CH₂), 3.26 (s, 3H, CH₃); ¹³C {1H} NMR (Acetone-d₆) δ 147.5 (C-10), 146.6 (C-9), 128.7 (C-6), 125.8 (C-5), 123.7 (C-7), 120.2 (C-8), 73.9 (CH₂), 42.5 (CH₃); LRMS (ESI) *m/z*: 245.1 (M+H)⁺; HRMS (ESI) *m/z* calcd. for C₈H₉N₂O₅S [M+H]⁺: 245.0490, found: 245.0489

6-amino-1-methyl-1H-benzo[e][1,3,4]oxathiazine 2,2-dioxide (20, ICT13047).



25 mL flask was charged with compound **24** (70.0 mg, 0.28 mmol) and EtOAc (3 mL). Palladium on carbon (10% (w/w), 4.00 mg) was then added carefully. The reaction mixture was stirred at R.T under hydrogen for 24h. The mixture was filtered through celite and concentrated to give (50.0 mg, 83%) of the *title compound* as yellowish white solid; m.p. 150.9-151.7 °C; IR: 3394, 3345, 3001, 2710, 1623, 1589, 1507, 1423, 1340, 1320 cm⁻¹; ¹H NMR (CDCl₃) δ 6.93 (d, *J* = 8.3 Hz, 1H, H-8), 6.39 (dd, *J* = 8.3, 1.2 Hz, 1H, H-7), 6.36 (d, *J* = 1.2 Hz, 1H, H-5), 4.95 (s, 2H, CH₂), 4.04 – 3.77 (s, 2H, NH₂), 3.07 (s, 3H, CH₃); ¹³C {¹H} NMR (CDCl₃) δ 146.9 (C-10), 143.5 (C-6), 128.6 (C-9), 117.5 (C-8), 110.3 (C-7), 107.7 (C-5), 74.2 (CH₂), 39.7 (CH₃); LRMS (ESI) *m/z*: 215.1 (M+H)⁺; HRMS (ESI) *m/z* calcd. for C₈H₁₁N₂O₃S [M+H]⁺: 215.0485, found: 215.0485.

7-nitro and 7-nitro-2H-benzo[b][1,4]oxazin-3(4H)-one. (26, ICT13004), (27, ICT13011).

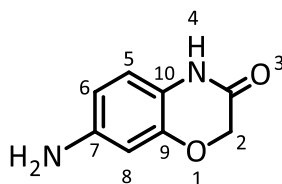


To a solution of 2H-benzo[b][1,4]oxazin-3(4H)-one **25** (0.90 g, 6.04 mmol) in glacial acetic (8 mL) acid, sodium nitrite (0.51 g, 7.39 mmol) was added. Solution of glacial acetic acid (5 mL) and concentrated nitric acid (3.5 mL) was prepared and added drop wise to the previous solution, the colourless solution turned to yellow. The reaction solution was left stirring at room temperature for 4 h. The solution was then poured into a beaker contain mixture of ice and water (50 g) and the precipitate powder filtered, collected and dried. The crude product was separated and purified by chromatography (EtOAc:PE, 2:8 v/v) to the two isomers. The first isomer, 2-nitro-2H-benzo[b][1,4]oxazin-3(4H)-one **26** (0.33 g, 28%) was yellow colour powder. The second isomer, 1-nitro-2H-benzo[b][1,4]oxazin-3(4H)-one **27** (0.77 g, 66%) was white powder;

Synthesis of compound **26** by different route: 500 mL round bottom flask was charged with 2-amino-5 nitro phenol (5 g, 32.4 mmol) and 200 mL acetonitrile. Sodium bicarbonate (10.9 g, 129 mmol) was added to previous solution and was left stirring for 10 minutes. The mixture was put in an ice-salt bath to keep the temperature at 0 C°. To this stirring mixture, 2-chloroacetylchloride (4.75 g, 0.04 mmol) was added dropwise and mixture was left stirring on ice bath for 40 minutes. The reaction mixture was then refluxed on an oil bath for 2 h. Acetonitrile was removed under reduced pressure to obtain yellow colour

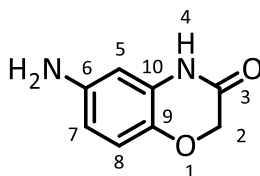
powder. The product was recrystallized using ethanol:water (1:1) to give the title compound (4.2 g, 67%); compound 26; the proton and ^{13}C data were in agreement with previously published data ¹⁵⁷; m.p. 219-220 °C (Lit., 219-222 °C) ¹²⁴; IR: 3144, 3081, 2965, 2886, 1794, 1698, 1670, 1601, 1525, 1504 cm^{-1} ; ^1H NMR (DMSO- d_6) δ 11.10 (s, 1H, NH), 7.88 (dd, $J = 9.1, 2.7$ Hz, 1H, H-6), 7.75 (d, $J = 2.7$ Hz, 1H, H-8), 7.19 (d, $J = 9.1$ Hz, 1H, H-5), 4.78 (s, 2H, CH_2); ^{13}C { ^1H } NMR (DMSO- d_6) δ 163.7 (CO), 148.6 (C-9), 141.7 (C-7), 127.6 (s, C-10), 119.1 (C-8), 116.5 (C-6), 110.7 (C-5), 66.7 (CH_2); LRMS (ESI) m/z : 195.09 ($\text{M}+\text{H}$)⁺; HRMS (ESI) m/z calcd. for $\text{C}_8\text{H}_7\text{O}_4\text{N}_2$ [$\text{M}+\text{H}$]⁺: 195.0400, found: 195.0397; compound 27; the proton and ^{13}C data were in agreement with previously published data ¹⁵⁸. m.p. 220.2-223.7 °C (Lit., 219-222 °C)¹⁵⁹; IR: 3134, 3082, 2955, 2872, 1792, 1693, 1672, 1604, 1534, 1523 cm^{-1} ; ^1H NMR (DMSO- d_6) δ 11.35 (s, 1H, NH), 7.91 (dd, $J = 9.1, 2.7$ Hz, 1H, H-7), 7.77 (d, $J = 2.7$ Hz, 1H, H-5), 7.06 (d, $J = 9.1$ Hz, 1H, H-8), 4.76 (s, 2H, CH_2); ^{13}C { ^1H } NMR (DMSO- d_6) δ 164.7 (CO), 142.8 (C-9), 142.2 (C-6), 133.8 (C-10), 118.7 (C-7), 115.6 (C-8), 111.4 (C-5), 66.5 (CH_2); LRMS (ESI) m/z : 195.06 ($\text{M}+\text{H}$)⁺; HRMS (ESI) m/z calcd. for $\text{C}_8\text{H}_7\text{O}_4\text{N}_2$ [$\text{M}+\text{H}$]⁺: 195.0400, found: 195.0397.

7-amino-2H-benzo[b][1,4]oxazin-3(4H)-one. (21, ICT13008).



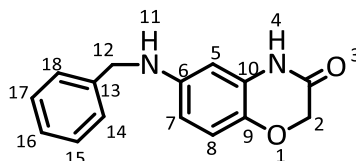
Mixture of compound **26** (0.33 g, 1.70 mmol) and 10% w/w palladium on carbon (0.1g) was suspended in ethanol (40 mL). The reaction mixture was left stirring under hydrogen overnight. The reaction mixture was filtered, using celite as filtering agent, and concentrated to give the title compound (0.26 g, 94%) as solid white powder; the proton and ^{13}C data were in agreement with previously published data ¹⁵⁷; m.p. 213.2-214 °C (Lit., 212-215 °C) ¹²⁴; IR: 3374, 3315, 3190, 2985, 2904, 1672, 1614, 1515, 1436, 1405 cm^{-1} ; ^1H NMR (DMSO- d_6) δ 10.47 (s, 1H, NH), 6.59 (d, J = 8.6 Hz, 1H, H-5), 6.16 (d, J = 2.5 Hz, 1H, H-8), 6.10 (dd, J = 8.6, 2.5 Hz, 1H, H-6), 4.87 (s, 2H, NH_2), 4.27 (s, 2H, CH_2); ^{13}C { ^1H } NMR (DMSO- d_6) δ 165.6 (CO), 144.2 (C-9), 134.0 (C-7), 127.6 (C-10), 116.3 (C-5), 108.1 (C-6), 101.3 (C-8), 66.9 (CH_2); LRMS (ESI) m/z : 165.01 (M+H)⁺.

6-amino-2H-benzo[b][1,4]oxazin-3(4H)-one (30, ICT13010).



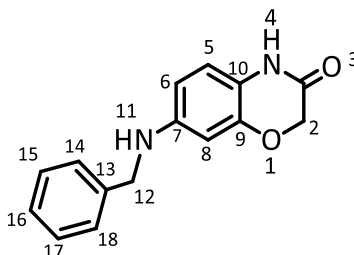
Mixture of compound **27** (0.40g, 2.06 mmol) and 10% w/w palladium on carbon (0.1g) was suspended in ethanol (40 mL). The reaction mixture was left stirring under hydrogen overnight. The reaction mixture was filtered, using celite as filtering agent, and concentrated to give the title compound (0.30g, 88%) as a pink powder; the proton and ¹³C data were in agreement with previously published data ¹⁵⁸; m.p. 232.1-132.6 °C (Lit., >228 °C) ¹⁵⁹; IR: 3361, 3325, 3204, 2982, 2912, 1662, 1614, 1525, 1426, 1409 cm⁻¹; ¹H NMR (DMSO-d₆) δ 10.28 (s, 1H, NH), 6.84 (d, *J* = 8.4 Hz, 1H, H-8), 6.56 (d, *J* = 2.5 Hz, 1H, H-5), 6.17 (dd, *J* = 8.4, 2.5 Hz, 1H, H-7), 4.89 (s, 2H, NH₂), 4.41 (s, 2H, CH₂); ¹³C {¹H} NMR (DMSO-d₆) δ 206.5 (CO), 163.8 (C-9), 145.0 (C-6), 144.1 (C-10), 116.2 (C-8), 107.8 (C-7), 101.8 (C-5), 66.7 (CH₂); LRMS (ESI) m/z: 165.01 (M+H)⁺.

6-(benzylamino)-2H-benzo[b][1,4]oxazin-3(4H)-one (34, ICT13012).



To a solution of 6-amino-(2H-benzo[b][1,4]oxazin-3(4H)-one) **27** (0.40 g, 2.43 mmol) in dichloromethane (50 mL), 3 equivalent of benzaldehyde **31** (0.65 g, 6.12 mmol) was added. The reaction mixture was left stirring over moderate speed for 48 hours. Small amount from the reaction mixture enough to run proton NMR was taken and dried to monitor formation of the imine, compound **32**. ^1H NMR (DMSO) δ 10.80 (s, 1H, NH), 8.64 (s, 1H, CHN), 7.91 (d, $J = 7.0$, Hz, 2H, H-14, H-18), 7.79 (d, $J = 2.9$ Hz, 1H, H-5), 7.51 (dd, $J = 7.8, 2.7$ Hz, 3H, H-15, H-16, H-17), 6.98 (d, $J = 8.2$ Hz, 1H, H-8), 6.96 (dd, $J = 8.2, 2.9$ Hz, 1H, H-7), 4.60 (s, 2H, CH_2O). Half equivalent of sodium borohydride (70.0 mg, 1.85 mmol) was added to the reaction mixture and was left stirring over moderate speed, 24 hours. The mixture then concentrated to give yellow solid materials. The solid product was purified by flash column chromatography (EtOAc:PE, 2:8 v/v) to give the title compound as brown solid (0.48 g, 78%); m.p. 160.5-160.9 $^\circ\text{C}$; ^1H NMR (CDCl_3) δ 9.08 (s, 1H, NH), 7.24 (m, 5H, H-14, H-15, H-16, H-17, H-18), 6.58 (d, $J = 8.3$ Hz, 1H, H-8), 6.20 (d, $J = 2.4$ Hz, 1H, H-5), 6.16 (dd, $J = 8.3, 2.4$ Hz, 1H, H-7), 4.47 (s, 2H, CH_2O), 4.20 (s, 2H, CH_2N); ^{13}C { ^1H } NMR (CDCl_3) δ 165.5 (CO), 145.5 (C-13), 144.8 (C-9), 139.0 (C-6), 128.7 (overlapping C-15, C-17), 127.4 (overlapping C-16, C-18), 127.8 (C-14). 116.8 (C-10), 111.2 (C-7), 105.3 (C-8), 107.1 (C-5), 71.3 (CH_2), 48.5 (CH_2N); LRMS (ESI) m/z: 255.14 (M+H) $^+$.

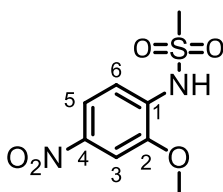
7-(benzylamino)-2H-benzo[b][1,4]oxazin-3(4H)-one (35, ICT13016).



250 mL round bottom flask was charged with 7-amino-(2H-benzo[b][1,4]oxazin-3(4H)-one) **26** (0.38g, 2.32mmol) and dichloromethane (50 mL). One equivalent of benzaldehyde **31** (0.65 g, 6.12 mmol) was then added to previously stirring solution. The reaction mixture was left stirring over moderate speed 48 hours at room temperature under nitrogen condition. Small amount from the reaction mixture enough to run proton NMR was taken and dried to monitor formation of the imine, compound **33**. ^1H NMR (CDCl_3) δ 10.84 (s, 1H, NH), 8.66 (s, 1H, CHN), 7.95 (d, $J = 7.0$, Hz, 2H, H-14, H-18), 7.81 (d, $J = 2.9$ Hz, 1H, H-8), 7.52 (m, 3H, H-15, H-16, H-17), 7.08 (d, $J = 8.2$ Hz, 1H, H-5), 6.96 (dd, $J = 8.2$, 2.9 Hz, 1H, H-7), 4.60 (s, 2H, CH_2). Half equivalent of sodium borohydride (70.0 mg, 1.85 mmol) was added and the mixture was left stirring over moderate speed for 24 hours. The reaction mixture then concentrated to give yellow solid materials. The solid product was purified by flash column chromatography (EtOAc:PE, 2:8 v/v) to give the title compound as brown solid (0.40 g, 67%); m.p. 139.1-139.9 °C (Lit., 138-140 °C) ¹²⁴; ^1H NMR (CDCl_3) δ 8.08 (s, 1H, NH), 7.23 (m, 5H, H-14, H-15, H-16, H-17, H-18), 6.81 (d, $J = 8.3$ Hz, 1H, H-5), 6.18 (d, $J = 2.4$ Hz, 1H, H-8), 6.13 (dd, $J = 8.3$, 2.4 Hz, 1H, H-6), 4.79 (s, 2H, CH_2O), 4.30 (s, 2H, CH_2N); ^{13}C {1H} NMR (CDCl_3) δ 168.1 (CO), 153.1 (C-9), 144.0 (C-7), 139.9 (overlapping C-14, C-18), 128.5 (C-13), 126.9 (overlapping C-15, C-

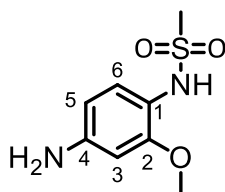
17), 126.3 (C-16), 123.3 (C-5), 115.2 (C-10), 110.1 (C-6), 96.5 (C-8), 69.3 (CH₂), 48.2 (CH₂N); LRMS (ESI) m/z: 255.14 (M+H)⁺.

N-(2-methoxy-4-nitrophenyl)methanesulfonamide (38, ICT13019).



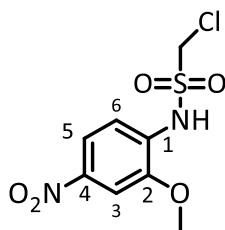
Solution of 2-methoxy-4-nitroaniline **37** (1.00 g, 5.94 mmol) in dry pyridine (5 mL) was treated dropwise with methanesulfonyl chloride **36** (0.55 mL, 7.13 mmol) with stirring and cooling to 0 °C. After the addition was over, the mixture was stirred for 5h at R.T and then poured over ice and water. The solid formed was filtered, washed with water and recrystallized from acetone-hexane to give the title compound (1.20 g, 82%) as yellow powder; m.p. 146.7-147 °C (Lit., 146 °C) ¹⁶⁰; IR: 3257, 3119, 3028, 2937, 1588, 1530, 1495, 1450, 1417, 1350 cm⁻¹; ¹H NMR (CDCl₃) δ 7.95 (d, *J* = 2.5 Hz, 1H, H-3) 7.92 (dd, *J* = 8.6, 2.5 Hz, 1H, H-5), 7.49 (d, *J* = 8.6 Hz, 1H, H-6), 7.28 (s, 1H, NH) 3.96 (s, 3H, OCH₃), 3.16 (s, 3H, SCH₃). ¹³C {¹H} NMR (CDCl₃) δ 157.8 (C-2), 149.8 (C-4), 133.1 (C-6), 128.4 (C-1), 116.3 (C-5), 107.8 (C-3), 56.9 (OCH₃), 43.7 (SCH₃); LRMS (ESI) m/z: 247.2 (M+H)⁺.

N-(4-amino-2-methoxyphenyl)methanesulfonamide (22, ICT13029).



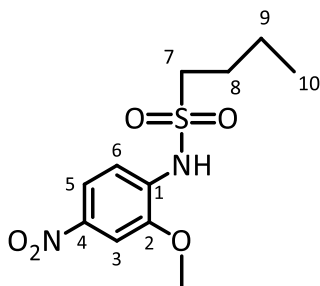
250 mL flask was charged with N-(2-methoxy-4-nitrophenyl) methanesulfonamide **38** (0.67 g, 2.72 mmol) and MeOH (20 mL). Palladium on carbon (10% (w/w), 67 mg) was then added carefully. The reaction mixture was stirred at R.T under hydrogen for 24h. The mixture was filtered through celite and concentrated. The residue was then purified by crystallization EtOAc-PE to give (0.50 g, 85%) of the title compound; m.p. 193.7-194 °C (Lit., 193-194 °C)¹⁶¹; IR: 3447, 3369, 2931, 1629, 1588, 1530, 1495, 1450, 1417, 1350 cm⁻¹; ¹H NMR (CDCl₃) δ 7.19 (s, 1H, NH), 6.94 (d, *J* = 9.2 Hz, 1H, H-6), 6.19 (dd, *J* = 9.2, 2.4 Hz, 1H, H-5), 6.15 (d, 2.4 Hz, 1H, H-3) 3.81 (s, 3H, OCH₃), 3.31 (s, 3H, SCH₃); ¹³C {¹H} NMR (CDCl₃) δ 157.4 (C-2), 150.1 (C-4), 132.9 (C-6), 112.2 (C-1), 107.2 (C-5), 98.8 (C-3), 55.8 (OCH₃), 43.4 (SCH₃); LRMS (ESI) m/z: 217.0 (M+H)⁺.

Chloro-N-(2-methoxy-4-nitrophenyl)methanesulfonamide (41, ICT13018).



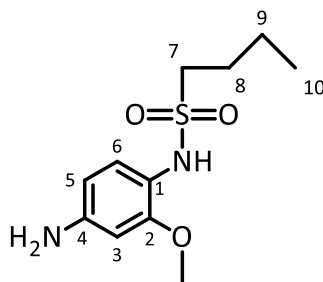
To solution of 2-methoxy-4-nitroaniline **37** (1.00 g, 5.94 mmol) in dry pyridine (5 mL), chloromethanesulfonyl chloride (0.64 mL, 7.13 mmol) was added drop wise. The mixture was then stirred and cooled 0 °C. After the addition was over, the mixture was stirred for 5h at R.T and then poured over ice and water. The solid was filtered, washed with water and recrystallized from acetone-hexane to give the title compound (1.50 g, 90%) as yellow crystals; m.p. 171.2-171.7 °C; IR: 3255, 3096, 3016, 2956, 1592, 1525, 1499, 1454, 1434, 1393 cm⁻¹; ¹H NMR (CDCl₃) δ 7.85 (dd, *J* = 8.7, 2.4 Hz, 1H, H-5), 7.74 (d, *J* = 2.4 Hz, 1H, H-3), 7.65 (d, *J* = 8.7 Hz, 1H, H-6), 7.40 (s, 1H, NH), 4.53 (s, 2H, CH₂), 3.97 (s, 3H, OCH₃); ¹³C {¹H} NMR (CDCl₃) δ 148.1 (C-2), 144.6 (C-4), 131.7 (C-1), 117.5 (C-6), 117.3 (C-5), 106.2 (C-3), 56.7 (CH₂), 54.5 (CH₃); LRMS (ESI) *m/z*: 281.2 (M+H)⁺.

N-(2-methoxy-4-nitrophenyl)butanesulfonamide (42, ICT13022).



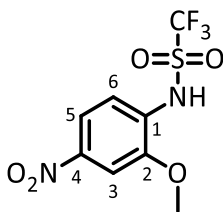
To a stirred solution of 2-methoxy-4-nitroaniline **37** (1.00 g, 5.94 mmol) in dry pyridine (5 mL) was treated dropwise with butane-1-sulfonyl chloride (0.92 mL, 7.13 mmol) with stirring and cooling to 0 °C. After the addition was over, the mixture was stirred for 5h at R.T and then poured over ice and water. The solid was filtered, washed with water and recrystallized from acetone-hexane to give the title compound (1.20 g, 70%) as brown solid; m.p. 98.3-98.9 °C; IR: 3475, 3319, 3095, 2924, 2871, 1732, 1621, 1594, 1499, 1466 cm⁻¹; ¹H NMR (CDCl₃) δ 7.85 (dd, *J* = 8.8, 2.4 Hz, 1H, H-5), 7.71 (d, *J* = 2.4 Hz, 1H, H-3), 7.58 (d, *J* = 8.8 Hz, 1H, H-6), 7.15 (s, 1H, NH), 3.94 (s, 3H, OCH₃), 3.09 (t, *J* = 7.9 Hz, 2H, H-7), 1.73 (m, 2H, H-8), 1.36 (m, 2H, H-9), 0.84 (t, *J* = 7.4 Hz, 3H, H-10); ¹³C {¹H} NMR (CDCl₃) δ 147.4 (C-2), 143.6 (C-4), 133.0 (C-1), 117.7 (C-6), 116.1 (C-5), 106.0 (C-3), 56.5 (OCH₃), 52.2 (C-8), 25.4 (C-7), 21.3 (C-9), 13.4 (C-10); LRMS (ESI) m/z: 289.3 (M+H)⁺.

N-(4-amino-2-methoxyphenyl)butanesulfonamide (48, ICT13036).



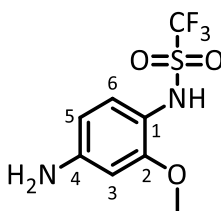
100 mL flask was charged with N-(2-methoxy-4-nitrophenyl) butane-1-sulfonamide **42** (0.5 g, 1.73 mmol) and ethyl acetate (20 mL). Palladium on carbon (10% (w/w) (10.4 mg, 0.037 mmol) was then added carefully. The reaction mixture was stirred at R.T under hydrogen for 24h. The mixture was filtered through celite and concentrated to give *the* title compound as yellow solid (0.40 g, 89%); m.p. 180.2-180.9 °C; IR: 3436, 3364, 3293, 3259, 2962, 2933, 1635, 1613, 1592, 1512 cm⁻¹; ¹H NMR (CDCl₃) δ 7.19 (d, *J* = 8.7 Hz, 1H, H-6), 6.29, (s, 1H, NH), 6.19 (dd, *J* = 8.7, 2.5 Hz, 1H, H-5), 6.18 (d, *J* = 2.5 Hz, 1H, H-3), 3.74 (s, 3H, OCH₃), 2.92 (t, *J* = 8.0 Hz, 2H, H-7), 1.69 (m, 2H, H-8), 1.30 (m, 2H, H-9), 0.81 (t, *J* = 7.4 Hz, 3H, H-10); ¹³C {¹H} NMR (CDCl₃) δ 151.8 (C-2), 145.6 (C-4), 125.0 (C-6), 116.4 (C-1), 107.3 (C-5), 98.4 (C-3), 55.5 (C-8), 50.4 (OCH₃), 25.3 (C-7), 21.5 (C-9), 13.8 (C-10); LRMS (ESI) *m/z*: 259.4 (M+H)⁺; HRMS (ESI) *m/z* calcd. for C₁₁H₁₉N₂O₃S [M+H]⁺: 259.1111, found: 259.1113.

Trifluoro-N-(2-methoxy-4-nitrophenyl)methanesulfonamide (43, ICT13060).



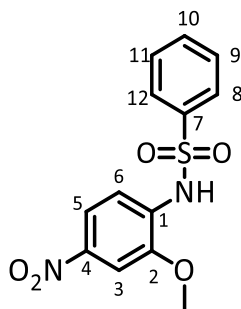
To a stirred suspension of 2-methoxy-4-nitroaniline **37** (0.50 g, 2.97 mmol) and sodium bicarbonate (124 mg, 1.47 mmol) in dichloromethane (10 mL), maintained at 0 °C under nitrogen atmosphere was added trifluoromethanesulfonic anhydride (0.49 mL, 2.97 mmol). The reaction mixture was brought to room temperature and was stirred for 6 h. Hydrochloric acid solution (10 mL, 2M) was added to the reaction mixture. Organic components were extracted with DCM (3x50mL). The combined organic extracts were dried over anhydrous MgSO₄, filtered and stripped of solvent under reduced pressure. The residue was purified by flash column chromatography (EtOAc:PE, 2:8 v/v) to give the title compound as yellow needles (0.70 g, 78%); m.p: 105.2-105.6 °C (Lit., 103-105 °C)¹; IR: 3471, 3381, 3257, 2923, 1592, 1501, 1446, 1417, 1377, 1328 cm⁻¹; ¹H NMR (CDCl₃) δ 7.86 (dd, *J* = 8.7, 2.4 Hz, 1H, H-5), 7.75 (d, *J* = 2.4 Hz, 1H, H-3), 7.63 (d, *J* = 8.7 Hz, 1H, H-6), 7.43 (s, 1H, NH), 3.98 (s, 3H, OCH₃); ¹³C {¹H} NMR (CDCl₃) δ 148.6 (C-2), 145.3 (C-4), 129.7 (C-1), 124.5 (q, *J_F* = 298.9 Hz, CF₃), 118.7 (C-6), 117.2 (C-5), 106.2 (C-3), 56.8 (OCH₃); LRMS (ESI) *m/z*: 301.2 [M+H]⁺; HRMS (ESI) *m/z* calcd. For C₈H₈F₃N₂O₅S [M+H]⁺: 301.0101, found: 301.0104.

Trifluoro-N-(4-amino-2-methoxyphenyl)methanesulfonamide (49, ICT13063).



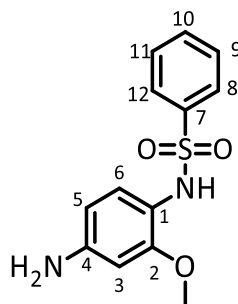
Palladium on carbon 10% w/w (0.10 g) was added to a solution of compound **43** (0.20 g, 0.66 mmol) in ethanol (20 mL). The reaction mixture was left stirring under hydrogen overnight. The reaction mixture was filtered, using celite as filtering agent, and concentrated to give the title compound (0.16 g, 89 %) as brown solid; m.p: 123.3-124.7 °C (Lit., 123-124 °C)²; IR: 3494, 3443, 3393, 3276, 2950, 2845, 1609, 1593, 1513, 1470 cm⁻¹; ¹H NMR (CDCl₃) δ 7.19 (s, 1H, NH), 7.14 (d, *J* = 8.9 Hz, 1H, H-6), 6.17 (dd, *J* = 8.9, 2.4 Hz, 1H, H-5), 6.15 (d, *J* = 2.4 Hz, 1H, H-3), 3.74 (s, 3H, OCH₃); ¹³C {¹H} NMR (CDCl₃) δ 153.5 (C-2), 147.2 (C-4), 126.6 (C-6), 120.0 (q, *J_F* = 298.9 Hz, CF₃), 113.9 (C-1), 106.9 (C-5), 98.3 (C-3), 55.5 (OCH₃); LRMS (ESI) *m/z*: 271.1 (M+H)⁺; HRMS (ESI) *m/z* calcd. for C₈H₁₀F₃N₂O₃S[M+H]⁺: 271.0359 found: 271.0361.

N-(2-methoxy-4-nitrophenyl)benzenesulfonamide (44, ICT13021).



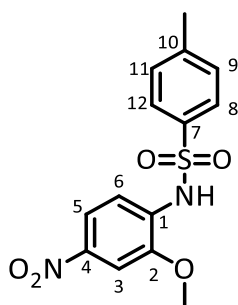
A 250 size flask was charged with 2-methoxy-4-nitroaniline **37** (1.00 g, 5.94 mmol) and dry pyridine (5 mL). The solution was treated dropwise with benzenesulfonyl chloride (0.90 mL, 7.13 mmol) with constant stirring and cooling to 0 °C. After the addition was over, the mixture was stirred for 5h at R.T and then poured over ice and water. The solid was filtered, washed with water and recrystallized from acetone-cyclo-hexane to give the title compound (1.50 g, 81%) as pale yellow crystals; m.p. 181.1-182 °C; IR: 3284, 3237, 3067, 2939, 1592, 1518, 1496, 1447, 1396, 1355 cm⁻¹; ¹H NMR (CDCl₃) δ 7.89 (d, *J* = 7.3, 2H, H-8, H-12), 7.86 (dd, *J* = 9.1, 2.4 Hz, 1H, H-5), 7.67 (d, *J* = 2.4 Hz, 1H, H-3), 7.64 (d, *J* = 9.1, Hz, 1H, H-6), 7.60 (d, *J* = 7.3, Hz, 1H, H-10), 7.52 (d, *J* = 7.4 Hz, 2H, H-9, H-11), 7.28 (s, 1H, NH), 3.91 (s, 3H, OCH₃); ¹³C {¹H} NMR (CDCl₃) δ 147.8 (C-2), 143.9 (C-7), 138.7 (C-4), 133.7 (C-10), 132.5 (C-1), 129.3 (overlapping C-8, C-12), 127.1 (overlapping C-9, C-11), 117.4 (C-6), 117.2 (C-5), 105.9 (C-3), 56.4 (OCH₃); LRMS (ESI) *m/z*: 309.3 (M+H)⁺.

N-(4-amino-2-methoxyphenyl)benzenesulfonamide (50, ICT13035).



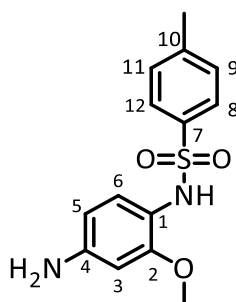
100 mL flask was charged with N-(2-methoxy-4-nitrophenyl) benzenesulfonamide **44** (0.50 g, 1.62 mmol) and ethyl acetate (20 mL). Palladium on carbon (10% (w/w) (8.0 mg, 0.03 mmol) was then added carefully. The reaction mixture was stirred at R.T under hydrogen for 24h. The mixture was filtered through celite and concentrated to give the title compound as brown solid (0.40 g, 88%); m.p. 173-173.9 °C; IR: 3436, 3364, 3291, 3060, 2935, 1646, 1615, 1595, 1511, 1472 cm⁻¹; ¹H NMR (CDCl₃) δ 7.58 (d, *J* = 8.0 Hz, 2H, H-8, H-12), 7.40 (d, *J* = 7.6 Hz, 1H, H-10), 7.31 (d, *J* = 8.0 Hz, 2H, H-9, H-11), 7.24 (d, *J* = 8.6 Hz, 1H, H-6), 6.43 (s, 1H, NH), 6.17 (dd, *J* = 8.6, 2.4 Hz, 1H, H-5), 5.94 (d, *J* = 2.4 Hz, 1H, H-3), 3.29 (s, 3H, OCH₃); ¹³C {¹H} NMR (CDCl₃) δ 152.4 (C-2), 145.8 (C-4), 139.2 (C-7), 132.4 (C-10), 128.3 (overlapping C-9, C-11), 127.3 (overlapping C-8, C-12), 126.1 (C-6), 116.1 (C-1), 107.2 (C-5), 98.3 (C-3), 55.1 (OCH₃); LRMS (ESI) *m/z*: 279.3 (M+H)⁺; HRMS (ESI) *m/z* calcd. for C₁₃H₁₅N₂O₃S [M+H]⁺: 279.0798, found: 279.0801.

N-(2-methoxy-4-nitrophenyl)-4-methylbenzenesulfonamide (45, ICT13020).



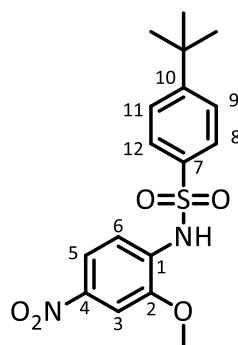
To solution of 2-methoxy-4-nitroaniline **37** (1.00 g, 5.94 mmol) in dry pyridine (5 mL), 4-methylbenzene-1-sulfonyl chloride (1.35 g, 7.13 mmol) was added drop wise. The mixture was then stirred and cooled 0 °C. After the addition was over, the mixture was stirred for 5h at R.T and then poured over ice and water. The solid was filtered, washed with water and recrystallized from ethanol-hexane to give the title compound (1.20 g, 62%) as brown powder; m.p. 175-175.6 °C; IR: 3284, 2941, 1593, 1525, 1496, 1444, 1397, 1356, 1341, 1323 cm⁻¹; ¹H NMR (CDCl₃) δ 7.75 (dd, *J* = 8.8, 2.4 Hz, 1H, H-5), 7.69 (d, *J* = 7.6, 2H, H-8, H-12), 7.58 (d, *J* = 2.4 Hz, 1H, H-3), 7.52 (d, *J* = 8.8 Hz, 1H, H-6), 7.39 (s, 1H, NH), 7.20 (d, *J* = 7.6 Hz, 2H, H-9, H-11), 3.82 (s, 3H, OCH₃), 2.32 (s, 3H, Ar-CH₃); ¹³C {¹H} NMR (CDCl₃) δ 147.7 (C-2), 144.73 (C-4), 143.69 (C-10), 135.72 (C-7), 132.65 (C-1), 129.92 (overlapping C-8, C-12), 127.2 (overlapping C-9, C-11), 117.4 (C-6), 116.8 (C-5), 105.8 (C-3), 56.4 (OCH₃), 21.6 (Ar-CH₃); LRMS (ESI) m/z: 323.2 (M+H)⁺.

N-(4-amino-2-methoxyphenyl)-4-methylbenzenesulfonamide (51, ICT13034).



100 mL flask was charged with N-(2-methoxy-4-nitrophenyl)-4-methylbenzenesulfonamide **45** (0.50 g, 1.55 mmol) and ethyl acetate (20 mL). Palladium on carbon (10% (w/w) (8.0 mg, 0.03 mmol) was then added carefully. The reaction mixture was stirred at R.T under hydrogen for 24h. The mixture was filtered through celite and concentrated to give the title compound as yellow needles (0.38 g, 83%); m.p: 172.8-173 °C; IR: 3467, 3377, 3261, 1615, 1595, 1512, 1453, 1439, 1401, 1329 cm^{-1} ; ^1H NMR (CDCl_3) δ 7.47 (d, $J = 8.2$ Hz, 2H, H-8, H-12), 7.21 (d, $J = 8.3$ Hz, 1H, H-6), 7.09 (d, $J = 8.2$ Hz, 2H, H-9, H-11), 6.44 (s, 1H, NH), 6.16 (dd, $J = 8.3, 2.3$ Hz, 1H, H-5), 5.96 (d, $J = 2.3$ Hz, 1H, H-3), 3.33 (s, 3H, OCH_3), 2.28 (s, 3H, Ar-CH_3); ^{13}C { ^1H } NMR (CDCl_3) δ 151.1 (C-2), 144.5 (C-10), 142.1 (C-7), 135.2 (C-4), 127.9 (overlapping C-8, C-12), 126.3 (overlapping C-9, C-11), 126.2 (C-6), 115.4 (C-1), 106.2 (C-5), 97.3 (C-3), 54.1 (OCH_3), 20.4 (Ar-CH_3); LRMS (ESI) m/z : 293.34 ($\text{M}+\text{H}$) $^+$

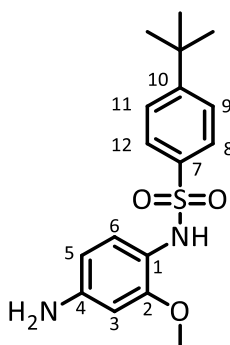
N-(4-nitro-2-methoxyphenyl)-1-(tert-butyl)benzenesulfonamide (40, ICT13062).



A solution of 2-methoxy-4-nitroaniline **37** (0.25 g, 1.48 mmol) and 4-tert-butylbenzenesulfonyl chloride **61** (0.41 g, 1.77 mmol) in pyridine (10 mL) was added dropwise at 0 °C, and mixture kept stirring under nitrogen at room temperature for 6 h. Hydrochloric acid solution (10 mL, 2M) was added to the solution mixture. The organic components were then extracted with ethyl acetate (3x50mL). The combined organic extracts were dried over anhydrous MgSO₄, filtered and the solvent was removed under reduced pressure. The crude was purified by using flash column chromatography (EtOAc:PE, 2:8 v/v) to give the title compound as a light yellow needles (0.42 g, 77%); m.p: 135.0-135.2 °C; IR: 3265, 2966, 1593, 1514, 1438, 1402, 1357, 1335, 1289, 1253 cm⁻¹; ¹H NMR (CDCl₃) δ 7.86 (dd, *J* = 8.9, 2.4 Hz, 1H, H-5), 7.82 (d, *J* = 8.6, 2H, H-8, H-12), 7.68 (d, *J* = 2.4 Hz, 1H, H-3), 7.63 (d, *J* = 8.9 Hz, 1H, H-6), 7.51 (d, *J* = 8.6, 2H, H-9, H-11), 7.47 (s, 1H, NH), 3.92 (s, 3H, OCH₃), 1.33 (s, 9H, (CH₃)₃); ¹³C {¹H} NMR (CDCl₃) δ 157.6 (C-10), 147.7 (C-2), 144.7 (C-4), 135.7 (C-7), 132.7 (C-1), 127.0 (overlapping C-8, C-12), 126.3 (overlapping C-9, C-11), 117.5 (C-6), 116.6 (C-5), 105.8 (C-3), 56.4 (OCH₃), 35.2 (C(CH₃)₃), 30.9

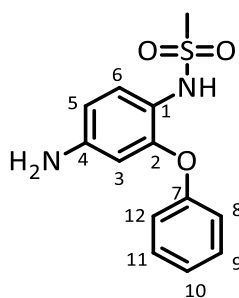
(C(CH₃)₃); LRMS (ESI) m/z: 365.1 (M+H)⁺; HRMS (ESI) m/z calcd. for C₁₇H₂₁N₂O₅S [M+H]⁺: 365.1166, found: 365.1168.

N-(4-amino-2-methoxyphenyl)-1-(tert-butyl)benzenesulfonamide (52, ICT13070).



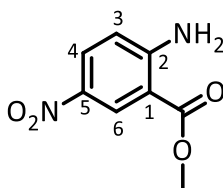
Palladium on carbon (10% (w/w), 67.0 mg) was added to a solution of compound **40** (54.0 mg, 0.15 mmol) in ethanol (10 mL). The reaction mixture was left stirring under hydrogen overnight. The mixture was filtered through celite and concentrated. The residue was then purified by flash column chromatography (EtOAc:PE, 2:8 v/v) to give the title compound (37.0 mg, 73%) as brownish white powder; m.p: 150.0-150.6 °C; IR: 3475, 3378, 3235, 2955, 1614, 1594, 1509, 1469, 1456, 1440 cm^{-1} ; ^1H NMR (CDCl_3) δ 7.49 (d, $J = 8.6$ Hz, 2H, H-8, H-12), 7.30 (d, $J = 8.6$ Hz, 2H, H-9, H-11), 6.41 (d, $J = 8.4$ Hz, 1H, H-6), 6.17 (dd, $J = 8.4, 2.4$ Hz, 1H, H-5), 5.95 (d, $J = 2.4$ Hz, 1H, H-3), 3.26 (s, 3H, OCH_3), 1.22 (s, 9H, $\text{C}(\text{CH}_3)_3$); ^{13}C { ^1H } NMR (CDCl_3) δ 156.1 (C-10), 152.4 (C-2), 145.7 (C-4), 136.2 (C-7), 126.6 (overlapping C-8, C-12), 126.1 (C-6), 125.3 (overlapping C-9, C-11), 116.3 (C-1), 107.2 (C-5), 98.2 (C-3), 55.2 (OCH_3), 35.0 ($\text{C}(\text{CH}_3)_3$), 31.0 ($\text{C}(\text{CH}_3)_3$); LRMS (ESI) m/z : 335.2 ($\text{M}+\text{H}$) $^+$; HRMS (ESI) m/z calcd. for $\text{C}_{17}\text{H}_{23}\text{N}_2\text{O}_3\text{S}$ [$\text{M}+\text{H}$] $^+$: 335.1424, found: 335.1426.

N-(4-amino-2-phenoxyphenyl)methanesulfonamide (58, ICT13050).



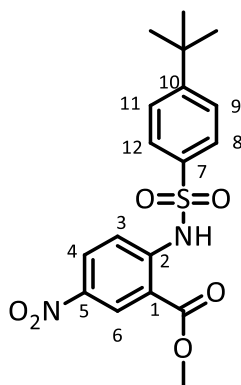
100 mL flask was charged with N-(4-nitro-2-phenoxyphenyl) methanesulphonamide **57** (0.20 g, 0.64 mmol) and ethyl acetate (20 mL). Palladium on carbon (10% (w/w)) was then added carefully. The reaction mixture was stirred at R.T under hydrogen for 24h. The mixture was filtered through celite and concentrated to give the title compound as brown solid (0.16 g, 92%); m.p. 198.1-198.8 °C (Lit., 198 °C) ¹⁶²; ¹H NMR (CDCl₃) δ 7.44 (d, *J* = 8.4 Hz, 2H, H-8, H-12), 7.15 (d, *J* = 8.4 Hz, 2H, H-9, H-11), 7.10 (d, *J* = 8.3 Hz, 1H, H-10), 6.30 (d, *J* = 2.1 Hz, 1H, H-6), 6.12 (dd, *J* = 9.1, 2.1 Hz, 1H, H-5), 6.03 (d, *J* = 9.1 Hz, 1H, H-3), 2.94 (s, 3H, CH₃); ¹³C {¹H} NMR (CDCl₃) δ 154.5 (C-7), 141.4 (C-2), 140.6 (C-4), 125.7 (overlapping C-8, C-12), 121.9 (C-10), 121.0 (C-1), 119.5 (overlapping C-9, C-11), 118.4 (C-6), 110.9 (C-5), 103.2 (C-3), 42.8 (CH₃); LRMS (ESI) *m/z*: 279.4 (M+H)⁺

Methyl 2-amino-5-nitrobenzoate (60, ICT13064).



Round bottom flask was charged with 2-amino-5-nitrobenzoic acid **59** (0.20 g, 1.09 mmol) and 20 mL of methanol. The reaction solution was treated with thionyl chloride (0.23 mL, 3.27 mmol) dropwise and refluxed overnight. After cooling to room temperature, water was added and extracted with ethyl acetate (3x50 mL). The combined organic extracts were dried over anhydrous MgSO₄, filtered and the solvent was evaporated under reduced pressure to give the title compound (0.19 mg, 88%). as yellow needles; m.p: 167.1-167.0 °C (Lit., 167-169 °C) ¹⁶³; IR: 3470, 3357, 2964, 1703, 1624, 1597, 1563, 1510, 1483, 1433 cm⁻¹; ¹H NMR (Acetone-d₆) δ 8.72 (d, *J* = 2.7 Hz, 1H, H-6), 8.12 (dd, *J* = 9.2, 2.7 Hz, 1H, H-4), 7.56 (s, 2H, NH₂), 6.97 (d, *J* = 9.2 Hz, 1H, H-3), 3.92 (s, 3H, OCH₃); ¹³C {¹H} NMR (Acetone-d₆) δ 168.6 (C=O₂CH₃), 157.2 (s, C-2), 138.3 (C-5), 129.4 (C-4), 129.1 (C-6), 116.8 (C-3), 110.4 (C-1), 52.4 (OCH₃); LRMS (ESI) *m/z*: 197.1 (M+H)⁺; HRMS (ESI) *m/z* calcd. for C₈H₉N₂O₄ [M+H]⁺: 197.0557, found: 197.0555.

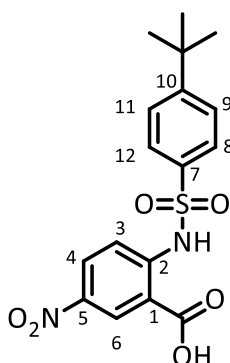
Methyl 2-(4-(tert-butyl)phenylsulfonamido)-5-nitrobenzoate (62, ICT13067).



To stirred solution of methyl 2-amino-5-nitrobenzoate **60** (0.10 g, 0.51 mmol) in THF (5 mL), two equivalent of sodium hydride as a 65% dispersion in mineral oil (24.0 mg, 1.0 mmol) was added in portions at room temperature over 20 min. 4-tert-butylbenzenesulfonyl chloride **61** (0.14 g, 0.61 mmol) was then added dropwise, and the mixture was left stirring overnight at room temperature. The reaction mixture was poured into hydrochloric acid (10 mL, 2M) and reaction mixture was extracted with ethyl acetate (3x50 mL). The combined organic extracts were dried over anhydrous MgSO₄, filtered and the solvent was removed under reduced pressure. The crude material was purified by flash column chromatography (EtOAc:PE, 2:8 v/v) to give the *title compound* (0.15 g, 75%) as yellow powder; m.p: 161.3-161.5 °C; IR: 2958, 1695, 1612, 1588, 1520, 1489, 1438, 1408, 1335, 1262 cm⁻¹; ¹H NMR (Acetone-d₆) δ 11.02 (s, 1H, NH), 8.63 (d, *J* = 2.5 Hz, 1H, H-6), 8.25 (dd, *J* = 9.2, 2.5 Hz, 1H, H-4), 7.83 (d, *J* = 8.6 Hz, 2H, H-8, H-12), 7.76 (d, *J* = 9.2 Hz, 1H, H-3), 7.53 (d, *J* = 8.6 Hz, 2H, H-9, H-11), 3.94 (s, 3H, OCH₃), 1.16 (s, 9H, C(CH₃)₃); ¹³C {¹H} NMR (Acetone-d₆) δ 167.6 (C=O), 158.8 (C-10), 146.3 (C-2), 142.4 (C-5), 137.0 (C-7), 130.1 (C-4), 128.0 (overlapping C-8, C-12), 127.8 (C-6), 127.5 (overlapping C-9, C-11), 118.6 (C-3), 115.6 (C-1), 53.7 (OCH₃), 35.8 (C(CH₃)₃), 31.1 (C(CH₃)₃);

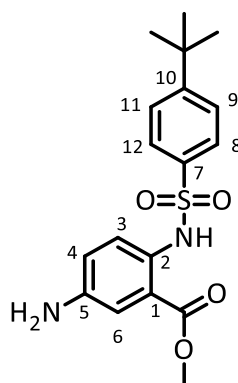
LRMS (ESI) m/z: 393 (M+H)⁺; HRMS (ESI) m/z calcd. for C₁₈H₂₄O₆N₃S
[M+NH₄]⁺: 410.1380, found: 410.1374

2-(4-(tert-butyl)phenylsulfonamido)-5-nitrobenzoic acid (63, ICT13074).



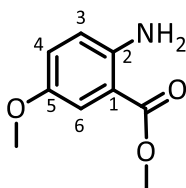
Solution of Sodium hydroxide (10 mL, 3M) was added to compound **62** (0.15 g, 0.38 mmol) and was reflux heated for 1 h. hydrochloric acid (10 mL, 2M) was added and reaction mixture was extracted with ethyl acetate (3x50 mL). The combined organic extracts were dried over anhydrous MgSO₄, filtered and the solvent was evaporated under reduced pressure to give the title compound (0.13 g, 90%) as whitish yellow powder; m.p: 115.3-115.9 °C; ¹H NMR (Acetone-d₆) δ 8.72 (d, *J* = 2.4 Hz, 1H, H-6), 8.40 (dd, *J* = 9.1, 2.4 Hz, 1H, H-4), 7.94 (d, *J* = 8.6 Hz, 2H, H-8, H-12), 7.83 (d, *J* = 9.1, 1H, H-3), 7.68 (d, *J* = 8.6 Hz, 2H, H-9, H-11), 1.12 (s, 9H, C(CH₃)₃); ¹³C {¹H} NMR (Acetone-d₆) δ 177.7 (CO₂H), 169.7 (C-10), 167.4 (C-2), 157.2 (C-7), 128.5 (C-5), 127.1 (C-6), 126.3 (overlapping C-8, C-12), 125.6 (overlapping C-9, C-11), 116.9 (C-4), 116.1 (C-3), 112.0 (C-1), 35.0 (C(CH₃)₃), 29.5 (C(CH₃)₃); LRMS (ESI) m/z: 377.86 (M-H)⁻; HRMS (ESI) m/z calcd. for C₁₈H₂₂O₆N₃S [M+NH₄]⁺: 393.1115, found: 393.1115.

Methyl 5-amino-2-(4-(tert-butyl)phenylsulfonamido)benzoate (64, ICT13089).



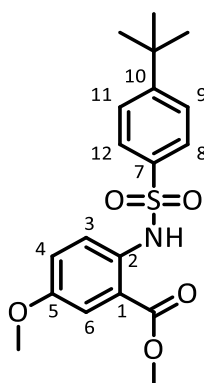
Round bottom flask was charged with compound **62** (20.0 mg, 0.05 mmol) and EtOAc (30 mL). Palladium on carbon (10% (w/w)) was then added carefully. The reaction mixture was stirred at R.T under hydrogen for 24h. The mixture was filtered through celite and concentrated to give (15.0 mg 82%) of the *title compound* as yellow crystals; m.p: 110.2-110.7 °C; IR: 3478, 3361, 3008, 2948, 1678, 1628, 1591, 1575, 1519, 1469 cm^{-1} ; ^1H NMR (Acetone- d_6) δ 9.46 (s, 1H, NH), 7.44 (d, $J = 8.6$ Hz, 2H, H-8, H-12), 7.39 (d, $J = 8.6$ Hz, 2H, H-9, H-11), 7.30 (d, $J = 8.9$ Hz, 1H, H-3), 6.99 (d, $J = 2.8$ Hz, 1H, H-6), 6.79 (dd, $J = 8.9, 2.8$ Hz, 1H, H-4), 4.69 (s, 2H, NH_2), 3.60 (s, 3H, OCH_3), 1.24 (s, 9H, $(\text{CH}_3)_3$); ^{13}C { ^1H } NMR (Acetone- d_6) δ 156.3 ($\underline{\text{C}}\text{O}_2\text{CH}_3$), 155.8 (C-10), 142.3 (C-5), 138.5 (C-7), 127.4 (C-2), 125.4 (overlapping C-8, C-12), 125.3 (C-3), 125.2 (overlapping C-9, C-11), 120.7 (C-4), 119.6 (C-6), 114.4 (C-1), 51.6, (OCH_3), 51.3 ($\underline{\text{C}}(\text{CH}_3)_3$), 34.3 ($\text{C}(\underline{\text{C}}\text{H}_3)_3$); LRMS (ESI) m/z : 363.07 ($\text{M}+\text{H}^+$); HRMS (ESI) m/z calcd. for $\text{C}_{18}\text{H}_{23}\text{O}_4\text{N}_2\text{S}$ [$\text{M}+\text{H}^+$]: 363.1373, found: 363.1374

Methyl 2-amino-5-methoxybenzoate (67, ICT13093).



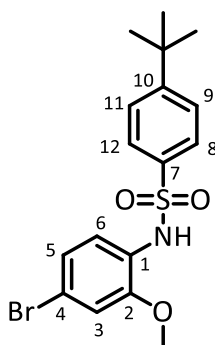
Round bottom flask was charged with 2-amino-5-methoxybenzoic acid **68** (0.20 g, 1.19 mmol) and 20 mL of methanol. The reaction solution was treated with thionyl chloride (0.10 mL, 3.57 mmol) dropwise and refluxed overnight. After cooling to room temperature, the reaction was with water and extracted with ethyl acetate (3x50 mL). The combined organic extracts were dried over anhydrous MgSO₄, filtered and the solvent was evaporated under reduced pressure to give the title compound (0.19 mg, 88%) as black solid; m.p: 37.1-37.8 °C (Lit., 37-38 °C) ¹⁶⁴; ¹H NMR (Acetone-d₆) δ 7.15 (d, *J* = 1.4 Hz, 1H, H-6), 6.82 (dd, *J* = 8.9, 1.4 Hz, 1H, H-4), 6.64 (d, *J* = 8.9 Hz, 1H, H-3), 5.94 (s, 2H, NH₂), 3.69 (s, 3H, OCH₃), 3.57 (s, 3H, CO₂CH₃); ¹³C {¹H} NMR (Acetone-d₆) δ 168.8 (C=O), 150.8 (C-5), 147.2 (C-2), 124.0 (C-4), 119.1 (C-3), 113.4 (C-6), 110.2 (C-1), 55.9 (OCH₃), 51.8 (CO₂CH₃); LRMS (ESI) *m/z*: 182.0 (M+H)⁺; HRMS (ESI) *m/z* calcd. for C₉H₁₂NO₃ [M+H]⁺: 182.1511, found: 182.1522

Methyl 2-(4-(tert-butyl)phenylsulfonamido)-5-methoxybenzoate (66, ICT13108).



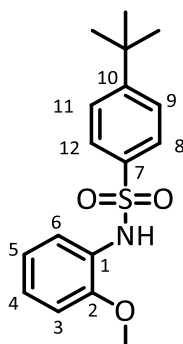
To solution of methyl 2-amino-5-methoxybenzoate **67** (0.10 g, 0.55 mmol) in pyridine (10 mL), solution of 4-tert-butylbenzenesulfonyl chloride **61** (0.15 g, 0.66 mmol) in DCM was added dropwise at 0 °C. The solution was left stirring at room temperature for 5 h. 2M hydrochloric acid (10 mL, 2M) was added and reaction solution was extracted with ethyl acetate (3x50 mL). The combined organic extracts were dried over anhydrous MgSO₄, filtered and the solvent was evaporated under reduced pressure. The resultant material was purified by flash column chromatography (EtOAc:PE, 2:8 v/v) to give the *title compound* (0.15 g, 72%) as brownish red solid; m.p: 146.4-146.8 °C; ¹H NMR (CDCl₃) δ 9.89 (s, 1H, NH), 7.59 (d, *J* = 8.3 Hz, 2H, H-8, H-12), 7.33 (d, *J* = 8.3 Hz, 2H, H-9, H-11), 7.28 (d, *J* = 3.2 Hz, 1H, H-6), 6.99 (dd, *J* = 9.1, 1.4 Hz, 1H, H-4), 6.88 (dd, *J* = 9.1, 1.4 Hz, 1H, H-3), 3.79 (s, 3H, OCH₃), 3.59 (s, 3H, CO₂CH₃), 1.20 (s, 9H, C(CH₃)₃); ¹³C {¹H} NMR (CDCl₃) δ 156.9 (C=O), 155.8 (C-10), 136.6 (C-5), 133.8 (C-2), 127.0 (overlapping C-8, C-12), 125.8 (overlapping C-9, C-11), 123.6 (C-7), 122.7 (C-1), 120.9 (C-4), 118.6 (C-3), 114.7 (C-6), 55.6 (OCH₃), 52.4 (CO₂CH₃), 35.8 (C(CH₃)₃), 31.0 (C(CH₃)₃); LRMS (ESI) *m/z*: 378.18.0 (M+H)⁺; HRMS (ESI) *m/z* calcd. for C₁₉H₂₄O₅NS [M+H]⁺: 378.1370, found: 378.1371.

***N*-(4-bromo-2-methoxyphenyl)-4-(*tert*-butyl)benzenesulfonamide (70, ICT13122).**



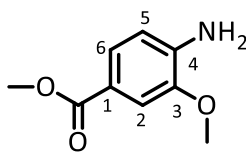
Solution of 4-bromo-2-methoxyaniline **69** (0.10 g, 0.49 mmol) in dry pyridine (10 mL) was treated dropwise with solution of 4-(*tert*-butyl) benzene-1-sulfonyl chloride **61** (88.6 mg, 0.59 mmol) in DCM. The reaction mixture was left stirring for 5h. Hydrochloric acid (10 mL, 2M) was added and mixture reaction was extracted with ethyl acetate (3x50 mL). The combined organic extracts were dried over anhydrous MgSO₄, filtered and the solvent was stripped off under reduced pressure. The resultant material was purified by flash column chromatography (EtOAc:PE, 2:8 v/v) to give the *title compound* (0.12 g, 61 %) as white crystals; m.p: 112.2-112.7 °C; ¹H NMR (Acetone-d₆) δ 8.08 (s, 1H, NH), 7.60 (d, *J* = 8.6 Hz, 2H, H-8, H-12), 7.45 (d, *J* = 8.6 Hz, 2H, H-9, H-11), 7.30 (d, *J* = 8.4 Hz, 1H, H-6), 6.95 (dd, *J* = 8.4, 1.8 Hz, 1H, H-5), 6.91 (d, *J* = 1.8 Hz, 1H, H-3), 3.47 (s, 3H, OCH₃), 1.21 (s, 9H, C(CH₃)₃); ¹³C {¹H} NMR (Acetone-d₆) δ 157.2 (C-10), 152.7 (C-2), 138.1 (C-7), 127.8 (overlapping C-8, C-12), 126.7 (C-4), 126.6 (overlapping C-9, C-11), 124.8 (C-6), 124.3 (C-5), 118.7 (C-1), 115.5 (C-3), 56.4 (OCH₃), 34.9 (C(CH₃)₃), 31.3 (C(CH₃)₃); LRMS (ESI) m/z: 399.87 (M+H)⁺; HRMS (ESI) m/z calcd. for C₁₇H₂₁O₃NBrS: 398.0420, found: 398.0421 and 400.041 50:50 [M+H]⁺

N-(2-methoxyphenyl)tert-butylbenzenesulfonamide (71, ICT13078).



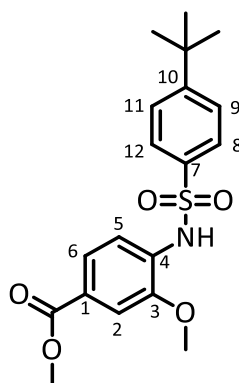
To solution of 2-methoxyaniline **72** (50.0 mg, 0.40 mmol) in dry pyridine (5 mL), solution of 4-tert-butylbenzenesulfonyl chloride **61** (0.11 g, 0.48 mmol) in DCM was added dropwise at 0 °C. The mixture was stirred under nitrogen for 5h at R.T and then poured over ice and water. The solid was filtered, washed with water and extracted with ethyl acetate (3x50 mL). The combined organic extracts were dried over anhydrous MgSO₄, filtered and the solvent was evaporated under reduced pressure. The resultant crude material was purified by flash column chromatography (EtOAc:PE, 2:8 v/v) to give the title compound (0.10 mg, 78%) as grey crystals; m.p: 172.9-173.3 °C; IR: 3252, 2962, 2927, 2866, 1637, 1595, 1547, 1498, 1466, 1444 cm⁻¹; ¹H NMR (CDCl₃) δ 7.60 (d, *J* = 8.8 Hz, 2H, H-8, H-12), 7.45 (dd, *J* = 7.7, 1.5 Hz, 1H, H-6), 7.33 (d, *J* = 8.8 Hz, 2H, H-9, H-11), 6.97 (dt, *J* = 7.7, 1.5 Hz, 1H, H-4), 6.91 (s, 1H, NH), 6.83 (td, *J* = 7.7, 1.0 Hz, 1H, 1H, H-5), 6.66 (dd, *J* = 8.1, 0.8 Hz, 1H, H-3), 3.54 (s, 3H, OCH₃), 1.23 (s, 9H, C(CH₃)₃); ¹³C {¹H} NMR (CDCl₃) δ 155.5 (C-10), 148.5 (C-2), 135.3 (C-7), 126.0 (overlapping C-8, C-12), 125.0 (C-1), 124.6 (overlapping C-9, C-11), 124.2 (C-6), 120.1 (C-4), 120.1 (C-5), 109.5 (C-3), 54.5 (OCH₃), 34.0 (C(CH₃)₃), 30.0 (C(CH₃)₃); LRMS (ESI) *m/z*: 320.1 (M+H)⁺; HRMS (ESI) *m/z* calcd. for C₁₇H₂₂O₃N₂S [M+NH₄]⁺: 320.1315, found: 320.1316

Methyl 4-amino-3-methoxybenzoate (74, ICT13084).



Round bottom flask was charged with 4-amino-3-methoxybenzoic acid **73** (0.30 g, 1.79 mmol) and 20 mL of methanol. The reaction solution was treated with thionyl chloride (0.23 mL, 5.37 mmol) dropwise and refluxed overnight. After cooling to room temperature, water was added and extracted with ethyl acetate (3x50 mL). The combined organic extracts were dried over anhydrous MgSO₄, filtered and the solvent was evaporated under reduced pressure to give the title compound (0.24 g, 73%) as brown powder; m.p: 127.6-128.2 °C (Lit., 127-129 °C)¹⁶⁵; ¹H NMR (Acetone-d₆) δ 7.33 (dd, *J* = 8.2, 1.8 Hz, 1H, H-6), 7.26 (d, *J* = 1.8 Hz, 1H, H-2), 6.59 (d, *J* = 8.2 Hz, 1H, H-5), 5.05 (s, 2H, NH₂), 3.75 (s, 3H, CO₂CH₃), 3.68 (s, 3H, OCH₃); ¹³C {¹H} NMR (Acetone-d₆) δ 165.3 (C=O), 144.5 (C-3), 141.6 (C-4), 122.7 (C-6), 116.5 (C-1), 111.0 (C-5), 109.5 (C-2), 53.7 (CO₂CH₃), 49.5 (OCH₃); LRMS (ESI) *m/z*: 182.8 (M+H)⁺; HRMS (ESI) *m/z* calcd. for C₉H₁₂NO₃ [M+H]⁺: 182.1913, found: 181.1901.

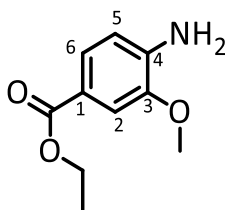
Methyl 4-(4-(tert-butyl)phenylsulfonamido)-3-methoxybenzoate (75, ICT13069).



To solution of methyl 4-amino-3-methoxybenzoate **74** (0.50 g, 2.75 mmol) in pyridine (10 mL), solution of 4-tert-butylbenzenesulfonyl chloride **61** (0.76 g, 3.26 mmol) in DCM was added dropwise at 0 °C. The mixture was left stirring at room temperature for 5 h. Hydrochloric acid (10 mL, 2M) was added and reaction mixture was extracted with ethyl acetate (3x50 mL). The combined organic extracts were dried over anhydrous MgSO₄, filtered and the solvent was evaporated under reduced pressure. The resultant material was purified by flash column chromatography (EtOAc:PE, 2:8 v/v) to give the *title compound* (0.80 g, 77%) as yellow crystals; m.p: 155.3-155.8 °C; IR: 3364, 3212, 2964, 1706, 1672, 1609, 1592, 1508, 1468, 1443 cm⁻¹; ¹H NMR (CDCl₃) δ 7.68 (d, *J* = 8.7 Hz, 2H, H-8, H-12), 7.54 (dd, *J* = 8.6, 1.5 Hz, 1H, H-6), 7.48 (d, *J* = 8.6 Hz, 1H, H-5), 7.38 (d, *J* = 8.7 Hz, 2H, H-9, H-11), 7.36 (d, *J* = 1.5 Hz, 1H, H-2), 7.25 (s, 1H, NH), 3.80 (s, 3H, CO₂CH₃), 3.72 (s, 3H, OCH₃), 1.22 (s, 9H, C(CH₃)₃); ¹³C {¹H} NMR (CDCl₃) δ 166.5 (C=O), 157.1 (C-10), 147.9 (C-3), 136.0 (C-7), 130.7 (C-4), 127.0 (overlapping C-8, C-12), 126.0 (overlapping C-9, C-11), 125.8 (C-1), 123.1 (C-6), 117.8 (C-5), 111.3 (C-2), 55.9 (OCH₃), 52.2 (CO₂CH₃),

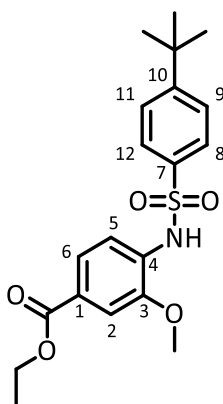
35.1 (C(CH₃)₃), 31.0 (C(CH₃)₃); LRMS (ESI) m/z: 378.1 (M+H)⁺; HRMS (ESI)
m/z calcd. for C₁₉H₂₄NO₅S [M+H]⁺: 378.1371, found: 378.1370

Ethyl 4-amino-3-methoxybenzoate (77, ICT13111).



Round bottom flask was charged with methyl 4-amino-3-methoxybenzoic acid **73** (0.50 g, 2.98 mmol) and 30 mL of ethanol. The reaction solution was treated with thionyl chloride (0.61 mL, 8.91 mmol) dropwise and refluxed overnight. After cooling to room temperature, the reaction was with water and extracted with ethyl acetate (3x50 mL). The combined organic extracts were dried over anhydrous MgSO₄, filtered and the solvent was evaporated under reduced pressure to give the title compound (0.48 g, 82%) as a brown solid; m.p: 84.0-84.7 °C (Lit., 84-85 °C) ¹⁶⁶; ¹H NMR (CDCl₃) δ 7.47 (dd, *J* = 8.4, 1.7 Hz, 1H, H-6), 7.37 (d, *J* = 1.7 Hz, 1H, H-2), 6.57 (d, *J* = 8.4 Hz, 1H, H-5), 4.24 (q, *J* = 7.1 Hz, 2H, CH₂), 4.14 (s, 2H, NH₂), 3.80 (s, 3H, OCH₃), 1.28 (t, *J* = 7.1 Hz, 3H, CH₂CH₃); ¹³C {¹H} NMR (CDCl₃) δ 166.9 (C=O), 146.1 (C-3), 141.1 (C-4), 124.0 (C-6), 119.8 (C-1), 113.0 (C-5), 111.1 (C-2), 60.4 (CH₂), 55.5 (OCH₃), 14.5 (CH₂CH₃); LRMS (ESI) *m/z*: 196 (M+H)⁺; HRMS (ESI) *m/z* calcd. for C₁₀H₁₄NO₃ [M+H]⁺: 196.2112, found: 196.2105.

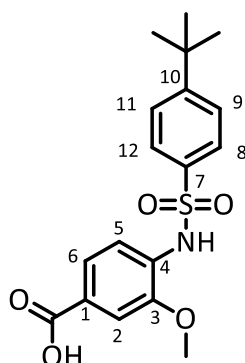
Ethyl 4-(4-(tert-butyl)phenylsulfonamido)-3-methoxybenzoate (76, ICT13113).



Solution of ethyl 4-amino-3-methoxybenzoate **77** (0.15 g, 0.76 mmol) in pyridine (15 mL) was treated dropwise with solution of 4-tert-butylbenzenesulfonyl chloride **61** (0.21 g, 0.92 mmol) in DCM at 0 °C. The solution was left stirring at room temperature for 5 h. 2M hydrochloric acid (10 mL) was added to reaction mixture. Organic components were then extracted with ethyl acetate (3x50 mL). The combined organic extracts were dried over anhydrous MgSO₄, filtered and the solvent was removed under reduced pressure. The resultant material was purified by flash column chromatography (EtOAc:PE, 2:8 v/v) to give the *title compound* (0.25 g, 84 %) as yellowish white solid; m.p: 129.3-129.8 °C; IR: 3354, 3252, 2961, 1712, 1672, 1606, 1592, 1507, 1462, 1433 cm⁻¹; ¹H NMR (Acetone-d₆) δ 7.68 (d, *J* = 8.6 Hz, 2H, H-8, H-12), 7.50 (dd, *J* = 8.3, 1.5 Hz, 1H, H-6), 7.47 (d, *J* = 8.3 Hz, 1H, H-5), 7.45 (d, *J* = 8.6 Hz, 2H H-9, H-11), 7.33 (d, *J* = 1.5 Hz, 1H, H-2), 4.17 (q, *J* = 7.1 Hz, 2H, CH₂), 3.63 (s, 3H, OCH₃), 1.19 (t, *J* = 7.2 Hz, 3H, CH₂CH₃), 1.16 (s, 9H, C(CH₃)₃); ¹³C {¹H} NMR (Acetone-d₆) δ 166.1 (C=O), 157.5 (C-10), 150.2 (C-3), 138.1 (C-7), 132.0 (C-4), 127.9 (overlapping C-8, C-12), 127.5 (overlapping C-9, C-11), 126.8 (C-1), 123.2 (s, C-6), 120.1 (s, C-5), 112.4 (s, C-2), 61.5 (CH₂), 56.3 (OCH₃), 35.7 (C(CH₃)₃),

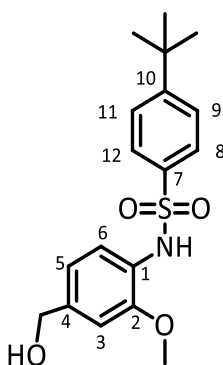
31.2 (C(CH₃)₃), 14.5 (CH₂CH₃); LRMS (ESI) m/z: 392.1 (M+H)⁺; HRMS (ESI)
m/z calcd. for C₂₀H₂₆O₅NS [M+H]⁺: 392.1526, found: 392.1522

4-(4-(tert-butyl)phenylsulfonamido)-3-methoxybenzoic acid (78, ICT13072).



Solution of Sodium hydroxide (10 mL, 3M) was added to compound **75** (0.40 g, 1.06 mmol) and was reflux heated for 1h. Hydrochloric acid (10 mL, 2M) was added and reaction mixture was extracted with ethyl acetate (3x50 mL). The combined organic extracts were dried over anhydrous MgSO₄, filtered and the solvent was evaporated under reduced pressure to give the *title compound* (0.28 g, 72 %) as wheat brown powder; m.p: 175.1-175.6 °C; IR: 2963, 1692, 1607, 1593, 1528, 1465, 1445, 1399, 1347, 1325 cm⁻¹; ¹H NMR (Acetone-d₆) δ 7.68 (d, *J* = 7.4 Hz, 2H, H-8, H-12), 7.48 (dd, *J* = 8.8, 1.4 Hz, 1H, H-6), 7.46 (d, *J* = 8.8 Hz, 1H, H-5), 7.43 (d, *J* = 7.4 Hz, 2H, H-9, H-11), 7.35 (d, *J* = 1.4 Hz, 1H, H-2), 3.64 (s, 3H, OCH₃), 1.17 (s, 9H, C (CH₃)₃); ¹³C {¹H} NMR (Acetone-d₆) δ 170.5 (C=O₂CH₃), 164.3 (C-10), 152.5 (C-3), 145.0 (C-7), 137.8 (C-4), 131.6 (C-8, C-12), 127.8 (C-9, C-11), 126.8 (C-1), 123.6 (C-6), 120.2 (C-5), 112.7 (C-2), 56.3 (OCH₃), 55.4 (C(CH₃)₃), 35.7 (C(CH₃)₃); LRMS (ESI) m/z: 364.1 (M+H)⁺; HRMS (ESI) m/z calcd. for C₁₈H₂₅O₅N₂S [M+NH₄]⁺: 381.1479, found: 381.1478

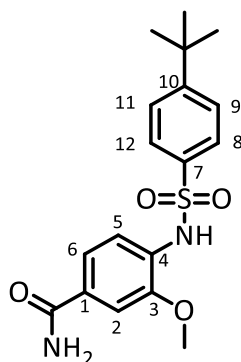
***N*-(4-(hydroxymethyl)-2-methoxyphenyl) *tert*-butylbenzenesulfonamide
(79, ICT13091).**



Under nitrogen atmosphere compound **75** (0.10 g, 0.26) was dissolved in dry THF (10 mL). The temperature was cooled to -78 using dry ice and acetone. 1.2 equivalent of Lithium triethylborohydride (super hydride) in THF (0.36 mL, 0.31 mmol) was added carefully and mixture was left stirring for 5 h until the reaction completed. The reaction was then warmed to room temperature and quenched with methanol and water and then was extracted over ice and water. The solid was filtered, washed with water and extracted with ethyl acetate (3x50 mL). The combined organic extracts were dried over anhydrous MgSO₄, filtered and the solvent was evaporated under reduced pressure. The resultant material was purified by flash column chromatography (EtOAc:PE, 2:8 v/v) to give the *title compound* (80.0 mg, 88%) as yellow powder; m.p: 130.0-130.6 °C; IR: 3254, 2963, 2870, 1595, 1509, 1462, 1432, 1394, 1365, 1336 cm⁻¹; ¹H NMR (CDCl₃) δ 7.61 (d, *J* = 8.7 Hz, 2H, H-8, H-12), 7.40 (d, *J* = 8.3, 1H, H-6), 7.34 (d, *J* = 8.7 Hz, 2H, H-9, H-11), 7.19 (s, 1H, OH), 6.94 (s, 1H, NH), 6.79 (dd, *J* = 8.3, 1.8 Hz, 1H, H-5), 6.73 (d, *J* = 1.8, 1H, H-3), 4.54 (s, 2H, CH₂), 3.56 (s, 3H, CH₃), 1.20 (s, 9H, (CH₃)₃); ¹³C {¹H} NMR (CDCl₃) δ 156.6 (C-10), 149.5 (C-2), 138.0 (C-7), 136.2 (C-1), 127.0 (overlapping C-8, C-12), 125.8 (overlapping C-9, C-11), 125.3 (C-4), 120.8 (C-6), 119.4 (C-5), 109.2 (C-3), 64.6 (CH₂), 55.0 (OCH₃),

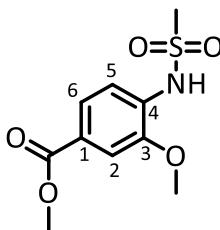
35.0 (C(CH₃)₃), 32.2 (C(CH₃)₃); LRMS (ESI) m/z: 350.1 (M+H)⁺; HRMS (ESI)
m/z calcd. for C₁₈H₂₄O₄NS [M+H]⁺: 350.1421, found: 350.1424.

4-(4-(tert-butyl)phenylsulfonamido)-3-methoxybenzamide (80, ICT13092).



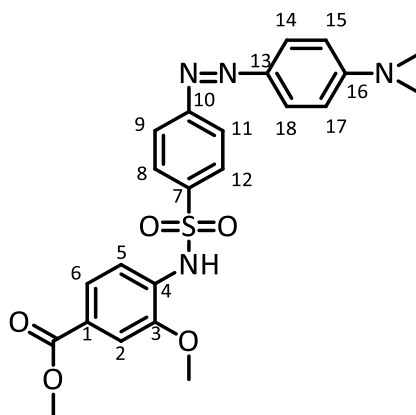
Under nitrogen atmosphere compound **75** (0.20 g, 0.52 mmol) was dissolved in Ammonium hydroxide (50mL, 35%) and mixture was left stirring at room temperature for 5 days. The reaction mixture was then washed with water and extracted with ethyl acetate (3x50 mL). The combined organic extracts were dried over anhydrous MgSO₄, filtered and the solvent was evaporated under reduced pressure. The resultant material was purified by flash column (EtOAc:PE, 2:8 v/v) to give the *title compound* (0.15 g, 79 %) as white crystals; m.p: 115.4-115.9 °C; IR: 3460, 3216, 2966, 1665, 1606, 1573, 1513, 1453, 1389, 1336 cm⁻¹; ¹H NMR (CDCl₃) δ 7.65 (d, *J* = 8.5 Hz, 2H, H-8, H-12), 7.45 (d, *J* = 8.4 Hz, 1H, H-5), 7.37 (d, *J* = 8.5 Hz, 2H, H-9, H-11), 7.28 (d, *J* = 1.5 Hz, 1H, H-2), 7.23 (dd, *J* = 8.4, 1.5 Hz, 1H, H-6), 3.66 (s, 3H, OCH₃), 1.20 (s, 9H, C(CH₃)₃); ¹³C {¹H} NMR (CDCl₃) δ 168.9 (CONH₂), 157.1 (C-10), 148.7 (C-3), 135.9 (C-7), 129.6 (C-4), 129.5 (C-1), 126.9 (overlapping C-8, C-12), 126.0 (overlapping C-9, C-11), 119.8 (C-6), 118.5 (C-5), 110.3 (C-2), 56.0 (d, *J* = 21.8 Hz, OCH₃), 35.1 (C(CH₃)₃), 30.9 (C(CH₃)₃); LRMS (ESI) m/z: 363.1 (M+H)⁺; HRMS (ESI) m/z calcd. for C₁₈H₂₃O₄N₂S [M+H]⁺: 363.1373, found: 363.1380

Methyl 3-methoxy-4-(methylsulfonamido)benzoate (81, ICT13073).



To solution of methyl 4-amino-3-methoxybenzoate **74** (0.20 g, 1.10 mmol) in pyridine (10 mL), methylsulfonyl chloride (0.15 g, 1.32 mmol) was added dropwise at 0 °C. The mixture was left stirring at room temperature for 5 h. Hydrochloric acid (10 mL, 2M) was added and reaction mixture was extracted with ethyl acetate (3x50 mL). The combined organic extracts were dried over anhydrous MgSO₄, the mixture was filtered and the solvent was evaporated under reduced pressure. The resultant crude materials was purified by flash column chromatography (EtOAc:PE, 2:8 v/v) to give the *title compound* (0.21 g, 73 %) as white powder; m.p: 124.8-125.0 °C; IR: 3267, 3014, 2933, 1715, 1604, 1594, 1508, 1472, 1451, 1433 cm⁻¹; ¹H NMR (Acetone-d₆) δ 7.66 (dd, *J* = 8.3, 1.8 Hz, 1H, H-6), 7.61 (d, *J* = 1.8 Hz, 1H, H-2), 7.59 (d, *J* = 8.3 Hz, 1H, H-2), 3.98 (s, 3H, OCH₃), 3.89 (s, 3H, CO₂CH₃), 3.10 (s, 3H, SO₂CH₃); ¹³C {¹H} NMR (Acetone-d₆) δ 166.8 (C=O), 150.0 (C-3), 132.6 (C-4), 127.0 (C-6), 123.5 (C-1), 119.6 (C-5), 112.5 (C-2), 56.5 (OCH₃), 52.3 (CO₂CH₃), 40.1 (s, SO₂CH₃); LRMS (ESI) *m/z*: 258.93.1 (M-H); HRMS (ESI) *m/z* calcd. for C₁₀H₁₄O₅NS [M+H]⁺: 260.0587, found: 260.0589.

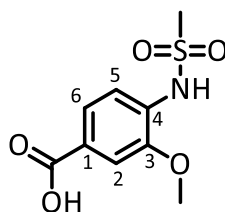
Methyl 4-(4-((4-(dimethylamino)phenyl)diazenyl)phenylsulfonamido)-3-methoxybenzoate (82, ICT13085).



To solution of methyl 4-amino-3-methoxybenzoate **74** (0.10 g, 0.55 mmol) in pyridine (8 mL), Dabsyl chloride (0.21 g, 0.66 mmol) was added dropwise at 0 °C. The solution was left stirring at room temperature for 5 h. Hydrochloric acid (10 mL, 2M) was added and reaction mixture was extracted with ethyl acetate (3x50 mL). The combined organic extracts were dried over anhydrous MgSO₄, filtered and the solvent was evaporated under reduced pressure. The resultant material was purified by flash column chromatography (EtOAc:PE, 2:8 v/v) to give the *title compound* (0.23 g, 89 %) as a light red crystals; m.p: 114.7-114.9 °C; ¹H NMR (Acetone-d₆) δ 7.91 (d, *J* = 8.9 Hz, 2H, H-8, H-12), 7.72 (d, *J* = 8.9 Hz, 2H, H-9, H-11) 7.70 (d, *J* = 8.6 Hz, 2H, H-14, H-18), 7.33 (dd, *J* = 8.4, 1.8 Hz, 1H, H-6), 7.27 (d, *J* = 8.4 Hz, 1H, H-5), 7.24 (d, *J* = 1.8 Hz, 1H, H-2), 6.75 (d, *J* = 8.6 Hz, 2H, H-15, H-17), 3.68 (s, 3H, OCH₃), 3.64 (s, 3H, CO₂CH₃), 2.99 (s, 6H, N(CH₃)₂); ¹³C {¹H} NMR (Acetone-d₆) δ 164.6 (CO₂CH₃), 155.5 (C-10), 154.4 (C-16), 151.3 (C-3), 144.0 (C-13), 142.5 (C-7), 128.7 (overlapping C-8, C-12), 128.4 (C-4), 126.1 (overlapping C-9, C-11), 125.8 (C-1), 123.6 (C-6), 122.2 (overlapping C-14, C-18), 117.4 (C-5) 112.3 (overlapping C-15, C-17), 111.8 (C-2), 55.3 (OCH₃), 51.3 (CO₂CH₃), 40.0 (N(CH₃)₂); LRMS (ESI) m/z:

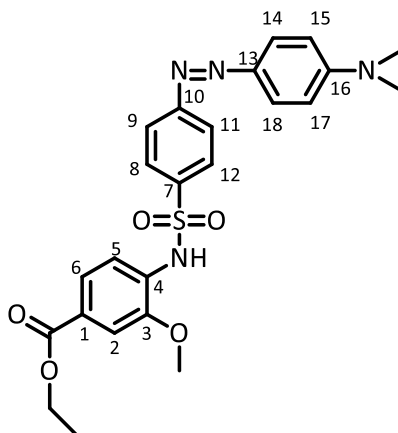
469.13 (M+H)⁺; HRMS (ESI) m/z calcd. for C₂₃H₂₃O₅N₄S [M-H]⁻: 467.1395,
found: 467.1388.

3-methoxy-4-(methylsulfonamido)benzoic acid (83, ICT13071).



Solution of Sodium hydroxide (10 mL, 3M) was added to methyl 3-methoxy-4-(methylsulfonamido)benzoate **81** (0.30 g, 1.15 mmol) and was reflux heated for 1 h. Hydrochloric acid (10 mL, 2M) was added and reaction mixture was extracted with ethyl acetate (3x50 mL). The combined organic extracts were dried over anhydrous MgSO₄, filtered and the solvent was evaporated under reduced pressure to give the title compound (0.23 g, 93%) as white powder. The proton NMR data was in agreement with previously published data ¹⁶⁷; m.p: 185.0-185.6 °C; IR: 3237, 2928, 1676, 1608, 1591, 1510, 1467, 1431, 1393, 1329 cm⁻¹; ¹H NMR (Acetone-d₆) δ 7.70 (dd, *J* = 8.3, 1.7 Hz, 1H, H-6), 7.64 (d, *J* = 1.7 Hz, 1H, H-2), 7.60 (d, *J* = 8.3 Hz, 1H, H-5), 3.97 (s, 3H, OCH₃), 3.08 (s, 3H, SO₂CH₃); ¹³C {¹H} NMR (Acetone-d₆) δ 165.8 (CO₂H), 149.8 (C-3), 131.6 (C-4), 127.0 (C-6), 123.8 (C-1), 119.7 (C-5), 112.7 (C-2), 56.5 (OCH₃), 40.0 (SO₂CH₃); LRMS (ESI) *m/z*: 246.02 (M+H)⁺; HRMS (ESI) *m/z* calcd. for C₉H₁₅O₅N₂S [M+NH₄]⁺: 263.0696, found: 263.0699

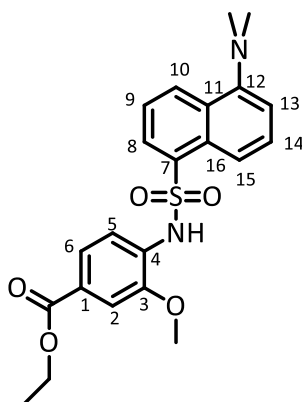
Ethyl 4-(4-((4-(dimethylamino)phenyl)diazenyl)phenylsulfonamido)-3-methoxybenzoate (84, ICT13114).



Round bottom flask was charged with ethyl 4-amino-3-methoxybenzoate **77** (0.10 g, 0.51 mmol) in presence of pyridine (15 mL). Dabsyl chloride (0.19 g, 0.61 mmol) dissolved in DCM was added dropwise at 0 °C to the reaction solution. The solution was left stirring at room temperature for 5h. 2M hydrochloric acid (10 mL, 2M) was added and reaction mixture was extracted with ethyl acetate (3x50 mL). The combined organic extracts were dried over anhydrous MgSO₄, filtered and the solvent was stripped of under reduced pressure. The resultant material was purified by flash column chromatography (EtOAc:PE, 2:8 v/v) to give the *title compound* (0.15 g, 60 %) as dark red crystals; m.p: 176.1-176.3 °C; IR: 3225, 2854, 1696, 1601, 1586, 1547, 1524, 1446, 1413, 1348 cm⁻¹; ¹H NMR (Acetone-d₆) δ 8.52 (s, 1H, NH), 7.85 (d, *J* = 8.4 Hz, 2H, H-8, H-12), 7.74 (d, *J* = 8.4 Hz, 2H, H-9, H-11), 7.70 (d, *J* = 8.4 Hz, 2H, H-14, H-18). 7.49 (dd, *J* = 8.2, 1.2 Hz, 1H, H-6), 7.38 (d, *J* = 8.2 Hz, 1H, H-5), 7.33 (d, *J* = 1.2 Hz, 1H, H-2), 6.75 (d, *J* = 8.4 Hz, 2H, H-15, H-17), 4.23 (q, *J*=7.0 Hz, 2H, CH₂), 3.64 (s, 3H, OCH₃), 3.01 (s, 6H, N(CH₃)₂), 1.18 (s, 3H, CH₂CH₃); ¹³C {¹H} NMR (Acetone-d₆) δ 166.9 (C=O), 166.7 (C-10), 146.7 (C-16), 143.3 (C-3), 125.5 (C-13), 124.8 (C-7), 124.6 (overlapping C-8, C-12),

124.4 (C-1), 123.0 (C-4), 119.3 (overlapping C-9, C-11), 113.2 (C-6), 113.1 (overlapping C-14, C-18) 111.8 (C-5), 111.7 (overlapping C-15, C-17), 111.6 (C-2), 60.4 (CH₂), 56.4 (OCH₃), 55.7 (N(CH₃)₂), 15.2 (CH₂CH₃); LRMS (ESI) m/z: 483.3 (M+H)⁺; HRMS (ESI) m/z calcd. for C₂₄H₂₇O₅N₄S [M+H]⁺: 483.1697, found: 483.1685

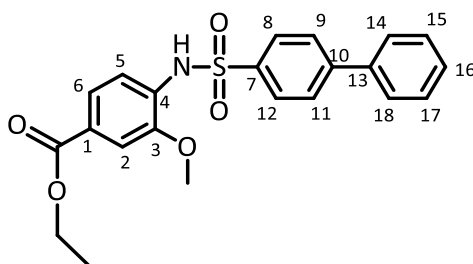
Ethyl 4-(5-(dimethylamino)naphthalene-1-sulfonamido)-3-methoxybenzoate (85, ICT13130).



Ethyl 4-amino-3-methoxybenzoate **77** (0.10 g, 0.51 mmol) was dissolved in dry pyridine (10 mL). The reaction temperature was brought to 0 °C and solution of dansyl chloride (0.16 g, 0.59 mmol) in DCM was added dropwise and was left stirring for 5 h. Hydrochloric acid (10 mL, 2M) was added and the reaction solution was extracted with ethyl acetate (3x50 mL). The combined organic extracts were dried over anhydrous MgSO₄, filtered and the solvent was evaporated under reduced pressure. The resultant material was purified by flash column chromatography (EtOAc:PE, 2:8 v/v) to give the *title compound* (0.21 g, 96 %) as brown solid; m.p: 142.0-142.6 °C; IR: 3269, 2927, 2852, 1708, 1605, 1588, 1574, 1507, 1461, 1433 cm⁻¹; ¹H NMR (CDCl₃) δ 8.42 (d, *J* = 8.8 Hz, 1H, H-8), 8.25 (d, *J* = 8.8 Hz, 1H, H-15), 8.17 (d, *J* = 7.3, Hz, 1H, H-10), 7.52 (dd, *J* = 7.3, 8.8 Hz, 1H, H-14), 7.48 (s, 1H, NH), 7.44 (dd, *J* = 8.4, 1.6 Hz, 1H, H-6), 7.41 (d *J* = 8.4, 1H, H-5), 7.36 (dd, *J* = 7.3, 8.8 Hz, 1H, H-9), 7.25 (d, *J* = 1.6 Hz, 1H, H-2), 7.10 (d, *J* = 7.3 Hz, 1H, H-13), 4.21 (q, *J* = 7.1 Hz, 2H, CH₂), 3.56 (s, 3H, OCH₃), 2.78 (s, 6H, N(CH₃)₂), 1.26 (t, *J* = 7.1 Hz, 3H, CH₂CH₃); ¹³C {¹H} NMR (CDCl₃) δ 166.0 (C=O), 152.0 (C-12), 147.9 (C-7), 133.8 (C-3), 131.1 (C-8), 130.6 (C-4), 130.3 (C-10), 129.8 (C-16), 129.5 (C-1), 128.4 (C-14),

126.1 (C-5), 122.9 (C-6), 118.5 (C-15), 117.7 (C-9), 115.2 (C-13), 112.3 (C-11),
111.2 (C-2), 61.0 (CH₂), 55.8 (OCH₃), 45.4 (N(CH₃)₂), 14.3 (CH₂CH₃); LRMS
ESI (-ve) m/z: 427.03 (M-H)⁻; HRMS (ESI) m/z calcd. for C₂₂H₂₅O₅N₂S [M+H]⁺:
429.1479, found: 429.1473.

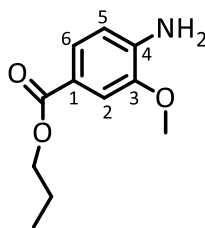
Ethyl 4-([1,1'-biphenyl]-4-ylsulfonamido)-3-methoxybenzoate (86, ICT13126).



Round bottom flask was charged with ethyl 4-amino-3-methoxybenzoate **77** (0.10 g, 0.51 mmol) in presence of pyridine (15 mL). Solution of [1,1'-biphenyl]-4-sulfonyl chloride (15.0 mg, 0.059 mmol) in DCM was added dropwise at 0 °C to the reaction solution. The solution was left stirring at room temperature for 5h. Hydrochloric acid (10 mL, 2M) was added and the reaction mixture was extracted with ethyl acetate (3x50 mL). The combined organic extracts were dried over anhydrous MgSO₄, filtered and the solvent was evaporated under reduced pressure. The resultant material was purified by flash column chromatography (EtOAc:PE, 2:8 v/v) to give the *title compound* (0.20 g, 95%) as yellow crystals; m.p: 120.8-121.0 °C; IR: 3213, 2977, 2940, 1697, 1601, 1565, 1506, 1480, 1462, 1438 cm⁻¹; ¹H NMR (CDCl₃) δ 7.81 (d, *J* = 8.3 Hz, 2H, H-8, H-12), 7.59–7.52 (m, 4H, H-9, H-11, H-15, H-17), 7.48 (d, *J* = 1.5 Hz, 1H, H-2), 7.44 (d, *J* = 8.1, 1.5 Hz, 1H, H-6) 7.39 – 7.32 (m, 3H, H-14, H-16, H-18), 7.30 (d, *J* = 8.1 Hz, 1H, H-5), 7.28 (s, 1H, NH), 4.26 (q, *J* = 7.1 Hz, 2H, CH₂), 3.73 (s, 3H, OCH₃), 1.28 (t, *J* = 7.1 Hz, 3H, CH₂CH₃); ¹³C {¹H} NMR (CDCl₃) δ 166.0 (C=O₂CH₂), 148.1 (C-3), 146.1 (C-13), 139.0 (C-7), 137.4 (C-10), 130.3 (C-4), 129.0 (overlapping C-15, C-17), 128.6 (C-16), 127.7 (overlapping C-14, C-18), 127.6 (overlapping C-8, C-12), 127.2 (overlapping C-9, C-11), 126.6 (C-1), 123.1 (C-6), 118.2 (C-5), 111.3 (C-2), 61.1 (CH₂), 56.0 (OCH₃), 14.3 (CH₂CH₃);

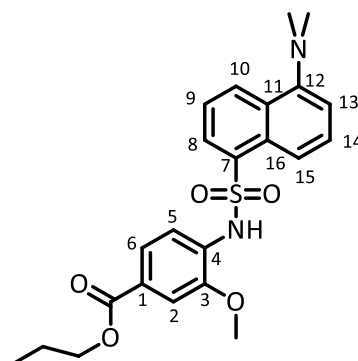
LRMS (ESI) m/z: 410.95 (M-H)⁻; HRMS (ESI) m/z calcd. for C₂₂H₂₂O₅NS
[M+H]⁺: 412.1213, found: 412.1211.

Propyl 4-amino-3-methoxybenzoate (ICT13142).



Round bottom flask was charged with 4-amino-3-methoxybenzoic acid **73** (0.10 g, 0.59 mmol) and 30 mL of propanol. The reaction solution was treated with thionyl chloride (0.12 mL, 1.77 mmol) dropwise and refluxed overnight. After cooling to room temperature, acidic water was added and extracted with ethyl acetate (3x50 mL). The combined organic extracts were dried over anhydrous MgSO_4 , filtered and the solvent was evaporated under reduced pressure to give to give the title compound (95.0 mg, 76 %) as brown solid; m.p: 39.6-40.4 °C; IR: 3416, 3039, 2844, 2599, 1713, 1623, 1537, 1503, 1456, 1419 cm^{-1} ; ^1H NMR (Acetone- d_6) δ 7.80 (dd, $J = 8.4, 1.4$ Hz, 1H, H-6), 7.78 (d, $J = 1.4$ Hz, 1H, H-2), 7.53 (d, $J = 8.4$ Hz, 1H, H-5), 4.32 (t, $J = 6.6$ Hz, 2H, OCH_2), 4.03 (s, 3H, OCH_3), 1.80 (m, 2H, CH_2CH_3), 1.03 (t, $J = 7.4$ Hz, 3H, CH_2CH_3); ^{13}C { ^1H } NMR (Acetone- d_6) δ 165.5 ($\text{C}=\text{O}_2\text{CH}_2$), 147.4 (C-3), 137.8 (C-4), 123.2 (C-6), 121.3 (C-1), 116.0 (C-5), 111.1 (C-2), 65.5 (OCH_2), 55.6 (OCH_3), 21.6 (CH_2CH_3), 10.3 (CH_2CH_3); LRMS (ESI) m/z : 210 ($\text{M}+\text{H}^+$); HRMS (ESI) m/z calcd. for $\text{C}_{11}\text{H}_{16}\text{NO}_3$ [$\text{M}+\text{H}^+$]: 210.1034, found: 210.1012

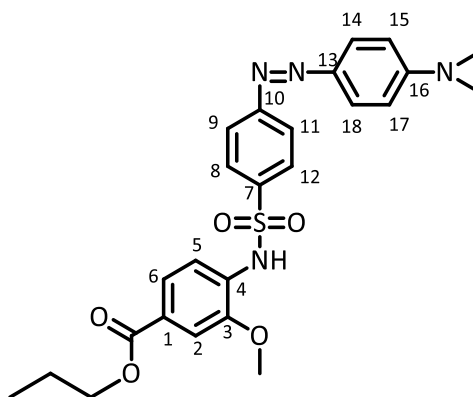
Propyl 4-(5(dimethylamino) naphthalene-1-sulfonamido)-3-methoxybenzoate (87, ICT13143).



Propyl 4-amino-3-methoxybenzoate (0.10 g, 0.47 mmol) was dissolved in dry pyridine (10 mL). The reaction temperature was brought to 0 °C and dansyl chloride (0.15 g, 0.57 mmol) was then added dropwise and solution was left stirring for 5h. Hydrochloric acid (10 mL, 2M) was added and reaction mixture was extracted with ethyl acetate (3x50 mL). The combined organic extracts were dried over anhydrous MgSO₄, filtered and the solvent was evaporated under reduced pressure. The resultant material was purified by flash column chromatography (EtOAc:PE, 2:8 v/v) to give the *title compound* (0.19 g, 91 %) as yellowish green crystals; m.p: 161.2-162 °C; IR: 3267, 2937, 2788, 1708, 1606, 1588, 1574, 1507, 1455, 1433 cm⁻¹; ¹H NMR (CDCl₃) δ 8.43 (d, *J* = 8.8 Hz, 1H, H-8), 8.25 (d, *J* = 8.8 Hz, 1H, H-15), 8.17 (d, *J* = 7.3 Hz, 1H, H-10), 7.53 (dd, *J* = 7.3, 8.8 Hz, 1H, H-14), 7.49 (s, 1H, NH), 7.46 (dd, *J* = 8.4, 1.6 Hz, 1H, H-6), 7.38 (d, *J* = 8.4 Hz, 1H, H-5), 7.35 (dd, *J* = 7.3, 8.8 Hz, 1H, H-9), 7.25 (d, *J* = 1.6 Hz, 1H, H-2), 7.10 (d, *J* = 8.3 Hz, 1H, H-13), 4.12 (t, *J* = 6.7 Hz, 2H, OCH₂), 3.56 (s, 3H, OCH₃), 2.78 (s, 6H, N(CH₃)₂), 1.65 (m, 2H, CH₂CH₃), 0.90 (t, *J* = 7.4 Hz, 3H, CH₂CH₃); ¹³C {¹H} NMR (CDCl₃) δ 166.0 (CO₂CH₂), 152.0 (C-12), 147.9 (C-7), 133.9 (C-3), 131.1 (C-8), 130.6 (C-4), 130.3 (C-10), 129.8 (C-16), 129.5 (C-1), 128.4 (C-14), 126.1 (C-5), 122.9 (C-6), 118.5 (C-15), 118.3

(C-9), 115.2 (C-13), 112.1 (C-11), 111.2 (C-2), 66.5 (OCH₂), 55.8 (OCH₃), 45.4 (N(CH₃)₂), 22.0 (CH₂CH₃), 10.4 (CH₂CH₃); LRMS (ESI) m/z: 443.01 (M+H)⁺; HRMS (ESI) m/z calcd. for C₂₃H₂₇O₅N₂S [M+H]⁺: 443.1635, found: 443.1628.

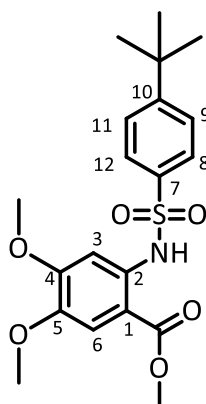
Propyl 4-(4-((4-(dimethylamino)phenyl)diazenyl)phenylsulfonamido)-3-methoxybenzoate (88, ICT13144).



Round bottom flask was charged with propyl 4-amino-3-methoxybenzoate (0.10 g, 0.47 mmol) in presence of pyridine (15 mL). Solution of dabsyl chloride (0.18 g, 0.57 mmol) in DCM was added dropwise at 0 °C to the reaction solution. The solution was left stirring at room temperature for 5h. Hydrochloric acid (10 mL, 2M) was added and reaction mixture was extracted with ethyl acetate (3x50 mL). The combined organic extracts were dried over anhydrous MgSO₄, filtered and the solvent was evaporated under reduced pressure. The resultant material was purified by flash column chromatography (EtOAc:PE, 2:8 v/v) to give the *title compound* (0.20 g, 85%) as dark red solid; m.p: 145.5-145.9 °C; IR: 3260, 2930, 2780, 1736, 1643, 1601, 1527, 1413, 1330, 1220 cm⁻¹; ¹H NMR (Acetone-d₆) δ 8.58 (s, 1H, NH), 7.86 (d, *J* = 8.4 Hz, 2H, H-8, H-12), 7.79 (d, *J* = 8.4 Hz, 2H, H-9, H-11), 7.76 (d, *J* = 8.4 Hz, 2H, H-14, H-18). 7.50 (dd, *J* = 8.2, 1.2 Hz, 1H, H-6), 7.49 (d, *J* = 8.2 Hz, 1H, H-5), 7.34 (d, *J* = 1.2 Hz, 1H, H-2), 6.83 (d, *J* = 8.4 Hz, 2H, H-15, H-17), 4.07 (t, *J* = 6.6 Hz, 2H, OCH₂), 3.65 (s, 3H, OCH₃), 3.08 (s, 6H, N(CH₃)₃), 1.61 (m, 2H, CH₂CH₃), 0.85 (t, *J* = 7.4 Hz, 3H, CH₂CH₃); ¹³C {¹H} NMR (Acetone-d₆) δ 166.3 (C=O), 153.8 (C-10), 144.2 (C-16), 140.4 (C-3), 131.9 (C-13), 129.3 (C-7), 128.2 (overlapping C-8, C-

12), 128.0 (C-1), 127.4 (C-4), 123.2 (overlapping C-9, C-11), 122.5 (overlapping C-14, C-18), 120.8 (C-6), 114.3 (C-5), 113.5 (overlapping C-15, C-17), 112.4 (C-2), 67.0 (OCH₂), 56.4 (OCH₃), 40.9 (N(CH₃)₃), 22.7 (CH₂CH₃), 10.7 (CH₂CH₃); LRMS (ESI) m/z: 497.02 (M+H)⁺; HRMS (ESI) m/z calcd. for C₂₅H₂₉O₅N₄S [M+H]⁺: 497.1853, found: 497.1842.

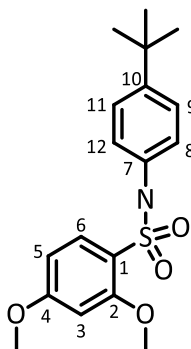
Methyl 2-(4-(tert-butyl)phenylsulfonamido)-4,5-dimethoxybenzoate (90, ICT13068).



To solution of methyl 2-amino-4, 5-dimethoxybenzoate **91** (0.10 g, 0.47 mmol) in dry pyridine (10 mL), solution of 4-tert-butylbenzenesulfonyl chloride **61** (0.13 g, 0.56 mmol) in DCM was added dropwise at 0 °C. The mixture was left stirring at R.T for 5 h. Hydrochloric acid solution (10 mL, 2M) was added to the reaction mixture. Organic components were extracted with ethyl acetate (3x50 mL). The combined organic extracts were dried over anhydrous MgSO₄, filtered and the solvent was evaporated under reduced pressure. The resultant material was purified by flash column chromatography (EtOAc:PE, 2:8 v/v) to give the title compound (0.15 g, 78 %) as brown crystals; m.p: 144.7-144.9 °C; IR: 2967, 1672, 1618, 1592, 1518, 1466, 1438, 1402, 1359, 1256 cm⁻¹; ¹H NMR (CDCl₃) δ 10.38 (s, 1H, NH), 7.63 (dd, *J* = 8.6, 2.0 Hz, 2H, H-8, H-12), 7.34 (dd, *J* = 8.6, 2.0 Hz, 2H, H-9, H-11), 7.24 (d, *J* = 5.9 Hz, 2H, H-3, H-6), 3.85 (s, 3H, CO₂CH₃), 3.75 (s, 6H, O(CH₃)₂), 1.21 (s, 9H, C(CH₃)₃); ¹³C {¹H} NMR (CDCl₃) δ 167.8 (C=O), 156.7 (C-5), 153.9 (C-10), 144.6 (C-1), 136.2 (C-4), 136.0 (C-7), 127.0 (overlapping C-8, C-12), 125.9 (overlapping C-9, C-11), 112.0 (C-3), 108.2 (C-2), 103.2 (C-6), 56.1 (O(CH₃)₂), 52.2 (CO₂CH₃), 35.1 (C(CH₃)₃), 31.0

(C(CH₃)₃); LRMS (ESI) m/z: 408.1 (M+H)⁺; HRMS (ESI) m/z calcd. for
C₂₀H₂₆O₆NS [M+H]⁺: 408.1475, found: 408.1469

***N*-4-(*tert*-butyl)phenyl)-2,4-dimethoxybenzenesulfonamide (**95**, ICT13121).**



2,4-dimethoxybenzene-1-sulfonyl chloride **93** (0.19 g, 0.80 mmol) was first dissolved in THF (15 mL) and was left stirring over 15 minutes. 4-(*tert*-butyl)aniline **94** (0.10 g, 0.67 mmol) was added dropwise to the solution and mixture was left stirring under nitrogen for 5h. Hydrochloric acid (10 mL, 2M) was added and extracted with ethyl acetate (3x50 mL). The combined organic extracts were dried over anhydrous MgSO₄, filtered and the solvent was removed under reduced pressure. The crude material was purified by flash column chromatography (EtOAc:PE, 2:8 v/v) to give the *title compound* (0.20 g, 85%) as white powder; m.p: 188.5-188.9 °C; IR: 3258, 2961, 1598, 1576, 1511, 1465, 1439, 1419, 1396, 1364 cm⁻¹; ¹H NMR (CDCl₃) δ 7.67 (d, *J* = 8.5 Hz, 1H, H-6), 7.16 (*J* = 8.6 Hz, 2H, H-8, H-12), 6.93 (s, 1H, NH), 6.92 (*J* = 8.6 Hz, 2H, H-9, H-11), 6.40 (d, *J* = 2.1 Hz, 1H, H-3), 6.38 (dd, *J* = 8.5, 2.1 Hz, 1H, H-5), 3.91 (s, 3H, OCH₃), 3.72 (s, 3H, OCH₃), 1.14 (s, 9H, C(CH₃)₃); ¹³C {¹H} NMR (CDCl₃) δ 164.9 (C-4), 157.7 (C-2), 148.0 (C-10), 134.2 (C-7), 132.7 (C-6), 126.0 (overlapping C-8, C-10), 121.1 (overlapping C-9, C-11), 118.7 (C-1), 104.4 (C-5), 99.3 (C-3), 56.3 (OCH₃), 55.7 (OCH₃), 34.2 (C(CH₃)₃), 31.2 (C(CH₃)₃); LRMS (ESI) *m/z*: 350.98 (M+H)⁺; HRMS (ESI) *m/z* calcd. for C₁₈H₂₄O₄NS [M+H]⁺: 350.1421, found: 350.1422

4.1.3. Experimental procedures for Western blot

All general chemicals, media and media supplements were obtained from Sigma-Aldrich (Poole, UK) unless otherwise specified. Rabbit Monoclonal antibody anti CCR7 [Y59], Abcam (Massachusetts, USA), Polyclonal goat anti rabbit linked to horseradish peroxidase conjugated secondary antibody (Dako, Ely, United Kingdom), Mouse monoclonal antibody anti- β -actin (Sigma Aldrich), polyclonal rabbit anti mouse linked to horseradish peroxidase (Dako), Nitrocellulose membrane and Amersham Hyper-film enhanced chemiluminescence detection reagent were obtained from GE Healthcare Life Sciences.

Cells and cell culture

All cell lines were obtained from the American Type Culture Collection (ATCC, Middlesex, UK), except for MCF-7 AND MCF-7 ADR were purchased from NCI. The cells were cultured in 75 cm² cell culture flasks (T-75) as monolayers in 10% Foetal Calf Serum (FCS), sodium pyruvate (1 mM) and L-glutamine (2 mM) RPMI-1640 medium (Sigma-Aldrich), at 37 °C , 95% air and 5% CO₂ atmosphere.

Determination of protein concentration

The Bradford assay was used to determine the protein concentration in each sample solution ¹⁶⁸. Serial dilutions started from 1 mg/ml, 0.5 mg/ml, 0.25 mg/ml, 0.125 mg/ml and 0.0625 mg/ml of BSA and blank dissolved in distilled water were prepared to create a standard curve of absorbance. Dilution of the protein samples were prepared to have 50 μ L in total. 1.5 ml of the Bradford reagent was added to each 50 μ L tube containing BSA, blank and samples

dilutions and the tubes were vortex mixed and allowed to stand for 15 minutes at room temperature to give enough time for the Coomassie Brilliant Blue dye to conjugate with the protein. The BSA standard concentration was analysed using a spectrophotometer (Cary 50 BIO UV-Visible) at a wavelength of 595nm. Results obtained from samples were calculated from the standard curve to get the protein concentration.

Method:

A panel of 10 cell pellets were first harvested from different cell lines which believed to have expression of CCR7 receptor based on literature review. Each pellet obtained is collection of three 75% confluent T-75 flasks. Cells were first washed with 10 ml of HBSS and collected in an Eppendorf tube, cell suspension was centrifuged at a speed of 13,000 rcf for 5 minutes at 22 °C to obtain the pellet and discard liquid layer. Pellets were then suspended in 2 X volume of protein extraction buffer. After the protein concentration was determined for each cell pellet, specific amount of protein was mixed with buffer solution and vortex mixed, centrifuged and heated in water bath for 10 minutes at 60 °C. 5 µl of PageRuler™ Plus Prestained Protein Ladder (Thermo Scientific) and the desired concentration of proteins were loaded on a 12% polyacrylamide gel for 20 min at 80 V and then 1 hour at 160 V constant voltage. The voltage was stopped when the dye reached 1 cm from the bottom of the gel. Transfer membrane and all pads and filters were soaked in the transfer buffer making sure that no bubbles are formed.

Blotting

The protein was transferred from polyacrylamide gel to nitrocellulose membrane (GE Healthcare Life Sciences) in presence of transfer buffer, the whole stack including transfer paper, gel and blotting papers were held vertically in the transfer buffer and the tank was connected to a power supply at 58 mA for 2 hours on ice. The membrane was placed in blocking solution (Marvel skimmed milk) on a rocker platform for one hour at room temperature. The membrane was then incubated with diluted rabbit monoclonal antibody anti CCR7 [Y59] (Abcam) primary antibody on the plate overnight at 4 °C. The membrane was washed with wash solution (0.5 % Tween PBS) for 15 minutes three times, washed solution was discarded. The membrane was incubated with the diluted horseradish peroxidase conjugated secondary antibody (Dako) in blocking solution for about one hour at room temperature on the rocker plate. Again, the membrane was washed three times and the washing solution was discarded. The final step was to detect CCR7 protein availability on these cell lines by using the reporter enzyme which linked to the antibody which gives colorimetric reaction during exposing to the appropriate substrate. The CCR7 protein was detected by incubating membrane with Amersham Hyper-film enhanced chemiluminescence (ECL) for about 10 minutes. The film was then developed in Multigrade Paper Developer solution (Ilford), washed with water and fixed in Rapid Film and Paper Fixer solution (Ilford) for 2 minutes and left to dry. Because the molecular weight of the ligand is close to the molecular weight of beta actin, the blots were stripped using stripping buffer (15 g glycine, 1 g SDS, 10 ml Tween20, Adjust pH to 2.2 Bring volume up to 1 L with ultrapure water) for 1 hour at 25 °C and re-probed with mouse monoclonal anti-β-actin (Sigma

Aldrich), which recognize proteins with band size 42 kDa to assess loading density. The primary antibody was incubated overnight at 4°C and same steps used in detecting the CCR7 receptor were repeated.

4.1.4. Experimental procedure for calcium flux assay

Chemicals and biologicals

All general chemicals, media and media supplements were obtained from Sigma-Aldrich unless otherwise specified. Recombinant CCL19 (and CCL21 were purchased from R&D Systems (Abingdon, UK). CCR7 antagonists were synthesised at the Institute of Cancer Therapeutics (University of Bradford, UK). Fluo-4 NW dye mix (Catalogue number F36206), (Component A), Probenecid, water soluble (Component B) and Assay buffer (1X HBSS, 20 mM HEPES) (Component C, included in starter pack only) were purchased from life technologies, UK. 96-well black-wall, flat bottom, microtiter plate (catalogue number 27614033) were purchased from Costar (Massachusetts, USA).

Cells and cell culture

Human glioblastoma-astrocytoma, epithelial-like cell line (U-87-MG), human T cell lymphoblast-like cell line (CCRF-CEM), human pancreatic carcinoma epithelial-like cell line (Panc-1) were obtained from the American Type Culture Collection (ATCC, Middlesex, UK). Human oral squamous cell carcinoma (OSC-19) was a generous gift from Dr Faye Johnson, MD Anderson Cancer Centre, Houston, USA. OSC-19 cell line was chosen because it was reported within our research group to have high expression of CCR7. CCRF and Panc-1 cell lines were chosen because they were reported in literature to have high expression of CCR7 receptor. U-87-MG cell line is a cell line amongst panel of

cell lines which showed remarkable expression on western blot assay. The cells were cultured in 75 cm² cell culture flasks (T-75) as monolayers in 10% Foetal Calf Serum (FCS), sodium pyruvate (1 mM) and L-glutamine (2 mM) RPMI-1640 medium (Sigma-Aldrich), at 37 °C , 95% air and 5% CO₂ atmosphere.

Method

Cells were seeded into each well of 96-well black-wall, flat bottom, microtiter plate at a density of 5 x 10⁴ cells per well. After 24 h, the growth medium was replaced with 100µl of the dye loading solution (Molecular Probes™ Fluo-4 NW (no wash), Invitrogen F36206). The plates were incubated at 37 °C for 30 minutes and at room temperature for an additional 30 minutes. 20µL of a given concentration of the antagonist in medium, or plain medium as control, was added to each well and the plate was incubated at 37 °C for 15 minutes and at room temperature for an additional 30 minutes. The plate was transferred into a Fluoroskan Ascent FL instrument (ThermoScientific) and the fluorescence in response to the addition of 20µl chemokine (to give 100 nM in-well concentration) was measured at room temperature (Ex 485 nm, Em 538 nm). IC₅₀ is calculated as the concentration of the antagonist required to half the maximal response to chemokine using Prism software. Data is presented as the mean ±SE of at least 3 independent experiments.

Making the reagents

Following the manufacturing instructions, 1 ml of the assay buffer (component C) was added to the container labelled as component B (probenecid) and vortex mix in order to make a 250 mM stock solution of probenecid. 10 ml of the assay buffer (component C) and 100µl of the probenecid solution (component B) was added to the component A (containing the Fluo-4 NW dye). The mixture was

shaked well for 2 minutes in the vortex mixer to make sure the dye dissolved properly. This dye loading solution is sufficient for one 96-well microplate as 100µl of the dye is loaded to each well.

Preparation of ligands CCL21 and CCL19

Both ligands are prepared the same way considering the differences in molecular weight. For example, 25µg lyophilized CCL21 (MW = 12 kDa) was reconstituted by adding 100µL of sterile phosphate-buffered-saline solution (PBS) containing 0.1% BSA to afford 100µL of 2.083×10^{-5} M stock solution. First, both ligand were used to determine the concentration to be used in the assay, so serial dilutions were taken place. The first dilution was prepared by adding 100µL of stock solution to 900µL of assay buffer (without probenecid) to afford 2.083×10^{-6} M solution (1000µL). If 20µL of this solution is added to 100µL of assay buffer (120µL), the final concentration of CCL21 is 3.47×10^{-7} . Taking into account the 700µl which is used to purge the system and number of wells repeated in each assay (75µL for 3 runs and 225µL is left for next dilutions). CCL21 showed better activity, so 100 nM of CCL21 was conducted from the EC₅₀ curve to be used for the whole assay. Taking into account the dead volume of pipes in the fluoroskan, 700µL, and number of wells used in each run, CCL21 is calculated to make 100nm in the wells (140µL total volume).

Preparation of antagonist solutions

A stock solution of each compound was prepared by dissolving known amount of compound in 100 µl DMSO, to generate 100mM stock solution. The first top concentration was made by adding 2 µL of the stock solution to an Eppendorf tube containing 198 µL of assay buffer without probenecid to give a 1mM

solution (containing 1% DMSO v/v). When the 20 μ L of first dilution solution is added directly to the well (total volume 140 μ L: 100 μ L loading dye mixture + 20 μ L ligand + 20 μ L antagonist) the final concentration of the molecule in cell suspension is 142 μ M, containing 0.14% DMSO.

4.1.5. Experimental procedure for Agarose Spot Method.

Chemicals and biologicals

Recombinant CXCL12, CCL19 and CCL21 were purchased from R&D Systems. Ultrapure™ low-melting agarose was purchased from Invitrogen (Paisley, UK). CXCR4 antagonist AMD3100 (catalogue number 3299)¹⁶⁹, was purchased from Tocris Biosciences (Westwoods Business Park, Ellisville, Missouri USA). CCR7 antagonist compound **75** and compound **3** were synthesised at the Institute of Cancer Therapeutics (University of Bradford, UK).

Cells and cell culture

Human primary glioblastoma cell line (U87-MG), human colon adenocarcinoma cell line (DLD-1), human colorectal adenocarcinoma cell line (HT-29) human prostate PC-3 and colorectal SW-480 adenocarcinoma cell lines were obtained from the American Type Culture Collection (ATCC). The cells were cultured in 75 cm² cell culture flasks (T-75) as monolayers in 10% Foetal Calf Serum (FCS), sodium pyruvate (1 mM) and L-glutamine (2 mM) RPMI-1640 medium (Sigma-Aldrich), at 37 °C, 95% air and 5% CO₂ atmosphere.

Equipment

Disposable glass-bottomed plastic 35mm petri dishes with lid were purchased from iBidi (Glasgow, United Kingdom). These dishes have a usable glass

surface area with a 20 mm diameter. Images were observed using LumaScopes 500 (Etaluma, Inc. Carlsbad, CA) with 20x objectives. A Nikon Eclipse TI confocal microscope was used to record a movie of cells migration.

Method

100 mg of low-melting point agarose was placed into a 100-mL beaker and dissolved into 20 mL PBS to make a 0.5% agarose solution. This was heated until boiling on a hot plate, and swirled to facilitate complete dissolution. Once all agarose particles were dissolved, the beaker was taken off of the heat and cooled down to 40 °C. Stock solutions of the appropriate chemokines were prepared as following. For example, 10µg lyophilized CXCL12 (MW = 8004 Da) was reconstituted by adding 100µL of sterile phosphate-buffered-saline solution (PBS) containing 0.1% BSA to afford a 12.5 µM stock solution. To prepare a 100 nM CXCL12/agarose solution, 1.6 µL of the CXCL12 stock solution was mixed with 18.4 µL of PBS. The resulting 20µL was then mixed with 180 µL of 0.5% agarose solution at 40 °C. To prepare CCL21 (MW = 12 kDa) is prepared as: 25ug lyophilized CCL21 is reconstituted by adding 100µL of sterile phosphate-buffered- saline solution containing 0.1% BSA. This affords a stock solution of 20.83uM. To prepare a 100 nM CCL21/agarose solution, 0.96 µL of the CCL21 stock solution was mixed with 19.03 µL of PBS. The resulting 20µL was then mixed with 180 µL of 0.5% agarose solution at 40 °C. To prepare CCL19 (MW = 8800 D) is prepared as: 25ug lyophilized CCL19 is reconstituted by adding 100µL of sterile phosphate-buffered-saline solution containing 0.1% BSA. This affords a stock solution of 28.41uM. To prepare a 100 nM CCL19/agarose solution, 0.70 µL of the CCL19 stock solution was mixed with 19.29 µL of PBS. The resulting 20µL was then mixed with 180 µL of 0.5%

agarose solution at 40 °C. To prepare the control agarose solution, 20µl of PBS was placed in an Eppendorf tube and mixed with 180 µL of 0.5% agarose solution at 40°C. Stock solutions of the appropriate antagonists were prepared as following. To prepare AMD3100, 100mM stock solution of AMD3100 was prepared by dissolving 7.945 mg of the drug (MW= 794.5) into 100µL of deionized water (stock solution). This stock solution was aliquoted according to experiment need and stored at -20 C°. Stock solution (100mM) was further diluted to 1mM (10µL stock + 990µL medium, 1mL total) in separate eppendorf tube (1mL is needed because medium containing drug is discarded after incubation for 4 hours to change the 0.1% medium). Then serial dilutions were prepared as follow, to make 200µM AMD3100, 800µL medium containing cells + 200µL of 1mM AMD3100 solution (1mL total). To make 100µM AMD3100, add 900µL medium containing cells to 100µL of 1mM AMD3100 solution (1mL total). To make 50µM AMD3100, add 950µL medium containing cells to 50µL of 1mM AMD3100 solution (1mL total). To prepare compound **75**, 100mM stock solution of compound **75** was prepared by dissolving 3.7745 mg of the drug (MW= 377.45) into 100µL of DMSO (stock solution). To prepare compound **3**, 100mM stock solution of compound **75** was prepared by dissolving 2.00 mg of the drug (MW= 200.22) into 100µL of DMSO (stock solution). These stock solutions were aliquoted according to experiment need and stored at -20 C°. The required diluted concentrations were then prepared the same way as shown in AMD3100 compound.

The ends of 200µl pipette tips (catalogue number 70.760.211; Sarstedt, Leicester, UK) were cut with scissors by about 2 mm in order to facilitate the transfer of the viscous agarose solution and the formation of the spot. Using

these cut pipette tips, 10µl drops of agarose solution (either control containing only PBS, or containing chemokine) were applied onto each of the quadrants of the petri dish. Depending on the purpose of the experiment, spots containing the same chemokine (to allow the results to be obtained in duplicate or triplicate) or different chemokines (to allow comparison) can be applied for each dish. If required, the spots can be identified by writing on the backside of the glass. The petri dish containing the spots was then cooled for exactly 5 minutes in a 4 °C fridge to allow the agarose spot to set. 1 ml of cell suspension in 10% FCS media, either containing the antagonist(s), or control (no agent), was plated into the dishes which were then incubated at 37 °C, 5% CO₂ to allow the cells to adhere. The cell density was about 6.0 x 10⁴/ml, after 4 hours, the culture media was replaced with 0.1% FCS. After 16 h, the agarose spots were analysed by counting total number of invading cells using a microscope. A movie was taken for the cells migrating using Nikon Eclipse TEZ000-U confocal microscope. Images obtained were analysed by Fiji/ImageJ software. Data is presented as the mean ±SE of at least 3 independent experiments.

5. References

1. Burger JA, Kipps TJ. CXCR4: a key receptor in the crosstalk between tumor cells and their microenvironment. *Blood*. 2006;107(5):1761-7.
2. Hanahan D, Weinberg RA. Hallmarks of cancer: the next generation. *Cell*. 2011;144(5):646-74.
3. Yokota J. Tumor progression and metastasis. *Carcinogenesis*. 2000;21(3):497-503.
4. Koizumi K, Hojo S, Akashi T, Yasumoto K, Saiki I. Chemokine receptors in cancer metastasis and cancer cell-derived chemokines in host immune response. *Cancer science*. 2007;98(11):1652-8.
5. Tannock IF, Hill RP. *The basic science of oncology*. New York: McGraw-Hill; 1998.
6. Murakami T, Cardones AR, Hwang ST. Chemokine receptors and melanoma metastasis. *Journal of dermatological science*. 2004;36(2):71-8.
7. Foon KA. *Biological therapy of cancer*. *Breast cancer research and treatment*. 1986;7(1):5-14.
8. Hassan S, Baccarelli A, Salvucci O, Basik M. Plasma Stromal Cell-Derived Factor-1: Host Derived Marker Predictive of Distant Metastasis in Breast Cancer. *Clinical cancer research*. 2008;14(2):446-54.
9. Pienta KJ, Robertson BA, Coffey DS, Taichman RS. The Cancer Diaspora: Metastasis beyond the seed and soil hypothesis. *Clinical cancer research*. 2013;19(21):5849-55.
10. Miyazaki H, Takabe K, Yeudall WA. Chemokines, chemokine receptors and the gastrointestinal system. *World j gastroenterol*. 2013;19(19):2847.

11. Janeway C, Travers P, Hunt S. Immunobiology: the immune system in health and disease: Current Biology; 1996.
12. Cabral GA, Raborn ES, Griffin L, Dennis J, Marciano-Cabral F. CB2 receptors in the brain: role in central immune function. British journal of pharmacology. 2008;153(2):240-51.
13. Fu H, Karlsson J, Bylund J, Movitz C, Karlsson A, Dahlgren C. Ligand recognition and activation of formyl peptide receptors in neutrophils. Journal of leukocyte biology. 2006;79(2):247-56.
14. Murdoch C, Finn A. Chemokine receptors and their role in inflammation and infectious diseases. Blood. 2000;95(10):3032-43.
15. Locati M, Bonecchi R, Corsi MM. Chemokines and Their Receptors Roles in Specific Clinical Conditions and Measurement in the Clinical Laboratory. American Journal of Clinical Pathology Pathology Patterns Reviews. 2005;123(Suppl 1):S82-S95.
16. Vaddi K, Keller M, Newton M. The Chemokine Factsbook: Ligands and Receptors: Academic Press; 1997.
17. Ali S, Lazennec G. Chemokines: novel targets for breast cancer metastasis. Cancer and Metastasis Reviews. 2007;26(3-4):401-20.
18. Lolis E, Murphy JW. The Structural Biology of Chemokines. In: Harrison JK, Lukacs NW, editors. The Chemokine Receptors. Totowa, NJ: Humana Press; 2007. p. 9-30.
19. Hattermann K, Holzenburg E, Hans F, Lucius R, Held-Feindt J, Mentlein R. Effects of the chemokine CXCL12 and combined internalization of its receptors CXCR4 and CXCR7 in human MCF-7 breast cancer cells. Cell Tissue Res. 2014;357(1):253-66.

20. Shim H, Oishi S, Fujii N, editors. Chemokine receptor CXCR4 as a therapeutic target for neuroectodermal tumors. *Seminars in cancer biology*; 2009: Elsevier.
21. Chung ACK, Lan HY. Chemokines in renal injury. *Journal of the American Society of Nephrology*. 2011;22(5):802-9.
22. de Munnik SM, Smit MJ, Leurs R, Vischer HF. Modulation of cellular signaling by herpesvirus-encoded G protein-coupled receptors. *Frontiers in pharmacology*. 2015;6.
23. Struyf S, Gouwy M, Dillen C, Proost P, Opdenakker G, Van Damme J. Chemokines synergize in the recruitment of circulating neutrophils into inflamed tissue. *European journal of immunology*. 2005;35(5):1583-91.
24. Zou Y-R, Kottmann AH, Kuroda M, Taniuchi I, Littman DR. Function of the chemokine receptor CXCR4 in haematopoiesis and in cerebellar development. *Nature*. 1998;393(6685):595-9.
25. Lazenec G, Richmond A. Chemokines and chemokine receptors: new insights into cancer-related inflammation. *Trends Mol Med*. 2010;16(3):133-44.
26. Rossi D, Zlotnik A. The biology of chemokines and their receptors. *Annual review of immunology*. 2000;18(1):217-42.
27. Fernandez EJ, Lolis E. Structure, function, and inhibition of chemokines. *Annual review of pharmacology and toxicology*. 2002;42(1):469-99.
28. Ransohoff RM, Suzuki K, Proudfoot AEI, Hickey WF, Harrison JK. *Universes in Delicate Balance: Chemokines and the Nervous System: Chemokines and the Nervous System*: Elsevier; 2002.
29. Herndon RM. *Multiple sclerosis: immunology, pathology, and pathophysiology*: Demos Medical Publishing; 2003.

30. Xing YN, Xu XY, Nie XC, Yang X, Yu M, Xu HM, et al. Role and clinicopathologic significance of CXC chemokine ligand 16 and chemokine (C-X-C motif) receptor 6 expression in gastric carcinomas. *Hum Pathol.* 2012;43(12):2299-307.
31. Harrison JK, Lukacs NW. *The chemokine receptors*: Springer; 2007.
32. Vindrieux D, Escobar P, Lazennec G. Emerging roles of chemokines in prostate cancer. *Endocrine-related cancer.* 2009;16(3):663-73.
33. Karnoub AE, Weinberg RA. Chemokine networks and breast cancer metastasis. *Breast disease.* 2007;26(1):75-85.
34. Gangur V, Birmingham NP, Thanavorakul S. Chemokines in health and disease. *Veterinary immunology and immunopathology.* 2002;86(3):127-36.
35. Rosenkilde MM, Schwartz TW. The chemokine system—a major regulator of angiogenesis in health and disease. *Apmis.* 2004;112(7-8):481-95.
36. Foti M, Granucci F, Aggujaro D, Liboi E, Luini W, Minardi S, et al. Upon dendritic cell (DC) activation chemokines and chemokine receptor expression are rapidly regulated for recruitment and maintenance of DC at the inflammatory site. *International immunology.* 1999;11(6):979-86.
37. Esche C, Stellato C, Beck LA. Chemokines: key players in innate and adaptive immunity. *Journal of investigative dermatology.* 2005;125(4):615-28.
38. Robertson MJ. Role of chemokines in the biology of natural killer cells. *Journal of leukocyte biology.* 2002;71(2):173-83.
39. Kakinuma T, Hwang ST. Chemokines, chemokine receptors, and cancer metastasis. *Journal of leukocyte biology.* 2006;79(4):639-51.

40. Müller A, Homey B, Soto H, Ge N, Catron D, Buchanan ME, et al. Involvement of chemokine receptors in breast cancer metastasis. *Nature*. 2001;410(6824):50-6.
41. Johnson Z, Power CA, Weiss C, Rintelen F, Ji H, Ruckle T, et al. Chemokine inhibition-why, when, where, which and how? *Biochemical Society Transactions*. 2004;32(2):366-77.
42. Crane IJ, Wallace CA, McKillop-Smith S, Forrester JV. Control of chemokine production at the blood–retina barrier. *Immunology*. 2000;101(3):426-33.
43. Xiang Z-l, Zeng Z-c, Tang Z-y, Fan J, Zhuang P-y, Liang Y, et al. Chemokine receptor CXCR4 expression in hepatocellular carcinoma patients increases the risk of bone metastases and poor survival. *BMC Cancer*. 2009;9(1):176.
44. Yu Y, Sweeney MD, Saad OM, Crown SE, Handel TM, Leary JA. Chemokine-Glycosaminoglycan Binding SPECIFICITY FOR CCR2 LIGAND BINDING TO HIGHLY SULFATED OLIGOSACCHARIDES USING FTICR MASS SPECTROMETRY. *Journal of Biological Chemistry*. 2005;280(37):32200-8.
45. Kim B-T, Kitagawa H, Tamura J-i, Saito T, Kusche-Gullberg M, Lindahl U, et al. Human tumor suppressor EXT gene family members EXTL1 and EXTL3 encode α 1, 4-N-acetylglucosaminyltransferases that likely are involved in heparan sulfate/heparin biosynthesis. *PNAS*. 2001;98(13):7176-81.
46. Yan D, Lin X. Shaping morphogen gradients by proteoglycans. *Cold Spring Harbor perspectives in biology*. 2009;1(3).
47. Linkes W. *Progress in Chemokine Research*: Nova Publishers; 2007.

48. Mellado M, Rodríguez-Frade JM, Mañes S, Martínez-A C. Chemokine signaling and functional responses: the role of receptor dimerization and TK pathway activation. *Annu Rev Immunol.* 2001;19:397-421.
49. Richmond A. NF- κ B, chemokine gene transcription and tumour growth. *Nature Reviews Immunology.* 2002;2(9):664-74.
50. Jatiani SS, Baker SJ, Silverman LR, Reddy EP. JAK/STAT Pathways in Cytokine Signaling and Myeloproliferative Disorders Approaches for Targeted Therapies. *Genes & cancer.* 2010;1(10):979-93.
51. Stadtmann A, Zarbock A. CXCR2: from bench to bedside. *Frontiers in immunology.* 2015;3:263.
52. Owen JL, Mohamadzadeh M. Macrophages and chemokines as mediators of angiogenesis. *Frontiers in Physiology.*4:159.
53. Lu H, Ouyang W, Huang C. Inflammation, a key event in cancer development. *Molecular Cancer Research.* 2006;4(4):221-33.
54. Peddareddigari VG, Wang D, DuBois RN. The tumor microenvironment in colorectal carcinogenesis. *Cancer Microenvironment.* 2010;3(1):149-66.
55. Orimo A, Gupta PB, SgROI DC, Arenzana-Seisdedos F, Delaunay T, Naeem R, et al. Stromal fibroblasts present in invasive human breast carcinomas promote tumor growth and angiogenesis through elevated SDF-1/CXCL12 secretion. *Cell.* 2005;121(3):335-48.
56. Koontongkaew S. The Tumor Microenvironment Contribution to Development, Growth, Invasion and Metastasis of Head and Neck Squamous Cell Carcinomas. *Journal of Cancer.* 2013;4(1):66.

57. Cabioglu N, Yazici MS, Arun B, Broglio KR, Hortobagyi GN, Price JE, et al. CCR7 and CXCR4 as novel biomarkers predicting axillary lymph node metastasis in T1 breast cancer. *Clin Cancer Res.* 2005;11(16):5686-93.
58. Segerer S, Nelson PJ, SchlÖNdorff D. Chemokines, chemokine receptors, and renal disease: from basic science to pathophysiologic and therapeutic studies. *Journal of the American Society of Nephrology.* 2000;11(1):152-76.
59. Kawaguchi M, Kokubu F, Matsukura S, Ieki K, Odaka M, Watanabe S, et al. Induction of CXC chemokines, growth-related oncogene α expression, and epithelial cell-derived neutrophil-activating protein-78 by ML-1 (interleukin-17F) involves activation of raf1-mitogen-activated protein kinase kinase-extracellular signal-regulated kinase 1/2 pathway. *Journal of Pharmacology and Experimental Therapeutics.* 2003;307(3):1213-20.
60. Luster AD. Chemokines--chemotactic cytokines that mediate inflammation. *New England journal of medicine.* 1998;338(7):436-45.
61. Wang Z, Ma Q, Liu Q, Yu H, Zhao L, Shen S, et al. Blockade of SDF-1/CXCR4 signalling inhibits pancreatic cancer progression in vitro via inactivation of canonical Wnt pathway. *British journal of cancer.* 2008;99(10):1695-703.
62. Schwiebert LM. *Chemokines, Chemokine Receptors and Disease*: Elsevier; 2005.
63. Burger JA, Kipps TJ. CXCR4: a key receptor in the crosstalk between tumor cells and their microenvironment. *Blood.* 2006;107(5):1761-7.
64. Stein JV, Nombela-Arrieta C. Chemokine control of lymphocyte trafficking: a general overview. *Immunology.* 2005;116(1):1-12.

65. Weng AP, Shahsafaei A, Dorfman DM. CXCR4/CD184 immunoreactivity in T-cell non-Hodgkin lymphomas with an overall Th1–Th2+ immunophenotype. *American journal of clinical pathology*. 2003;119(3):424-30.
66. Cardones AR, Murakami T, Hwang ST. CXCR4 enhances adhesion of B16 tumor cells to endothelial cells in vitro and in vivo via β 1 integrin. *Cancer research*. 2003;63(20):6751-7.
67. McGrath KE, Koniski AD, Maltby KM, McGann JK, Palis J. Embryonic expression and function of the chemokine SDF-1 and its receptor, CXCR4. *Developmental biology*. 1999;213(2):442-56.
68. Takabatake Y, Sugiyama T, Kohara H, Matsusaka T, Kurihara H, Koni PA, et al. The CXCL12 (SDF-1)/CXCR4 axis is essential for the development of renal vasculature. *Journal of the American Society of Nephrology*. 2009;20(8):1714-23.
69. Fulton AM. *Chemokine Receptors in Cancer*: Springer; 2009.
70. Murdoch C. CXCR4: chemokine receptor extraordinaire. *Immunological reviews*. 2000;177(1):175-84.
71. Dar A, Kollet O, Lapidot T. Mutual, reciprocal SDF-1/CXCR4 interactions between hematopoietic and bone marrow stromal cells regulate human stem cell migration and development in NOD/SCID chimeric mice. *Experimental hematology*. 2006;34(8):967-75.
72. Zoughlami Y, Voermans C, Brussen K, van Dort KA, Kootstra NA, Maussang D, et al. Regulation of CXCR4 conformation by the small GTPase Rac1: implications for HIV infection. *Blood*. 2012;119(9):2024-32.

73. Chen S, Lin F, Shin ME, Wang F, Shen L, Hamm HE. RACK1 regulates directional cell migration by acting on G β γ at the interface with its effectors PLC β and PI3K γ . *Molecular biology of the cell*. 2008;19(9):3909-22.
74. Alblas J, Ulfman L, Hordijk P, Koenderman L. Activation of Rhoa and ROCK are essential for detachment of migrating leukocytes. *Molecular biology of the cell*. 2001;12(7):2137-45.
75. Furusato B, Mohamed A, Uhlén M, Rhim JS. CXCR4 and cancer. *Pathology international*. 2010;60(7):497-505.
76. Otsuka S, Bebb G. The CXCR4/SDF-1 chemokine receptor axis: a new target therapeutic for non-small cell lung cancer. *J Thorac Oncol*. 2008;3(12):1379-83.
77. Hunter K, Welch DR, Liu ET. Genetic background is an important determinant of metastatic potential. *Nature genetics*. 2003;34(1):23-4.
78. Choi HY, Saha SK, Kim K, Kim S, Yang GM, Kim B, et al. G protein-coupled receptors in stem cell maintenance and somatic reprogramming to pluripotent or cancer stem cells. *BMB Rep*. 2015;48(2):68-80.
79. Zlotnik A, Yoshie O, Nomiya H. The chemokine and chemokine receptor superfamilies and their molecular evolution. *Genome biology*. 2006;7(12):243.
80. Liu Y, Ji R, Li J, Gu Q, Zhao X, Sun T, et al. Correlation effect of EGFR and CXCR4 and CCR7 chemokine receptors in predicting breast cancer metastasis and prognosis. *J Exp Clin Cancer Res*. 2010;29(1):16.
81. Scholten DJ. Chemokine Receptors CXCR3 and CXCR7: Allosteric Ligand Binding, Biased Signaling, and Receptor Regulation [PhD]. Amsterdam: Vrije Universiteit; 2012.

82. Noor S, Wilson EH. Role of CC chemokine receptor type 7 and its ligands during neuroinflammation. *Age*. 2012;15:17.
83. Mburu YK, Egloff AM, Walker WH, Wang L, Seethala RR, Van Waes C, et al. Chemokine receptor 7 (CCR7) gene expression is regulated by NF- κ B and activator protein 1 (AP1) in metastatic squamous cell carcinoma of head and neck (SCCHN). *Journal of Biological Chemistry*. 2012;287(5):3581-90.
84. Love M, Sandberg JL, Ziarek JJ, Gerarden KP, Rode RR, Jensen DR, et al. Solution structure of CCL21 and identification of a putative CCR7 binding site. *Biochemistry*. 2012;51(3):733-5.
85. Pease JE, Williams TJ. The attraction of chemokines as a target for specific anti-inflammatory therapy. *British journal of pharmacology*. 2006;147(S1):S212-S21.
86. Otero C, Groettrup M, Legler DF. Opposite fate of endocytosed CCR7 and its ligands: recycling versus degradation. *Journal of Immunology*. 2006;177(4):2314-23.
87. Förster R, Davalos-Misslitz AC, Rot A. CCR7 and its ligands: balancing immunity and tolerance. *Nature Reviews Immunology*. 2008;8(5):362-71.
88. Yoshida R, Imai T, Hieshima K, Kusuda J, Baba M, Kitaura M, et al. Molecular cloning of a novel human CC chemokine EBI1-ligand chemokine that is a specific functional ligand for EBI1, CCR7. *J Biol Chem*. 1997;272(21):13803-9.
89. Reif K, Ekland EH, Ohl L, Nakano H, Lipp M, Förster R, et al. Balanced responsiveness to chemoattractants from adjacent zones determines B-cell position. *Nature*. 2002;416(6876):94-9.

90. Scandella E, Men Y, Legler DF, Gillessen S, Prikler L, Ludewig B, et al. CCL19/CCL21-triggered signal transduction and migration of dendritic cells requires prostaglandin E2. *Blood*. 2004;103(5):1595-601.
91. Nicolson GL. Autocrine and paracrine growth mechanisms in cancer progression and metastasis. In: JR B, editor. *Encyclopedia of Cancer*. 2nd ed. San Diego: Elsevier Science; 2002. p. 165-77.
- 92 Förster R, Davalos-Miszlitz AC, Rot A. CCR7 and its ligands: balancing immunity and tolerance. *Nature Reviews Immunology*. 2008;8(5):362-71.
93. Okada T, Cyster JG. CC chemokine receptor 7 contributes to Gi-dependent T cell motility in the lymph node. *Journal of Immunology*. 2007;178(5):2973-8.
94. Yamashita N, Tashimo H, Matsuo Y, Ishida H, Yoshiura K, Sato K, et al. Role of CCL21 and CCL19 in allergic inflammation in the ovalbumin-specific murine asthmatic model. *Journal of allergy and clinical immunology*. 2006;117(5):1040-6.
95. Schneider MA, Meingassner JG, Lipp M, Moore HD, Rot A. CCR7 is required for the in vivo function of CD4+ CD25+ regulatory T cells. *Journal of experimental medicine*. 2007;204(4):735-45.
96. Yang B-G, Tanaka T, Jang MH, Bai Z, Hayasaka H, Miyasaka M. Binding of lymphoid chemokines to collagen IV that accumulates in the basal lamina of high endothelial venules: its implications in lymphocyte trafficking. *Journal of Immunology*. 2007;179(7):4376-82.
97. Zidar DA, Violin JD, Whalen EJ, Lefkowitz RJ. Selective engagement of G protein coupled receptor kinases (GRKs) encodes distinct functions of biased ligands. *PNAS*. 2009;106(24):9649-54.

98. Riol-Blanco L, Sánchez-Sánchez N, Torres A, Tejedor A, Narumiya S, Corbí AL, et al. The chemokine receptor CCR7 activates in dendritic cells two signaling modules that independently regulate chemotaxis and migratory speed. *Journal of Immunology*. 2005;174(7):4070-80.
99. Verzijl D, Ijzerman AP. Functional selectivity of adenosine receptor ligands. *Purinergic signalling*. 2011;7(2):171-92.
100. Comerford I, Harata-Lee Y, Bunting MD, Gregor C, Kara EE, McColl SR. A myriad of functions and complex regulation of the CCR7/CCL19/CCL21 chemokine axis in the adaptive immune system. *Cytokine & growth factor reviews*. 2013.
101. DeWire SM, Ahn S, Lefkowitz RJ, Shenoy SK. β -arrestins and cell signaling. *Annu Rev Physiol*. 2007;69:483-510.
102. Nandagopal S, Wu D, Lin F. Combinatorial guidance by CCR7 ligands for T lymphocytes migration in co-existing chemokine fields. *PLoS one*. 2011;6(3):e18183.
103. Allaire M-A, Dumais N. Involvement of the MAPK and RhoA/ROCK pathways in PGE₂-mediated CCR7-dependent monocyte migration. *Immunology Letters*. 2012;146(1):70-3.
104. Ishigami S, Natsugoe S, Nakajo A, Tokuda K, Uenosono Y, Arigami T, et al. Prognostic value of CCR7 expression in gastric cancer. *Hepatogastroenterology*. 2007;54(76):1025-8.
105. Wiley HE, Gonzalez EB, Maki W, Wu MT, Hwang ST. Expression of CC chemokine receptor-7 and regional lymph node metastasis of B16 murine melanoma. *J Natl Cancer Inst*. 2001;93(21):1638-43.

106. Marinissen MJ, Gutkind JS. G-protein-coupled receptors and signaling networks: emerging paradigms. *Trends Pharmacol Sci.* 2001;22(7):368-76.
107. Fang L, Hwang ST. Roles for CCR7 in cancer biology. *Chemokine receptors in cancer*: Springer; 2009. p. 93-108.
108. Sánchez-Sánchez N, Riol-Blanco L, de la Rosa G, Puig-Kröger A, García-Bordas J, Martín D, et al. Chemokine receptor CCR7 induces intracellular signaling that inhibits apoptosis of mature dendritic cells. *Blood.* 2004;104(3):619-25.
109. Palmqvist C, Wardlaw AJ, Bradding P. Chemokines and their receptors as potential targets for the treatment of asthma. *British journal of pharmacology.* 2007;151(6):725-36.
110. Vinader V, Afarinkia K. A beginner's guide to chemokines. *Future Med Chem.* 2012;4(7):845-52.
111. Ott TR, Lio FM, Olshefski D, Liu XJ, Struthers RS, Ling N. Determinants of High-Affinity Binding and Receptor Activation in the N-Terminus of CCL-19 (MIP-3 β). *Biochemistry.* 2004;43(12):3670-8.
112. Ott TR, Lio FM, Olshefski D, Liu X-J, Ling N, Struthers RS. The N-terminal domain of CCL21 reconstitutes high affinity binding, G protein activation, and chemotactic activity, to the C-terminal domain of CCL19. *Biochemical and biophysical research communications.* 2006;348(3):1089-93.
113. Sasaki M, Hasegawa H, Kohno M, Inoue A, Ito MR, Fujita S. Antagonist of secondary lymphoid-tissue chemokine (CCR ligand 21) prevents the development of chronic graft-versus-host disease in mice. *Journal of Immunology.* 2003;170(1):588-96.

114. Ott TR, Pahuja A, Nickolls SA, Alleva DG, Struthers RS. Identification of CC chemokine receptor 7 residues important for receptor activation. *Journal of Biological Chemistry*. 2004;279(41):42383-92.
115. Otero C, Eisele PS, Schaeuble K, Groettrup M, Legler DF. Distinct motifs in the chemokine receptor CCR7 regulate signal transduction, receptor trafficking and chemotaxis. *Journal of Cell Science*. 2008;121(16):2759-67.
116. Kohout TA, Nicholas SL, Perry SJ, Reinhart G, Junger S, Struthers RS. Differential desensitization, receptor phosphorylation, β -arrestin recruitment, and ERK1/2 activation by the two endogenous ligands for the CC chemokine receptor 7. *Journal of Biological Chemistry*. 2004;279(22):23214-22.
117. Proudfoot AEI, Power CA, Rommel C, Wells TNC, editors. Strategies for chemokine antagonists as therapeutics. *Seminars in immunology*; 2003: Elsevier.
118. Carter PH. Chemokine receptor antagonism as an approach to anti-inflammatory therapy: 'just right' or plain wrong? *Current opinion in chemical biology*. 2002;6(4):510-25.
119. Koopmann W, Ediriwickrema C, Krangel MS. Structure and function of the glycosaminoglycan binding site of chemokine macrophage-inflammatory protein-1 β . *Journal of Immunology*. 1999;163(4):2120-7.
120. Chen G, Chen S-M, Wang X, Ding X-F, Ding J, Meng L-H. Inhibition of chemokine (CXC motif) ligand 12/chemokine (CXC motif) receptor 4 axis (CXCL12/CXCR4)-mediated cell migration by targeting mammalian target of rapamycin (mTOR) pathway in human gastric carcinoma cells. *Journal of Biological Chemistry*. 2012;287(15):12132-41.

121. Gladue RPPGR, Martin WHPGR, Poss CSPGR. Treatment of T-cell mediated diseases. Google Patents; 2002.
122. Grombein CM, Hu Q, Rau S, Zimmer C, Hartmann RW. Heteroatom insertion into 3, 4-dihydro-1H-quinolin-2-ones leads to potent and selective inhibitors of human and rat aldosterone synthase. *European journal of medicinal chemistry*. 2015;90:788-96.
123. Zhang L, Liu W, Mao F, Zhu J, Dong G, Jiang H, et al. Discovery of Benzylidene Derivatives as Potent Syk Inhibitors: Synthesis, SAR Analysis, and Biological Evaluation. *Archiv der Pharmazie*. 2015;348(7):463-74.
124. Piao Z-T, Guan L-P, Zhao L-M, Piao H-R, Quan Z-S. Synthesis of novel 7-benzylamino-2H-1, 4-benzoxazin-3 (4H)-ones as anticonvulsant agents. *European journal of medicinal chemistry*. 2008;43(6):1216-21.
125. Mierke DF, Giragossian C. Peptide hormone binding to G-protein-coupled receptors: Structural characterization via NMR techniques. *Medicinal research reviews*. 2001;21(5):450-71.
126. Luttrell DK, Luttrell LM. Not so strange bedfellows: G-protein-coupled receptors and Src family kinases. *Oncogene*. 2004;23(48):7969-78.
127. Medler KF. Calcium signaling in taste cells: regulation required. *Chemical senses*. 2010;35(9):753-65.
128. Patergnani S, Suski JM, Agnoletto C, Bononi A, Bonora M, De Marchi E, et al. Calcium signaling around mitochondria associated membranes (MAMs). *Cell Communication and Signaling*. 2011;9(1):1.
129. Lodish H, Berk A, Zipursky S. *Molecular cell biology*. 4th ed. New York: WH Freeman; 2000.

130. Jensen EC. The basics of western blotting. *The anatomical record*. 2012;295(3):369-71.
131. Shuyi Y, Juping D, Zhiquan Z, Qiong P, Wuyang J, Ting L, et al. A critical role of CCR7 in invasiveness and metastasis of SW620 colon cancer cell in vitro and in vivo. *Cancer biology & therapy*. 2008;7(7):1037-43.
132. Tutunea-Fatan E, Majumder M, Xin X, Lala PK. The role of CCL21/CCR7 chemokine axis in breast cancer-induced lymphangiogenesis. *Molecular cancer*. 2015;14(1):1.
133. Chen L, Liu X, Zhang H-Y, Du W, Qin Z, Yao Y, et al. Upregulation of chemokine receptor CCR10 is essential for glioma proliferation, invasion and patient survival. *Oncotarget*. 2014;5(16):6576-83.
134. Peng C, Zhou K, An S, Yang J. The effect of CCL19/CCR7 on the proliferation and migration of cell in prostate cancer. *Tumor Biology*. 2015;36(1):329-35.
135. Chi B-J, Du C-L, Fu Y-F, Zhang Y-N, Wang RW. Silencing of CCR7 inhibits the growth, invasion and migration of prostate cancer cells induced by VEGFC. *International journal of clinical and experimental pathology*. 2015;8(10):12533.
136. Na IK, Busse A, Scheibenbogen C, Ghadjar P, Coupland SE, Letsch A, et al. Identification of truncated chemokine receptor 7 in human colorectal cancer unable to localize to the cell surface and unreactive to external ligands. *International Journal of Cancer*. 2008;123(7):1565-72.
137. Cunningham HD, Shannon LA, Calloway PA, Fassold BC, Dunwiddie I, Vielhauer G, et al. Expression of the CC chemokine receptor 7 mediates

metastasis of breast cancer to the lymph nodes in mice. *Translational oncology*. 2010;3(6):354-61.

138. Wilson JL, Burchell J, Grimshaw MJ. Endothelins induce CCR7 expression by breast tumor cells via endothelin receptor A and hypoxia-inducible factor-1. *Cancer research*. 2006;66(24):11802-7.

139. Schimanski CC, Schwald S, Simiantonaki N, Jayasinghe C, Gönner U, Wilsberg V, et al. Effect of chemokine receptors CXCR4 and CCR7 on the metastatic behavior of human colorectal cancer. *Clinical Cancer Research*. 2005;11(5):1743-50.

140. Cai W, Tao J, Zhang X, Tian X, Liu T, Feng X, et al. Contribution of homeostatic chemokines CCL19 and CCL21 and their receptor CCR7 to coronary artery disease. *Arteriosclerosis, thrombosis, and vascular biology*. 2014;34(9):1933-41.

141. Ramirez PW, Famiglietti M, Sowrirajan B, DePaula-Silva AB, Rodesch C, Barker E, et al. Downmodulation of CCR7 by HIV-1 Vpu results in impaired migration and chemotactic signaling within CD4⁺ T cells. *Cell reports*. 2014;7(6):2019-30.

142. Fisher T. Fluo-4 NW Calcium Assay Kit Catalog number F36205: Thermo Fisher; 2006 [Available from: <https://www.thermofisher.com/order/catalog/product/F36205>.

143. Bruserud Ø. The chemokine system in experimental and clinical hematology. Preface. *Curr Top Microbiol Immunol*. 2010;341:v-vi.

144. Horuk R. Chemokine receptor antagonists: overcoming developmental hurdles. *Nat Rev Drug Discov*. 2009;8(1):23-33.

145. Hulkower KI, Herber RL. Cell migration and invasion assays as tools for drug discovery. *Pharmaceutics*. 2011;3(1):107-24.
146. Zigmond SH. Ability of polymorphonuclear leukocytes to orient in gradients of chemotactic factors. *J Cell Biol*. 1977;75(2 Pt 1):606-16.
147. Zicha D, Dunn GA, Brown AF. A new direct-viewing chemotaxis chamber. *J Cell Sci*. 1991;99 (Pt 4):769-75.
148. Muinonen-Martin AJ, Veltman DM, Kalna G, Insall RH. An improved chamber for direct visualisation of chemotaxis. *PLoS One*. 2010;5(12):e15309.
149. Wiggins H, Rappoport J. An agarose spot assay for chemotactic invasion. *Biotechniques*. 2010;48(2):121-4.
150. Vinader V, Al-Saraireh Y, Wiggins HL, Rappoport JZ, Shnyder SD, Patterson LH, et al. An agarose spot chemotaxis assay for chemokine receptor antagonists. *J Pharmacol Toxicol Methods*. 2011;64(3):213-6.
151. Fricker SP, Anastassov V, Cox J, Darkes MC, Grujic O, Idzan SR, et al. Characterization of the molecular pharmacology of AMD3100: a specific antagonist of the G-protein coupled chemokine receptor, CXCR4. *Biochem Pharmacol*. 2006;72(5):588-96.
152. Kodama J, Hasengaowa, Kusumoto T, Seki N, Matsuo T, Ojima Y, et al. Association of CXCR4 and CCR7 chemokine receptor expression and lymph node metastasis in human cervical cancer. *Ann Oncol*. 2007;18(1):70-6.
153. Wagner PL, Moo TA, Arora N, Liu YF, Zarnegar R, Scognamiglio T, et al. The chemokine receptors CXCR4 and CCR7 are associated with tumor size and pathologic indicators of tumor aggressiveness in papillary thyroid carcinoma. *Ann Surg Oncol*. 2008;15(10):2833-41.

154. Arigami T, Natsugoe S, Uenosono Y, Yanagita S, Arima H, Hirata M, et al. CCR7 and CXCR4 expression predicts lymph node status including micrometastasis in gastric cancer. *Int J Oncol.* 2009;35(1):19-24.
155. Schneider CA, Rasband WS, Eliceiri KW. NIH Image to ImageJ: 25 years of image analysis. *Nat Meth.* 2012;9(7):671-5.
156. Schreiner C, Bauer J, Margolis M, Juliano RL. Expression and role of integrins in adhesion of human colonic carcinoma cells to extracellular matrix components. *Clin Exp Metastasis.* 1991;9(2):163-78.
157. Argade A, Bhamidipati S, Li H, Sylvain C, Clough J, Carroll D, et al. Design, synthesis of diaminopyrimidine inhibitors targeting IgE-and IgG-mediated activation of Fc receptor signaling. *Bioorganic & medicinal chemistry letters.* 2015;25(10):2122-8.
158. Verho O, Gustafson KP, Nagendiran A, Tai CW, Bäckvall JE. Mild and Selective Hydrogenation of Nitro Compounds using Palladium Nanoparticles Supported on Amino-Functionalized Mesocellular Foam. *ChemCatChem.* 2014;6(11):3153-9.
159. Shridhar D, Gandhi S, Rao KS. A Facile synthesis of 2-alkyl (aryl)-6-and-7-nitro-3-oxo-3, 4-dihydro-2H-1, 4-benzoxazines. *Synthesis.* 1982;1982(11):986-7.
160. Hanson JR, Saberi H. Comparative orienting effects of the methanesulfonamide group in aromatic nitration. *Journal of Chemical Research.* 2004;2004(7):460.
161. Cain BF, Atwell GJ, Denny WA. Potential antitumor agents. 16. 4'-(Acridin-9-ylamino) methanesulfonanilides. *Journal of medicinal chemistry.* 1975;18(11):1110-7.

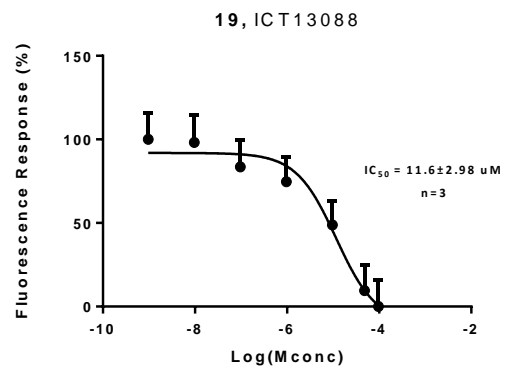
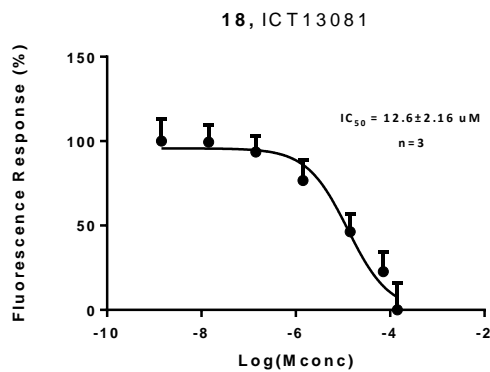
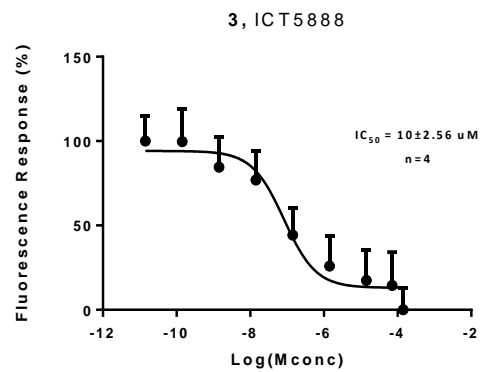
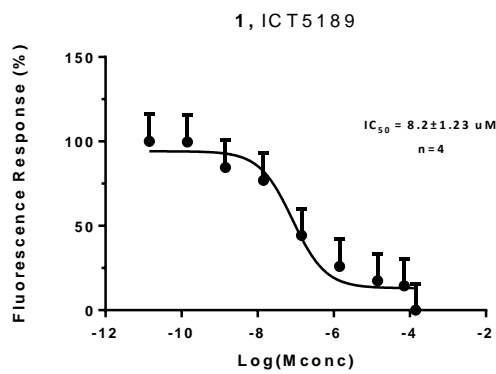
162. Pericherla S, Mareddy J, Rani D, Gollapudi PV, Pal S. Chemical modifications of nimesulide. *Journal of the Brazilian Chemical Society*. 2007;18(2):384-90.
163. O'Rand M, inventor; University of North Carolina at Chapel Hill, assignee. Small molecules for inhibiting male fertility patent WO/2015/138919. 2015.
164. Kovács D, Molnár-Tóth J, Blaskó G, Fejes I, Nyerges M. Synthesis of New Pyrazolo [1, 5- α] quinazoline Derivatives. *Synth Comm*. 2015;45(14):1675-80.
165. Macielag M, Greco M, Zhang YM, Teleha C, inventors; Janssen Pharmaceutica Nv, assignee. Quinoline derivatives useful as cb-1 inverse agonists patent WO2015130444 A1. 2015.
166. Tang PC, Zhang N, Zhang B, Wang W, Zheng H, Wu L, inventors; shanghai hengrui pharmaceutical co., ltd, assignee. Dihydropteridinone derivatives, preparation process and pharmaceutical use thereof patent WO/2011/035534. 2014.
167. Ayesa S, Lindquist C, Agback T, Benkestock K, Classon B, Henderson I, et al. Solid-phase parallel synthesis and SAR of 4-amidofuran-3-one inhibitors of cathepsin S: effect of sulfonamides P3 substituents on potency and selectivity. *Bioorganic & medicinal chemistry*. 2009;17(3):1307-24.
168. Kruger NJ. The Bradford method for protein quantitation. *Basic protein and peptide protocols*. 1994:9-15.
169. De Clercq E. The bicyclam AMD3100 story. *Nature Reviews Drug Discovery*. 2003;2(7):581-7.

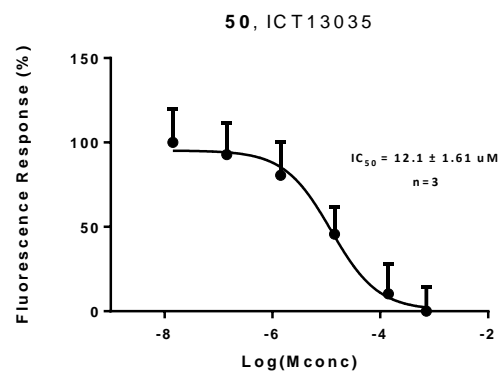
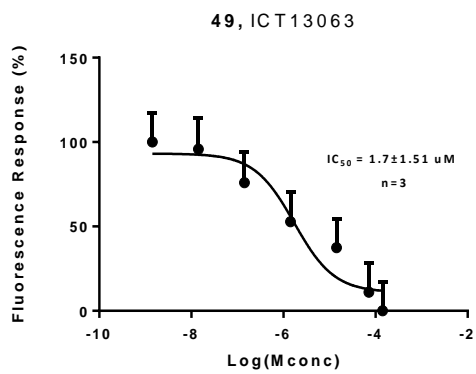
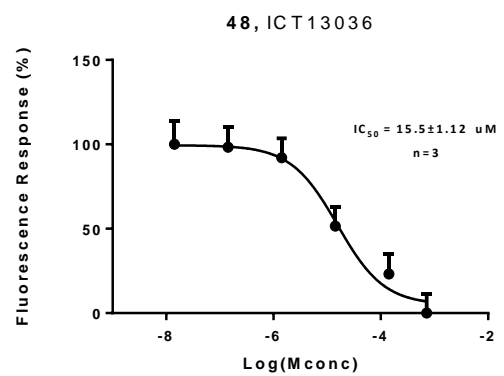
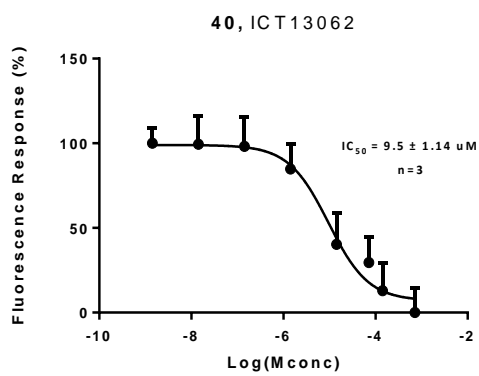
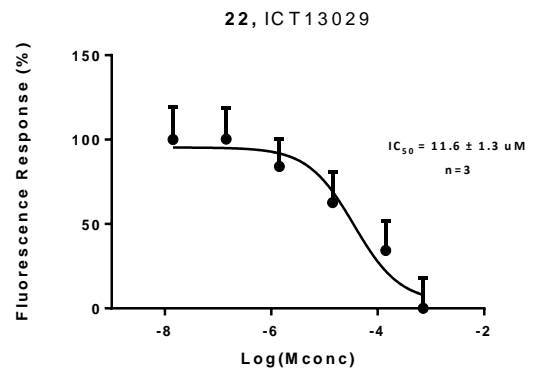
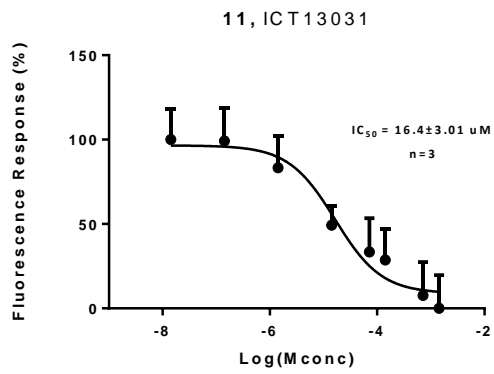
170. Liang CC, Park AY, Guan JL. In vitro scratch assay: a convenient and inexpensive method for analysis of cell migration in vitro. *Nat Protoc.* 2007;2(2):329-33.

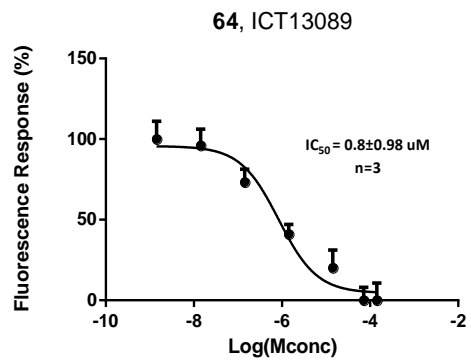
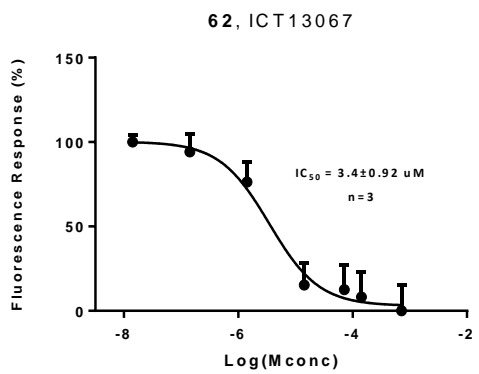
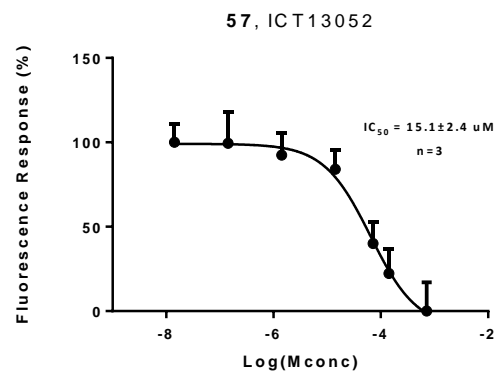
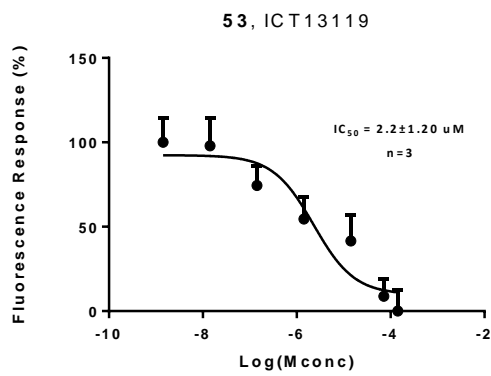
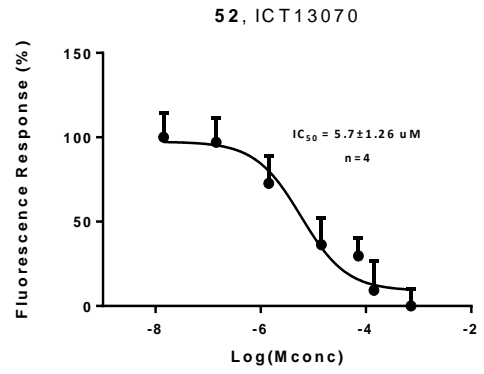
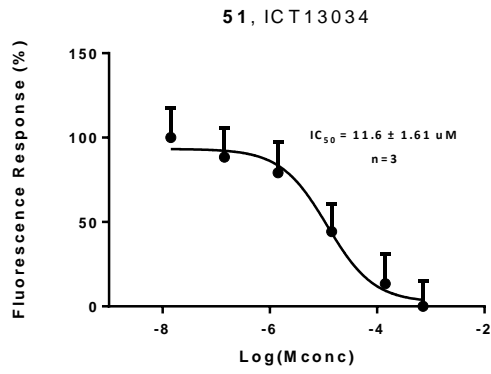
171. Stein JV, Nombela-Arrieta C. Chemokine control of lymphocyte trafficking: a general overview. *Immunology.* 2005;116(1):1-12.

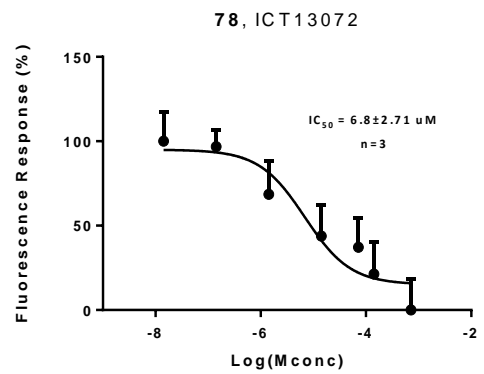
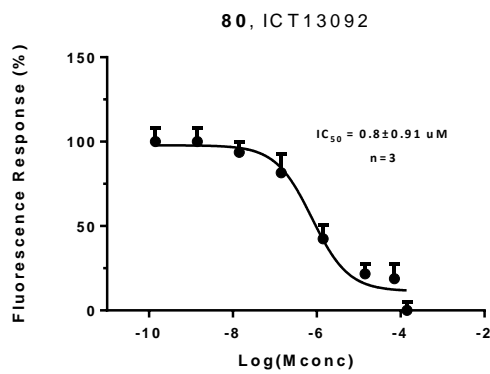
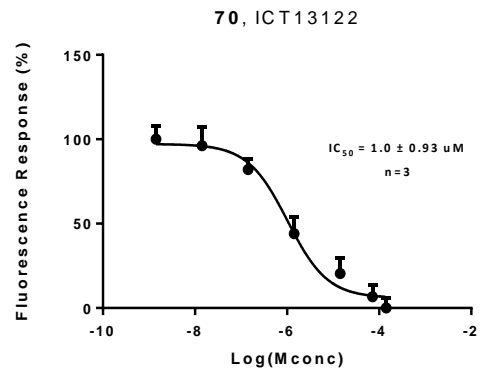
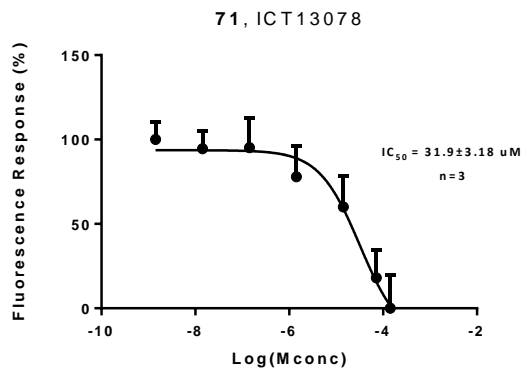
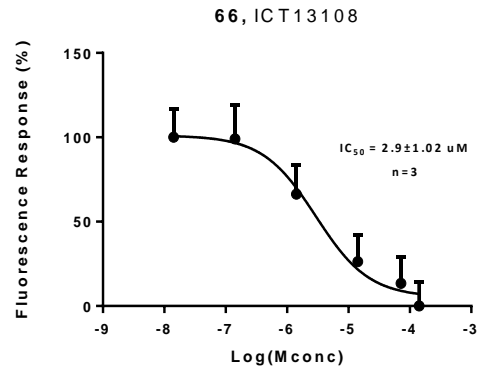
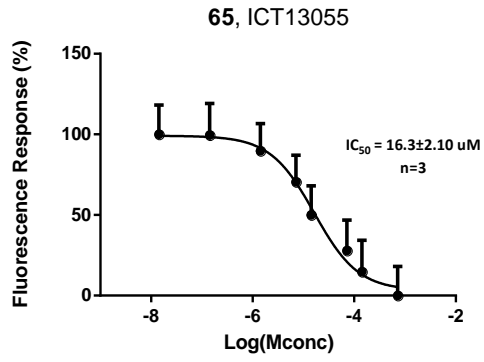
Appendix I Evaluating activity of Different compounds using calcium flux assay.

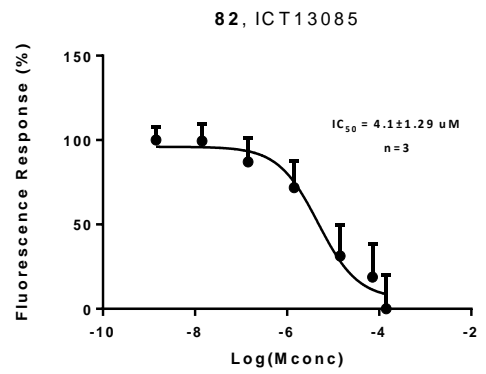
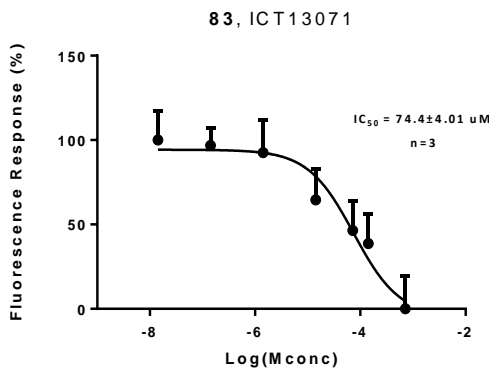
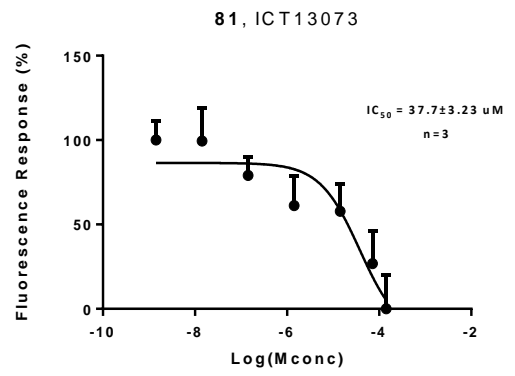
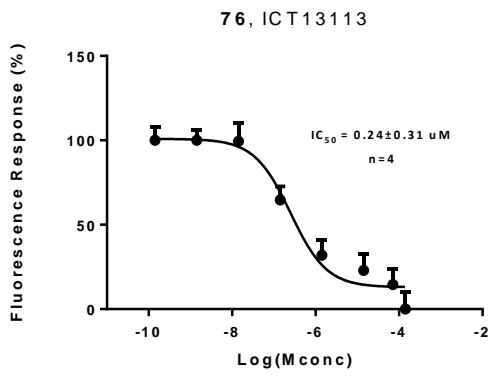
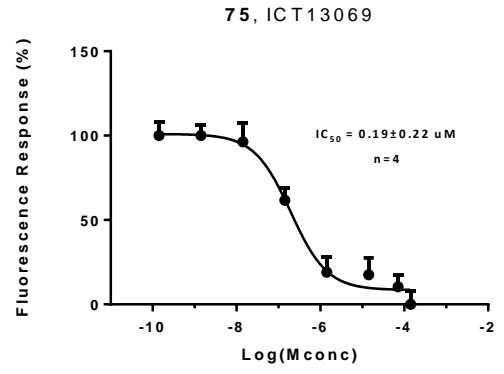
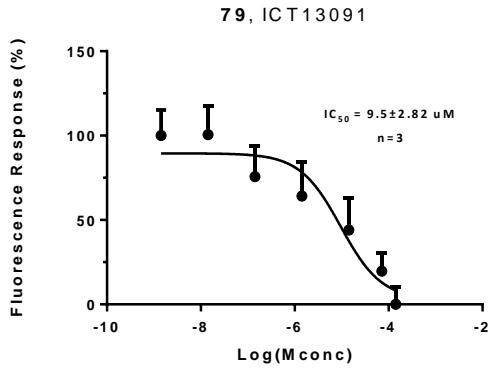
1. Dose Dependant Response (IC_{50}) curves for CCR7 receptor antagonists using OSC-19 cell line.

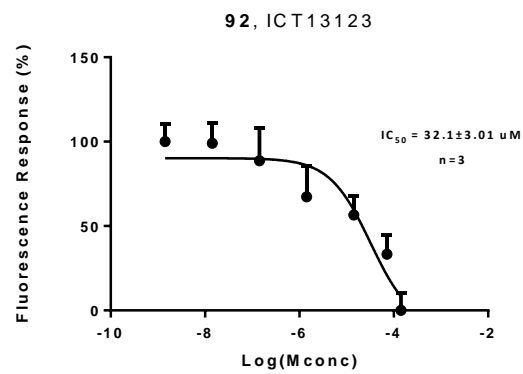
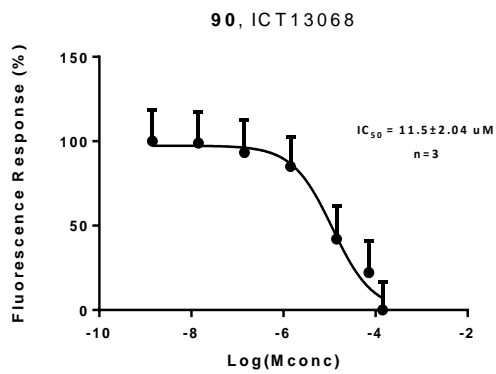
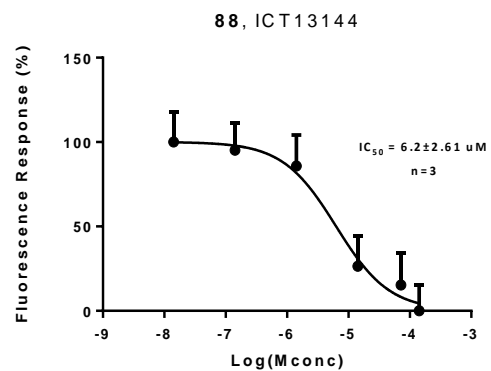
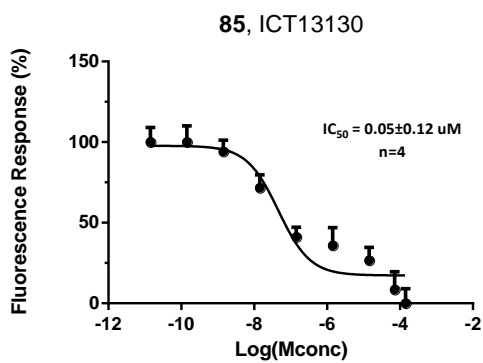
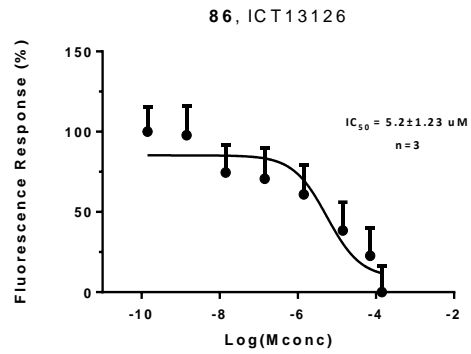
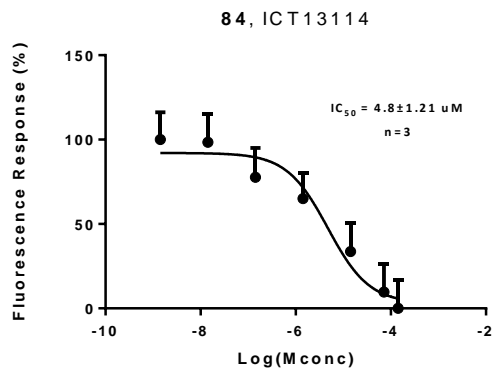


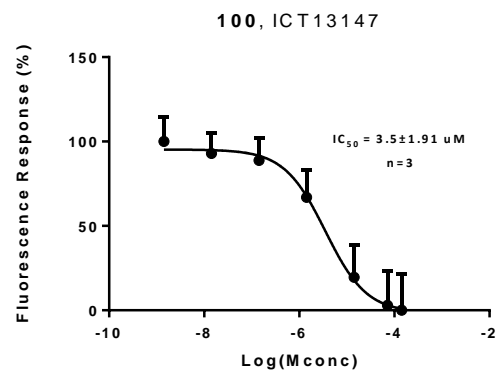
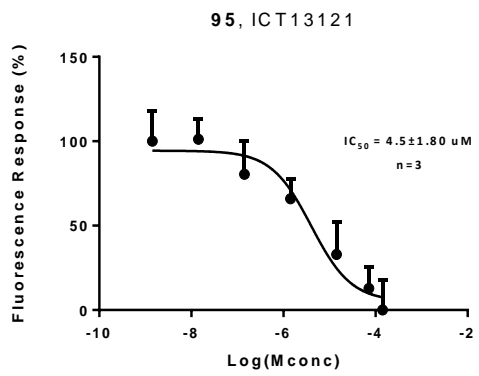
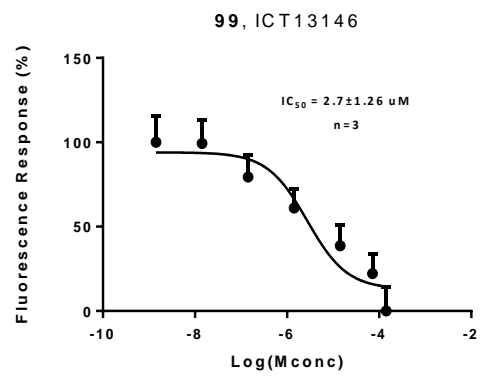
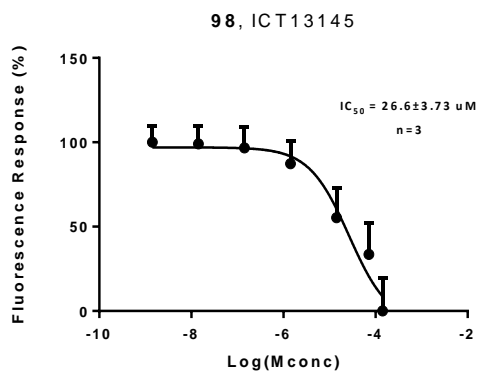
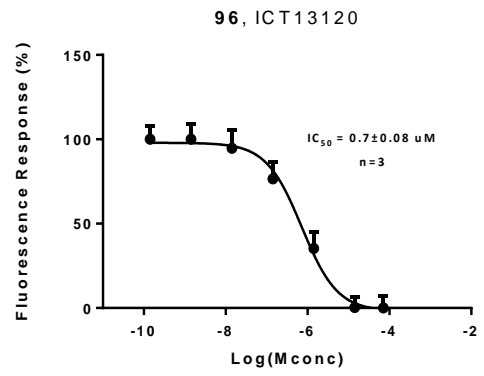
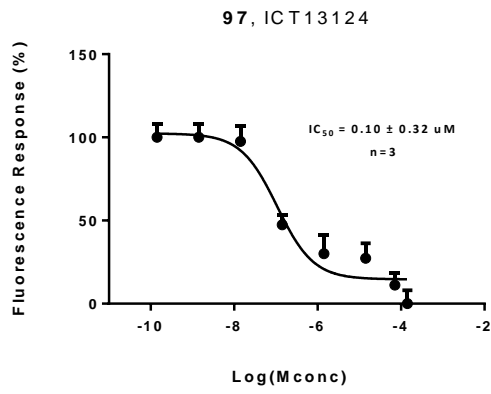












2. Evaluating activity of different compound using two different concentration.

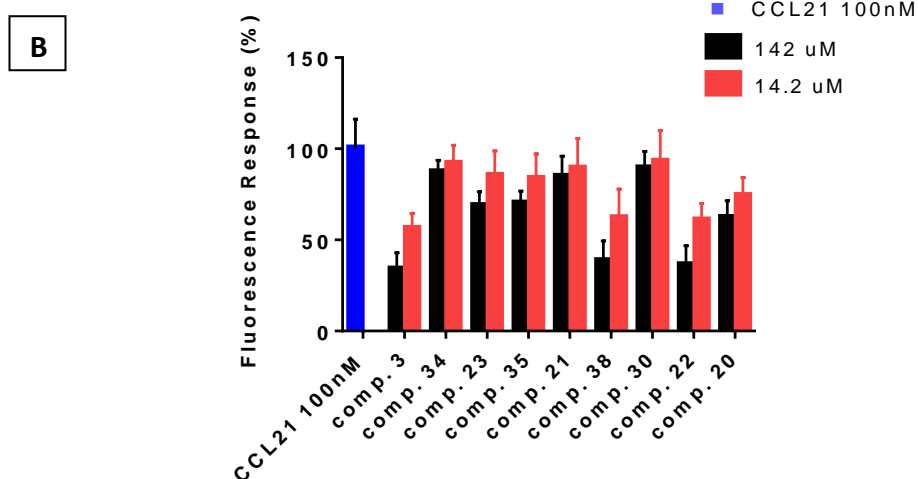
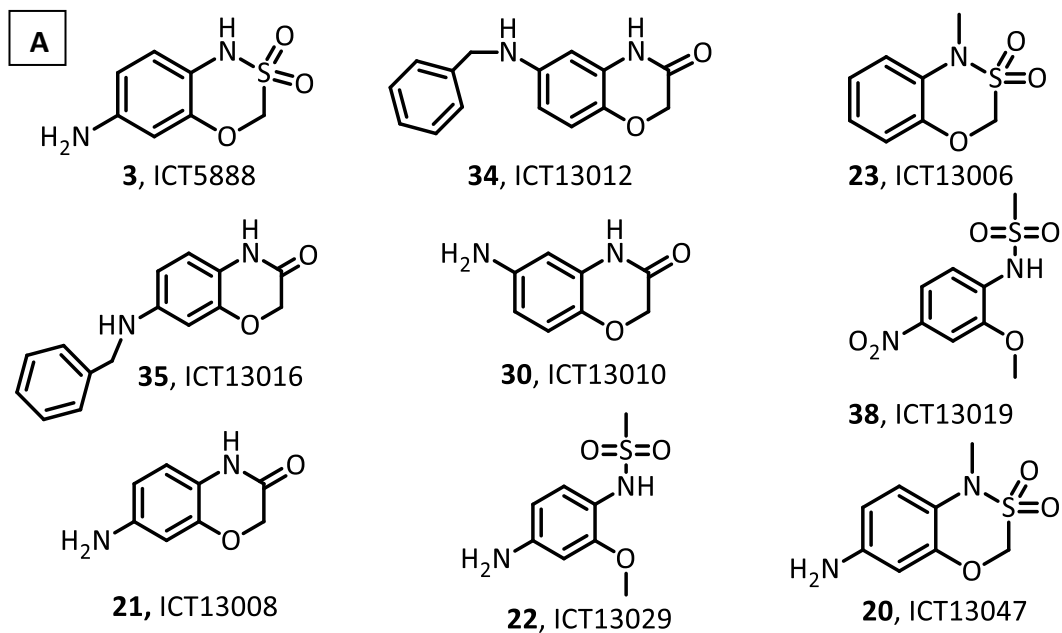


Figure 46 (A) Different compound **3** (ICT5888) analogues were tested using two different concentration, **(B)** Activity of the analogues were assessed by calcium flux assay.

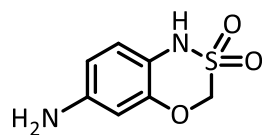
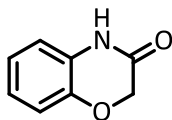
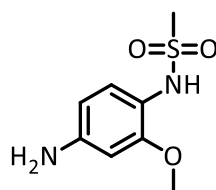
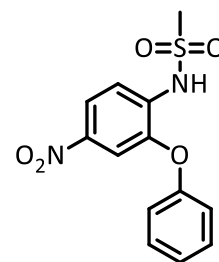
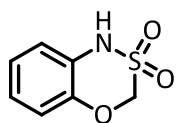
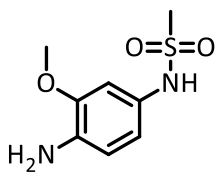
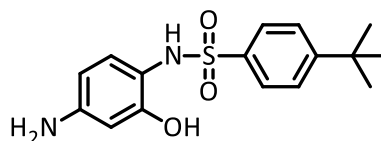
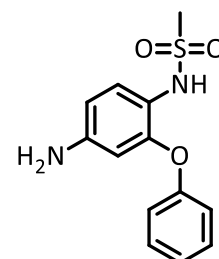
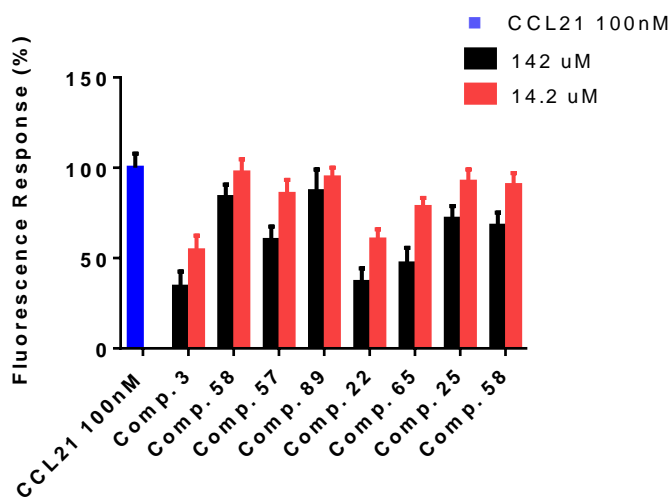
A**3**, ICT5888**25**, ICT13007**22**, ICT13029**57**, ICT13052**5**, ICT13001**89**, ICT13053**65**, ICT13055**58**, ICT13050**B**

Figure 47 (A) number of different compound **3**, ICT5888 analogues were tested using two different concentration **(B)** Activity of these analogues were assessed by calcium flux assay.

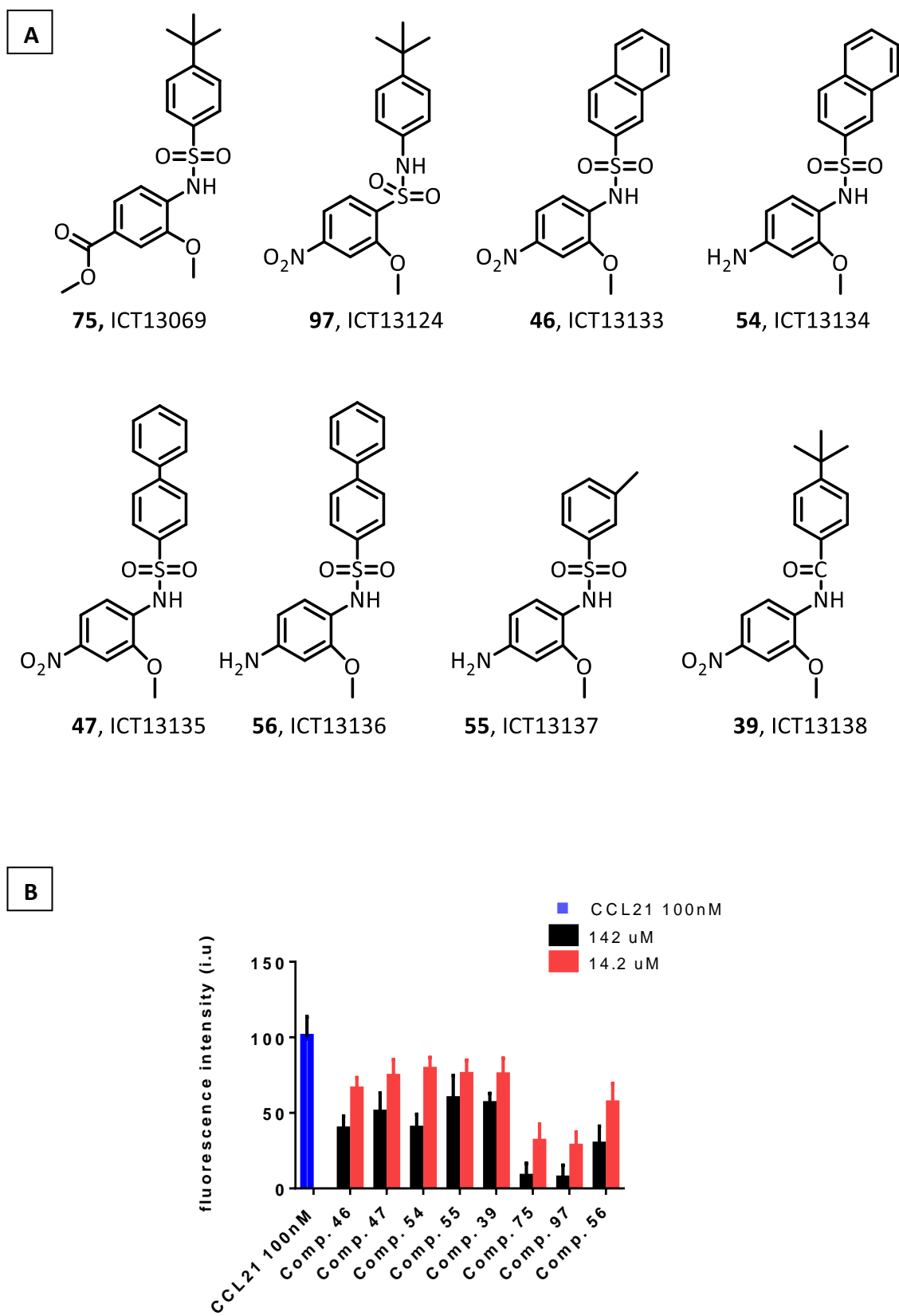
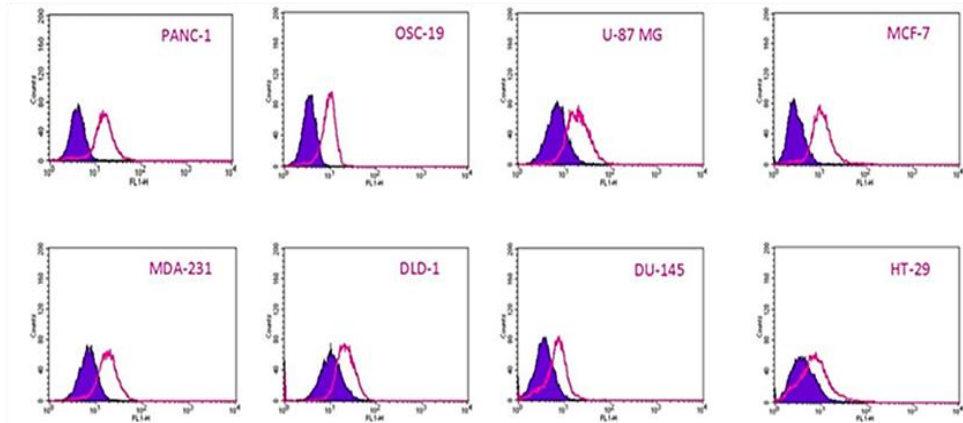


Figure 48 (A) number of different analogues were tested using two different concentration **(B)** Activity of different molecules were assessed by calcium flux assay.

Appendix II CCR7 and CXCR4 membranous receptor expression using flow cytometry assay

(A)



(B)

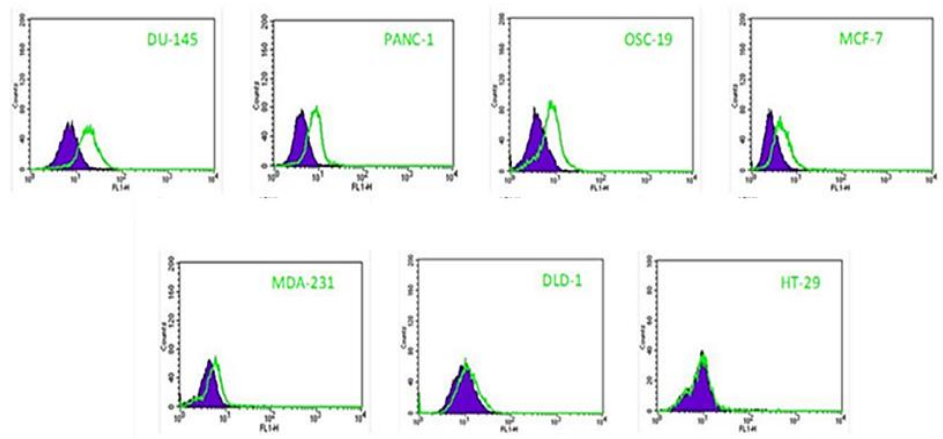
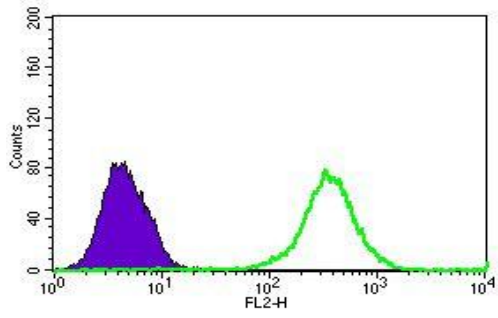
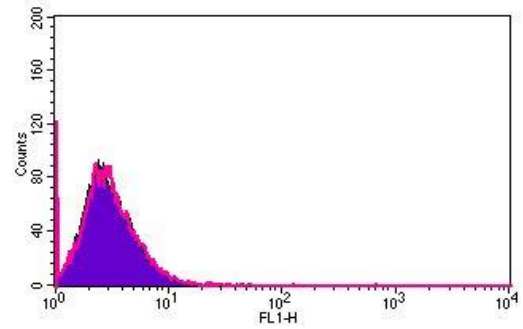


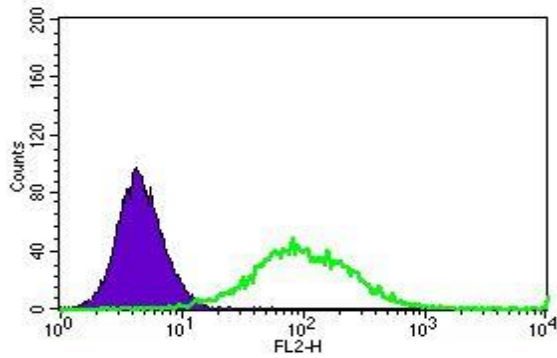
Figure 49 CCR7 and CXCR4 membranous protein expression: **(A)** CCR7 is expressed in all cell lines (the pink curve). The more shifted the unfilled curve (CCR7 stained) from the filled curve (isotype control), the higher the expression. **(B)** CXCR4 is expressed in 6 cell lines the unfilled curve (CXCR4 stained). (This work was conducted by Mrs. Haneen Bashir)



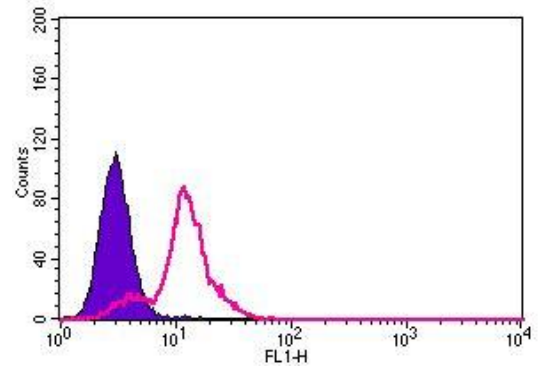
CXCR4 expression on SW480 cells



CCR7 expression on SW480 cells



CXCR4 expression on PC-3 cells



CCR7 expression on PC-3 cells

Figure 50 Expression of CCR7 and CXCR4 receptor in SW48 and PC-3 cells using flow cytometry. High expression of CXCR4 receptor while no expression of CCR7 receptor on SW480 cells. CXCR4 receptor has more expression than CCR7 receptor on PC-3 cells. (This work was conducted by Mrs. Haneen Bashir).

Appendix III Evaluating the cytotoxicity of some compounds using MTT assay.

Compound	IC ₅₀
3 , ICT5888	680 ± 20 μM (n=3)
75 , ICT13069	190 ± 20 μM (n=3)
52 , ICT13070	> 250 μM (n=3)
78 , ICT13072	> 250 μM (n=3)
70 , ICT13122	45 ± 5 μM (n=3)
76 , ICT13113	80 ± 5 μM (n=3)
22 , ICT13029	140 ± 20 μM (n=3)

Table 16 cytotoxicity results obtained from MTT assay. (This work was conducted by Mrs. Haneen Bashir)

Appendix IV Evaluating efficacy of compound 75 using scratch assay.

1. Assessment of PC-3 cells aptitude toward different chemoattractant

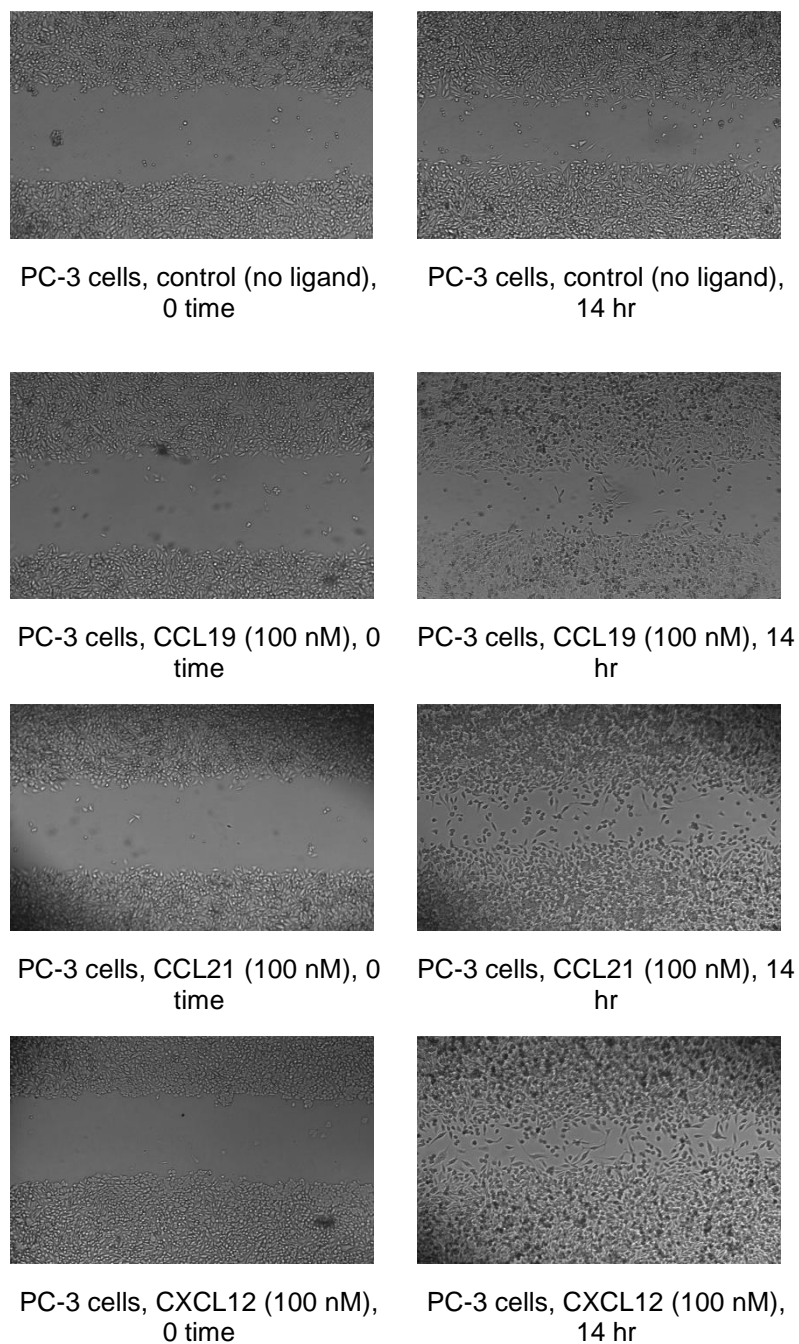
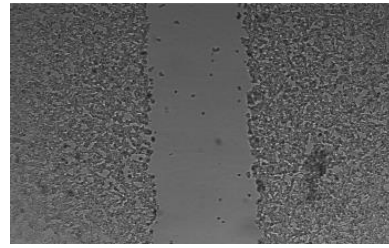
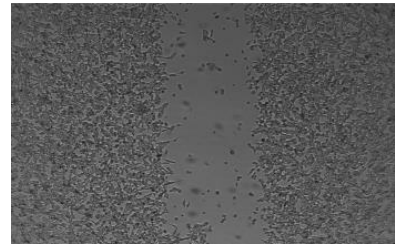


Figure 51 Scratch were made on confluent monolayers of PC-3 cells. Cells were treated with CCL21 at 100 nM, CCL19 at 100 nM and CXCL12 100 nM or no ligand added (control). Wound healing is accelerated toward CXCL12 more than CCL21 and the least was observed with CCL19. (This work was conducted by Mrs. Haneen Bashir)

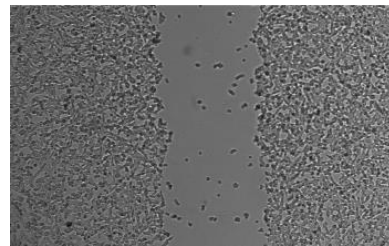
2. Assessment of SW480 cells aptitude toward different chemoattractants



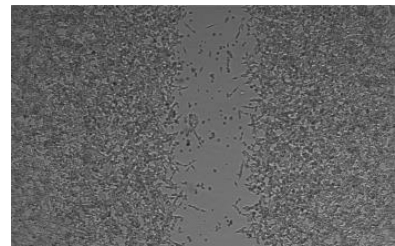
SW480 cells, control (no ligand), 0 time



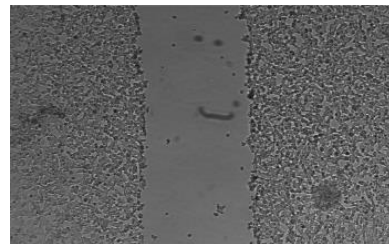
SW480 cells, control (no ligand), 21 hr



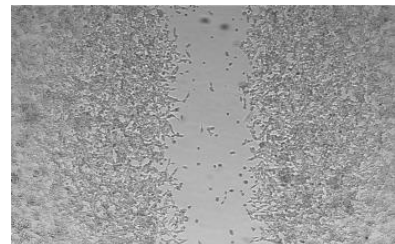
SW480 cells, CCL19 (100 nM), 0 time



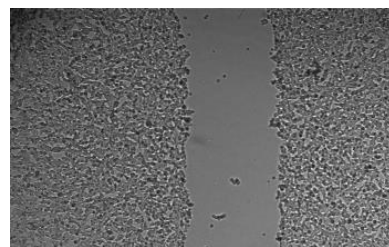
SW480 cells, CCL19 (100 nM), 21 hr



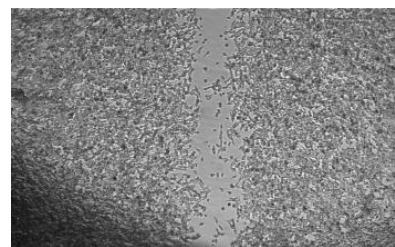
SW480 cells, CCL21 (100 nM), 0 time



SW480 cells, CCL21 (100 nM), 21 hr



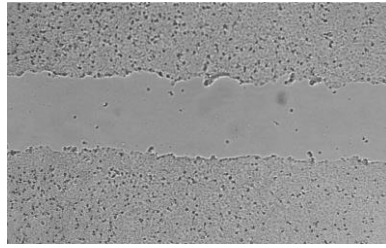
SW480 cells, CXCL12 (100 nM), 0 time



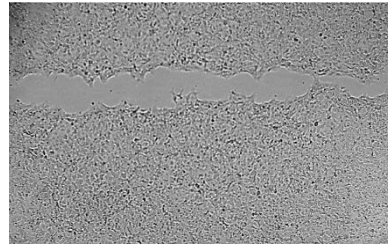
SW480 cells, CXCL12 (100 nM), 21 hr

Figure 52 Scratch were made on confluent monolayers of SW480 cells. Cells were treated with CCL21 at 100 nM, CCL19 at 100 nM and CXCL12 100 nM or no ligand added (control). Wound healing is accelerated toward CXCL12 but not CCL21 neither CCL19. (This work was conducted by Mr. Roshan Patel)

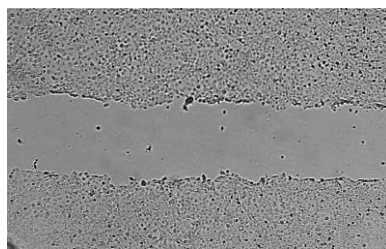
3. Assessment of potency of compound 75 using OSC-19 cells.



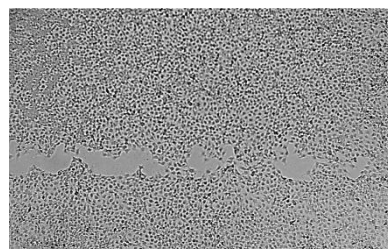
OSC-19 cells, control (no ligand), 0 time



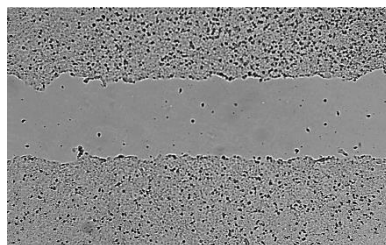
OSC-19 cells, control (no ligand), 18 hr



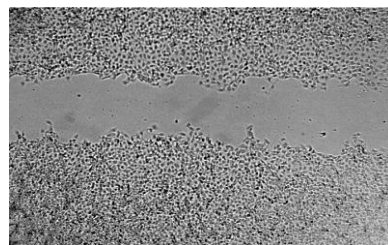
OSC-19 cells, CCL21 (10 nM), 0 time



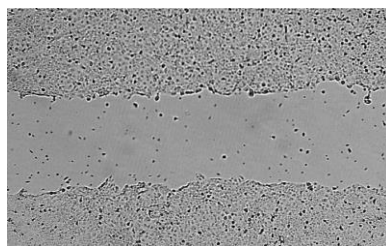
OSC-19 cells, CCL21 (10 nM), 18 hr



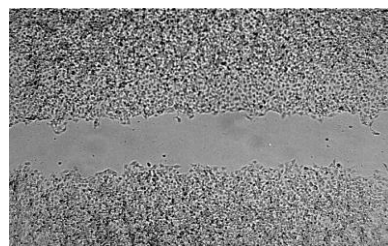
OSC-19 cells, CCL21 (10 nM) + 100 μM compound 75, 0 time



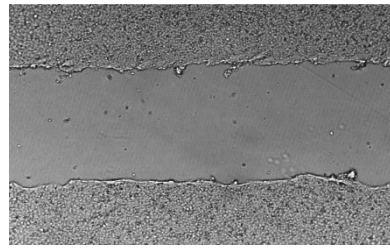
OSC-19 cells, CCL21 (10 nM) + 100 μM compound 75, 18 hr



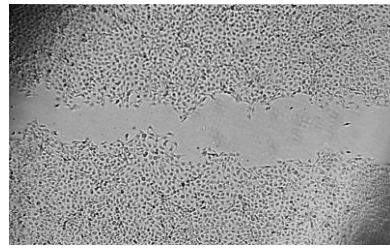
OSC-19 cells, CCL21 (10 nM) + 10 μM compound 75, 0 time



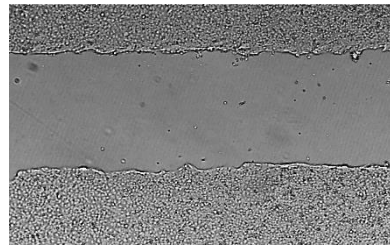
OSC-19 cells, CCL21 (10 nM) + 10 μM compound 75, 18 hr



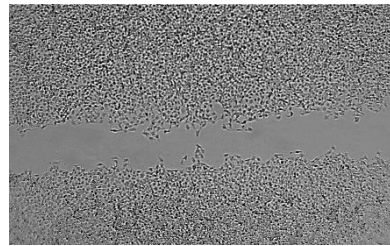
OSC-19 cells, CCL21 (10 nM) +
1 μM compound **75**, 0 time



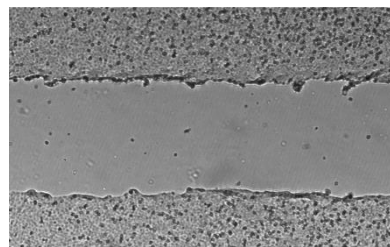
OSC-19 cells, CCL21 (10 nM) +
1 μM compound **75**, 18 hr time



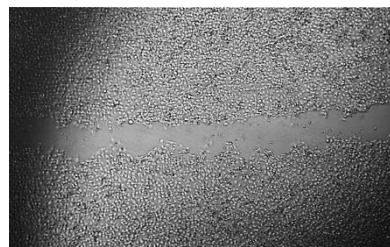
OSC-19 cells, CCL21 (10 nM) +
100 nM compound **75**, 0 time



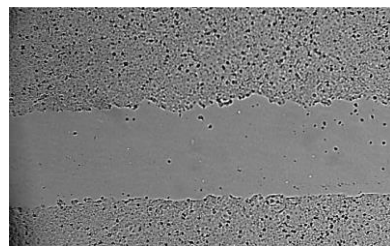
OSC-19 cells, CCL21 (10 nM) +
100 nM compound **75**, 18 hr



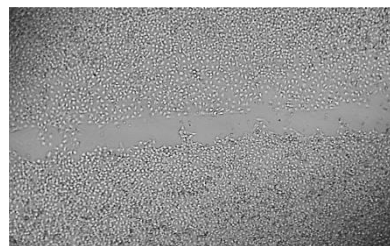
OSC-19 cells, CCL21 (10 nM) +
10 nM compound **75**, 0 time



OSC-19 cells, CCL21 (10 nM) +
10 nM compound **75**, 18 hr



OSC-19 cells, CCL21 (10 nM) +
1 nM compound **75**, 0 time



OSC-19 cells, CCL21 (10 nM) +
1 nM compound **75**, 18 hr

Figure 53 ICT13069 inhibits cell migration in dose dependent manner, OSC-19 cells were treated with ICT13069 at different concentrations for 2 h before adding CCL21.

(This work was conducted by Mrs. Haneen Bashir)